

Different strategies to prepare anti-inflammatory biomaterial coatings with in vitro and in vivo studies on efficacy and mechanisms

Dissertation

zur Erlangung des
Doktorgrades der Naturwissenschaften (Dr. rer. nat.)

der

Naturwissenschaftlichen Fakultät I – Biowissenschaften –

der Martin-Luther-Universität
Halle-Wittenberg,

vorgelegt

von Frau Dipl. Pharm. Hala Alkhoury

geb. am 10.09.1988 in Damaskus

Gutachter: Prof. Dr. rer. nat. habil. Thomas Groth
Prof. Dr. Markus Pietzsch
Prof. Dr. Gloria Gallego Ferrer

Halle (Saale), 23-11-2020

To my family

Table of Contents

Abbreviations.....	5
Graphical abstract.....	8
Abstract.....	9
Zusammenfassung.....	11
Chapter 1.....	13
Introduction.....	13
1. Biomaterials, biocompatibility and implant-related complications	14
2. General overview on inflammation in health and disease.....	15
3. Host response to biomaterials	17
3.1. Protein adsorption, opsonisation, activation of coagulation and complement	17
3.2. Macrophages as key players during acute and chronic inflammation	19
3.3. The nuclear transcription factor NF- κ B signalling pathway.....	22
3.4. Role of cytokines and metalloproteinases in inflammation	24
3.5. Foreign body giant cell formation and fibrosis on biomaterial implants	25
4. Control of inflammation by non-steroidal anti-inflammatory drugs (NSAIDs) and glycosaminoglycans	27
4.1. Nanoparticle-based systems for drug delivery of NSAID and other anti-inflammatory drugs	27
4.2. Chemistry and biology of hyaluronan, heparin and chitosan	29
5. Different approaches towards anti-inflammatory surfaces	34
5.1. Brief survey on anti-inflammatory strategies of materials' modification	34
6. Aim of the thesis	36
Chapter 2: Covalent immobilization of glycosaminoglycans to reduce the inflammatory effects of biomaterials.....	47
Chapter 3: Study on the potential mechanism of anti-inflammatory activity of covalently immobilized hyaluronan and heparin	56

Chapter 4: Studies on the mechanisms of anti-inflammatory activity of heparin- and hyaluronan-containing multilayer coatings-targeting NF-κB signalling pathway.....	71
Chapter 5: Tissue response to biphasic calcium phosphate covalently modified with either heparin or hyaluronic acid in a mouse subcutaneous implanation model.....	90
Chapter 6: Anti-inflammatory surface coatings based on polyelectrolyte multilayers of heparin and polycationic nanoparticles of Naproxen-bearing polymeric drugs	122
Chapter 7.....	134
Summary and future perspectives.....	134
Acknowledgment.....	136
Publication list with declaration of self-contribution to research articles	139
Curriculum vitae	144
Selbstständigkeitserklärung	146

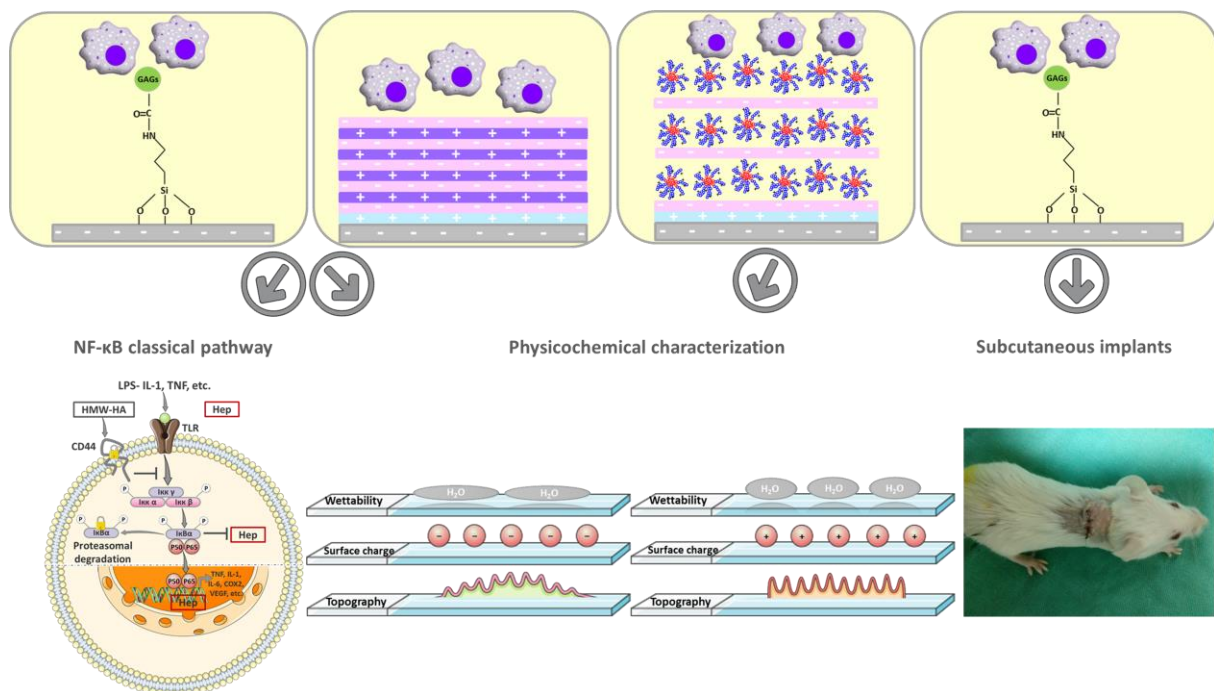
Abbreviations

AAS	- antibiotic antimycotic solution
AFM	- atomic force microscopy
AP	- alternative pathway
APTES	- 3-amino propyl triethoxy silane
ARD	- ankyrin repeat-containing domain
ARDS	- acute respiratory distress syndrome
ATIII	- antithrombin III
BCP	- biphasic calcium phosphate
BSA	- bovine serum albumin
Chi	- chitosan
CLSM	- confocal laser scanning microscopy
COPD	- chronic obstructive pulmonary disease
COS	- chitosan oligosaccharide
CP	- classical pathway
CS	- chondroitin sulfate
DAMPs	- danger-associated molecular patterns
DCs	- dendritic cells
DC-STAMP	- dendritic cell-specific transmembrane protein
DD	- deacetylation degree
DEX	- dexamethasone
DSMO	- dimethyl sulfoxide
ECM	- extracellular matrix
EDC	- 1-Ethyl-3-(3-dimethylaminopropyl) carbodiimide
ELISA	- enzyme-linked immunosorbent assay
FBGCs	- foreign body giant cells
FBR	- foreign body response
FBS	- fetal bovine serum
FGF	- fibroblast growth factor
FITC	- fluorescein isothiocyanate
FXII	- factor XII
GAG	- glycosaminoglycan
GM-CSF	- granulocyte macrophage colony-stimulating factor
HA	- hyaluronic acid / hyaluronan
HEMA	- hydroxyethyl methacrylate
Hep	- heparin

HMW-HA	- high molecular weight hyaluronic acid
IBD	- inflammatory bowel diseases
IF	- immunofluorescence
IFN-γ	- interferon- γ
IL-1ra	- interleukin 1 receptor antagonist
IL-1β	- Interleukin-1 β
LbL	- layer-by-layer
LBP	- LPS-binding protein
LMW-HA	- low molecular weight hyaluronic acid
LPS	- lipopolysaccharide
MBL	- mannose-binding lectin
MCP	- monocyte chemoattractant proteins
M-CSF	- macrophage colony-stimulating factor
MES	- acid 2-(N-morfolino) etansolfonico
MIP	- macrophage inhibitory protein
MMP	- matrix metalloproteinases
MR	- mannose receptors
MSCs	- mesenchymal stem cells
NaOH	- sodium hydroxide
NF-κB	- nuclear transcription factor- κ B
NHS	- N-hydroxysuccinimide
NK	- natural killer
NLRs	- nod-like receptors
NPs	- nanoparticles
PAMPs	- Pathogen-associated molecular patterns
PCL	- poly- ϵ -caprolactone
PDGF	- platelet-derived growth factor
PEG	- polyethylene glycol
PEI	- poly (ethylene imine)
PEMs	- polyelectrolyte multilayers
PEO	- poly(ethylene oxide)
pHEMA	- poly(2-hydroxyethyl methacrylate)
PLGA	- poly(lactic-co-glycolic acid)
PMA	- phorbol 12-myristate 13-acetate
PRRs	- pattern recognition receptors
PSS	- polystyrene sulfonate
PZC	- point of zero charge

QCM	- quartz crystal microbalance
RA	- rheumatoid arthritis
RCA	- regulator of complement activation
RFU	- relative fluorescence unit
RHD	- Rel homology domain
RNS	- reactive nitrogen species
ROS	- reactive oxygen species
SEM	- scanning electron microscopy
SR	- scavenger receptors
TAD	- C-terminal transactivation domain
TF	- tissue factor
TGF-β1	- transforming growth factor- β 1
TH1	- T-helper 1
TH2	- T-helper 2
TIMPs	- tissue inhibitors of metalloproteinases
TLR	- toll-like receptor
TNF	- tumour necrosis factor
Treg	- regulatory T-cell
VEGF	- vascular endothelial growth factor
WCA	- water contact angle
XPS	- X-ray photoelectron spectroscopy
ZP	- Zeta potential
α-MSH	- alpha melanocyte-stimulating hormone

Graphical abstract



General overview on thesis chapters. Two different methods were applied to model substrata of glass or silicone (grey base layer with negative charge). A priming layer of 3-aminopropyltriethoxysilane or poly (ethylene imine) (blue layer with positive charge) was adsorbed first. Then, glycosaminoglycans were immobilized either covalently as a monolayer or adsorptively as a multilayer using the layer-by-layer technique, which is based on alternating adsorption of the polyanions heparin or hyaluronan (pink layer with negative charge) and the polycation chitosan (purple layer with positive charge). THP-1 monocyte derived macrophages were utilized for the biological studies in attempt to evaluate the macrophage-related inflammatory responses. The work was focusing on the evaluation of anti-inflammatory activity of glycosaminoglycans in terms of physicochemical properties (wettability, surface charge and topography) as well as the potential mechanism toward the nuclear transcription factor-κB signalling pathway. Thereafter, an integration of multiple anti-inflammatory strategies was approached by incorporating Naproxen-encapsulated nanoparticles together with heparin. The work hypothesis was to investigate the cellular responses by showing short and potential long-term anti-inflammatory effects. Finally, preclinical in vivo studies were performed with covalent immobilization of glycosaminoglycans on biphasic calcium phosphate particles to investigate tissue response with subcutaneous implantation in mice.

Abstract

Chronic inflammation and fibrous encapsulation, which can occur after the implantation of biomaterials, severely limit the function of implants. This work was aimed to develop novel implant coatings for various biomedical applications using glycosaminoglycans such as hyaluronan, and heparin, since heparin and high-molecular hyaluronic acid are known to have anti-inflammatory effects. The glycosaminoglycans were immobilized either covalently as a monolayer or adsorptively as a multilayer using the layer-by-layer technique on model materials. An extension of the pharmaceutical effects of glycosaminoglycans should be achieved by application of nanoparticles containing Naproxen. The coatings were characterized by physical methods with respect to layer formation, wettability, zeta potential and topography. Macrophages are important effector cells that play a crucial role in inflammation. The effect of the coatings on macrophages in terms of cell adhesion, subsequent formation of foreign body giant cells and release of the pro-inflammatory cytokine IL-1 β compared to pro-inflammatory controls showed that these parameters were significantly reduced. In order to elucidate the mechanism of action of the immobilized glycosaminoglycans, studies were conducted that focused on the signal transduction of the nuclear transcription factor- κ B, which plays a central role in the expression of genes in leukocytes during inflammatory reactions. By using confocal laser scanning microscopy and immunoblotting, it could be shown an inhibition of the activation and translocation into the nucleus of the p65 subunit of nuclear transcription factor- κ B by heparin and hyaluronic acid. It was also illustrated that heparin in particular was taken up by cells through endocytosis and that both glycosaminoglycans were associated with the cell membrane of macrophages. Overall, it was observed that heparin has the strongest inhibitory effect on macrophages, which was related to the inhibition of the nuclear transcription factor- κ B signalling pathway. In order to investigate the anti-inflammatory effect of immobilized heparin and hyaluronic acid after successful in vitro detection, it was necessary to investigate whether this effect can also be found in vivo. Therefore, biphasic calcium phosphate materials were coated with both glycosaminoglycans and subcutaneously implanted into mice for 15 and 30 days. The histological studies showed a decrease in the number of multinucleated giant cells and a reduced vascularization of the tissue with both glycosaminoglycans. On the one hand, biphasic calcium phosphate-HA suppressed inflammatory reactions, but allowed the formation of new bone-like tissue. On the other hand, biphasic calcium phosphate-

Hep allowed osteogenesis in the subcutaneous bone-forming model and delayed the onset of the inflammatory reaction.

As a general conclusion, it can be stated that the designed systems represent novel approaches for biomaterials coating, which could represent promising strategies for achieving an inherent anti-inflammatory effect.

Zusammenfassung

Chronische Entzündungen und fibröse Verkapselungen, die nach der Implantation von Biomaterialien auftreten können, schränken die Funktion von Implantaten stark ein. Diese Arbeit zielte daher darauf ab, neuartige Beschichtungen für verschiedene biomedizinische Anwendungen zu entwickeln, bei denen Glykosaminoglykane wie Hyaluronan und Heparin eingesetzt werden, da vor allem Heparin und hochmolekulare Hyaluronsäure für eine entzündungshemmende Wirkung bekannt sind. Die Glykosaminoglykane wurden entweder kovalent als Monoschicht oder adsorptiv als Multischicht mit Hilfe der Layer-by-Layer-Technik auf Modellmaterialien immobilisiert. Eine Erweiterung der pharmazeutischen Wirkung sollte durch Auftragung von Nanopartikeln erreicht werden, die Naproxen enthalten. Die Beschichtungen wurden mit physikalischen Methoden hinsichtlich Schichtbildung, Benetzbarkeit, Zetapotential und Topographie charakterisiert. Makrophagen stellen dabei wichtige Effektorzellen dar, die eine entscheidende Rolle im Entzündungsgeschehen spielen. Die Wirkung der Beschichtungen auf Makrophagen hinsichtlich der Zelladhäsion, der anschließenden Bildung von Fremdkörper-Riesenzellen und die Freisetzung des pro-inflammatorischen Zytokins IL-1 β im Vergleich zu entzündungsfördernden Kontrollen, zeigte dass diese Parameter signifikant vermindert waren. Um den Wirkmechanismus der immobilisierten Glykosaminoglykane aufzuklären, wurden Studien durchgeführt, die sich mit der Wirkung der Glykosaminoglykane auf die Signaltransduktion des nukleären Transkriptionsfaktors- κ B konzentrierten, der eine zentrale Rolle bei der Expression von Genen in Leukozyten bei Entzündungsreaktionen spielt. Dabei konnte mit konfokaler Laser-scanning-Mikroskopie und Immunoblotting gezeigt werden, dass eine Hemmung der Aktivierung und Translokation in den Zellkern der p65-Untereinheit Signaltransduktion des nukleären Transkriptionsfaktors- κ B durch Heparin und Hyaluronsäure verursacht wird. Dabei konnte auch gezeigt werden, dass vor allem bei Heparin eine Aufnahme in Zellen durch Endozytose stattfindet und beide Glykosaminoglykane mit der Zellmembran der Makrophagen assoziiert sind. Insgesamt wurde deutlich, dass Heparin die stärkste Hemmwirkung auf Makrophagen besitzt, was mit der Hemmung der Signaltransduktion des nukleären Transkriptionsfaktors- κ B Signalwegs in Zusammenhang steht. Nach erfolgreichem in vitro-Nachweis der entzündungshemmenden Wirkung von immobilisiertem Heparin und Hyaluronsäure wurde untersucht, ob diese auch in vivo zu finden ist. Deshalb wurden biphasische Kalziumphosphatmaterialien mit beiden Glykosaminoglykane

beschichtet und subkutan in Mäuse für 15 und 30 Tage implantiert. Die histologischen Studien zeigten eine Abnahme der Anzahl vielkerniger Riesenzellen sowie eine verminderte Vaskularisierung des Gewebes bei beiden Glykosaminoglykane. Einerseits unterdrückte biphasische Kalziumphosphatmaterialien-HA Entzündungsreaktionen, erlaubte aber die Bildung neuen knochenähnlichen Gewebes. Auf der anderen Seite erlaubte biphasische Kalziumphosphatmaterialien-Hep die Osteogenese im subkutanen knochenbildenden Modell und verzögerte den Beginn der Entzündungsreaktion. Insgesamt lässt sich schlussfolgern, dass es sich bei den entwickelten Systemen um neuartige Ansätze der Beschichtung von Biomaterialien handelt, die vielversprechende Strategien zur Erzielung einer inhärenten entzündungshemmenden Wirkung bei Implantaten darstellen könnten.

Chapter 1

Introduction

This cumulative thesis consists of five publications. The first chapter represents a general introduction to the content of this thesis. Out of the five manuscripts, four have already been published and are assembled as chapter 2, 3, 4 and 6 including a summary at the beginning of each chapter. The fifth manuscript has been submitted to Journal of Biomedical Materials Research (JBMR) part A and represents chapter 5.

1. Biomaterials, biocompatibility and implant-related complications

Biomaterials are recognized for their importance in increasing the quality of the lives of patients in terms of replacing or augmenting a tissue, organ or restoring a biological function in the body [1]. Biomaterials science is a field that encompasses a steady and strong growth in different areas [2]. The interdisciplinary field of biomaterials brought researches in physics, chemistry and biology together. The first attempt of joint implantation was documented in the 1890s [3] while the first fully implantable pacemaker was reported in 1958 [4]. During these developments, the outcome of implantation became heavily dependent on the materials used for the devices. So far, metals and metal alloys, carbon, ceramics, polymers and composite materials thereof have found diverse usage in biomaterials field [5]. Polymers can be divided into two classes: non-biodegradable and degradable polymers. For instance, degradable polymers can be of either synthetic or biological origin. In addition, the degradation process can be based on either enzymatic and non-enzymatic hydrolysis [6]. For these processes the kind of bonds between the monomeric units of polymers plays an important role. Many of the natural polymers like glycosaminoglycans (GAGs) undergo enzymatic degradation, since the glycosidic bond is relatively stable against chemical hydrolysis [7]. By contrast, polyesters that are often used as synthetic, degradable polymers in medical applications degrade by chemical hydrolysis [8]. Moreover, biopolymers were the first biomaterials that were used clinically [9]. On the other hand, non-degradable polymers are beneficial when long-lasting biomaterials are needed like poly (methyl methacrylate) to be used as intraocular lenses, etc. [10, 11].

The biomaterial-associated adverse reactions are still an obstacle to their clinical application and therefore assessment of biocompatibility is essential for suitability of an implant. For example, toxicity and immunogenicity are factors evaluating the tolerability of an implant [12]. The potential cell death, impairment of cellular or tissue functions as well as chronic inflammation are signs of a low biocompatibility profile [13, 14]. After the surgical procedure of implantation, a trauma and injury of tissues occurs with a complex cascade of biological events including inflammatory responses and wound healing mechanisms. In addition, the healing procedure is sometimes interfered with the persistence of adverse reactions leading to additional complications such as immense pain, excessive inflammation, tissue destruction or even isolation and rejection of the implant [15]. In this regard, the implant surface properties in terms of shape mechanical properties, topography, porosity, and chemical composition have

been found to be essential variables influencing the host responses [16]. Other factors affecting the functioning and longevity of the implant are the age, sex, pharmacological status as well as the general health condition and lifestyle of the host [17]. Research efforts were applied for decades in attempt to control and reduce the adverse tissue-material response. Therefore, a systematic assessment in terms of biocompatibility and analysis of reasons for adverse effects is usually required. Effective technologies to control host responses elicited by the biomaterial can be only developed by a thorough understanding of the *in vitro* and *in vivo* tissue-material interactions [18].

2. General overview on inflammation in health and disease

The immune system provides an essential mechanism during infection or tissue injury defined as inflammation, which is considered as a key biochemical process evolved in higher organisms that acts as a self-protection [19]. Two types of immunity exist in the human body, which are specified as innate and adaptive. The non-specific and naturally existing in the body since birth is the innate one. In contrast, the adaptive immunity is specific to one pathogen and it is acquired when an infective agent invades the body or upon vaccination [20]. Moreover, it is well documented that inflammation has a close connection to innate immunity. The inflammatory pathways and their target tissue vary significantly between bacterial and viral infection [19]. For instance, it has been well established that immune cells sense pathogens of bacterial source immediately through specific receptors, which in turn modifies the vascular endothelial permeability. Subsequently, a systemic effect with excessive inflammatory cytokine production will be reached and will mediate acute phase proteins secretion like C-reactive protein and coagulation factors by the liver cells [19]. In contrast, the viral infection has a distinct signalling pathway through the production of another class of cytokines such as type-1 interferons (IFNs) (play central roles in antiviral responses) and also involves cytotoxic T lymphocytes [21]. Furthermore, there are symptoms associated with the *inflammare* (original Latin word of inflammation), which has a modern acronym called PRISH. It represents the classical symptoms of inflammation including pain, redness, immobility, swelling and heat [22]. In the case of tissue injury, a phase of acute inflammation, which is deemed as part of the innate immunity and the first line of inflammatory response against foreign invaders and danger molecules starts a few seconds to minutes after injury. The acute inflammation phase is

characterized by the presence of neutrophils (polymorphonuclear leukocytes, PMNs) [23]. In addition, irritation causes mast cells to recognize the foreign stimuli by cell-surface receptors and secrete factors like histamine, proteases, and tumour necrosis factor (TNF). Histamine mediates vasodilation to ease the permeability of white blood cells and some proteins [24, 25]. While, the released interleukin-4 and 13 (IL-4, IL-13) play a role in determining the extent and degree of the subsequent development of the foreign body reaction [26, 27]. In addition, the protease triggers protein catabolism while TNF causes cell death. Usually, IL-10, transforming growth factor- β (TGF- β) and glucocorticoids are the dominant anti-inflammatory mediators in inflammation's resolution as well as in involving monocytes for the clearance of cell debris [28]. However, the persistence of acute inflammation without resolution will lead to a chronic phase, which is generally essential to eliminate the persistence stimulus like infection or chronic cellular injury [29]. The chronic inflammation is a major hallmark of abnormal inflammatory responses, which usually lasts from several months to years and eventually causes inflammatory diseases. Indeed, neurodegenerative diseases, chronic obstructive pulmonary disease (COPD), obesity, type 2 diabetes, asthma, acute respiratory distress syndrome (ARDS), inflammatory bowel diseases (IBD), rheumatoid arthritis (RA) and cancer are examples of clinical disorders related to chronic inflammation [30, 31]. On the other hand, it should be emphasized here that wounds would never heal without the aid of the inflammation process.

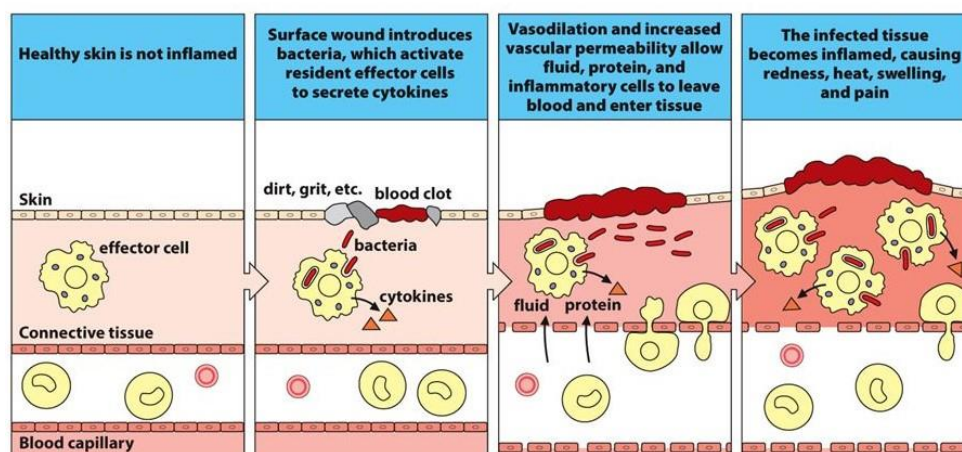


Figure 1: illustrative overview of an established state of inflammation at the site of infection as a result of the innate immunity. The figure is adopted from [32].

3. Host response to biomaterials

3.1. Protein adsorption, opsonisation, activation of coagulation and complement

Host responses following the injury of an implantation process can be followed by a sequence of events represented as blood-material interaction, provisional matrix formation, inflammation, foreign body response (FBR) and fibrous encapsulation [33]. However, a desired immune response can be established with an appropriate engineering of the implant surface in terms of composition and properties [34]. Indeed, wettability and charge of a biomaterial are highly influencing protein adsorption and subsequent cell adhesion. For instance, proteins tend to adsorb at higher ratios on positively charged surfaces when compared to negatively charged ones due to the strong Coulomb attractive forces [35]. In addition, certain hydrophilic surfaces allow less protein adsorption due to steric repulsion as a result of hydrophilic macromolecules immobilization like poly(ethylene oxide) (PEO) [36]. Subsequently, it is well documented that an activation of the coagulation cascade, complement system, fibrinolytic system, kinin-generating system and platelets take place after protein adsorption [37, 38].

The damages to tissue and blood vessels trigger activation of the intrinsic and extrinsic pathways of the coagulation cascade by initiators named as factor XII (FXII) and tissue factor (TF) that are causing platelet activation and fibrin polymerization, respectively [39, 40]. The TF is a cellular lipoprotein released from damaged cells or expressed in activated monocytes, granulocytes and endothelial cells. While, the contact activation (FXII) is an inducer for the intrinsic system on negatively charged substrates followed by generation of thrombin as a result of the downstream cascade of protein reactions [41]. However, contact activation of FXII is limited and cannot induce clot formation alone and thus it is not sufficient for the whole coagulation cascade [42]. Therefore, a combination of contact activation, platelet adhesion and activation as well as the presence of leukocytes is all together required for the biomaterial-associated blood coagulation [42, 43]. For instance, the platelets activate the co-factor V into co-factor Va while both the intrinsic and extrinsic coagulation pathways activate the factor X into FXa, which eventually allow the cleavage of prothrombin into thrombin. Thus, thrombin initiates fibrin formation, which will form at the end a stable fibrous mesh [44]. A provisional matrix around the implant is formed by the fibrin clot, which has major tasks to stop bleeding, to attract and activate blood platelets as well as to act as a reservoir of cytokines, chemokines, growth factors and other bioactive compounds.

Moreover, fibrin is a major component of the provisional matrix, which will aid in angiogenesis [45].

Furthermore, an activation of the complement system can be initiated with biomaterial contact if surfaces are rich in nucleophilic groups like hydroxyl and amino groups [46]. The complement systems acts either by involving leukocyte function of innate immunity or by direct lysis in destroying and removing the microorganisms and apoptotic cells [47]. It consists of nearly 30 tightly regulated proteins. Three biochemical pathways are involved in the complement system activation by the C3 convertase; the classical pathway (CP), the mannose-binding lectin (MBL) and the alternative pathway (AP) [23]. The C3a, C3b, C5a and the membrane attack complex C5b-9 products are formed from the C3 convertase, which is the most abundant complement protein in blood [46]. Mast cell degranulation, PMNs and monocyte recruitment, release of reactive oxygen and nitrogen species (ROS, RNS) as well as platelet adhesion are all triggered by the anaphylatoxins C3a and C5a [47]. However, the regulator of complement activation (RCA) proteins adjusts the complement activation by inhibiting the C3 and C5 convertase, which eventually prevent the release of anaphylatoxic peptides C3a and C5a in order to avoid possible damage to the host tissue [46, 48]. Moreover, the adsorbed protein layer on biomaterials is associated with the classical complement activation mainly via C1. For instance, IgG binds to C1q providing initiation of the C3 convertase, which will eventually initiate an onset of the inflammatory responses as well as the alternative complement pathway [39, 49].

The tight crosstalk among the extent of injury and nature of implant material (during the surgical procedure), the different activated systems, as well as the provisional matrix should be well orchestrated to limit the following inflammatory cascades. Therefore, an appropriate engineering of the surface composition and properties is highly essential to establish a desired immune response. For instance, surface wettability, charge, and surface topography influence greatly the inflammatory process [35].

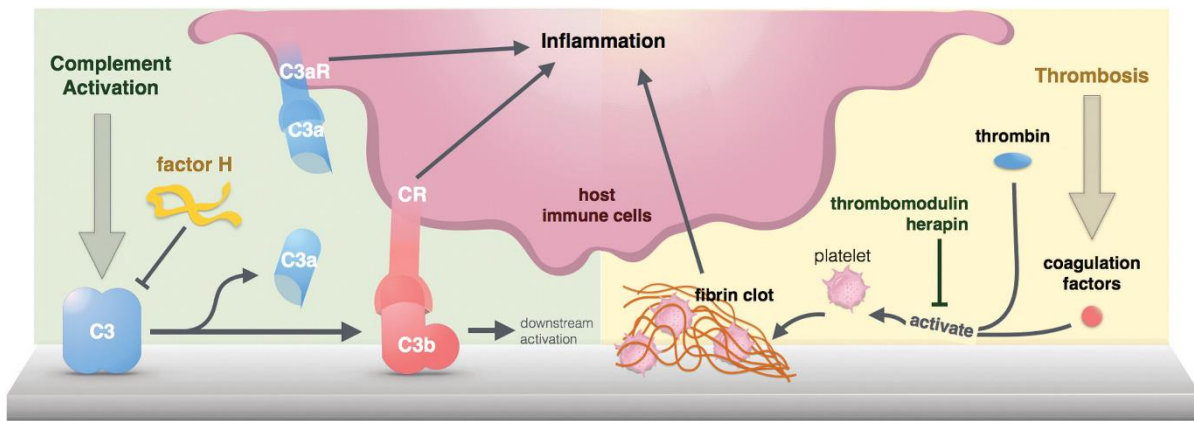


Figure 2: Schematic overview of the immune response toward biomaterials in terms of inducing the complement activation and thrombosis. An activation of the complement system C3aR to C3 convertase formation, which will further promote the inflammatory activation (**left**). The formation of fibrin clot is resulted by the binding of coagulation factors and activation of platelets (**right**). The figure is adopted from [50].

3.2. Macrophages as key players during acute and chronic inflammation

The initiation of inflammation is usually accompanied and orchestrated by immune cells that leave the circulation to the site of injury. Indeed, neutrophils reach the injury site within 24 h while the macrophages and lymphocytes reach there after 48 h. Other immune cells involved in the inflammation process are dendritic and mast cells [51]. In addition, non-immune cells such as epithelial, endothelial and fibroblast cells also contribute to the inflammatory processes [19]. The monocytes are signalled by chemo-attractants (such as complement factors C3a, C3b, C5a and C5b-9) to leave the bone marrow, to enter the bloodstream and finally to reach the target tissues. In addition, monocytes are precursors that undergo differentiation into macrophages [52]. Macrophages are essential components of the innate immune system performing a multitude of functions as effector cells in monitoring tissue damage as well as presence of pathogens by generating and resolving the inflammatory reaction. Moreover, macrophages play a role by shaping tissue architecture and development and clearing apoptotic cells, which means they are regenerating tissues through maintaining tissue homeostasis [53]. Pattern recognition receptors (PRRs) are macrophage-related and are able to recognize pathogen-associated molecular patterns (PAMPs; specialized molecular structures found on pathogens) and damage- or danger-associated molecular patterns (DAMPs; or alarmins, endogenous equivalent of PAMPs released

from cells at implant site). Thus, the PRR upregulate transcription of genes, which encode pro-inflammatory cytokine release and other inflammatory responses [15]. The alarm signals that are defined as alarmins include ATP, uric acid and heat shock proteins and are recognized by macrophages and other immune cells like dendritic cells (DCs). Transmembrane proteins such as Toll-like receptors (TLRs), C-type lectin receptors or cytoplasmic proteins such as Nod-like receptors (NLRs) are PRR related. In bacterial infection, phagocytosis take place by activation of several surface receptors such as scavenger receptors (SR) and mannose receptors (MR) [54]. Moreover, macrophages are able to alter their own phenotype through autocrine signalling and thus make them very heterogeneous in their functions and effects. Monocyte derived macrophages (M0) are classified as classically activated, wound healing and regulatory. They undergo endogenous stimuli released by either the innate or adaptive immunity. The natural killer (NK) cells and the interferon- γ (IFN γ) released by T-helper 1 (TH1) during innate and adaptive immunity respectively as well as the granulocyte macrophage colony-stimulating factor (GM-CSF) are priming monocyte differentiation into M1 macrophages [55, 56]. In addition, TNF- α or gram-negative bacterial endotoxin lipopolysaccharide (LPS) in combination with IFN γ induce also differentiation to classically-activated M1 phenotype [53, 57]. During the cell-mediated immune response, the pro-inflammatory M1 macrophages possess microbicidal and tumoricidal functions by releasing cytotoxic substances such as ROS like superoxide and hydroxyl radicals, as well as lysosomal content including elastase, hydrolases [58, 59]. In addition, the secretion of pro-inflammatory cytokines such as IL-1, IL-6, and TNF as well as IL-12 and IL-23 by classical macrophages play a role in host response [60, 61]. However, production of IL-1, IL-6, and IL-23 lead to recruitment of a subset of pro-inflammatory T helper cells named as TH17 cells that also related to regulatory T cells (Treg) formerly known as suppressor T cells. The recruitment of TH17 cells lead to release of IL-17 that contributes to polymorphous leukocyte recruitment, which eventually cause immunopathology like RA and IBD [60, 61]. Furthermore, IL-4 produced from basophils and mast cells in innate immunity or by T-helper 2 (TH2) cells in adaptive immunity allow transformation of monocytes and macrophages (M0) into the so-called wound-healing or M2 macrophages [55]. In addition, macrophage colony-stimulating factors (M-CSFs) act as a priming agent while IL-13 and IL-10 may also activate M2 phenotype [62]. Furthermore, the M2 macrophages are related to a resolution phase associated with repair, wound healing and tissue remodelling. They

express low levels of IL-12 and IL-23 and high levels of IL-10 (an anti-inflammatory cytokine), growth factors such as vascular endothelial growth factor (VEGF), TGF- β , fibroblast growth factor (FGF) and platelet-derived growth factor (PDGF) [23, 63]. In addition, the M2 macrophages have increased expression of SR, MR as well as galactose receptors [64]. Thereafter, the regulatory macrophages limit inflammation and dampen the immune response through IL-10 release [65]. It is well documented that the monocyte-derived macrophages are not terminally differentiated into M1 or M2, however the phenotype is highly dependent on the microenvironment signals [66, 67]. For instance, M1 macrophages resistant to TLR responses lead to a stop of pro-inflammatory cytokines release and achieve the ability to release anti-inflammatory IL-10 [67, 68]. While M2 macrophages upon exposure to IFN and LPS, can express cytokine phenotypes characteristic of M1 phenotype. Therefore, a protective feature, which allows healing and repair together with rapid response to a pathogen is represented by the complex remarkable state of macrophage plasticity, making macrophages an interesting target in the context of immunomodulation [69, 70]. At the site of inflammation, increased infiltration of monocytes and macrophages occurs through chemoattractants released by macrophages such as IL-8, GM-CSF, G-CSF, monocyte chemoattractant proteins (MCP-1-4), macrophage inhibitory protein (MIP-1 α and β). However, upon the resolution of inflammation, no further recruitment of cells as well as no more secretion of these chemokines are noticed [63].

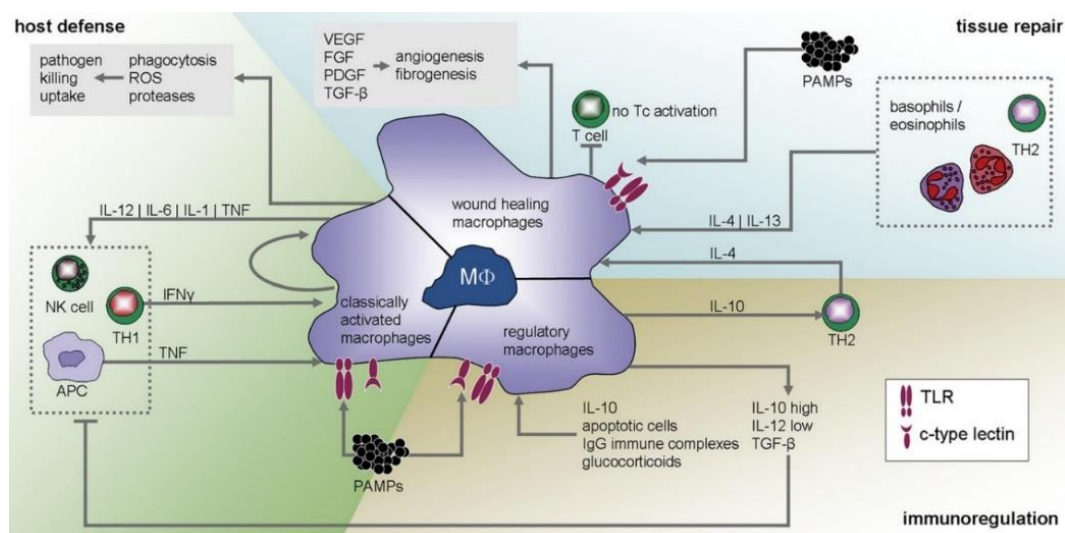


Figure 3: Macrophage classifications of different phenotypic profiles leading to different host response, wound healing, and immune regulation. The figure is adopted from [23].

3.3. The nuclear transcription factor NF- κ B signalling pathway

The nuclear transcription factor- κ B (NF- κ B) pathway, which was discovered in 1986 by David Baltimore [71], is considered to be essential in physiological processes. It is well documented that the development and regulation of the immune system, cell proliferation, cell death as well as inflammation are all regulated by the NF- κ B [72]. A wide variety of illnesses like auto immunity diseases, atherosclerosis, neurodegeneration, and cancer are also associated with NF- κ B pathway [73]. The structural homologous transcription factors related to this signalling pathway are named as NF- κ B1, NF- κ B2, RelA, RelB, and c-Rel, which are binding to κ B enhancers as homo- or hetero-dimers [74]. Furthermore, a Rel homology domain (RHD; responsible for dimerization, inhibitor binding, nuclear translocation and DNA-binding) is shared in all NF- κ B subunits. In contrast, C-terminal transactivation domain (TAD) (enable the binding of nuclear co-activators and subsequent positive regulation of gene expression) is only found in p65, RelB and c-Rel [75, 76]. Furthermore, a long, ankyrin repeat-containing domain (ARD) at their C terminus instead of the TAD domain are found in p50 (p105 precursor) and p52 (p100 precursor) and therefore cannot activate target gene expression as a homodimer [77]. A wide variety of signals induce the NF- κ B transcription factors, such as viral and microbial toxins, cytokines, ROS, exogenous peroxides, pathogens, injuries, immunoreceptors (TLP receptors, mainly TLR4 present in human monocytes and macrophages), antigen receptors, growth factor receptors, as well as physical, oxidative and genotoxic stress [78, 79]. Furthermore, there are two distinct pathways leading to NF- κ B activation, which are called canonical (classical) and non-canonical (alternative). The inhibitory proteins I κ Bs kinase (IKK) complex consists of NF- κ B essential modulator (NEMO), a scaffold sensing protein and catalytic kinase subunits of IKK α and/or IKK β [80]. The activation of I κ B kinase is considered the common regulatory step for both pathways. In details, the canonical pathway is activated by (IKK) β and utilizes the three canonical I κ B proteins I κ B α , I κ B β and I κ B ϵ while the non-canonical pathway is activated through IKK α , and utilizes the p52 precursor protein p100 [81]. In un-stimulated cells and by focusing on the canonical pathway, the inhibitory proteins I κ Bs sequester the NF- κ B proteins in the cytoplasm. However, activation of I κ Bs (IKK-mediated) and phosphorylation allow the degradation and translocation of I κ B to the nucleus as well as the activation of specific target gene expression [82]. Therefore, NF- κ B is considered a rapid acting (transient) and cyclical transcription factor in the presence of continual inducers [73, 80]. As an example, a

repeated degradation and re-synthesis of I κ B (activation and inactivation of NF- κ B) will cause nuclear NF- κ B DNA-binding activity to appear and disappear approximately every 30–60 min in mouse fibroblasts [80, 83]. In this thesis, LPS, potent microbial initiator of inflammation, which binds to LPS-binding protein (LBP) in serum and is recognized by CD14 was used [84]. Studies have shown that LPS is also recognized by TLRs (TLR4 and TLR2) and integrins CD11c and/or CD18, which activate different signalling pathways [84]. In this context, specifically important is the nuclear factor NF- κ B pathway that is responsible for pro-inflammatory gene expression. An illustration scheme of the activation and deactivation of the classical signalling pathway of NF- κ B is shown in **Figure 3**.

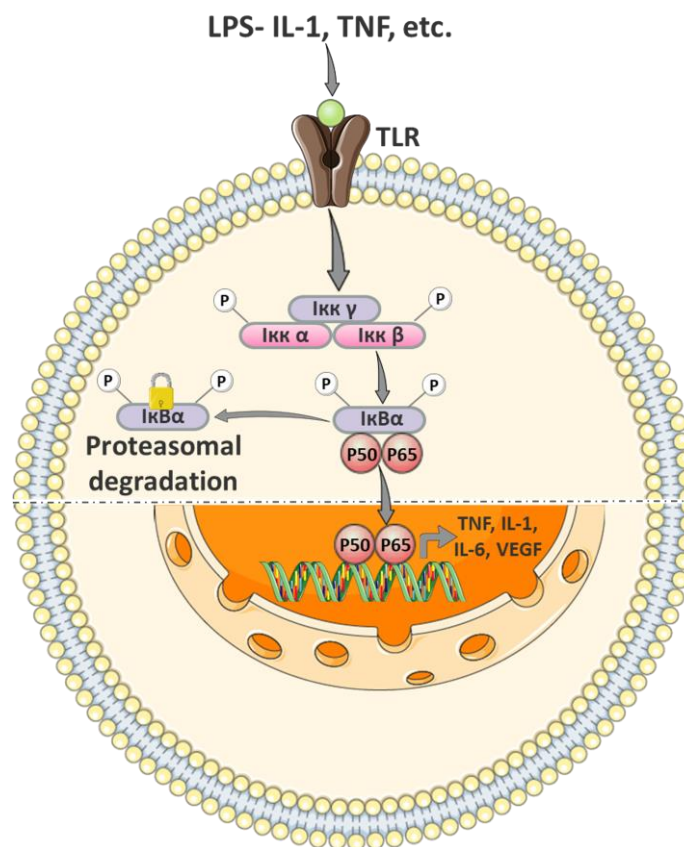


Figure 4: Illustration scheme of the canonical (classical) nuclear factor- κ B(NF- κ B) signalling pathway. A wide variety of signals activate the NF- κ B transcription factor like tumour necrosis factor (TNF), IL-1 and Toll-like receptor (TLR) ligands, such as lipopolysaccharide (LPS). The IKK kinase will phosphorylate the I κ B α protein leading to the dissociation of I κ B α with further proteasomal degradation. The activated subunits p50 and p65 will be translocated into the nucleus and will bind to specific sequences of DNA. Pro-inflammatory cytokines, chemokines and growth factors such as TNF, IL-1, IL-6 and vascular endothelial growth factor (VEGF) will be released.

3.4. Role of cytokines and metalloproteinases in inflammation

Cytokines are cell regulators acting at nano-to-pico molar concentrations playing an important role in many physiological responses of the cell and tissue activities during inflammation and FBR [85]. They also modulate haematopoiesis, neurogenesis, embryogenesis, and oncogenesis [85, 86]. Moreover, cytokines are defined as a diverse group of soluble proteins and peptides released by a wide variety of cells including B cells, mast cells, neutrophils, basophils and eosinophils. However, the predominant producers of cytokines are macrophages and T helper cells [87]. Monokines (produced from monocytes), lymphokines (produced from lymphocytes) and interleukins (produced from leukocytes) are synonyms of cytokines [88]. In addition, cytokines possess autocrine action on cells that secrete them, paracrine on nearby cells or endocrine on distant cells. They are acting either synergistically, antagonistically or redundantly (similar functions can be stimulated by different cytokines) [87, 88].

Cytokines are also classified as pro- or anti-inflammatory as well as pro- or anti-wound healing depending on the exerted effects [87]. Examples of cytokines with effects as pro-inflammatory and anti-wound healing are TNF- α , IL-6, IL-2 and IL-8 because of their collective ability in promoting inflammation [16, 89]. In contrast, interleukin 1 receptor antagonist (IL-1ra), TGF- β , IL-4 and IL-13 are examples of an anti-inflammatory and pro-wound healing that either inhibit cytokines release or suppress the cell receptor binding, which cause hindering of the inflammation cascade [89]. In addition, the cytokine family consists of two unique cytokines named as IL-1 β and IL-10 because they adapt the extremes of responses [63]. For instance, IL-10 is the most potent cytokine as it suppresses inflammatory and wound healing cells activation as well as pro-inflammatory cytokines production and thus is considered as anti-inflammatory and anti-wound healing [87]. Moreover, IL-1 β activates the monocytes, lymphocytes and fibroblast and therefore it is classified as pro-inflammatory and pro-wound healing cytokine. In addition, gram-negative bacterial endotoxins such as LPS trigger also the secretion of IL-1 β [89, 90]. The activity of IL-1 β is related to bacterial infection causing pathophysiology [90]. Nevertheless, IL-6 is classified as both pro- and anti-inflammatory cytokine. It is reported that IL-6 downregulates pro-inflammatory cytokines IL-1 and TNF- α by up-regulating IL-1ra and soluble TNF- α receptor respectively [91]. It also develops cell-specific and humoral immune responses by B cell and T cell proliferation and activation as well as immunoglobulin secretion in

chronic inflammation [92]. Besides, a new classification of cytokines in TH1 and TH2 subcategories was pointed out by Brodbeck et al. The TH1 represents TNF- α , IL-1 β and IL-8 while TH2 subgroup includes IL-6, IL-10 and IL-1ra [16]. Apart from cytokines, certain enzymes are also involved in inflammatory as well as tissue regeneration process. Especially important among the proteolytic enzymes is the class of matrix metalloproteinases (MMPs), which can be classified into different groups such as gelatinases (MMP-2,-9), matrilysins (MMP-7,-26), collagenases (MMP-1, -8, -13, -18) and stromelysins (MMP-3,-10) [93]. MMPs are secreted by adherent macrophages and foreign body giant cells (FBGCs) and their functionality involves decomposition of extracellular matrix (ECM) proteins, promotion of cell migration, growth, differentiation, fibrous capsule formation, angiogenesis and tissue remodelling [31, 63]. The MMPs are zinc-dependent protein and they are either anchored to the cell surface or secreted into the extracellular space [31, 94]. In addition, tissue inhibitors of metalloproteinases (TIMPs) lead to activity loss of the MMPs and may result in diseases such as arthritis, cancer, atherosclerosis, aneurysms, nephritis, tissue ulcers, and fibrosis [93, 94].

3.5. Foreign body giant cell formation and fibrosis on biomaterial implants

A persistent stage of inflammation upon biomaterial implantation is driving the activated macrophages to take cues from the microenvironment in attempt to resolve the foreign material [66]. Hence, the wide range of transient polarization states of macrophages play a significant role in the inflammation cascade and as a morphologic variant, they can coalesce into FBGCs [95, 96]. Moreover, multinucleated giant cell formation will be triggered when macrophages fail to engulf foreign material with a particle size between 10-100 μm [48]. In addition, cytokines as well as adhesion molecules are two main factors in FBGCs formation. The FBGCs are regarded as a hallmark of chronic inflammation and FBR [45, 97]. For instance, activated T lymphocytes at the implant site are assumed to be the source of IL-4 and IL-13, which induce macrophage fusion on biomaterial surfaces in vivo and in vitro [96, 98]. Moreover, collagen, fibronectin, laminin, fibrinogen, and vitronectin are a variety of proteins that also promote FBGC formation. It is reported that only vitronectin supports macrophage adhesion and fusion even all proteins support initial monocyte adhesion [99]. In addition, chemotaxis like the chemoattractant CCL2 guides macrophage to each other in attempt to form FBGCs [100]. Furthermore, fusogenic molecules

including MR CD44 [101], (CD206) [102], CD47 [103], dendritic cell-specific transmembrane protein (DC-STAMP) [104] and E-cadherin [105] are required for cell-cell fusion and allow fusion on the biomaterial [23, 106]. Literature pointed out that the surface physicochemical properties play a significant role in the fusion extent dictated by protein adsorption and integrin receptors [107]. For example, IgG and complement factors as well as $\beta 1$ and $\beta 2$ integrin receptors mediate macrophage adhesion and fusion [108, 109]. However, the $\beta 1$ and $\beta 2$ integrins have distinct roles. For instance, mediation of initial monocyte adhesion by interactions with a diversity of ligands including fragments of complement C3, fibrinogen, factor X, and high-molecular weight kininogen is accomplished by $\beta 2$ integrins [110]. While $\beta 1$ integrin is dominating in monocyte differentiation into macrophages and is strongly expressed in FBGCs [109, 111]. IL-4 and IL-13 cytokines are not only responsible for FBGCs formation but also for the activation of wound healing M2 phenotype, therefore FBGCs have an anti-inflammatory cytokine expression [112]. In addition, the pro-inflammatory effect of ROS, degradative enzymes and the secretion of pro-inflammatory chemokines is antagonized by the anti-inflammatory cytokines secreted by fused macrophage [113]. The release of enzymes like collagenase, elastase and proteinase, which aid with angiogenesis and tissue regeneration is also achieved by FBGCs [97]. Subsequently, IL-4 stimulates FBGCs release of FGF, transforming growth factor- $\beta 1$ (TGF- $\beta 1$), PDGF and VEGF, which eventually induce the fibroblast growth and differentiation into myofibroblast [114, 115]. In addition, not only the growth factors secreted by FBGCs but also the alternatively activated “M2” phenotype produce pro-fibrotic factors (PDGF and TGF- $\beta 1$), which stimulate fibroblasts proliferation and collagen synthesis [33, 116]. Hence, the fibrous encapsulation is considered the final stage of host response toward implanted biomaterials. This phase is represented by the dynamic interaction between macrophages and fibroblasts. The fibroblast cells will differentiate into myofibroblasts [117]. The latter enhances α -smooth muscle actin expression, wound healing promotion and scar formation [118]. Thereafter, an increased secretion of collagen and tissue contraction will further cause fibrosis and scarring [118, 119]. Thus, the formed fibrous capsules around the biomaterial will eventually lead to impaired functionality and longevity of drug delivery devices, various biosensors, tissue-engineering scaffolds as well as artificial organs [120, 121]. Therefore, implant modification, which is leading to reduced number of adherent macrophages, limited recruitment of additional immune cells as well as polarization of M2 phenotype during early host

response will mitigate an impaired implantation process [122]. An illustrative scheme of the host response of biomaterial implantation is shown in **Figure 5**.

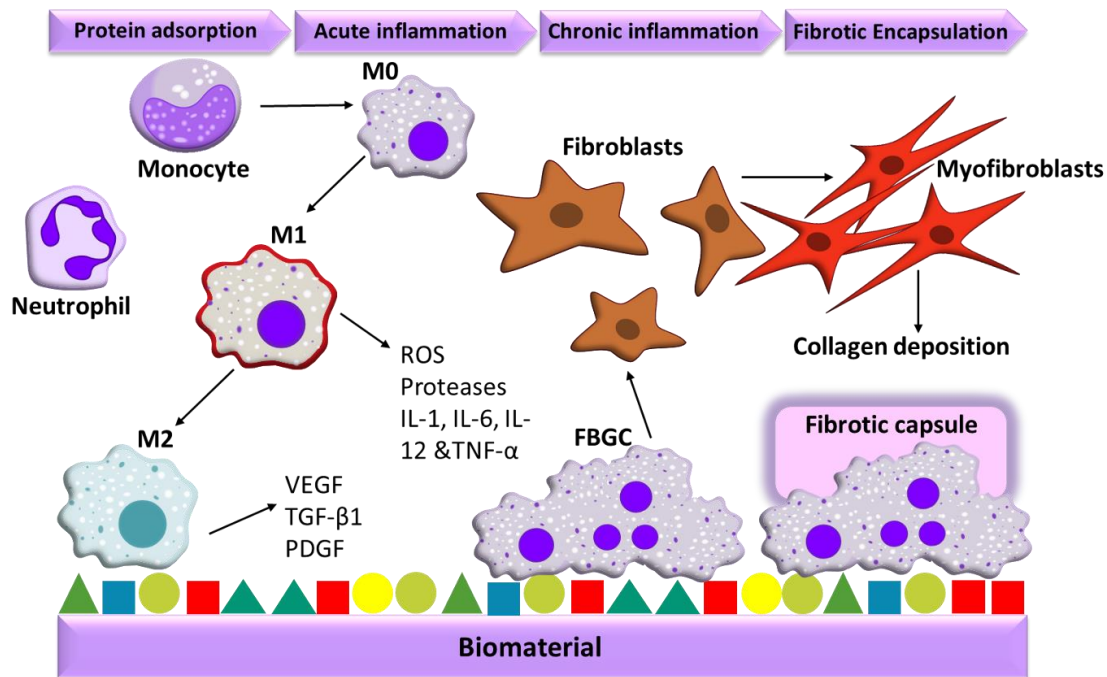


Figure 5: Host responses toward implanted biomaterials. First, immediate serum proteins adsorb (■, ●, ▲) on implanted biomaterial. Second, immune cells of neutrophils and monocytes are recruited to the implant site. “M1” phenotypic macrophages are differentiated from monocyte during acute inflammation while “M2” phenotype with pro-healing capacities is polarized during chronic inflammatory stage. The M2 macrophages fuse to form foreign body giant cells (FBGCs) in order to increase the phagocytic ability. Activated fibroblasts differentiate into myofibroblasts allowing collagen deposition. Eventually, failure of the implant is reached with the formed thick fibrotic capsule around the biomaterial.

4. Control of inflammation by non-steroidal anti-inflammatory drugs (NSAIDs) and glycosaminoglycans

4.1. Nanoparticle-based systems for drug delivery of NSAID and other anti-inflammatory drugs

NSAIDs belong to a wide range of chemical classes such as propionic acids (Naproxen, Ibuprofen), acetic acids (Indomethacin, Diclofenac) and enolic acids (Piroxicam), acetylated (Aspirin) and non-acetylated (sodium and magnesium salicylate) carboxylic acids. They are essential classes of medications for their anti-

inflammatory effects in the treatment of musculoskeletal sprains, RA, osteoarthritis beside their analgesic and anti-pyritic effects [123]. NSAIDs comprise a wide variety of inhibitory mechanisms including prevention of neutrophil chemotaxis and adhesion, inhibition of platelet aggregation, reduction in release of ROS and other lysosomal enzymes and most importantly and mainly the suppression effect on the COX enzymes by reducing prostaglandin production [124]. Focusing in particular on the Naproxen NSAID, which anti-inflammatory effects are due to the inhibition of COX-2 activity while the side effects are related to inhibiting of COX-1 including irritation of gastric mucosa and headaches. However, it is classified as a non-selective inhibitor of both COX isoforms, which greatly suppresses functions of leukocytes at the site of inflammation. In addition, Naproxen is used in diseases such as ankylosing spondylitis and RA [124]. Naproxen as well as most of other NSAIDs are considered weakly acidic, having a pK_a value between 3 and 5 [125]. Besides, it also has a hydrophobic nature making its encapsulation within a shell preferable for a sustained release and dissolution of drug as it allows low permeability of water [126]. Therefore, a new advancement in the biomaterial field was accomplished with the development of drug-encapsulated nanoparticles (NPs) that can be fabricated by natural or synthetic polymers. The outer shell can be prepared by organic materials like dextrans, poly(lactic-co-glycolic acid) (PLGA), poly-L-arginine, poly- ϵ -caprolactone (PCL) as well as poly (1-vinylimidazole) [127, 128]. Drug-encapsulated NPs have a multitude of advantages including controlled time-dependent release, co-loading of multiple drugs, tissue-targeted delivery, reduced toxicity and lower risk of enzymatic degradation [128, 129]. It can be also used in a wide variety of different applications as anti-cancer drug and gene delivery systems, etc. [128]. Furthermore, stimuli (temperature, ionic strength, pH as well as enzymatic activities)-responsive NPs were investigated in order to improve the efficacy in terms of drug release at the target site [130]. In addition, the diffusion and biodegradation of the outer polymer shell that forms further the NPs is playing an essential role in the release of the encapsulated drug. Moreover, NPs can be prepared of two biopolymers named as block copolymer or as gradient copolymer [131, 132]. The amphiphilic nature of a controlled gradient copolymer composition along the macromolecular chain tend to form micelles and allow high drug loading capacity. Suarez et al. prepared in their studies polymer drug conjugates using gradient copolymerization made of poly (1-vinylimidazole) hydrophilic shell, which is encapsulating different NSAIDs like Ibuprofen and Naproxen that form the hydrophobic

core region [133]. Indeed, the imidazole-based ligands are able to chelate metal ions like Zn^{2+} and thus inhibiting the MMP functionality [133]. The combined anti-inflammatory effects of 1-vinylimidazole and Naproxen gave importance for these NPs to be studied thoroughly for their anti-inflammatory effects when immobilized in multilayer system as biomaterial modification tool, which was analysed herein [134]. The structure of Naproxen encapsulated NPs is shown in the following **Figure 6**.

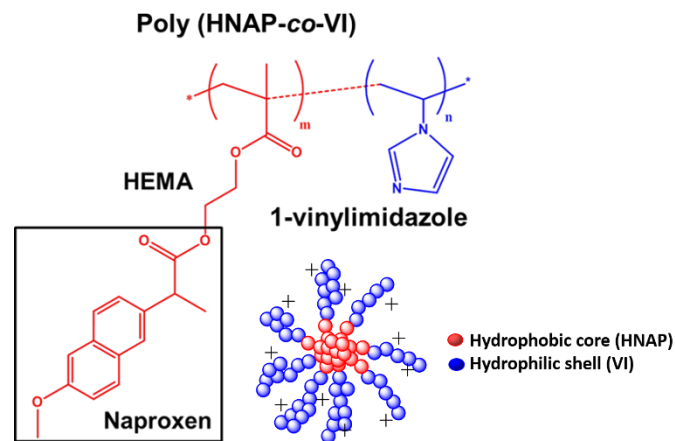


Figure 6: The chemical structure of the Naproxen-encapsulated nanoparticles. The synthesis of the hydroxyethyl methacrylate (HEMA) derivatives of naproxen were carried out through a carbodiimide mediated Steglich esterification reaction. The copolymer poly(HNAP-co-VI) was synthesized by free radical polymerization in solution combining HNAP and 1-vinylimidazol (VI). The Naproxen is located in the core while outer shell is made of 1-vinylimidazole.

4.2. Chemistry and biology of hyaluronan, heparin and chitosan

Hyaluronic acid (HA) is the only non-sulphated GAG. It is an anionic molecule due to the presence of carboxyl and hydroxyl groups in its backbone structure. HA is not covalently bound to a core protein to form proteoglycans [7]. It has a chemical structure consisting of repeating disaccharide units of D-glucuronic acid and N-acetyl-D glucosamine linked together via alternating β -1,4 and β -1,3 glycosidic bonds that form the linear polysaccharide [135, 136].

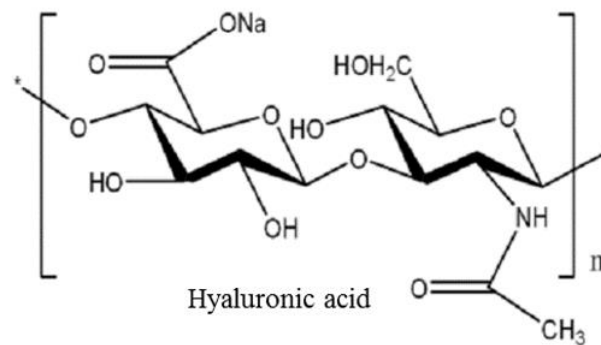


Figure 7: The chemical structure of hyaluronic acid (HA) consisting of D-glucuronic acid and D-N-acetyl glucosamine. Adopted from [137].

Notably, the equatorial side chains cause the formation of a polar and hydrophilic face while the axial hydrogen atoms of about eight CH groups form a non-polar and relatively hydrophobic face [138]. Hence, HA is anionic under acidic pH as it has a pK_a value of nearly 3.0. In addition, it has a molecular mass up to ~4 million Daltons and an average disaccharide length of ~1 nm [139]. Furthermore, HA is abundant in animals and bacteria and highly distributed throughout synovial fluid, vitreous humour and connective, epithelial and neural tissues of mammals like humans [140]. HA has many advantages, which allow its utilization as drug delivery vehicles; it is also biodegradable, biocompatible, non-toxic, and an important joint lubricant [141]. The consistency, biocompatibility and hydrophilicity of HA have made it an excellent moisturizer in cosmetic creams as well as to be used as dermal filler [140, 142]. In addition, HA in the ECM mostly is bound to hyaluronan-binding proteins (versican and aggrecan) [143]. Different size and amount of HA is found after injuries. High molecular weight (HMW)-HA can be degraded to low molecular form of HA through action of hyaluronidases, ROS as well as by mechanical forces. Both forms of HA will remain in the injured tissue until a resolution state of inflammation is accomplished. In addition, the size of HA plays a significant role towards inflammation. It is reported that the HMW-HA has anti-inflammatory properties while the low molecular weight (LMW)-HA has pro-inflammatory characteristics [144]. In contrast, other literature such as a work by Mizrahy et al. pointed out that LMW-HA oppose the ability to proliferate cells through its activation of the immune system and thus having anti-inflammatory effects [145, 146]. Furthermore, Zhou et al. explained the HA related effects with TLR in promoting and inhibiting the inflammation. It was reported that LMW-HA interacts with TLR-2 and TLR-4 (TLR-4 is activated PAMPs, like LPS) and thus activates the TLR signalling [33,

144]. Activation of the TLR will eventually lead to NF- κ B activation and thus translocation to the nucleus. It will also cause an increase of the pro-inflammatory cytokine release such as IL-1 β , TNF α , and IL-6, driving chemokine expression, inducing cleavage of CD44 and inhibit its cross-linking ability [144]. In contrast, the HMW-HA inhibits the TRL signalling through its binding to CD44 receptors mediated by low-affinity hydrogen bonds and thus suppressing the NF- κ B signalling pathway [33, 147]. HMW-HA prevents also cell growth and differentiation and increases expression of anti-inflammatory cytokines like IL-2, IL-10 and TGF- β . The binding of HMW-HA to CD44 receptors is of particular importance as it is considered a major cell surface glycoprotein expressed by many different cell types. It also interprets cues from the ECM into signals that affect growth, activation, survival and differentiation as well as plays a role in immune homeostasis, eliminate the LMW fragments of HA, and reduce phagocytosis by macrophage [148].

Heparin has the highest negative charge density among all known biomacromolecules due to the presence of a large number of negatively charged functional groups such as sulfate monoesters, sulfamido groups and carboxyl groups [149]. Its chemical structure is composed of alternating saccharide units of N-acetylated or N-sulfated D-glucosamine, that are α (1-4)- or β (1-4)-linked to uronic acids (L-iduronic or D-glucuronic acid) [150]. In particular, the main disaccharide of heparin is composed of iduronic acid, which is sulfated at the carbon 2 (IdoA2S) and N-sulfated glucosamine, which is additionally sulfated at C6 (GlcNS6S) [7]. The structure of Hep is illustrated in **Figure 8**.

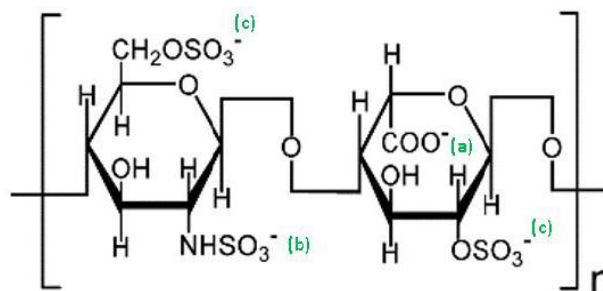


Figure 8: The chemical structure of disaccharide repeating unit of heparin consisting of 2-O-sulfated iduronic acid and 6-O-sulfated, N-sulfated glucosamine. The structure illustrates the L-iduronic acid (**left**) and the glucosamine (**right**). The negatively charged groups are (a) carboxyl, (b) sulfamido and (c) sulfate monoesters. Adopted from [150].

Moreover, heparin has a molecular weight of 5-25 KDa; at physiological pH both carboxyl and sulfate groups are ionized. The carboxylate group has a $pK_a \sim 3.3$ and the O-sulfo and N-sulfo have pK_a value between $\sim 1.0-1.5$ [151, 152]. Notably, heparin is a hydrophilic polymer holding $\sim 2-10\%$ water. The negative charge of heparin is maintained through a wide pH range, which makes the ionic interactions with a wide variety of ECM proteins, enzymes, cytokines and growth factors at physiological conditions possible. Heparin is released by mast cells due to external stimuli such as interaction of antigens with cell-surface bound IgE antibodies [153]. It has many therapeutic applications in the treatment of burns, ulcerative colitis, pulmonary disease, cancer, neurodegenerative diseases, and venous thrombosis [154]. Besides, the anti-coagulant property of heparin is an important feature. This effect is established through the binding of heparin to antithrombin III (ATIII) mediated pathways, which further inhibits the initial activation coagulation enzymes and thus prevents clot growth [152]. Moreover, literatures reported anti-inflammatory effects of heparin in its soluble form while less research was adduced toward the immobilized form. Reports showed that heparin suppresses the complement system, which is part of the initiation cascade of inflammation, inactivates chemokines and improves blood compatibility through its anticoagulant effects [154]. Heparin prevents also the activation and recruitment of inflammatory cells into tissue through inhibition of the selectin-mediated cell adhesion [155]. In details, heparin inhibits the binding of L-selectin and P-selectin (responsible of loose interaction between the endothelium and the neutrophils) to counter-ligands [156, 157]. Additionally, heparin inhibits leukocyte activation, migration and adhesion, making it a useful as anti-inflammatory agent [156]. In addition, it was reported to exert inhibitory effects on the canonical NF- κ B signalling pathway, which eventually downregulates gene expression of adhesion molecules as well as the pro-inflammatory cytokine release [158, 159]. Two different mechanisms of actions were addressed toward the NF- κ B pathway. One is based on the inhibition of the phosphorylation of NF- κ B from the cytoplasm into the nucleus through the electrostatic conjugation between the negatively charged Hep and the positively charged subunits p50-p65 of NF- κ B [159]. The second is based on the translocation of phosphorylated p65 into the nucleus. Here, the uptake of Hep molecules through endocytosis will block the binding of the translocated NF- κ B to the DNA [160].

Chitosan (Chi) is a bioactive polysaccharide of marine or fungi origin, which is composed of N-acetyl-D-glucosamine linked together by glycosidic β (1–4) bond [161,

162]. In addition, the linear biopolymer Chi has an amino group (C2) and 2 hydroxyl groups (C3 and C6) [161]. Chi is usually derived from alkaline deacetylation of chitin [163]. The viscosity of Chi is related to the molecular weight as well as the deacetylation degree (DD) of chitin, which is considered the most essential parameter in determining the properties as well as the applications of Chi [164]. For instance, the DD of Chi is usually between 60 to 95% however the ~85% DD is resulting in the presence of a large number of free amine groups. Conversely, some researches indicate that a DD of 50% is considered Chi [165].

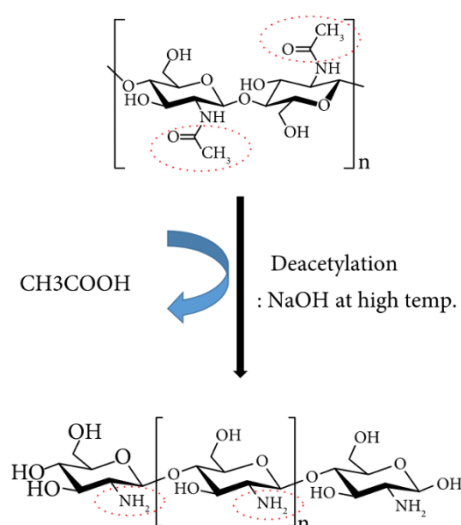


Figure 9: Schematic presentation of chitin deacetylation with alkaline. Adopted from [166].

Furthermore, the pK_a value of Chi is ranging between 6.46 and 7.32 and therefore the amino groups are protonated under acidic pH [167]. It is insoluble in water with pH above pK_a value as well as in alkaline solutions. In contrast, the polycationic character of Chi through amino groups protonation allow its dissolution in water and is also related to the interaction with wide variety of ions and molecules [168]. This eventually make Chi an attractive molecule in fabricating functional materials to be used in biomedical, pharmaceutical, tissue engineering, drug delivery and gene therapy applications [169]. Hence, Chi has many biological activities as antioxidant, antimicrobial, anticoagulant and anti-inflammatory [166]. Furthermore, Chi can be slowly degraded by chitosanases as well as lysozymes [163]. It is considered a biodegradable, bioresorbable, biocompatible and nontoxic molecule [170]. In addition, the three-dimensional structure of Chi can absorb and retain high amounts of water, allowing it to swell without the need to completely dissolve and thus behaving as a

hydrogel [165, 171]. Chi has an anti-bacterial activity on diverse type of microorganisms, including fungi, viruses and bacteria due to its cationic nature, which leads to its biocidal properties [172, 173]. In addition, the anti-inflammatory activity of high and low molecular weight (MW) Chi was test by Davydova et al. [174]. Indeed, Chi with MWs of both 115 kDa and 5.2 kDa have shown induction of anti-inflammatory IL-10 cytokine expression in animal blood and suppression of colitis progress. It was concluded that the MW has no influence on the anti-inflammatory activity of Chi [166, 174]. In addition, it is reported that the chitosan oligosaccharide (COS) has inhibitory effect toward the NF- κ B [175]. The diverse properties of Chi making it an attractive molecule, which was also extensively used in multilayers formation for biomedical applications [176, 177].

5. Different approaches towards anti-inflammatory surfaces

5.1. Brief survey on anti-inflammatory strategies of materials' modification

The adverse tissue-implant effects are reported as chronic inflammation and fibrotic encapsulation, which may eventually lead to implant failure. Therefore, several approaches were developed to obtain anti-inflammatory surfaces. Chemical and physical modifications, cell-based strategies, controlled release of anti-inflammatory agents as well as immunomodulatory strategies have been extensively studied to modulate the immune response. Examples of chemical and physical modifications are highly focused on surface geometry, topography, wettability, charge and surface chemistry as described earlier in section 3.1. In fact, tailoring surface properties of biomaterials provided beneficial outcomes [178]. For instance, different size, shape, and geometric alignment will lead to a significant influence toward many cell population in terms of adhesion, migration, arrangement and differentiation [179, 180]. Moreover, passivation of biomaterials by using non-biofouling coatings is another approach to minimize protein adsorption due to steric repulsion and hydration forces, which will lead to less activation of coagulation and complements, less immune globulins adsorption, less adhesive protein binding and hence less recruitment and adhesion of leukocytes at the implantation site [15, 181]. Examples of anti-fouling materials are poly(2-hydroxyethyl methacrylate) (pHEMA), poly(acrylamide) and polyethylene glycol (PEG) however PEG has proved to be most efficient [158]. Furthermore, Zhou et al. investigated different terminal methyl (CH₃), amine (NH₂), hydroxyl (OH) and carboxyl

(COOH) groups in an in vitro co-culture model of macrophage and fibroblast. The outcome of the study showed that the highest level of inflammatory reactions was found on the hydrophobic CH₃ surface, while the lowest was observed on hydrophilic/anionic COOH surface [182]. Another promising strategy is the incorporation of tissue-specific or stem cells into a scaffold or suitable hydrogel, which can be efficiently used in tissue regeneration. It is essential to know that a cross talk between embedded cells and immune cells (such as macrophages) will have an impact on the host response. For instance, macrophages interact with stem cells through paracrine or juxtacrine signalling [183]. In addition, mesenchymal stem cells (MSCs), for example, exerts an immunomodulatory effect when embedded in a PEG hydrogel and allow reduction of fibrotic responses in vivo [184]. Furthermore, the most effective biomolecular method is to naturally modulate the immune response by decorating biomaterials with endogenous molecules as was previously addressed by Kim et al. [15, 185]. In addition, biomolecules such as ECM proteins, complement and thrombotic inhibitors, growth factors as well as cytokines can be combined in attempt to reach synergistic effects [185]. Dexamethasone (DEX), alpha melanocyte-stimulating hormone (α -MSH), NSAIDs and superoxide dismutase are other pharmacological anti-inflammatory agents [15, 158].

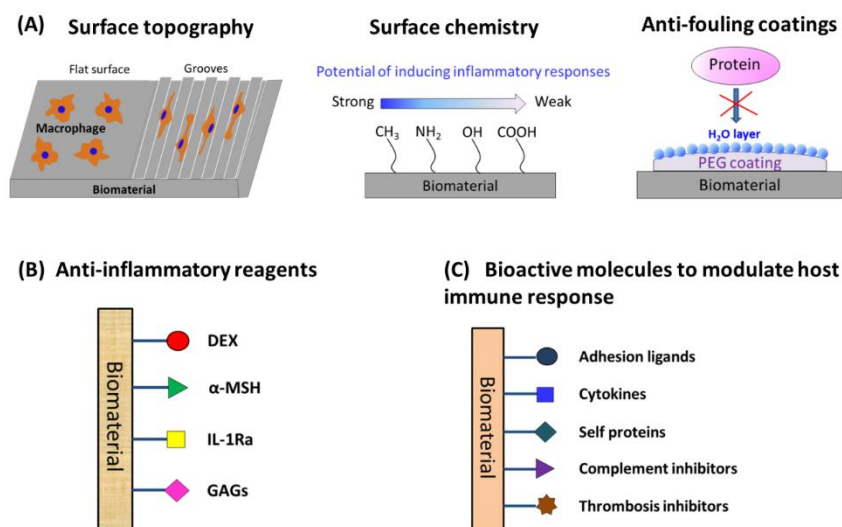


Figure 10: Schematic representation of different anti-inflammatory strategies. **(A)** Physical (surface topography), chemical and anti-fouling coatings (PEG- polyethylene glycol) modification. **(B)** Incorporation of anti-inflammatory agents (DEX- dexamethasone; α -MSH - alpha melanocyte-stimulating hormone; IL-1Ra - interleukin-1 receptor antagonists; GAGs- glycosaminoglycans). **(C)** Immunomodulation

approaches using bioactive molecules. All are examples of different methods that can alter the immune response. Adopted from [33].

6. Aim of the thesis

Although the attenuation of undesired effects of implants poses a challenge, studies were conducted to make biomaterials more biocompatible. Therefore, the aim of the thesis was to develop novel approaches of anti-inflammatory surface coatings based on immobilization of GAGs such as HA and Hep together with an extension involving Naproxen-conjugated NPs. Preclinical *in vivo* studies were also performed in terms of tissue responses of subcutaneous implants in mice. The anti-inflammatory properties of GAGs were studied based on their physicochemical properties in terms of wettability and surface charge as well as the potential mechanism of action toward the canonical signalling pathway of NF- κ B.

THP-1 derived macrophages were used, since macrophages play an essential role during the inflammation process. In all studies of this work, physicochemical characterizations were performed to examine the immobilization process of GAGs and resulting surface properties. In addition, different macrophage related inflammatory responses such as adhesion, fusion and pro-inflammatory cytokine (IL-1 β) release were the parameters in evaluating the anti-inflammatory properties of GAGs. Furthermore, immunofluorescence (IF) staining, immunoblotting, flow cytometry as well as confocal laser microscopy (CLSM) studying the uptake or association of GAGs by macrophages were performed to evaluate the mechanism of action of GAGs toward the NF- κ B signalling pathway. Moreover, the *in vivo* studies focused on histological analysis in terms of multinucleated giant cell formation, vascularization, expression of vasculogenic-related genes and expression of osteogenic genes. Overall, the different approaches of biomaterial coatings showed promising outcomes in achieving anti-inflammatory surface modifications. The results are reported herein.

References

1. Davis, J.R., *Handbook of Materials for Medical Devices*. 2003: ASM International.
 2. Ratner, B.D., et al., *Biomaterials science: a multidisciplinary endeavor*. 2004.
 3. Brand, R.A., M.A. Mont, and M. Manning, *Biographical Sketch: Themistocles Gluck (1853–1942)*. *Clinical Orthopaedics and Related Research®*, 2011. **469**(6): p. 1525-1527.
 4. Aquilina, O., *A brief history of cardiac pacing*. *Images in paediatric cardiology*, 2006. **8**(2): p. 17.
 5. Prakasam, M., et al., *Biodegradable materials and metallic implants—a review*. *Journal of functional biomaterials*, 2017. **8**(4): p. 44.
 6. Katti, D., et al., *Toxicity, biodegradation and elimination of polyanhydrides*. *Advanced drug delivery reviews*, 2002. **54**(7): p. 933-961.
 7. Köwitsch, A., G. Zhou, and T. Groth, *Medical application of glycosaminoglycans: a review*. *Journal of tissue engineering and regenerative medicine*, 2018. **12**(1): p. e23-e41.
 8. Sharkawi, T., et al., *Intravascular bioresorbable polymeric stents: a potential alternative to current drug eluting metal stents*. *Journal of Pharmaceutical Sciences*, 2007. **96**(11): p. 2829-2837.
 9. Nair, L.S. and C.T. Laurencin, *Biodegradable polymers as biomaterials*. *Progress in polymer science*, 2007. **32**(8-9): p. 762-798.
 10. Hollick, E.J., et al., *Biocompatibility of poly (methyl methacrylate), silicone, and AcrySof intraocular lenses: randomized comparison of the cellular reaction on the anterior lens surface*. *Journal of Cataract & Refractive Surgery*, 1998. **24**(3): p. 361-366.
 11. Hollick, E.J., et al., *The effect of polymethylmethacrylate, silicone, and polyacrylic intraocular lenses on posterior capsular opacification 3 years after cataract surgery*. *Ophthalmology*, 1999. **106**(1): p. 49-55.
 12. Wang, X., *Overview on biocompatibilities of implantable biomaterials*. 2013: INTECH Open Access Publisher.
 13. Gupta, A., T. Sakhivel, and S. Seal, *Recent development in 2D materials beyond graphene*. *Progress in Materials Science*, 2015. **73**(0): p. 44-126.
 14. Karger-Kocsis, J., H. Mahmood, and A. Pegoretti, *Recent advances in fiber/matrix interphase engineering for polymer composites*. *Progress in Materials Science*, 2015. **73**(0): p. 1-43.
 15. Vishwakarma, A., et al., *Engineering immunomodulatory biomaterials to tune the inflammatory response*. *Trends in biotechnology*, 2016. **34**(6): p. 470-482.
 16. Brodbeck, W., et al., *Biomaterial surface chemistry dictates adherent monocyte/macrophage cytokine expression in vitro*. *Cytokine*, 2002. **18**(6): p. 311-319.
 17. Williams, D.F., *On the mechanisms of biocompatibility*. *Biomaterials*, 2008. **29**(20): p. 2941-2953.
 18. Anderson, J.M., *Future challenges in the in vitro and in vivo evaluation of biomaterial biocompatibility*. *Regenerative biomaterials*, 2016. **3**(2): p. 73-77.
 19. Ahmed, A.U., *An overview of inflammation: mechanism and consequences*. *Frontiers in Biology*, 2011. **6**(4): p. 274.
 20. Hansson, G.K., et al., *Innate and adaptive immunity in the pathogenesis of atherosclerosis*. *Circulation research*, 2002. **91**(4): p. 281-291.
 21. Medzhitov, R., *Inflammation 2010: new adventures of an old flame*. *Cell*, 2010. **140**(6): p. 771-776.
-

22. Ferrero-Miliani, L., et al., *Chronic inflammation: importance of NOD2 and NALP3 in interleukin-1 β generation*. *Clinical & Experimental Immunology*, 2007. **147**(2): p. 227-235.
23. Franz, S., et al., *Immune responses to implants—a review of the implications for the design of immunomodulatory biomaterials*. *Biomaterials*, 2011. **32**(28): p. 6692-6709.
24. Tang, L., T.A. Jennings, and J.W. Eaton, *Mast cells mediate acute inflammatory responses to implanted biomaterials*. *Proceedings of the National Academy of Sciences*, 1998. **95**(15): p. 8841-8846.
25. Zdolsek, J., J.W. Eaton, and L. Tang, *Histamine release and fibrinogen adsorption mediate acute inflammatory responses to biomaterial implants in humans*. *Journal of translational medicine*, 2007. **5**(1): p. 31.
26. Murthy, T., et al., *Biological response modifiers*. *Int J Pharm Tech Res*, 2010. **2**: p. 2152-2160.
27. Chomarat, P. and J. Banchereau, *Interleukin-4 and Interleukin-13: Their similarities and discrepancies*. *International reviews of immunology*, 1998. **17**(1-4): p. 1-52.
28. Serhan, C.N. and J. Savill, *Resolution of inflammation: the beginning programs the end*. *Nature immunology*, 2005. **6**(12): p. 1191-1197.
29. Majno, G. and I. Joris, *Cells, tissues, and disease: principles of general pathology*. 2004: Oxford University Press.
30. Ward, P.A., *Acute and chronic inflammation*. *Fundamentals of inflammation*, 2010: p. 1-16.
31. Lee, I.-T. and C.-M. Yang, *Inflammatory signalings involved in airway and pulmonary diseases*. *Mediators of inflammation*, 2013. **2013**.
32. Parham, P., *The immune system*. 2014: Garland Science.
33. Zhou, G. and T. Groth, *Host Responses to Biomaterials and Anti-Inflammatory Design—a Brief Review*. *Macromol Biosci*, 2018. **18**(8): p. e1800112.
34. Williams, D.F., *The Williams Dictionary of Biomaterials*. 1999: Liverpool University Press.
35. Wilson, C.J., et al., *Mediation of biomaterial-cell interactions by adsorbed proteins: a review*. *Tissue engineering*, 2005. **11**(1-2): p. 1-18.
36. Amiji, M. and K. Park, *Surface Modification of Polymeric Biomaterials with Poly (ethylene oxide) A Steric Repulsion Approach*. 1994, ACS Publications.
37. Markiewski, M.M., et al., *Complement and coagulation: strangers or partners in crime?* *Trends Immunol*, 2007. **28**(4): p. 184-92.
38. Jenney, C.R. and J.M. Anderson, *Adsorbed IgG: a potent adhesive substrate for human macrophages*. *Journal of Biomedical Materials Research: An Official Journal of The Society for Biomaterials, The Japanese Society for Biomaterials, and The Australian Society for Biomaterials and the Korean Society for Biomaterials*, 2000. **50**(3): p. 281-290.
39. Gorbet, M.B. and M.V. Sefton, *Biomaterial-associated thrombosis: roles of coagulation factors, complement, platelets and leukocytes*. *Biomaterials*, 2004. **25**(26): p. 5681-5703.
40. Zhuo, R., C.A. Siedlecki, and E.A. Vogler, *Autoactivation of blood factor XII at hydrophilic and hydrophobic surfaces*. *Biomaterials*, 2006. **27**(24): p. 4325-4332.
41. Schmaier, A.H., *Contact activation: a revision*. *Thrombosis and haemostasis*, 1997. **78**(01): p. 101-107.
42. Sperling, C., et al., *Blood coagulation on biomaterials requires the combination of distinct activation processes*. *Biomaterials*, 2009. **30**(27): p. 4447-4456.

43. Fischer, M., C. Sperling, and C. Werner, *Synergistic effect of hydrophobic and anionic surface groups triggers blood coagulation in vitro*. Journal of Materials Science: Materials in Medicine, 2010. **21**(3): p. 931-937.
44. Heemskerk, J.W., E.M. Bevers, and T. Lindhout, *Platelet activation and blood coagulation*. THROMBOSIS AND HAEMOSTASIS-STUTTGART-, 2002. **88**(2): p. 186-194.
45. Anderson, J.M., *Biological responses to materials*. Annual review of materials research, 2001. **31**(1): p. 81-110.
46. Nilsson, B., et al., *The role of complement in biomaterial-induced inflammation*. Molecular immunology, 2007. **44**(1): p. 82-94.
47. Sarma, J.V. and P.A. Ward, *The complement system*. Cell and tissue research, 2011. **343**(1): p. 227-235.
48. Xia, Z. and J.T. Triffitt, *A review on macrophage responses to biomaterials*. Biomedical Materials, 2006. **1**(1): p. R1.
49. Tengvall, P., A. Askendal, and I. Lundström, *Ellipsometric in vitro studies on the activation of complement by human immunoglobulins M and G after adsorption to methylated silicon*. Colloids and Surfaces B: Biointerfaces, 2001. **20**(1): p. 51-62.
50. Kim, Y.K., E.Y. Chen, and W.F. Liu, *Biomolecular strategies to modulate the macrophage response to implanted materials*. J. Mater. Chem. B, 2016. **4**(9): p. 1600-1609.
51. Akira, S., S. Uematsu, and O. Takeuchi, *Pathogen recognition and innate immunity*. Cell, 2006. **124**(4): p. 783-801.
52. Sheikh, Z., et al., *Macrophages, foreign body giant cells and their response to implantable biomaterials*. Materials, 2015. **8**(9): p. 5671-5701.
53. Italiani, P. and D. Boraschi, *From monocytes to M1/M2 macrophages: phenotypical vs. functional differentiation*. Frontiers in immunology, 2014. **5**: p. 514.
54. Muñoz Carrillo, J.L., et al., *Physiology and pathology of innate immune response against pathogens*. 2017.
55. Duffield, J.S., *The inflammatory macrophage: a story of Jekyll and Hyde*. Clinical Science, 2003. **104**(1): p. 27-38.
56. Mackaness, G., *Cellular immunity and the parasite*, in *Immunity to Blood Parasites of Animals and Man*. 1977, Springer. p. 65-73.
57. O'Shea, J.J. and P.J. Murray, *Cytokine signaling modules in inflammatory responses*. Immunity, 2008. **28**(4): p. 477-487.
58. Schorlemmer, H., et al., *The selective release of lysosomal acid hydrolases from mouse peritoneal macrophages by stimuli of chronic inflammation*. British journal of experimental pathology, 1977. **58**(3): p. 315.
59. Rajagopalan, S., et al., *Reactive oxygen species produced by macrophage-derived foam cells regulate the activity of vascular matrix metalloproteinases in vitro. Implications for atherosclerotic plaque stability*. The Journal of clinical investigation, 1996. **98**(11): p. 2572-2579.
60. Langrish, C.L., et al., *IL-23 drives a pathogenic T cell population that induces autoimmune inflammation*. The Journal of experimental medicine, 2005. **201**(2): p. 233-240.
61. Bettelli, E., et al., *Reciprocal developmental pathways for the generation of pathogenic effector TH 17 and regulatory T cells*. Nature, 2006. **441**(7090): p. 235-238.
62. Vogel, D.Y., et al., *Human macrophage polarization in vitro: maturation and activation methods compared*. Immunobiology, 2014. **219**(9): p. 695-703.

63. Anderson, J.M., *In vitro and in vivo monocyte, macrophage, foreign body giant cell, and lymphocyte interactions with biomaterials*, in *Biological interactions on materials surfaces*. 2009, Springer. p. 225-244.
 64. Brown, B.N. and S.F. Badylak, *Expanded applications, shifting paradigms and an improved understanding of host–biomaterial interactions*. *Acta biomaterialia*, 2013. **9**(2): p. 4948-4955.
 65. Mosser, D.M., *The many faces of macrophage activation*. *Journal of Leukocyte Biology*, 2003. **73**(2): p. 209-212.
 66. Davies, L.C., et al., *Tissue-resident macrophages*. *Nature immunology*, 2013. **14**(10): p. 986.
 67. Bertrand, J.Y., et al., *Three pathways to mature macrophages in the early mouse yolk sac*. *Blood*, 2005. **106**(9): p. 3004-3011.
 68. Orkin, S.H. and L.I. Zon, *Hematopoiesis: an evolving paradigm for stem cell biology*. *Cell*, 2008. **132**(4): p. 631-644.
 69. Stout, R.D., et al., *Macrophages sequentially change their functional phenotype in response to changes in microenvironmental influences*. *The Journal of Immunology*, 2005. **175**(1): p. 342-349.
 70. Franz, S., et al., *Clearance of apo Nph induces an immunosuppressive response in pro-inflammatory type-1 and anti-inflammatory type-2 MΦ: Brief Definite Report*. *Autoimmunity*, 2009. **42**(4): p. 275-277.
 71. Baltimore, D., *Discovering NF-κB*. *Cold Spring Harbor perspectives in biology*, 2009. **1**(1): p. a000026.
 72. Hayden, M., Ghosh S. *Signaling to NF-κB*. *Genes Dev*, 2004. **18**: p. 2195-2224.
 73. Christian, F., E.L. Smith, and R.J. Carmody, *The regulation of NF-κB subunits by phosphorylation*. *Cells*, 2016. **5**(1): p. 12.
 74. Sun, S.C., *The noncanonical NF-κB pathway*. *Immunological reviews*, 2012. **246**(1): p. 125-140.
 75. Wan, F. and M.J. Lenardo, *Specification of DNA binding activity of NF-κB proteins*. *Cold Spring Harbor perspectives in biology*, 2009. **1**(4): p. a000067.
 76. Hayden, M.S. and S. Ghosh, *Shared principles in NF-κB signaling*. *Cell*, 2008. **132**(3): p. 344-362.
 77. Napetschnig, J. and H. Wu, *Molecular basis of NF-κB signaling*. *Annual review of biophysics*, 2013. **42**: p. 443-468.
 78. Oeckinghaus, A. and S. Ghosh, *The NF-κB family of transcription factors and its regulation*. *Cold Spring Harbor perspectives in biology*, 2009. **1**(4): p. a000034.
 79. Lawrence, T., *The nuclear factor NF-kappaB pathway in inflammation*. *Cold Spring Harb Perspect Biol*, 2009. **1**(6): p. a001651.
 80. Gilmore, T.D., *Introduction to NF-κ B: players, pathways, perspectives*. *Oncogene*, 2006. **25**(51): p. 6680-6684.
 81. Hoffmann, A., G. Natoli, and G. Ghosh, *Transcriptional regulation via the NF-κ B signaling module*. *Oncogene*, 2006. **25**(51): p. 6706-6716.
 82. Hayden, M.S. and S. Ghosh, *Signaling to NF-κB*. *Genes & development*, 2004. **18**(18): p. 2195-2224.
 83. Hoffmann, A. and D. Baltimore, *Circuitry of nuclear factor κB signaling*. *Immunological reviews*, 2006. **210**(1): p. 171-186.
 84. Triantafilou, M. and K. Triantafilou, *Lipopolysaccharide recognition: CD14, TLRs and the LPS-activation cluster*. *Trends in immunology*, 2002. **23**(6): p. 301-304.
 85. Balkwill, F. and F. Burke, *The cytokine network*. *Immunology today*, 1989. **10**(9): p. 299-304.
-

86. Stenvinkel, P., et al., *IL-10, IL-6, and TNF- α : central factors in the altered cytokine network of uremia—the good, the bad, and the ugly*. *Kidney international*, 2005. **67**(4): p. 1216-1233.
 87. Zhang, J.-M. and J. An, *Cytokines, inflammation and pain*. *International anesthesiology clinics*, 2007. **45**(2): p. 27.
 88. Nathan, C. and M. Sporn, *Cytokines in context*. *The Journal of cell biology*, 1991. **113**(5): p. 981-986.
 89. Brodbeck, W.G., et al., *In vivo leukocyte cytokine mRNA responses to biomaterials are dependent on surface chemistry*. *Journal of Biomedical Materials Research Part A: An Official Journal of The Society for Biomaterials, The Japanese Society for Biomaterials, and The Australian Society for Biomaterials and the Korean Society for Biomaterials*, 2003. **64**(2): p. 320-329.
 90. Morrison, D.C. and J.L. Ryan, *Endotoxins and disease mechanisms*. *Annual review of medicine*, 1987. **38**(1): p. 417-432.
 91. Xing, Z., et al., *IL-6 is an antiinflammatory cytokine required for controlling local or systemic acute inflammatory responses*. *The Journal of clinical investigation*, 1998. **101**(2): p. 311-320.
 92. Feghali, C.A. and T.M. Wright, *Cytokines in acute and chronic inflammation*. *Front Biosci*, 1997. **2**(1): p. d12-d26.
 93. Visse, R. and H. Nagase, *Matrix metalloproteinases and tissue inhibitors of metalloproteinases: structure, function, and biochemistry*. *Circulation research*, 2003. **92**(8): p. 827-839.
 94. Kulinsky, V., *Biochemical aspects of inflammation*. *Biochemistry (Moscow)*, 2007. **72**(6): p. 595-607.
 95. Anderson, J.M., *Multinucleated giant cells*. *Current opinion in hematology*, 2000. **7**(1): p. 40-47.
 96. Brodbeck, W.G., et al., *Lymphocytes and the foreign body response: lymphocyte enhancement of macrophage adhesion and fusion*. *Journal of Biomedical Materials Research Part A: An Official Journal of The Society for Biomaterials, The Japanese Society for Biomaterials, and The Australian Society for Biomaterials and the Korean Society for Biomaterials*, 2005. **74**(2): p. 222-229.
 97. McNally, A.K. and J.M. Anderson, *Macrophage fusion and multinucleated giant cells of inflammation*. *Adv Exp Med Biol*, 2011. **713**: p. 97-111.
 98. DeFife, K.M., et al., *Interleukin-13 induces human monocyte/macrophage fusion and macrophage mannose receptor expression*. *The Journal of Immunology*, 1997. **158**(7): p. 3385-3390.
 99. McNally, A.K., et al., *Vitronectin is a critical protein adhesion substrate for IL-4-induced foreign body giant cell formation*. *Journal of Biomedical Materials Research Part A: An Official Journal of The Society for Biomaterials, The Japanese Society for Biomaterials, and The Australian Society for Biomaterials and the Korean Society for Biomaterials*, 2008. **86**(2): p. 535-543.
 100. Kyriakides, T.R., et al., *The CC chemokine ligand, CCL2/MCP1, participates in macrophage fusion and foreign body giant cell formation*. *The American journal of pathology*, 2004. **165**(6): p. 2157-2166.
 101. Cui, W., et al., *The intracellular domain of CD44 promotes the fusion of macrophages*. *Blood*, 2006. **107**(2): p. 796-805.
 102. McNally, A.K., K.M. DeFife, and J.M. Anderson, *Interleukin-4-induced macrophage fusion is prevented by inhibitors of mannose receptor activity*. *The American journal of pathology*, 1996. **149**(3): p. 975.
-

103. Han, X., et al., *CD47, a ligand for the macrophage fusion receptor, participates in macrophage multinucleation*. Journal of Biological Chemistry, 2000. **275**(48): p. 37984-37992.
 104. Yagi, M., et al., *DC-STAMP is essential for cell–cell fusion in osteoclasts and foreign body giant cells*. The Journal of experimental medicine, 2005. **202**(3): p. 345-351.
 105. Moreno, J.L., et al., *IL-4 promotes the formation of multinucleated giant cells from macrophage precursors by a STAT6-dependent, homotypic mechanism: contribution of E-cadherin*. Journal of leukocyte biology, 2007. **82**(6): p. 1542-1553.
 106. Helming, L. and S. Gordon, *Molecular mediators of macrophage fusion*. Trends in cell biology, 2009. **19**(10): p. 514-522.
 107. Dadsetan, M., et al., *Surface chemistry mediates adhesive structure, cytoskeletal organization, and fusion of macrophages*. Journal of Biomedical Materials Research Part A: An Official Journal of The Society for Biomaterials, The Japanese Society for Biomaterials, and The Australian Society for Biomaterials and the Korean Society for Biomaterials, 2004. **71**(3): p. 439-448.
 108. Collier, T.O., et al., *Surface chemistry control of monocyte and macrophage adhesion, morphology, and fusion*. Journal of Biomedical Materials Research: An Official Journal of The Society for Biomaterials, The Japanese Society for Biomaterials, and The Australian Society for Biomaterials and the Korean Society for Biomaterials, 2000. **49**(1): p. 141-145.
 109. McNally, A.K. and J.M. Anderson, *$\beta 1$ and $\beta 2$ integrins mediate adhesion during macrophage fusion and multinucleated foreign body giant cell formation*. The American journal of pathology, 2002. **160**(2): p. 621-630.
 110. Berton, G. and C.A. Lowell, *Integrin signalling in neutrophils and macrophages*. Cellular signalling, 1999. **11**(9): p. 621-635.
 111. McNally, A.K., S.R. MacEwan, and J.M. Anderson, *α subunit partners to $\beta 1$ and $\beta 2$ integrins during IL-4-induced foreign body giant cell formation*. Journal of Biomedical Materials Research Part A: An Official Journal of The Society for Biomaterials, The Japanese Society for Biomaterials, and The Australian Society for Biomaterials and the Korean Society for Biomaterials, 2007. **82**(3): p. 568-574.
 112. Helming, L. and S. Gordon, *The molecular basis of macrophage fusion*. Immunobiology, 2008. **212**(9-10): p. 785-793.
 113. Anderson, J.M., A. Rodriguez, and D.T. Chang, *Foreign body reaction to biomaterials*. Seminars in Immunology, 2008. **20**(2): p. 86-100.
 114. Wynn, T.A. and L. Barron, *Macrophages: master regulators of inflammation and fibrosis*. Semin Liver Dis, 2010. **30**(3): p. 245-57.
 115. Ward, W.K., *A review of the foreign-body response to subcutaneously-implanted devices: the role of macrophages and cytokines in biofouling and fibrosis*. 2008, SAGE Publications.
 116. Mantovani, A., et al., *Macrophage polarization: tumor-associated macrophages as a paradigm for polarized M2 mononuclear phagocytes*. Trends in immunology, 2002. **23**(11): p. 549-555.
 117. Barron, L. and T.A. Wynn, *Fibrosis is regulated by Th2 and Th17 responses and by dynamic interactions between fibroblasts and macrophages*. American Journal of Physiology-Gastrointestinal and Liver Physiology, 2011. **300**(5): p. G723.
-

-
118. Serini, G., et al., *The fibronectin domain ED-A is crucial for myofibroblastic phenotype induction by transforming growth factor- β 1*. *The Journal of cell biology*, 1998. **142**(3): p. 873-881.
 119. Mutsaers, S.E., et al., *Mechanisms of tissue repair: from wound healing to fibrosis*. *The international journal of biochemistry & cell biology*, 1997. **29**(1): p. 5-17.
 120. Williams, D., *Tissue-biomaterial interactions*. *Journal of Materials science*, 1987. **22**(10): p. 3421-3445.
 121. Drury, J.L. and D.J. Mooney, *Hydrogels for tissue engineering: scaffold design variables and applications*. *Biomaterials*, 2003. **24**(24): p. 4337-4351.
 122. Hachim, D., et al., *Shifts in macrophage phenotype at the biomaterial interface via IL-4 eluting coatings are associated with improved implant integration*. *Biomaterials*, 2017. **112**: p. 95-107.
 123. Abukhalaf, I.K., et al., *Nonsteroidal Anti-inflammatory Drugs, Disease-Modifying Antirheumatic Drugs, and Agents Used in Gout*, in *Handbook of Drug Interactions*. 2012, Springer. p. 415-475.
 124. Suleyman, H., B. Demircan, and Y. Karagoz, *Anti-inflammatory and side effects of cyclo-oxygenase inhibitors*. *Pharmacological reports*, 2007. **59**(3): p. 247.
 125. Brooks, P.M. and R.O. Day, *Nonsteroidal antiinflammatory drugs—differences and similarities*. *New England Journal of Medicine*, 1991. **324**(24): p. 1716-1725.
 126. Mello, V.A.d. and E. Ricci-Júnior, *Encapsulation of naproxen in nanostructured system: structural characterization and in vitro release studies*. *Quimica Nova*, 2011. **34**(6): p. 933-939.
 127. Iqbal, P., J.A. Preece, and P.M. Mendes, *Nanotechnology: The “Top-Down” and “Bottom-Up” Approaches*. *Supramolecular chemistry: from molecules to nanomaterials*, 2012.
 128. Shah, N.J., et al., *Engineering Layer-by-Layer Thin Films for Multiscale and Multidrug Delivery Applications*. *Layer-by-Layer Films for Biomedical Applications*, 2015.
 129. Sharma, A., S.V. Madhunapantula, and G.P. Robertson, *Toxicological considerations when creating nanoparticle-based drugs and drug delivery systems*. *Expert opinion on drug metabolism & toxicology*, 2012. **8**(1): p. 47-69.
 130. Gao, W., J.M. Chan, and O.C. Farokhzad, *pH-responsive nanoparticles for drug delivery*. *Molecular pharmaceutics*, 2010. **7**(6): p. 1913-1920.
 131. Kim, B.-S., et al., *Hydrogen-bonded multilayer of pH-responsive polymeric micelles with tannic acid for surface drug delivery*. *Chemical communications*, 2009(28): p. 4194-4196.
 132. Nguyen, P.M., et al., *Extended release antibacterial layer-by-layer films incorporating linear-dendritic block copolymer micelles*. *Chemistry of Materials*, 2007. **19**(23): p. 5524-5530.
 133. Suarez, P., et al., *Self-assembling gradient copolymers of vinylimidazol and (acrylic)ibuprofen with anti-inflammatory and zinc chelating properties*. *Macromol Biosci*, 2013. **13**(9): p. 1174-84.
 134. Al-Khoury, H., et al., *Anti-inflammatory Surface Coatings Based on Polyelectrolyte Multilayers of Heparin and Polycationic Nanoparticles of Naproxen-Bearing Polymeric Drugs*. *Biomacromolecules*, 2019.
 135. Laurent, T.C., *Biochemistry of hyaluronan*. *Acta Oto-Laryngologica*, 1987. **104**(S442): p. 7-24.
 136. Garg, H.G. and C.A. Hales, *Chemistry and biology of hyaluronan*. 2004: Elsevier.
-

137. Bhattacharya, D., et al., *Impact of structurally modifying hyaluronic acid on CD44 interaction*. Journal of Materials Chemistry B, 2017. **5**(41): p. 8183-8192.
138. Köwitsch, A., et al., *Bioactivity of immobilized hyaluronic acid derivatives regarding protein adsorption and cell adhesion*. Biotechnology and applied biochemistry, 2011. **58**(5): p. 376-389.
139. Brown, M. and S.A. Jones, *Hyaluronic acid: a unique topical vehicle for the localized delivery of drugs to the skin*. Journal of the European Academy of Dermatology and Venereology, 2005. **19**(3): p. 308-318.
140. Necas, J., et al., *Hyaluronic acid (hyaluronan): a review*. Veterinarni medicina, 2008. **53**(8): p. 397-411.
141. Gotoh, S., et al., *Effects of the molecular weight of hyaluronic acid and its action mechanisms on experimental joint pain in rats*. Annals of the rheumatic diseases, 1993. **52**(11): p. 817-822.
142. Fakhari, A. and C. Berklund, *Applications and emerging trends of hyaluronic acid in tissue engineering, as a dermal filler and in osteoarthritis treatment*. Acta biomaterialia, 2013. **9**(7): p. 7081-7092.
143. Cataldi, A. and V. di Giacomo, *Extracellular Matrix: Immunity and Inflammation*, in *Extracellular Matrix for Tissue Engineering and Biomaterials*. 2018, Springer. p. 83-109.
144. Ruppert, S.M., et al., *Tissue integrity signals communicated by high-molecular weight hyaluronan and the resolution of inflammation*. Immunologic research, 2014. **58**(0): p. 186–192.
145. Mizrahy, S., et al., *Hyaluronan-coated nanoparticles: the influence of the molecular weight on CD44-hyaluronan interactions and on the immune response*. Journal of Controlled Release, 2011. **156**(2): p. 231-238.
146. Vistejnova, L., et al., *Low molecular weight hyaluronan mediated CD44 dependent induction of IL-6 and chemokines in human dermal fibroblasts potentiates innate immune response*. Cytokine, 2014. **70**(2): p. 97-103.
147. Jouy, F., et al., *Sulfated hyaluronan attenuates inflammatory signaling pathways in macrophages involving induction of antioxidants*. Proteomics, 2017. **17**(10): p. 1700082.
148. Ruffell, B., et al., *Differential use of chondroitin sulfate to regulate hyaluronan binding by receptor CD44 in inflammatory and interleukin 4-activated macrophages*. Journal of Biological Chemistry, 2011. **286**(22): p. 19179-19190.
149. Casu, B., *Structure and biological activity of heparin*, in *Advances in carbohydrate chemistry and biochemistry*. 1985, Elsevier. p. 51-134.
150. Ou, Y., et al., *Inhibition of urinary macromolecule heparin on aggregation of nano-COM and nano-COD crystals*. Molecules, 2015. **20**(1): p. 1626-1642.
151. Wang, H., D. Loganathan, and R.J. Linhardt, *Determination of the pKa of glucuronic acid and the carboxy groups of heparin by ¹³C-nuclear-magnetic-resonance spectroscopy*. Biochem. J, 1991. **278**: p. 689-695.
152. Rabenstein, D.L., *Heparin and heparan sulfate: structure and function*. Natural product reports, 2002. **19**(3): p. 312-331.
153. Bishop, J.R., M. Schuksz, and J.D. Esko, *Heparan sulphate proteoglycans fine-tune mammalian physiology*. Nature, 2007. **446**(7139): p. 1030-1037.
154. Severin, I.C., et al., *Glycosaminoglycan analogs as a novel anti-inflammatory strategy*. Frontiers in immunology, 2012. **3**.
155. Koenig, A., et al., *Differential interactions of heparin and heparan sulfate glycosaminoglycans with the selectins. Implications for the use of unfractionated and low molecular weight heparins as therapeutic agents*. The Journal of clinical investigation, 1998. **101**(4): p. 877-889.

-
156. Young, E., *The anti-inflammatory effects of heparin and related compounds*. Thrombosis research, 2008. **122**(6): p. 743-752.
 157. Nelson, R.M., et al., *Heparin oligosaccharides bind L-and P-selectin and inhibit acute inflammation*. 1993.
 158. Bridges, A.W. and A.J. García, *Anti-inflammatory polymeric coatings for implantable biomaterials and devices*. Journal of diabetes science and technology, 2008. **2**(6): p. 984-994.
 159. AlKhoury, H., et al., *Study on the potential mechanism of anti-inflammatory activity of covalently immobilized hyaluronan and heparin*. Journal of Biomedical Materials Research Part A, 2020.
 160. Lee, J.H., et al., *Heparin inhibits NF- κ B activation and increases cell death in cerebral endothelial cells after oxygen-glucose deprivation*. Journal of molecular neuroscience, 2007. **32**(2): p. 145-154.
 161. Dash, M., et al., *Chitosan—A versatile semi-synthetic polymer in biomedical applications*. Progress in polymer science, 2011. **36**(8): p. 981-1014.
 162. Silva, S.S., et al., *Plasma surface modification of chitosan membranes: characterization and preliminary cell response studies*. Macromolecular bioscience, 2008. **8**(6): p. 568-576.
 163. Lizardi-Mendoza, J., W.M.A. Monal, and F.M.G. Valencia, *Chemical characteristics and functional properties of chitosan*, in *Chitosan in the preservation of agricultural commodities*. 2016, Elsevier. p. 3-31.
 164. Gades, M.D. and J.S. Stern, *Chitosan supplementation and fat absorption in men and women*. Journal of the American dietetic Association, 2005. **105**(1): p. 72-77.
 165. Sánchez-Machado, D.I., et al., *Chitosan*, in *Nonvitamin and Nonmineral Nutritional Supplements*. 2019, Elsevier. p. 485-493.
 166. Kim, S., *Competitive biological activities of chitosan and its derivatives: Antimicrobial, antioxidant, anticancer, and anti-inflammatory activities*. International Journal of Polymer Science, 2018. **2018**.
 167. Boddohi, S., C.E. Killingsworth, and M.J. Kipper, *Polyelectrolyte multilayer assembly as a function of pH and ionic strength using the polysaccharides chitosan and heparin*. Biomacromolecules, 2008. **9**(7): p. 2021-2028.
 168. Rinaudo, M., *Chitin and chitosan: properties and applications*. Progress in polymer science, 2006. **31**(7): p. 603-632.
 169. Croisier, F. and C. Jérôme, *Chitosan-based biomaterials for tissue engineering*. European Polymer Journal, 2013. **49**(4): p. 780-792.
 170. Kean, T. and M. Thanou, *Biodegradation, biodistribution and toxicity of chitosan*. Advanced drug delivery reviews, 2010. **62**(1): p. 3-11.
 171. Jamnongkan, T. and S. Kaewpirom, *Controlled-release fertilizer based on chitosan hydrogel: phosphorus release kinetics*. Sci J Ubu, 2010. **1**(1): p. 43-50.
 172. Rodríguez-Núñez, J.R., et al., *Antimicrobial activity of chitosan-based films against Salmonella typhimurium and Staphylococcus aureus*. International journal of food science & technology, 2012. **47**(10): p. 2127-2133.
 173. Liu, Y., et al., *Molecular interactions, characterization and antimicrobial activity of curcumin–chitosan blend films*. Food Hydrocolloids, 2016. **52**: p. 564-572.
 174. Davydova, V., et al., *Cytokine-inducing and anti-inflammatory activity of chitosan and its low-molecular derivative*. Applied Biochemistry and Microbiology, 2016. **52**(5): p. 476-482.
 175. Yang, E.-J., et al., *Anti-inflammatory effect of chitosan oligosaccharides in RAW 264.7 cells*. Central European Journal of Biology, 2010. **5**(1): p. 95-102.
-

-
176. Yuan, W., et al., *pH-controlled construction of chitosan/alginate multilayer film: characterization and application for antibody immobilization*. *Langmuir*, 2007. **23**(26): p. 13046-13052.
 177. Lankalapalli, S. and V. Kolapalli, *Polyelectrolyte complexes: A review of their applicability in drug delivery technology*. *Indian journal of pharmaceutical sciences*, 2009. **71**(5): p. 481.
 178. McWhorter, F.Y., C.T. Davis, and W.F. Liu, *Physical and mechanical regulation of macrophage phenotype and function*. *Cellular and Molecular Life Sciences*, 2015. **72**(7): p. 1303-1316.
 179. Wang, S., et al., *Micro-/Nano-Scales Direct Cell Behavior on Biomaterial Surfaces*. *Molecules*, 2018. **24**(1).
 180. Pujari-Palmer, S., *Nanofeatures of Biomaterials and their Impact on the Inflammatory Response*. 2016, Acta Universitatis Upsaliensis.
 181. Swartzlander, M.D., et al., *Linking the foreign body response and protein adsorption to PEG-based hydrogels using proteomics*. *Biomaterials*, 2015. **41**: p. 26-36.
 182. Zhou, G., H. Loppnow, and T. Groth, *A macrophage/fibroblast co-culture system using a cell migration chamber to study inflammatory effects of biomaterials*. *Acta Biomater*, 2015. **26**: p. 54-63.
 183. Saleh, L.S. and S.J. Bryant, *The host response in tissue engineering: crosstalk between immune cells and cell-laden scaffolds*. *Current opinion in biomedical engineering*, 2018. **6**: p. 58-65.
 184. Swartzlander, M.D., et al., *Immunomodulation by mesenchymal stem cells combats the foreign body response to cell-laden synthetic hydrogels*. *Biomaterials*, 2015. **41**: p. 79-88.
 185. Kim, Y.K., E.Y. Chen, and W.F. Liu, *Biomolecular strategies to modulate the macrophage response to implanted materials*. *Journal of Materials Chemistry B*, 2016. **4**(9): p. 1600-1609.
-

Chapter 2

Summary – Covalent immobilization of glycosaminoglycans to reduce the inflammatory effects of biomaterials:

The incorporation of GAGs for their anti-inflammatory potential together with their ability to bind cytokines like growth factors, chemokines and enzymes (like lipoprotein lipase and heparin cofactor II), is of great importance to modulate the inflammatory responses to implanted biomaterials. Therefore, HA, chondroitin sulfate (CS), and Hep were used in this study to investigate their effects on macrophage responses. The three different GAGs were immobilized covalently on amino-functionalized substrata by 1-ethyl-3-(3-dimethylaminopropyl) carbodiimide (EDC)/N-hydroxysuccinimide (NHS) crosslinking chemistry. Physicochemical characterizations were performed in attempt to evaluate the successful immobilization method by water contact angle (WCA) and zeta potential (ZP) measurements. Results showed significant increase in wettability as well as in negative charges on all GAGs-modified surfaces. Moreover, the high content of sulfate monoesters and sulfamido groups in Hep resulted in making the Hep-modified surfaces the highest in wettability and negative surface charge. THP-1-derived macrophages were used to investigate the anti-inflammatory potential of the GAGs-modified samples. Macrophage adhesion, spreading, FBGC formation, β 1 integrin expression as well as pro-inflammatory cytokine of interleukin-1 β (IL-1 β) production were studied as essential parameters to evaluate the inflammation process. This study illustrated that the HA-modified surfaces with their hydrophilicity and some steric effects of HA expressed a slightly higher reduction of initial macrophage adhesion and spreading compared to CS- and Hep-modified surfaces. In contrast, it was observed that the different GAGs showed no pivotal significant difference among them toward the studied macrophage responses. Eventually, the covalent immobilization approach was used here because of its advantage of stable coating resulted from chemical bonding, which further could be used in an *in vivo* model to reduce adverse biomaterial-induced inflammatory responses.

Covalent immobilization of glycosaminoglycans to reduce the inflammatory effects of biomaterials

Guoying Zhou, Hala Al-Khoury, Thomas Groth

Biomedical Materials Group, Institute of Pharmacy, Martin Luther University Halle-Wittenberg, Halle - Germany

ABSTRACT

Background: The inflammatory responses evoked by artificial organs and implantation of devices like biosensors and guide wires can lead to acute and chronic inflammation, largely limiting the functionality and longevity of the devices with negative effects on patients.

Aims: The present study aimed to reduce the inflammatory responses to biomaterials by covalent immobilization of glycosaminoglycans (GAGs) on amino-terminated surfaces used as model biomaterials here.

Methods and results: Water contact angle (WCA) and zeta potential measurements showed a significant increase in wettability and negative charges on the GAG-modified surfaces, respectively, confirming the successful immobilization of GAGs on the amino-terminated surfaces. THP-1-derived macrophages were used as a model cell type to investigate the efficacy of GAG-modified surfaces in modulating inflammatory responses. It was found that macrophage adhesion, macrophage spreading morphology, foreign body giant cell (FBGC) formation, as well as $\beta 1$ integrin expression and interleukin-1 β (IL-1 β) production were all significantly decreased on GAG-modified surfaces compared to the initial amino-terminated surface.

Conclusions: This study demonstrates the potential of covalent GAG immobilization to reduce the inflammatory potential of biomaterials in different clinical settings.

Keywords: Cytokines, Foreign body giant cells, Glycosaminoglycans, Inflammation, Macrophages

Introduction

Biomaterial implants and medical devices are widely used today and their performance is crucial for the safety of patients and their quality of life (1). Nevertheless, the implantation of any foreign material or device will trigger a cascade of inflammatory responses, which can lead to chronic inflammation and fibrotic encapsulation, resulting in the failure of implants and devices (2). In addition, the periprosthetic inflammatory responses to wear particles released from implanted prosthetics can cause osteolysis, leading to aseptic loosening of joint prosthetics, which is one of the most frequent reasons for the failure of total joint replacement surgeries (3). Monocytes/macrophages play central roles in these inflammatory responses, acting as a first line of defense in order to phagocytose the bacterial and foreign materials (4). Furthermore, when facing materials that are much larger

sized than themselves, several macrophages fuse to form foreign body giant cells (FBGCs) in order to increase their phagocytosis ability (5). Their involvement in these processes also includes a variety of inflammatory mediators such as cytokines, chemokines and growth factors to attract other cell types like fibroblasts (6). In response to these signals, fibroblasts are activated and differentiate into myofibroblasts to produce extracellular matrix (ECM) proteins such as collagen, leading to implant encapsulation and potential failure of the device (7).

It has been confirmed that the surface properties of biomaterials, including surface chemistry, wettability, surface potential and topography, dictate the plasma protein adsorption into the material surface immediately after implantation, thereby affecting the subsequent cellular inflammatory responses to implants (8, 9). An appropriate design and/or modification of biomaterial surface properties has therefore been considered to be a useful strategy for reducing inflammatory responses and improving implant performance (10).

Many recent studies on preventing inflammatory responses have focused on the incorporation of various anti-inflammatory agents like dexamethasone (DEX), alpha melanocyte-stimulating hormone (α -MSH) and glycosaminoglycans (GAGs) to generate more biocompatible materials (10, 11). Of these, GAGs, linear unbranched polysaccharides such as hyaluronic acid (HA), chondroitin sulfate (CS), and heparin (Hep) are important components of ECM with various biological activities that also include some anti-inflammatory

Accepted: January 21, 2016

Published online: February 23, 2016

Corresponding author:

Prof. Dr. Thomas Groth
Biomedical Materials Group
Martin Luther University Halle-Wittenberg
Heinrich-Damerow-Strasse 4
06120 Halle (Saale), Germany
thomas.groth@pharmazie.uni-halle.de

© 2016 Wichtig Publishing



potential (12). GAGs participate in cell-matrix interactions and bind cytokines, growth factors, chemokines and enzymes affecting biological processes like cell migration, homing, growth, and differentiation, which is also related to inflammation (13). In addition, both CS and Hep can bind to L- and P-selectin, which impairs leukocyte adhesion, activation and transmigration activities (14). Furthermore, they can mediate anti-inflammatory effects by inhibition of nuclear factor- κ B (NF- κ B) translocation, which is a crucial transcription factor of many pro-inflammatory mediators, leading to suppression of pro-inflammatory cytokine production (15). By contrast, high molecular weight HA (HMW-HA) prevents inflammatory responses through interactions with CD44, which translates the signals from HA to down-regulate leukocyte activation, growth, and differentiation (16). Hence, the use of GAGs to modify biomaterial surfaces seems to be a promising tool to reduce or prevent the inflammatory potential of biomaterials. Moreover, our recent work showed that the deposition of GAG-chitosan multilayers on glass surfaces significantly reduced macrophage adhesion, fusion and down-regulated pro-inflammatory cytokine production (17).

The current study aimed to evaluate the effect of covalent immobilization of GAGs on material surface for reduction of the inflammatory responses of macrophages to biomaterials. For this purpose, GAGs were covalently immobilized onto an amino-terminated self-assembling monolayer (SAM) surface by 1-ethyl-3-(3-dimethylaminopropyl) carbodiimide (EDC)/N-hydroxysuccinimide (NHS) crosslinking chemistry (18). THP-1 cells were applied as a model monocyte system and differentiated into macrophage-like cells by treatment with phorbol-12-myristate-13-acetate (PMA) (19). By using the THP-1-derived macrophages, an anti-inflammatory GAG effect was observed in an *in vitro* setting. Results are reported in this article.

Materials and methods

Materials

Hyaluronic acid (HA, Mw~1.3 MDa) was provided by Innovent. Chondroitin sulfate sodium salt (CS, Mw~25 kDa) was purchased from Sigma-Aldrich. Heparin sodium salt (Hep, Mw~15 kDa) was provided by Serva. N-hydroxysuccinimide (NHS) and Triton X-100 were obtained from Sigma-Aldrich. Other compounds used were 3-aminopropyltriethoxysilane (APTES) (ABCR), 2-(N-morpholino)ethanesulfonic acid monohydrate (MES) (VWR International), ethylenediamine (Sigma-Aldrich) and 1-ethyl-3-(3-dimethylaminopropyl) carbodiimide (EDC) (Alfa Aesar).

Preparation of GAG-modified surfaces

Preparation of amino-terminated SAM

Round glass cover slips (ϕ 15 mm; Menzel) were cleaned with 0.5 M NaOH in 96% ethanol (Roth) for 2 hours. Subsequently, the slides were extensively rinsed with double-distilled water (10×5 minutes) and dried under nitrogen flow. The amino-terminated SAMs were obtained by immersing the cleaned glass slides in 2% (v/v) solution of APTES in

99.8% acetone (Roth) for 1 hour at room temperature (RT). After that, the surfaces were rinsed extensively with acetone, ethanol and washed with double-distilled water (8×5 minutes). Then the surfaces were dried with streaming nitrogen and baked for 1 hour at 100°C.

Immobilization of GAGs onto amino-terminated SAM

GAG solutions of HA, CS and Hep at 4 mg mL⁻¹ were first prepared by dissolution in freshly prepared MES-buffered solution (50 mM, pH 4.7). Subsequently, 5 mg mL⁻¹ of EDC and 3 mg mL⁻¹ of NHS were added respectively to the GAG solutions for 30 minutes each at RT. Thereafter, the amino-terminated glass surfaces were immersed in the EDC/NHS-activated GAG solutions for 24 hours. After that, 1 M ethylenediamine solution was added to inactivate the remaining reactive carboxyl species of the EDC linker (18). The surfaces were then rinsed with ethanol, washed with double-distilled water (8×5 minutes), and dried under nitrogen flow.

Characterization of GAG-modified surfaces

Surface wettability studies

Static water contact angle (WCA) measurements were conducted using the OCA 15+ device from Dataphysics, placing 5 droplets of 2 μ L fresh ultrapure water onto each surface at RT and applying the sessile drop method. The experiments were run in triplicate and mean and standard deviations of 2 independent experiments were calculated.

Surface potential measurements

Zeta potentials of amino-terminated SAM and GAG-modified surfaces were determined with a SurPASS device (Anton Paar). Glass cover slips with specific dimensions were used for sample preparation and zeta potential measurements. Two identically modified cover slips were fixed and placed opposite each other in the adjustable gap cell. The gap was adjusted to a distance where a flow rate of 100 to 150 mL minutes⁻¹ was achieved at a maximum overpressure of 300 mbar. One mM potassium chloride (KCl) was used as model electrolyte and 0.1 M hydrochloric acid (HCl) was used for pH titration. The pH value of KCl was adjusted to pH 10.5 using 1 M sodium hydroxide (NaOH) before starting the measurement. Then the measurements were performed by an automated titration program using titration steps of 0.03 μ L from pH 10.5 to 5.0 and 0.25 μ L from pH 5.0 to 3.0.

Cell experiments

Cell culture

Cells of the human monocytic cell line THP-1 (DSMZ) were cultured in RPMI-1640 medium (Biochrom) supplemented with 10% (v/v) fetal bovine serum (FBS; Biochrom), 1% (v/v) antibiotic-antimycotic solution (AAS; Promocell) at 37°C in a humidified 5% CO₂/95% air atmosphere using a NuAire DH Autoflow incubator. Suspended cells were passaged by



centrifugation. The old medium was removed and the cell pellet was resuspended in fresh medium every second day in order to maintain a cell density of $0.5\text{--}1.0 \times 10^6$ cells mL^{-1} . THP-1-derived macrophages were obtained by incubation of THP-1 cells with 200 nM phorbol-12-myristate-13-acetate (PMA; Sigma) in T75 cell culture flasks (Greiner Bio-One) for 48 hours. Afterwards, the differentiated macrophages were detached by incubation with 0.25% trypsin/0.02% EDTA (Biochrom) and used for seeding on the different surfaces.

Cell adhesion studies

THP-1-derived macrophages were seeded on amino-terminated SAM and GAG-modified surfaces at a cell density of 2.5×10^4 cells mL^{-1} in serum-free RPMI-1640 medium. Cultures were incubated at 37°C in a humidified 5% CO_2 /95% air atmosphere for 24 hours. Thereafter, the surfaces were gently washed with PBS once to remove nonadherent cells. Attached cells were fixed by methanol and stained with 10% (v/v) Giemsa (Merck) in ultrapure water. Cells were visualized with a transmitted light microscope (Axiovert 100; Zeiss) equipped with a CCD camera (Sony, MC-3254; AVT-Horn). The cell count on different surfaces was calculated using ImageJ software (version 1.46r).

Immunofluorescence staining of macrophages

Cells were treated and incubated as described above. After 24 hours of incubation, attached cells were fixed with 4% paraformaldehyde solution (Roti® Histofix; Roth) for 15 minutes. Then the cells were permeabilized with 0.1% (v/v) Triton X-100 for 10 minutes and rinsed twice with PBS. Nonspecific binding sites were blocked by incubation with 1% (w/v) bovine serum albumin (BSA; Merck) in PBS for 1 hour, while all antibodies were diluted in the same solution. At first, the cells were incubated with a mouse monoclonal antibody raised against vinculin (1:100, Sigma) for 30 minutes. After washing twice with PBS, a secondary goat antimouse antibody conjugated with CY2 (1:100, Dianova) was applied for another 30 minutes. Actin fibers and cell nuclei were stained by BODIPY®-Phalloidin (1:50, Invitrogen) and TO-PRO3 (1:500, Invitrogen), respectively, for an additional 30 minutes each. All fixation, washing, and staining steps were performed at RT. Finally, all samples were washed with PBS, dipped into ultrapure water, and mounted with Mowiol (Calbiochem) to object holders. All surfaces were examined by confocal laser scanning microscopy (CLSM; Zeiss) using a 63-fold oil immersion objective and images were processed with ZEN2011 software (Zeiss).

Foreign body giant cell (FBGC) characterization

The FBGC formation on different surfaces was evaluated after 10 days of incubation in serum-containing RPMI-1640 medium. The surfaces were gently washed with PBS once and the attached cells were fixed with cold methanol and stained with 10% (v/v) Giemsa (Merck) in ultrapure water. Cells were photographed using a transmitted light microscope equipped with a CCD camera and the area percentage of FBGC on different surfaces was calculated by ImageJ software.

$\beta 1$ integrin expression

The cells were treated as described above in FBGC characterization. The $\beta 1$ integrin expression on different surfaces was then evaluated by immunofluorescence staining (20). Cells were fixed with 4% paraformaldehyde solution (Roth), permeabilized with 0.1% (v/v) Triton X-100 (Sigma) for 10 minutes at RT and rinsed twice with PBS. Again, non-specific binding sites were blocked with 1% (w/v) BSA in PBS for 1 hour. Thereafter, cells were incubated with a mouse monoclonal antibody raised against $\beta 1$ integrin (1:50, Santa Cruz Biotechnology) for 30 minutes. After washing twice with PBS, a secondary goat anti mouse antibody conjugated with CY2 (1:100, Dianova) was applied for another 30 minutes. The nuclei were stained with TO-PRO3 (1:500, Invitrogen) for 30 minutes. Finally, all samples were mounted with Mowiol (Calbiochem) and examined with a confocal laser scanning microscope (CLM; Zeiss) using a 40-fold oil immersion objective. Images were processed with the ZEN2011 software (Zeiss).

Pro-inflammatory cytokine production

Thp-1-derived macrophages were seeded on amino-terminated SAM and GAG-modified surfaces at a cell density of 5.0×10^5 cells mL^{-1} and incubated for 24 minutes with or without $1 \mu\text{g mL}^{-1}$ lipopolysaccharide (LPS; Sigma) in serum-containing RPMI-1640 medium. After that, the medium supernatants of the untreated and LPS-challenged samples were collected and stored at -20°C until needed for investigation. The IL-1 β production on different surfaces was detected using enzyme-linked immunosorbent assay (ELISA) according to the manufacturers' instructions (Thermo Scientific).

Statistics

All data are represented as mean values \pm standard deviations (SD). Statistical examination was performed using 1-way analysis of variance (ANOVA) followed by post-hoc Tukey testing. The significance level was set as $p \leq 0.05$ and indicated by an asterisk. The number of samples has been indicated in the respective figure captions.

Results and discussion

Characterization of GAG-modified surfaces

The wettability of substrata after immobilization of different GAGs was evaluated by static water contact angle (WCA) measurements. Here, the covalent immobilization of different GAGs on amino-terminated surfaces resulted in varying wettability, as depicted by Figure 1. First, the amino-terminated SAM (NH_2) resulted in moderately wettable surfaces with $\text{WCA} \sim 53^\circ$, which is in line with previous reports (21). Further, the WCA significantly decreased after the immobilization of GAGs onto the NH_2 surface. This is due to the presence of hydrophilic sulfate and carboxylic acid groups of immobilized GAGs (22). Among the GAGs, the Hep-modified surface had the highest wettability, as indicated by the smallest WCA, followed by CS and HA. The highest wettability of Hep is due to its high content of sulfate monoesters and sulfamido groups



40

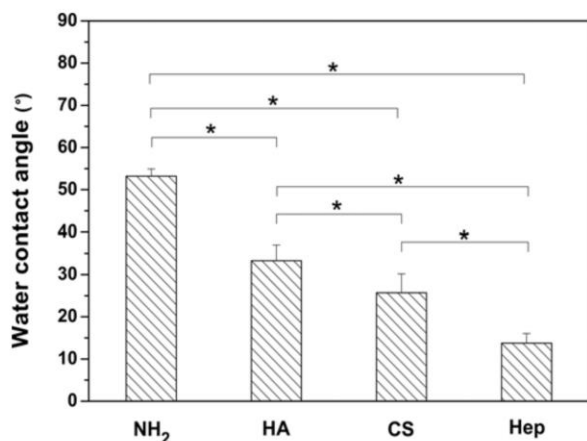


Fig. 1 - Static water contact angle (WCA) measurements for amino-terminated SAM (NH₂) and surfaces after immobilization of hyaluronic acid (HA), chondroitin sulfate (CS) and heparin (Hep) onto NH₂ SAM. Results are means ± SD of 2 independent experiments and triplicate samples for each condition, *p<0.05.

Covalent immobilization of GAGs to reduce inflammatory effects

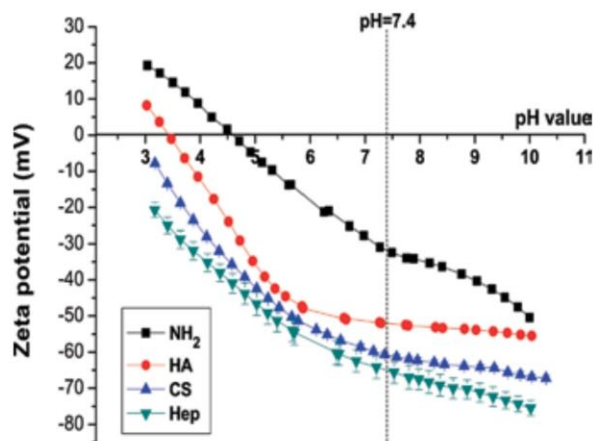


Fig. 2 - Zeta potential measurements of amino-terminated SAM (NH₂, ■) and surfaces after immobilization of hyaluronic acid (HA, ●), chondroitin sulfate (CS, ▲) and heparin (Hep, ▼) onto NH₂ SAM.

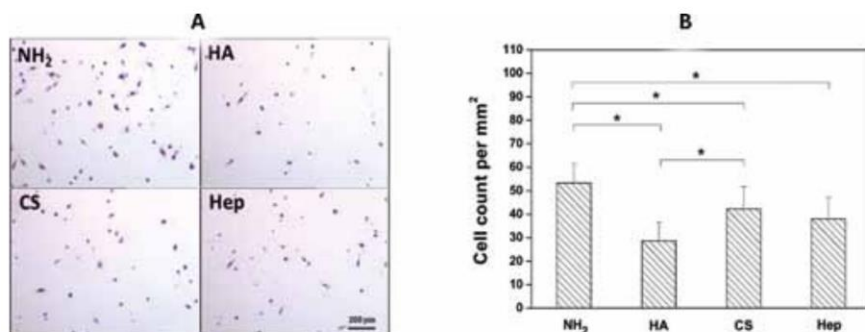


Fig. 3 - (A) Transmitted light microscopic images of adhering macrophages for 24 minutes of incubation in serum-free RPMI medium and then stained with Giemsa on amino-terminated SAM (NH₂) after immobilization of hyaluronic acid (HA), chondroitin sulfate (CS) and heparin (Hep) onto NH₂ surface. [Scale bar: 200 μm]. (B) Quantified macrophages per area adherent on NH₂, HA, CS and Hep surfaces after 24 minutes of incubation. Data represent mean ± SD, n = 4, *p<0.05.

(23). By contrast, CS possesses fewer sulfate groups than Hep, while HA possesses only carboxylic acid groups but not sulfate groups, resulting in the lower wettability of both compared to Hep.

The immobilization of GAGs onto the NH₂ surface also had a strong effect on the surface charge, indicated by different zeta potentials as shown in Figure 2. It can be seen that the NH₂ surface resulted in a positive zeta potential below pH 4.7, which is due to the protonation of amino groups in the low pH region (24). By contrast, a significant decrease in zeta potentials was observed for all GAG-modified surfaces. This is attributed to the deprotonation of sulfate and carboxylic groups, especially at the basic pH region. Furthermore, clear differences between the GAG-modified surfaces were found in zeta potentials. Hep had the lowest zeta potentials due to the highest content of sulfate groups, followed by CS and HA, which is consistent with the wettability shown by WCA measurements.

Adhesion and fusion of macrophages

THP-1 cells were used as a model monocyte system and differentiated into macrophages by PMA treatment. The adhesion

and spreading of the THP-1-derived macrophages were investigated on different GAG-modified surfaces in comparison with the NH₂ surface using histochemical (Fig. 3) as well as immunohistochemical (Fig. 4) techniques.

Figure 3 shows that macrophages adhered differently to the various surfaces. Here, the significantly highest cell count was found on the NH₂ surface (Fig. 3B). This is due to the high amount of amino groups, with resulting moderate wettability and the least negative surface potential at pH 7.4 (as observed with the WCA and zeta potential measurements). The finding of high cell adhesion is also well in line with many previous studies (25). By contrast, the cell adhesion on all GAG-modified surfaces was significantly reduced, which is obviously also related to the higher wettability and more negative potential of these surfaces. However, a first observation in this regard was that despite certain differences in surface properties among the GAGs-immobilized surfaces, no significant difference in adhesion of macrophages was observed.

Figure 4A shows the morphology of spreading macrophages on different surfaces by immunofluorescence staining of actin (red) and vinculin (green). It can be seen that



© 2016 Wichtig Publishing

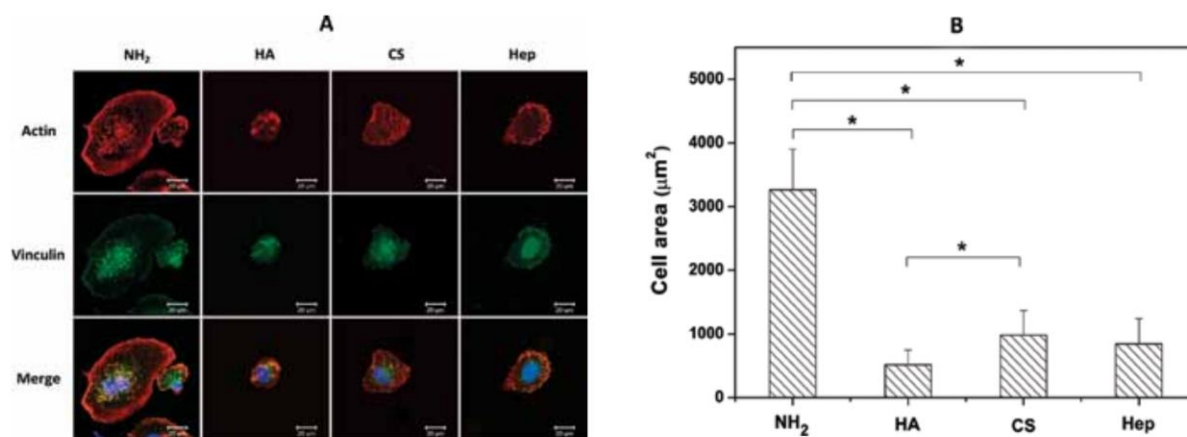


Fig. 4 - Representative confocal laser scanning microscopy (CLSM) images (A) and quantitative cell area (B) of macrophages after 24 minutes of incubation in serum-free RPMI medium on amino-terminated SAM (NH₂) and surfaces after immobilization of hyaluronic acid (HA), chondroitin sulfate (CS) and heparin (Hep) onto NH₂ SAM. The cells were stained for vinculin (green), actin (red), and nucleus (blue). [Scale bar: 20 μm].

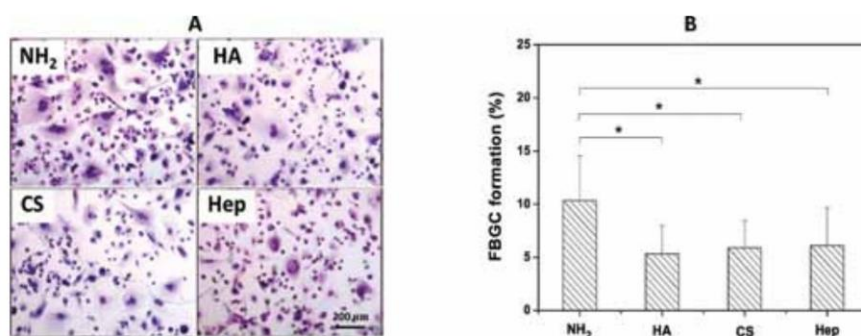


Fig. 5 - (A) Transmitted light microscopic images of Giemsa-stained foreign body giant cells (FBGCs) after 10 days of incubation on amino-terminated SAM (NH₂) and surfaces after immobilization of hyaluronic acid (HA), chondroitin sulfate (CS) and heparin (Hep) on NH₂ SAM [Scale bar: 200 μm]. (B) Quantified area percentage of FBGCs formed on NH₂, HA, CS and Hep surfaces after 10 days of incubation by quantitative evaluation of micrographs. Data represent mean ± SD, n = 10, *p < 0.05.

macrophages on the NH₂ surface seemed to adhere more strongly, indicated by a greater spreading of cells with a larger cell area than on the GAG-modified surfaces. Punctate actin structures were formed, especially at the periphery of macrophages. Furthermore, larger focal adhesion plaques were lacking. Instead, a rather clustered distribution of vinculin was found in the cells. This is also consistent with previous findings that podosome structures rather than focal contacts are the major adhesive structures present in macrophages adhering to surfaces (26). As expected, cell spreading on GAG-modified surfaces was largely suppressed compared to the NH₂ surface, as illustrated by the reduced actin and vinculin expression. Figure 4B shows the quantitative cell spreading area on various surfaces. The results revealed a significantly lower spreading area of macrophages on all GAG-modified surfaces in comparison to the NH₂ surface. Among the different GAGs, HA-modified surfaces once again showed the highest capacity for inhibiting cell spreading. By contrast, adhesion (Fig. 4A) and spreading (Fig. 4B) were slightly increased on CS- and Hep-modified surfaces, although they remained significantly lower than on the NH₂ surface. The reason for the enhanced adhesion and spreading on CS- and Hep-modified surfaces might be due to the increased content

of sulfate groups, which are reported to promote adhesion of several cell types (22, 27). Overall, the immobilization of GAGs onto the NH₂ surface showed significant effects in reducing macrophage adhesion and spreading compared to the original NH₂ SAM.

Macrophage fusion into FBGCs is a hallmark of chronic inflammation (28). Moreover, β1 integrin was reported to play a crucial role during macrophage fusion and FBGC formation (20). In need, the extent of FBGC formation and β1 integrin expression reflect the pro-inflammatory potential of a biomaterial *in vitro* and *in vivo* (2, 29). For these reasons, the macrophage fusion and β1 integrin expression in FBGCs were evaluated after 10 days of incubation on GAG-modified surfaces in comparison to the NH₂ surface (Figs. 5 and 6). Figure 5A shows that macrophage fusion was effectively inhibited on GAG-modified surfaces in comparison to the NH₂ surface. Marked macrophage fusion was observed on the NH₂ surface in terms of more (n ≥ 2) nuclei accumulation within an extensively spread cell body. By contrast, FBGCs with fewer nuclei and a reduced size of were found on all GAG-modified surfaces. Figure 5B depicts the area percentages of formed FBGCs on different surfaces, which provide quantitative confirmation of the findings in Figure 5A. Furthermore, β1 integrin

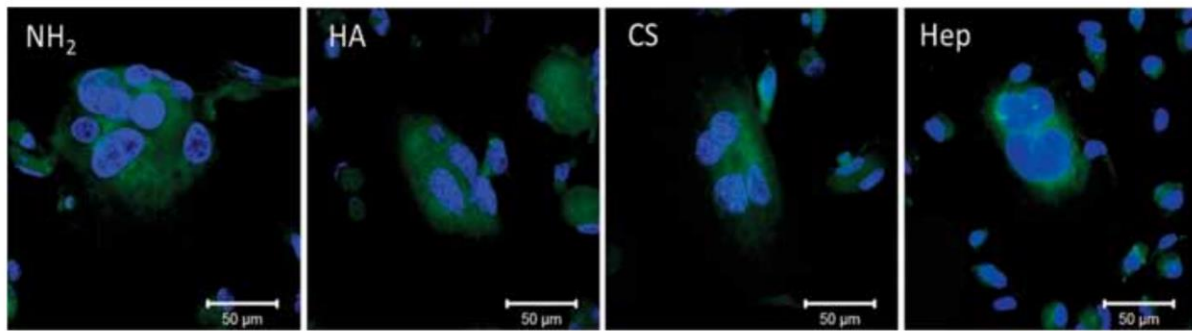


Fig. 6 - Expression of $\beta 1$ integrin was determined on fusing macrophages/FBGCs after 10 days of incubation on amino-terminated SAM (NH_2) and surfaces after immobilization of hyaluronic acid (HA), chondroitin sulfate (CS) and heparin (Hep) on NH_2 SAM. Cells were fixed with 4% paraformaldehyde and stained for $\beta 1$ integrin (green) and nuclei (blue) [Scale bar: 50 μm].

expression on different surfaces (Fig. 6) shows a trend similar to macrophage fusion data (Fig. 5). Here, a significant reduction of $\beta 1$ integrin expression (green staining) but also cell spreading was observed on GAG-modified surfaces in comparison to the NH_2 surface. It was also obvious in these studies that NH_2 SAM promoted FBGC formation as cells there had more nuclei per cell body than on GAG-modified surfaces. The highest extent of macrophage fusion on the NH_2 surface might be related to the higher macrophage number on this surface. This seems to increase the probability of macrophage fusion, since macrophage-macrophage fusion requires a certain cell adhesion density and spreading of the cells (30). For this reason, a higher degree of macrophage fusion is accompanied by a higher $\beta 1$ integrin expression. In other words, the surfaces that did not support initial macrophage adhesion and morphology development (cytoplasmic expansion) could not promote the ensuing macrophage fusion and $\beta 1$ integrin expression (30). Consequently, the more hydrophilic and negatively charged GAG-modified surfaces, which reduced initial macrophage adhesion and spreading, limited macrophage fusion and $\beta 1$ integrin expression significantly compared to NH_2 SAM. However, in addition to cell number, the release of cytokines has also been identified as an inducer of macrophage fusion, particularly IL-4 and IL-13 (31).

IL-1 β cytokine production

During implant-associated inflammation, macrophages are activated and play important roles in modulating the inflammatory responses by secreting a variety of soluble signals such as pro- or anti-inflammatory cytokines and chemokines (5). The production of pro-inflammatory cytokines such as IL-1 β , IL-6 and TNF- α in the cell cultures may reflect the potential of the biomaterial to induce inflammatory reactions (3, 29). Moreover, LPS is known as a strong stimulant for macrophage activation and can up-regulate the pro-inflammatory cytokine release (32). Since biomaterial implantation can sometimes also be accompanied by infection with gram-negative bacteria, the presence of endotoxin, i.e. LPS, is a possible complication. Therefore, the production of the pro-inflammatory cytokine IL-1 β was studied here in both the

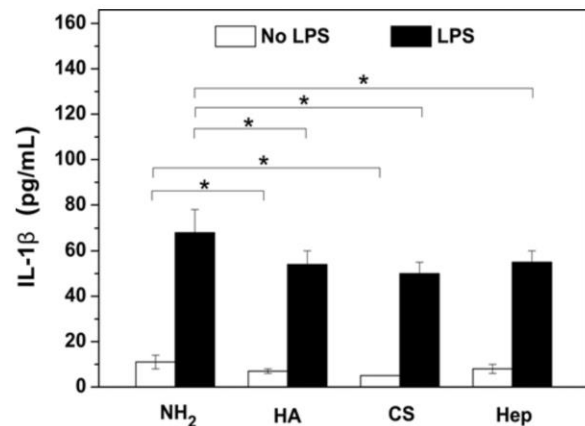


Fig. 7 - IL-1 β production of macrophages after 24 minutes of incubation in the absence (white bars) and presence (black bars) of lipopolysaccharide (LPS) on amino-terminated SAM (NH_2) and surfaces after immobilization of hyaluronic acid (HA), chondroitin sulfate (CS) and heparin (Hep) on NH_2 SAM. Data represent mean \pm SD, $n = 6$, * $p < 0.05$.

presence and absence of LPS treatment to investigate the inflammatory potential of all surfaces.

Figure 7 shows the IL-1 β production on different surfaces after 24 minutes of incubation with (black bars) or without (white bars) LPS stimulation. It was found that the NH_2 surface (11 ± 3 pg/mL) caused strong spreading and that the fusion of macrophages produced higher amounts of IL-1 β than surfaces modified with HA (7 ± 1 pg/mL) or CS (5 ± 0 pg/mL) in the absence of LPS stimulation. Likewise, IL-1 β production on surfaces modified with HA (54 ± 6 pg/mL), CS (50 ± 5 pg/mL) and Hep (55 ± 5 pg/mL) were significantly reduced compared to the NH_2 surface (68 ± 10 pg/mL) in the presence of LPS stimulation. The data show also that IL-1 β production by THP-1 derived macrophages was up-regulated on all surfaces after LPS treatment, which is well in line with previous findings also demonstrating the functionality of the cells (17, 33). The



reduction of pro-inflammatory cytokine IL-1 β release by GAG-modified surfaces is further evidence for their potential to inhibit the inflammatory potential of biomaterials.

The anti-inflammatory effects observed here might be attributed partly to the physicochemical properties of the GAG-modified surfaces. The immobilization of GAGs onto the NH₂ surface resulted in a significant increase in wettability and negative charges, which are believed to reduce protein adsorption and cell adhesion (18, 22, 25) and further impair macrophage fusion and the ensuing inflammatory responses (17). It can be also assumed that both the physicochemical properties of the GAG-modified surfaces as well as the physiologic roles of GAGs in regulating inflammatory responses resulted in the remarkable anti-inflammatory effect compared to the NH₂ surface (34, 35). Together, the present study and our previous work (17) demonstrate the remarkable inflammatory-inhibiting effects of GAGs. In this study we have provided another way of immobilizing GAGs onto surfaces, namely by covalent immobilization on biomaterial surfaces. An obvious advantage of the covalent immobilization is a more stable chemical bonding compared to adsorptive binding presented in a previous work (17). This method is more suitable for long-term, *in vivo* applications to reduce biomaterial-induced inflammatory responses.

Conclusions

In this study, different types of GAGs were covalently immobilized onto amino-terminated surfaces to evaluate their anti-inflammatory effects using a simple *in vitro* model. Static WCA and zeta potential measurements confirmed the successful immobilization of the GAGs resulting in more hydrophilic and negatively charged surfaces compared to the original substrate. The studies with macrophages derived from THP-1 demonstrated that the GAG-modified surfaces significantly reduced macrophage adhesion and spreading, FBGC formation, β 1 integrin expression and pro-inflammatory cytokine IL-1 β production compared to the amino-terminated surface. Among the GAGs, the HA-modified surface expressed a slightly higher reduction of initial macrophage adhesion and spreading compared to CS- and Hep-modified surfaces, possibly due to specific HA-CD44 interactions or steric effects of the larger HA molecules. Nevertheless, no significant differences were found regarding the other cellular responses among the different types of GAGs. Overall, the results suggest a great potential in reducing the inflammatory responses by covalent immobilization of GAGs onto NH₂-terminated glass used as model surface. More important, however, is the wide applicability of this method to real biomaterial surfaces to improve the biocompatibility of implantable artificial organs, glucose-detecting biosensors, catheters, and tissue engineering scaffolds.

Acknowledgement

The assistance of Mrs. M. Porobin in zeta potential measurement is gratefully acknowledged.

Disclosures

Financial support: G. Zhou thanks the China Scholarship Council for offering the scholarship to work in Germany.

Conflict of interest: None of the authors has financial interest related to this study to disclose.

References

- Martínez-Miguel P, de Sequera P, Albalade M, et al. Evaluation of a polynephron dialysis membrane considering new aspects of biocompatibility. *Int J Artif Organs*. 2015;38(1):45-53.
- Anderson JM. Biological responses to materials. *Annu Rev Mater Res*. 2001;31:81-110.
- Sun K, Li Y, Lu Z, Zhang L, Gao Z, Jin Q. Suppression of titanium particle-induced TNF-alpha expression and apoptosis in human U937 macrophages by siRNA silencing. *Int J Artif Organs*. 2013;36(7):522-527.
- Wynn TA, Barron L. Macrophages: master regulators of inflammation and fibrosis. *Semin Liver Dis*. 2010;30(03):245-257.
- Anderson JM, Rodriguez A, Chang DT. Foreign body reaction to biomaterials. *Semin Immunol*. 2008;20(2):86-100.
- Brodbeck WG, Nakayama Y, Matsuda T, Colton E, Ziats NP, Anderson JM. Biomaterial surface chemistry dictates adherent monocyte/macrophage cytokine expression *in vitro*. *Cytokine*. 2002;18(6):311-319.
- Barron L, Wynn TA. Fibrosis is regulated by Th2 and Th17 responses and by dynamic interactions between fibroblasts and macrophages. *Am J Physiol Gastrointest Liver Physiol*. 2011;300(5):G723-G728.
- Lourenço BN, Marchioli G, Song W, et al. Wettability influences cell behavior on superhydrophobic surfaces with different topographies. *Biointerphases*. 2012;7(1-4):46.
- Llopis-Hernández V, Rico P, Ballester-Beltrán J, Moratal D, Salmerón-Sánchez M. Role of surface chemistry in protein remodeling at the cell-material interface. *Plos One*. 2011;6:e19610-e.
- Franz S, Rammelt S, Scharnweber D, Simon JC. Immune responses to implants - a review of the implications for the design of immunomodulatory biomaterials. *Biomaterials*. 2011;32(28):6692-6709.
- Boontheekul T, Mooney DJ. Protein-based signaling systems in tissue engineering. *Curr Opin Biotechnol*. 2003;14(5):559-565.
- Severin IC, Soares A, Hantson J, et al. Glycosaminoglycan analogs as a novel anti-inflammatory strategy. *Front Immunol*. 2012;3:293.
- Gandhi NS, Mancera RL. The structure of glycosaminoglycans and their interactions with proteins. *Chem Biol Drug Des*. 2008;72(6):455-482.
- Young E. The anti-inflammatory effects of heparin and related compounds. *Thromb Res*. 2008;122(6):743-752.
- Iovu M, Dumais G, du Souich P. Anti-inflammatory activity of chondroitin sulfate. *Osteoarthritis Cartilage*. 2008;16(Suppl 3):S14-S18.
- Ruppert SM, Hawn TR, Arrigoni A, Wight TN, Bollyky PL. Tissue integrity signals communicated by high-molecular weight hyaluronan and the resolution of inflammation. *Immunol Res*. 2014;58(2-3):186-192.
- Zhou G, Niepel MS, Saretia S, Groth T. Reducing the inflammatory responses of biomaterials by surface modification with glycosaminoglycan multilayers. *J Biomed Mater Res A*. 2016;104(2):493-502.
- Köwitsch A, Yang Y, Ma N, Kuntsche J, Mäder K, Groth T. Bioactivity of immobilized hyaluronic acid derivatives regarding protein adsorption and cell adhesion. *Biotechnol Appl Biochem*. 2011;58(5):376-389.
- Park EK, Jung HS, Yang HI, Yoo MC, Kim C, Kim KS. Optimized THP-1 differentiation is required for the detection of responses to weak stimuli. *Inflamm Res*. 2007;56(1):45-50.



20. McNally AK, Anderson JM. Beta1 and beta2 integrins mediate adhesion during macrophage fusion and multinucleated foreign body giant cell formation. *Am J Pathol.* 2002;160(2):621-630.
21. Katzur V, Eichler M, Deigle E, et al. Surface-immobilized PAMAM-dendrimers modified with cationic or anionic terminal functions: physicochemical surface properties and conformational changes after application of liquid interface stress. *J Colloid Interface Sci.* 2012;366(1):179-190.
22. Yang Y, Köwitsch A, Ma N, et al. Functionality of surface-coupled oxidised glycosaminoglycans towards fibroblast adhesion. *J Bioact Compat Polym.* 2015:0883911515599999.
23. Wang HM, Loganathan D, Linhardt RJ. Determination of the pKa of glucuronic acid and the carboxy groups of heparin by ¹³C-nuclear-magnetic-resonance spectroscopy. *Biochem J.* 1991;278(Pt 3):689-695.
24. Shyue JJ, De Guire MR, Nakanishi T, Masuda Y, Koumoto K, Sukenik CN. Acid-base properties and zeta potentials of self-assembled monolayers obtained via in situ transformations. *Langmuir.* 2004;20(20):8693-8698.
25. Bacakova L, Filova E, Parizek M, Ruml T, Svorcik V. Modulation of cell adhesion, proliferation and differentiation on materials designed for body implants. *Biotechnol Adv.* 2011;29(6):739-767.
26. DeFife KM, Jenney CR, Colton E, Anderson JM. Cytoskeletal and adhesive structural polarizations accompany IL-13-induced human macrophage fusion. *J Histochem Cytochem.* 1999;47(1):65-74.
27. Amorim S, Pires RA, da Costa DS, Reis RL, Pashkuleva I. Interactions between exogenous FGF-2 and sulfonic groups: in situ characterization and impact on the morphology of human adipose-derived stem cells. *Langmuir.* 2013;29(25):7983-7992.
28. Kou PM, Babensee JE. Macrophage and dendritic cell phenotypic diversity in the context of biomaterials. *J Biomed Mater Res A.* 2011;96A(1):239-260.
29. Anderson JM, Miller KM. Biomaterial biocompatibility and the macrophage. *Biomaterials.* 1984;5(1):5-10.
30. McNally AK, Jones JA, Macewan SR, Colton E, Anderson JM. Vitronectin is a critical protein adhesion substrate for IL-4-induced foreign body giant cell formation. *J Biomed Mater Res A.* 2008;86A(2):535-543.
31. DeFife KM, Jenney CR, McNally AK, Colton E, Anderson JM. Interleukin-13 induces human monocyte/macrophage fusion and macrophage mannose receptor expression. *J Immunol.* 1997;158(7):3385-3390.
32. Loppnow H, Brade H, Dürrbaum I, et al. IL-1 induction-capacity of defined lipopolysaccharide partial structures. *J Immunol.* 1989;142(9):3229-3238.
33. Zhou G, Loppnow H, Groth T. A macrophage/fibroblast coculture system using a cell migration chamber to study inflammatory effects of biomaterials. *Acta Biomater.* 2015;26:54-63.
34. Ruppert SM, Hawn TR, Arrigoni A, Wight TN, Bollyky PL. Tissue integrity signals communicated by high-molecular weight hyaluronan and the resolution of inflammation. *Immunol Res.* 2014;58(2-3):186-192.
35. Iovu M, Dumais G, du Souich P. Anti-inflammatory activity of chondroitin sulfate. *Osteoarthritis Cartilage.* 2008;16(Suppl 3):S14-S18.



Chapter 3

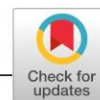
Summary – Study on the potential mechanism of anti-inflammatory activity of covalently immobilized hyaluronan and heparin:

This chapter concentrates on the mechanism of anti-inflammatory effects of GAGs with a particular focus on the canonical signal transduction pathway of NF- κ B. According to the aforementioned results in chapter 2, two distinct GAGs were chosen for the current study due to their significant results in reducing macrophage related inflammatory responses. Thus, HA and Hep were also covalently immobilized on amino-terminated surfaces by using EDC/NHS cross-linking chemistry. Additional physicochemical characterizations toward surface topography was performed with atomic force microscopy (AFM). WCA and ZP measurements were performed here as well to give an evidence of a successful surface modification process. The physicochemical results illustrated covalent immobilization of HA and Hep represented by lower contact angles and more negative surface potentials in comparison to the control amino-terminated surface. Macrophages differentiated from THP-1 monocytes were used to investigate the potential mechanism of the anti-inflammatory properties of GAGs in terms of NF- κ B. IF staining of p65 subunit was used to evaluate the nuclear to cytoplasmic ratio of p65 translocation. In addition, immunoblotting as well as the association or the uptake of fluorescein isothiocyanate (FITC)-labelled GAGs by macrophages were done. Besides, macrophage inflammatory responses were also studied in terms of the number and the aspect ratio of adherent macrophages, the fusion extent and the pro-inflammatory cytokine of IL-1 β release. Results pointed out that Hep had the highest partial inhibitory effect toward translocation of the p65 into the nucleus followed by HA. However, again no significant difference was shown between the different GAGs. Thereafter, both GAGs demonstrated lower expression of NF- κ B in the whole cell lysate with immunoblotting and macrophages showed a capability to associate or take up the FITC-labelled GAGs. The following outcomes are related to HA suppression to TLR signalling as well as binding to CD44 receptor. While, Hep either activates phosphorylation of p65 allowing its translocation to the nucleus with further inhibition of NF- κ B binding to DNA sequences or inhibits partially the NF- κ B translocation through the electrostatic binding of the positively charged

transcription factor to the anionic Hep, taken up by endocytosis. These effects of both GAGs will finally lead to down regulation of pro-inflammatory cytokine production and other inflammatory activities.

Received: 22 August 2019 | Revised: 7 January 2020 | Accepted: 10 January 2020

DOI: 10.1002/jbm.a.36885



ORIGINAL ARTICLE



Study on the potential mechanism of anti-inflammatory activity of covalently immobilized hyaluronan and heparin

Hala AlKhoury^{1,2} | Adrian Hautmann¹ | Frank Erdmann³ | Guoying Zhou¹ |
Sanja Stojanović^{4,5} | Stevo Najman^{4,5} | Thomas Groth^{1,2,6}

¹Department of Biomedical Materials, Institute of Pharmacy, Martin Luther University Halle Wittenberg, Halle (Saale), Germany

²Interdisciplinary Center of Materials Science, Martin Luther University Halle-Wittenberg, Halle (Saale), Germany

³Pharmaceutical Biology and Pharmacology Department, Institute of Pharmacy, Martin Luther University Halle Wittenberg, Halle (Saale), Germany

⁴Department of Biology and Human Genetics, Faculty of Medicine, University of Niš, Niš, Serbia

⁵Department for Cell and Tissue Engineering, Scientific Research Center for Biomedicine, Faculty of Medicine, University of Niš, Niš, Serbia

⁶Laboratory of Biomedical Nanotechnologies, Institute of Bionic Technologies and Engineering, I.M. Sechenov First Moscow State University, Moscow, Russian Federation

Correspondence

Thomas Groth, Department of Biomedical Materials, Institute of Pharmacy, Martin Luther University Halle Wittenberg, Heinrich Damerow Strasse 4, D 06120 Halle (Saale), Germany.
Email: thomas.groth@pharmazie.uni-halle.de

Funding information

Ministry of Education, Science and Technological Development of the Republic of Serbia; German Academic Exchange Service

Abstract

Inflammation and subsequent fibrotic encapsulation that occur after implantation of biomaterials are issues that fostered efforts in designing novel biocompatible materials to modulate the immune response. In this study, glycosaminoglycans (GAG) like hyaluronic acid (HA) and heparin (Hep) that possess anti-inflammatory activity were covalently bound to NH₂-modified surfaces using EDC/NHS cross-linking chemistry. Immobilization and physical surface properties were characterized by atomic forces microscopy, water contact angle studies and streaming potential measurements demonstrating the presence of GAG on the surfaces that became more hydrophilic and negatively charged compared to NH₂-modified. THP-1 derived macrophages were used here to study the mechanism of action of GAG to affect the inflammatory responses illuminated by studying macrophage adhesion, the formation of multinucleated giant cells (MNGCs) and IL-1 β release that were reduced on GAG-modified surfaces. Detailed investigation of the signal transduction processes related to macrophage activation was performed by immunofluorescence staining of NF- κ B (p65 subunit) together with immunoblotting. We studied also association and translocation of FITC-labeled GAG. The results show a significant decrease in NF- κ B level as well as the ability of macrophages to associate with and take up HA and Hep. These results illustrate that the anti-inflammatory activity of GAG is not only related to making surfaces more hydrophilic, but also their active involvement in signal transduction processes related to inflammatory reactions, which may pave the way to design new anti-inflammatory surface coatings for implantable biomedical devices.

KEYWORDS

cell adhesion and multinucleated giant cells formation, covalent immobilization, endocytosis immunoblotting, glycosaminoglycans, inflammation, macrophages, NF- κ B

1 | INTRODUCTION

Biomaterials are widely used to support and replace partially or completely tissues and organs to improve, augment, or restore biological functions (Brovold et al., 2018). However, implantation of biomaterials is followed by blood-material interaction, which leads to protein adsorption that can initiate an inflammatory cascade comprising injury, followed

by acute and chronic inflammation, formation of granulation tissue, foreign body response, and eventually fibrous encapsulation. This represents in the majority of cases an undesired event and is largely influenced by the characteristics of the implanted biomaterials, such as surface properties and compliance and shape (Vasconcelos, Águas, Barbosa, Pelegrin, & Barbosa, 2019; Velnar, Bunc, Klobucar, & Gradisnik, 2016). Macrophages play a significant role in the inflammation process and are

considered as key effector and dominant cells secreting pro-inflammatory cytokines such as IL-1 β and tumour necrosis factor- α (TNF α), chemokines and growth factors, such as monocyte chemoattracting protein 1 (MCP-1), transforming growth factor- β , and platelet-derived growth factor (Oishi & Manabe, 2018; Wynn & Vannella, 2016). In addition, macrophages may fuse on the biomaterial in an attempt to phagocytose the implant larger in size than themselves, forming foreign body giant cells, which represents also a sign of chronic inflammation (Kastellorizios, Tipnis, & Burgess, 2015; Moore & Kyriakides, 2015).

There is a multitude of attempts to dampen inflammatory response after biomaterial implantation. One capitalizes on passive mechanisms, based on hydrophilicity of materials and steric repulsion that shall reduce opsonization of the implant material. Hence, adsorption of proteins, like complement factors, immunoglobulins, coagulation factors, and others is reduced, which leads to decreased activation of leukocytes. However, it is difficult to have a long-term inhibition of protein adsorption. Therefore, the success of this approach is limited (Franz, Rammelt, Scharnweber, & Simon, 2011; Vroman, Adams, Fischer, & Munoz, 1980). Others are based on presence and release of anti-inflammatory drugs like nonsteroidal anti-inflammatory drugs (e.g., naproxen) that may reduce acute and chronic inflammation (Al-Khoury et al., 2019; Suarez et al., 2013). Quite recently, it was also discovered that biomaterial-induced inflammatory response can be attenuated by the use of glycosaminoglycans (GAG) like hyaluronic acid (HA) or heparin (Hep) that possess anti-inflammatory properties (Wu et al., 2015; Zhang et al., 2018). For instance, the presence of intact GAG like hyaluronan (HA) is considered as a tissue integrity signal that reduces inflammation through its binding to CD44, a cell-surface glycoprotein, which promotes the production of anti-inflammatory cytokines (IL-2 and IL-10; Altman et al., 2019; Chen et al., 2019). In addition, this interaction causes a negative regulation of the pro-inflammatory toll-like-receptor (TLR) signaling in which TLR is considered as an immunoreceptor mediator for NF- κ B activation (Avenoso et al., 2018). Furthermore, high molecular weight HA regulates T-cell populations by increasing the levels of transcription factor Foxp3 in regulatory T-cells (Tregs), a specialized sub-population of CD4+ T cells, thus promoting their function through enhanced anti-inflammatory cytokine production (Ruppert et al., 2014). On the other hand, the highly sulphated GAG heparin (Hep) has demonstrated many benefits in the prevention and treatment of venous thrombosis, pulmonary diseases, burns, but recently also in the control of inflammation (Paschoa, 2016; Shastri, Peterson, & Patel, 2017). Heparin can suppress the classical pathway of the complement system by regulating the complement factors C activity (Rent et al., 1975; Weiler, Edens, Linhardt, & Kapelanski, 1992), potentiating the C1 esterase inhibitor action (Caughman, Boackle, & Vesely, 1982), interfering with the binding of C1q to immune complexes (Golan, Burger, & Loos, 1982) and inhibiting the interaction of C1s with C4 and C2 (Loos, Volanakis, & Stroud, 1976). Heparin and Hep-related compounds like heparin sulphate also inactivate chemokines through its binding to Hep-binding proteins which eventually prevent the activation and recruitment of inflammatory cells into tissue (Poterucha, Libby, & Goldhaber, 2017; Young, 2008). It has been shown also to possess an inhibitory effect on the nuclear transcription factor- κ B (NF- κ B), which in

turn suppresses leukocyte activation as well as pro-inflammatory cytokine production (Qi, Zhang, & Wang, 2016). The NF- κ B signaling pathway is inhibited by two different mechanisms with Hep; first one is by inhibiting the translocation of the transcription factor into the nucleus, while the second one is that Hep interferes nonspecifically to DNA binding of NF- κ B in the nucleus (Lee, Lee, Seo, Kim, & Ahn, 2007).

It has been shown previously that the NF- κ B pathway is essential in a variety of physiological processes like control of the immune response, cell proliferation, and death (Hayden & Ghosh, 2004). It has been also identified as key factor in inflammation having a direct influence on downregulating cytokine release (Lawrence, 2009). In other words, the inhibition of NF- κ B can potentially reduce inflammatory-related gene activation and regulate the gene expression and production of pro-inflammatory cytokines, chemokines, and adhesion molecules (Thourani et al., 2000). The NF- κ B transcription factor family consists of a wide variety of subunits, which share the same Rel homology domain (RHD, a protein domain), responsible for dimerization, inhibitor binding, nuclear translocation, and DNA binding (Hayden & Ghosh, 2008; Wan & Lenardo, 2009). Therefore, during activation, the inhibitory protein family (I κ Bs) gets degraded, leaving the NF- κ B, which can then translocate to the nucleus (Hayden & Ghosh, 2004).

In previous studies, we have shown that both covalent monolayer and adsorptive multilayer immobilization of GAG on model surfaces led to a reduction of inflammatory response of macrophages (Zhou, Al-Khoury, & Groth, 2016; Zhou, Niepel, Saretia, & Groth, 2016). Here, we extend these finding focusing on the effect of covalently immobilized HA and Hep toward the inhibition of p65 subunit translocation to the nuclear area and of phosphorylation of NF- κ B protein family, which is related to activation of THP-1 monocyte-derived macrophages (Chanput, Mes, & Wichers, 2014) in terms of NF- κ B pathway suppression by these covalently immobilized GAGs.

2 | MATERIALS AND METHODS

2.1 | Chemicals for surface modification

Glass cover slips were obtained from Menzel GmbH (Bielefeld, Germany) of (\varnothing 12 and 15 mm) surfaces. Silicon wafers were provided from LG Siltron Inc. (Gumi, Korea) of (10 \times 10) mm² surface. In addition, 3-Aminopropyltriethoxysilane 98% (APTES) were delivered from ABCR GmbH & CO. KG (Karlsruhe, Germany). HA was provided as a kind gift from M. Schnabelrauch, Innovent e.V. (Jena, Germany), while heparin (Hep) was obtained from Serva (Heidelberg, Germany). 1-(3-Dimethylaminopropyl)-3-ethylcarbodiimide hydrochloride, 98 + % (EDC) was purchased from Thermo Fischer Kandel GmbH (Karlsruhe, Germany) while N-Hydroxy-succinimide 98% (NHS) was obtained from Sigma-Aldrich (Taufkirchen, Germany). Acetone \geq 99.5% was provided from Roth (Karlsruhe, Germany) and Ethylene diamine from Sigma-Aldrich (Taufkirchen, Germany). 2-(N-Morpholino) ethaneulphonic acid monohydrate (MES) was purchased from VWR International Ltd. (Hunter Boulevard, England). Ammonia and hydrogen peroxide were delivered from Th. Geyer GmbH & Co. KG 25% and Roth 30%

(Renningen, Karlsruhe, Germany), respectively. AFM tips were obtained from AppNano (Applied Nanostructures Inc., Santa Clara, CA).

2.1.1 | Preparation of amino-terminated surfaces

Silicon wafers and glass cover slips were used for modification with APTES to generate amino groups for subsequent immobilization of GAG. The substrates were cleaned using the Radio Corporation of America cleaning protocol which is based of mixing a solution of ammonia, hydrogen peroxide, and water (1:1:5, v/v/v) at 75°C for 10 min, respectively. Then, ultrapure water (6 × 5 min) was used to wash the substrates with a further drying step by a stream of nitrogen (Macek, 1993). Furthermore, 2% (v/v) solution of APTES in 99.8% acetone was prepared to immerse the substrates for 1 hr at room temperature (RT). The resulted NH₂-modified surfaces were rinsed extensively with acetone, ethanol and washed with double-distilled water (8 × 5 min) then dried with a stream of nitrogen.

2.1.2 | Immobilization of GAG onto amino-terminated surfaces

MES buffer at a concentration of 50 mM at pH 4.70 was prepared. GAG solutions of HA ($M_w \approx 1.3$ MDa) and heparin (Hep, $M_w \approx 15$ kDa) at a concentration of 2 mg ml⁻¹ were dissolved in the aforementioned buffer. Subsequently, EDC and NHS at a concentration of 5 and 3 mg ml⁻¹, respectively were added for 30 min at RT to the GAG solutions (Hermanson, 1996). Thereafter, the EDC/NHS-activated GAG solutions were immobilized on the NH₂-terminated surfaces for 24 hr with light protection. Afterward, an inactivation of the remaining reactive carboxyl species of the EDC linker was achieved by immersing the samples in 1 M ethylene diamine solution for 10 min. The slides were rinsed with ethanol and washed with double-distilled water (6 × 5 min) then dried under nitrogen flow (Köwitsch et al., 2011).

2.1.3 | Labelling of GAG

The fluorescein isothiocyanate (FITC)-labeled GAG were prepared to determine the localization of stained HA and Hep within the cells according to a protocol published recently (Kowitsch et al., 2014). HA and Hep at a concentration of 2 mg ml⁻¹ were dissolved in a 50 mM MES-buffer (pH adjusted to 4.75). Thereafter, ×2 mmol of EDC and ×2 mmol of NHS were added to the GAG solutions under continuous stirring for 1 hr with further pH adjustment to 7.0. The concentrations were adjusted to obtain 10% labeled carboxylic groups with fluorescein. Subsequently, a solution of 1 mg ml⁻¹ of 6-aminofluorescein in dimethyl sulfoxide was added overnight. Eventually, the solutions were dialyzed against double-distilled water for 3 days with a subsequent freeze drying step. All steps were performed under light protection.

2.2 | Characterization of surfaces

2.2.1 | Atomic force microscopy (AFM)

Surface topography of NH₂ and GAG-modified silicon wafers (Si) was investigated using AFM (Nano-R, Pacific Nanotechnology, Santa Clara, CA). The Si wafers (10 × 10 mm²) were probed in contact mode under ambient (air) laboratory conditions of temperature and humidity. AFM tips with 125 μm length, 35 μm width, 14–16 μm height, and tip radius of <10 nm were used for imaging. The used scan area was 10 × 10 μm² per image with a scan rate of 0.2 Hz and a resolution of (512 × 512 pixel²). Image processing was done using the Gwiddyon software (version 2.40).

2.2.2 | Water contact angle measurements

The sessile drop method was used for static water contact angle (WCA) measurements using OCA 15+ device from Dataphysics (Filderstadt, Germany). Here, five droplets of 2 μl ultrapure water were applied to each sample at RT. Consequently, the experimental values were used to calculate the mean and standard deviation of two independent experiments.

2.2.3 | Streaming potential measurements

Streaming potential measurements were performed with a SurPASS device (Anton Paar, Graz, Austria). Two identically modified glass slides were mounted oppositely into the adjustable measurement chamber. The flow of electrolyte (1 mM KCl in water) was adjusted to a distance to maintain 300 mbar as a maximum pressure. Hydrochloric acid (HCl) at concentration 0.1 M was used for pH titration. In addition, the pH value was adjusted to pH 10.5 using 1 M sodium hydroxide (NaOH) before starting a measurement. Finally, the measurements were carried out with an automated titration ranged from pH 10.5 to pH 2.25, which was adjusted by two titration steps: 0.03 ml from pH 10.5 to pH 5.0 and 0.25 ml from pH 5.0 to pH 3.0.

2.3 | Studies with THP-1 derived macrophages

2.3.1 | Cell culture

The THP-1 human monocytic cells (DSMZ, Braunschweig, Germany) were cultured in RPMI-1640 medium (Lonza, Wuppertal, Germany) supplemented with 10% (v/v) fetal bovine serum (FBS, Biochrom AG, Berlin, Germany) and 1% (v/v) antibiotic-antimycotic solution (AAS, Lonza, Wuppertal, Germany) at 37°C in a humidified 5% CO₂/95% air atmosphere using a NUAIRE® DH Autoflow incubator (NuAire, Plymouth, MN). Every second day the nonadherent cells were passaged to maintain a cell density of 1 × 10⁶ cells ml⁻¹. THP-1 derived macrophages were obtained by incubation of floating monocytes with 200 nM phorbol-12-myristate-13-acetate (PMA, Sigma Aldrich, Darmstadt, Germany) in T75 cell culture

flasks (Greiner Bio-One GmbH & Co. KG, Frickenhausen, Germany) for 48 hr, as reported in literature (Zhou et al., 2010). Thereafter, macrophages were detached using 0.25% trypsin/0.02% EDTA (Biochrom AG, Berlin, Germany) with further addition of serum-containing RPMI-1640 medium to stop the activity of trypsin. Eventually, the harvested cells were used for seeding on the different modified surfaces.

2.3.2 | Cell adhesion studies

The modified substrates were sterilized with 70% ethanol for 15 min and rinsed twice with phosphate buffer saline (PBS). Macrophages were seeded on either NH₂-terminated and HA- or Hep-modified surfaces at a cell density of 2.5×10^4 cells ml⁻¹ in serum-containing RPMI-1640 medium (10% FBS). Samples were incubated for 24 hr at 37°C in a humidified 5% CO₂/95% air atmosphere. Thereafter, the nonadherent cells were gently washed twice with PBS. Attached cells were fixed with cold methanol (Roth, Karlsruhe, Germany) for 10 min and stained with 10% (v/v) Giemsa (Merck KGaA, Darmstadt, Germany) in ultrapure water for another 10 min. The cells were photographed with a transmitted light microscope (Nikon ECLIPSE Ti2, Tokyo, Japan) equipped with a CCD camera (DCIN, 12 V, EXT1/0, Tokyo, Japan) to evaluate cell count and morphology using the ImageJ software (version 1.46r).

2.3.3 | Multinucleated giant cells (MNGCs) characterization

The MNGCs formation was evaluated after 10 days culture of macrophages seeded as described in the previous section using a cell density of 2.5×10^5 cells ml⁻¹. The higher cell density compared to cell adhesion experiments was chosen to permit aggregation of macrophages as prerequisite for their fusion. The modified surfaces with cells were gently washed twice with PBS. Attached cells were fixed with cold methanol and stained with 10% (v/v) Giemsa in ultrapure water as described in the adhesion studies. Micrographs of macrophages were taken by a transmitted light microscope equipped with a CCD camera (Axiovert 100, Carl Zeiss, Oberkochen, Germany) and the area percentage of MNGCs was calculated by the ImageJ software as described in our previous articles (Zhou, Al-Khoury, & Groth, 2016; Zhou, Niepel, et al., 2016).

2.3.4 | IL-1β production measurement

Macrophages were seeded at a cell density of 5.0×10^5 cells ml⁻¹ on the modified surfaces and incubated for 24 hr in presence or absence of 1 μg ml⁻¹ lipopolysaccharide (LPS, Sigma Aldrich, Darmstadt, Germany). The cytokine containing supernatants, both with LPS treatment and without LPS, were collected and stored at -20°C until needed for investigation. The IL-1β production was measured using an ELISA kit following the manufacturers' instructions (Thermo Scientific, Bonn, Germany).

2.3.5 | Immunofluorescence (IF) staining of NF-κB

The translocation of p65 subunit of NF-κB to the nuclear area was evaluated by immunostaining according to the method developed by Noursadeghi et al. (2008). FITC-labeled HA and Hep were immobilized on NH₂-modified slides. Macrophages were seeded on modified surfaces at a density of 2.5×10^5 cells ml⁻¹ in serum-containing RPMI 1640 medium and incubated for 48 hr at 37°C in a humidified 5% CO₂/95% air atmosphere. Two sets of samples were analyzed to compare between the absence and presence of 1 μg ml⁻¹ LPS (Sigma Aldrich). Thereafter, cells cultured on modified surfaces were fixed with 4% paraformaldehyde (Sigma Aldrich, Darmstadt, Germany) for 15 min, permeabilized with 0.1% (v/v) Triton[®] X-100 (Sigma-Aldrich, Taufkirchen, Germany) for 10 min at RT, and rinsed twice with PBS. The nonspecific binding sites were blocked with a 1% (w/v) bovine serum albumin ≥98% (BSA, Carl Roth GmbH, Halle (Saale), Germany) in PBS for 30 min. Subsequently, cells were incubated with monoclonal p65 subunit of NF-κB antibody (1:100, Santa Cruz Biotechnology, Dallas, TX) at 4°C overnight. After washing with PBS for 5 min on a shaker, a secondary monoclonal anti-rabbit IgG antibody conjugated with CY2 (1:200, Jackson Immunoresearch, Ely, UK) was applied for another 30 min at RT. The nuclei were stained with TO-PRO-3 (1:500, Invitrogen) for 40 min at RT. Finally, the samples were mounted on glass slides with polyvinyl alcohol (PVA, Sigma Aldrich, Darmstadt, Germany) and examined on confocal microscope LSM 710 (Carl Zeiss) using a 40-fold oil immersion objective. Image processing was done with ImageJ (v.1.52i). The TO-PRO-3 channel was used to mask a region of interest (ROI) representing the nucleus, while the Cy2 channel was used to mask a cellular ROI. Then the nuclear ROI was subtracted from the cellular ROI to obtain a cytosolic ROI. Finally, the fluorescence intensity was evaluated in the nuclear and cytosolic ROI and a ratio calculated. The principle of the method is visualized in Figure S1.

2.3.6 | Cell lysis for immunoblotting (IB)

Macrophages differentiated from THP-1 monocytic cell line as described above were seeded at cell density of 52×10^5 cells ml⁻¹ for 48 hr on NH₂ as well as GAG-modified samples (glass slides with a total area of 19.76 cm², Menzel GmbH, Bielefeld, Germany). The four-well plates (Greiner Bio-one, Leipzig, Germany) were placed on ice and the cells were washed twice with ice-cold PBS. Thereafter, cell lysate buffer (RIPA buffer) with protease and phosphatase inhibitors (ThermoFisher Scientific, Waltham, MA) was added and the macrophages were scraped using a cold plastic cell scraper. Subsequently, the cell lysates were gently transferred to precooled tubes and a constant agitation at 4°C for 30 min was maintained. In addition, the cell lysates were centrifuged at 4°C and 13,000 rpm for 20 min with subsequent storage of the supernatants at -80°C up to 1 month before performance of IB.

2.3.7 | Bicinchoninic acid protein assay

The bicinchoninic acid (BCA) test was performed according to the manual of the Pierce BCA Protein Assay Kit (Thermo Scientific, Bonn, Germany). A working solution was prepared by mixing 50 parts of BCA Reagent A with 1 part of BCA Reagent B. Thereafter, 25 μl of cell lysates were pipetted in a 96-well plate and 200 μl working solution was added. The samples were incubated for 30 min at 37°C. Then, the absorbance was measured at 562 nm with a plate reader (Fluostar Optima, BMG LABTECH, Offenburg, Germany).

2.3.8 | SDS-PAGE and Western blotting

Twenty-five micro liter of cell lysates were separated by PAGE using 15% SDS-polyacrylamide gels. Then, immunoblotting was done using nitrocellulose membranes (Schleicher & Schuell). Membranes were blocked in 3% (w/v) milk powder in TBS-T, probed with monoclonal antibodies against phospho-NF-κB (CST, #3033), NF-κB (Santa Cruz Biotechnology, sc-8008), and β-actin (MERCK, A1978), followed by incubation with HRP-labeled secondary antibodies and visualized with the enhanced chemiluminescence reaction (ThermoFisher Scientific) in a ChemiDoc Imaging System (Biorad). Obtained grayscale images were densitometrically analyzed by the Li-Cor Image Studio software using automatic background determination and subtraction function. Results of two samples were used to calculate means.

2.3.9 | Association of FITC-GAG with macrophages studied by confocal laser scanning microscopy

Macrophages were seeded on the NH₂-terminated and FITC-labeled HA and Hep modified surfaces at a concentration of 2.5×10^5 cells ml⁻¹ for 24 hr, then fixed for 10 min with 4% paraformaldehyde (Sigma Aldrich, Darmstadt, Germany). Afterward, the red fluorescent carbocyanine solution, a cytoplasmic membrane dye (DID, Biotium, Fremont, CA), was prepared at a ratio of 5 μl to 1 ml PBS, 0.5 ml, added to each sample and incubated for 10 min to stain macrophages. Eventually, all samples were washed twice with PBS, mounted on objective slides using polyvinyl alcohol (PVA, Sigma Aldrich, Darmstadt, Germany) and examined with confocal laser scanning microscopy (CLSM) using ×63 oil immersion objective (LSM 710, Carl Zeiss). Images were processed using the ZEN2011 software (Carl Zeiss).

2.3.10 | Uptake of FITC-GAG by macrophages studied with flow cytometry

Macrophages were seeded for 48 hr as described above preparing two sets of samples with presence and absence of LPS. Thereafter,

the modified surfaces were transferred to new well plates, gently washed with PBS. Then, 300 μl of 0.25% Trypsin was added for 3 min with further addition of serum-containing RPMI 1640 medium to stop the trypsin effect. The cells were scraped-off, centrifuged, washed once with PBS and re-suspended in 200 μl PBS. Finally, 100 μl cell suspension was transferred to 96-well plate and measured with a flow cytometry device (LSR Fortessa II, BD Bioscience, Germany). The data were analyzed with the FACS-Diva software (version 6.2).

2.4 | Statistics

Kruskal-Wallis and one-way analysis of variance (ANOVA) followed by posthoc Tukey's test using the Origin 8 Pro software (Origin Lab, Northampton, MA) were used for statistical calculations. Data are presented as mean values ± standard deviations (SD) or medians with box plots. The number of samples has been indicated in the respective figure captions. Statistical significance was considered for $p \leq .05$ and is indicated by asterisks in the figures.

3 | RESULTS

3.1 | Characterization of surface properties

The modified surfaces were investigated toward surface topography with AFM. It can be seen in Figure 1a that the immobilization of HA and heparin (Hep) resulted in slight changes of the topography in comparison to NH₂-modified control surfaces. In addition, smoother surfaces were achieved after the immobilization of both GAG, which was considered as an evidence of complete coating of the substratum with HA and Hep.

The wetting properties of plain NH₂-terminated surfaces and those modified by covalent immobilization of either HA or Hep were determined by static WCA measurements. Figure 1b demonstrates a significant increase in the hydrophilicity of GAG-modified samples compared to NH₂-terminated surfaces. In addition, a significant difference between the HA and Hep was found with Hep being the most hydrophilic surface. Furthermore, Figure 1c shows the zeta-potentials of samples in dependence on the pH of electrolyte solution (1 mM KCl). It shows a clear difference between all surfaces with a sequence of NH₂, HA, and Hep, which corresponded well with the chemical composition of substrata.

3.2 | Adhesion and fusion of macrophages

In Figure 2a, the micrographs of macrophages cultured for 24 hr on modified surfaces are shown, representing the adhesion and shape of cells. Macrophages showed highest adherence on the NH₂-terminated surfaces with a spread and elongated shape, while a lower quantity of cells with more round shape were seen on HA, while cells on Hep

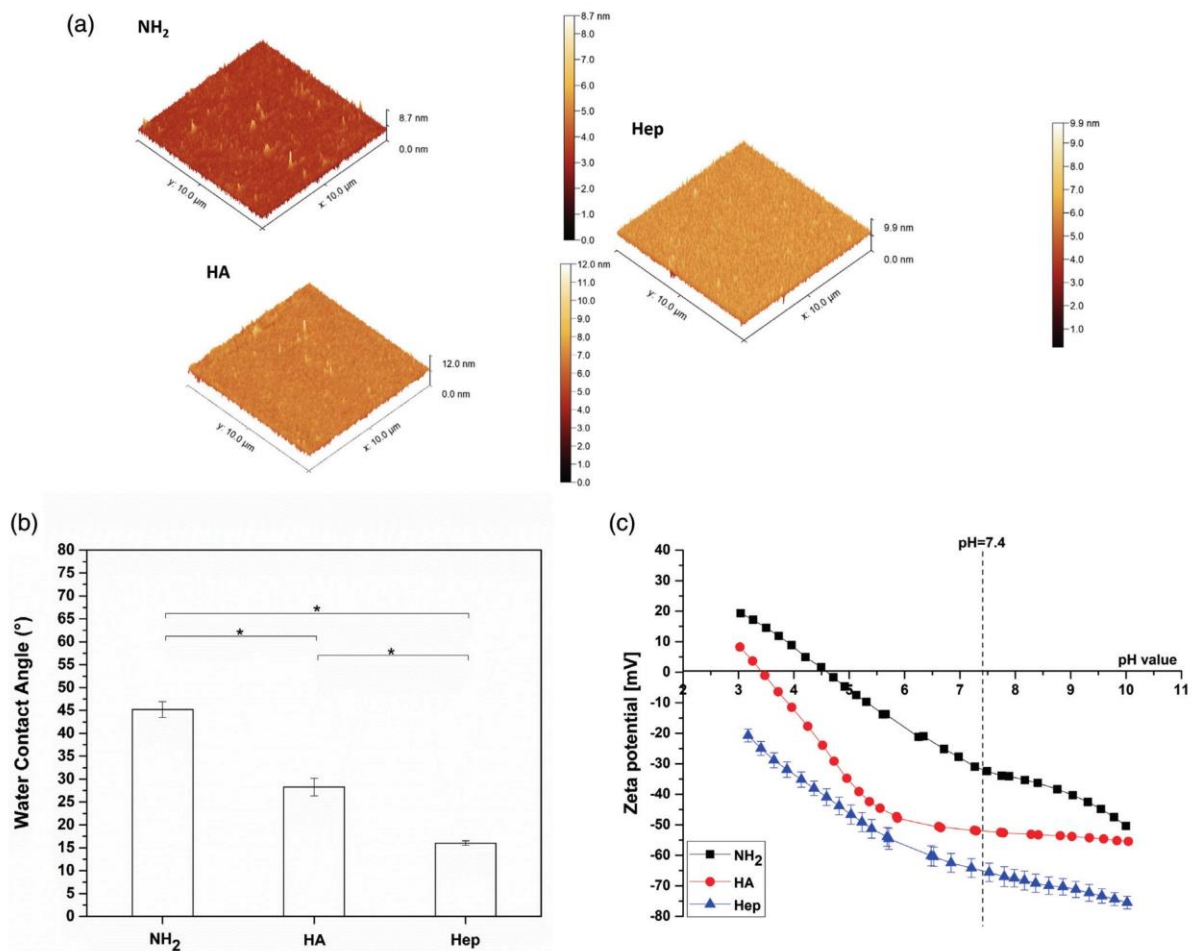


FIGURE 1 (a) Atomic force microscopy (AFM) images to visualize surface topography of the aminoterminated (NH₂) and NH₂ modified with covalent immobilization of either hyaluronic acid (HA) or heparin (Hep). (b) Static water contact angle measurements using the sessile drop method to characterize surface wettability of amino-terminated surfaces (NH₂) and covalent immobilization of either hyaluronic acid (HA) or heparin (Hep). Results are presented as means ± SD, **p* < .05, *n* = 5. (c) Zeta potentials of aminoterminated surfaces (NH₂) and covalent immobilization of either HA or Hep, abbreviated as (NH₂ [■], HA [●], and Hep [▲]), respectively. Results are presented as means ± SD in the pH range 10–3.0

were fewer and had a more elongated phenotype. The number of adherent macrophages per area shown in Figure 2b displays the highest cell adhesion on NH₂-terminated surfaces, followed by Hep, while the lowest adhesion of macrophages was found on HA-coated samples. In addition, Figure 2c shows the aspect ratio of adherent macrophages with a clear trend of enhanced cell polarization on the NH₂-terminated samples. By contrast, the mean and median values of aspect ratio illustrated a significant decrease on HA-modified samples and higher again on Hep-coated surface in accordance with the micrographs.

Figure 3a shows the micrographs of the MNGCs formation obtained after 10 days culture of cells in serum-containing medium. Evaluation of macrophage fusion showed that the significantly highest was observed on the NH₂ surfaces in terms of number of nuclei (≥2)

per cell body and size of MNGC. In contrast, the GAG-modified surfaces lowered significantly the fusion extent. Subsequently, image analysis software was used to evaluate the area percentage of the MNGC, which is illustrated in Figure 3b. The GAG-modified surfaces showed a significant reduced percentage of MNGC in comparison to the NH₂-coated samples

3.2.1 | IL-1β pro-inflammatory cytokine release

The IL-1β production was analyzed after 24 hr of cultivation of cells with (black bars) or without (white bars) LPS stimulation as shown in Figure 4. A higher release of IL-1β was noticed in cell culture supernatants of macrophages cultured on NH₂ samples both in presence or absence of LPS.

FIGURE 2 (a) Transmitted light microscopic images of adherent macrophages stained with 10% (v/v) Giemsa after 24 hr cultivation on the amino-terminated surfaces (NH₂) and covalent immobilization of either hyaluronic acid (HA) or heparin (Hep). (Scale bar: 100 μm). (b) Number of adherent macrophages per surface area after 24 hr of incubation. Data represent means ± SD, *n* = 5, **p* ≤ .05. (c) Aspect ratio of adherent macrophages. The box plot indicates the 25th and 75th percentile, the lowest and highest values are represented by the whiskers, whereas the median (horizontal line) and mean value (black square) are shown as well

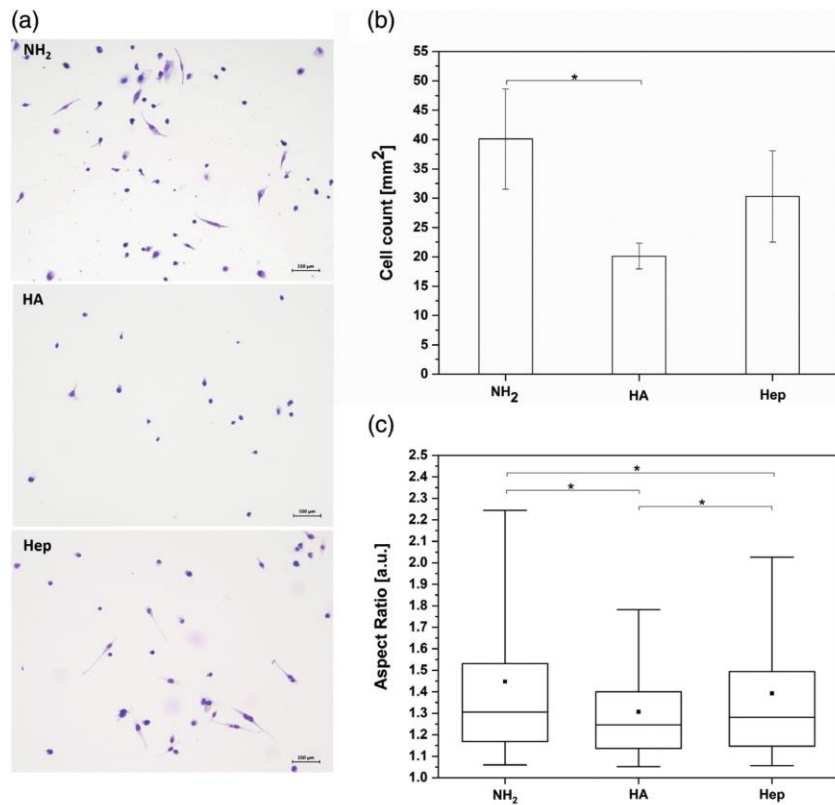
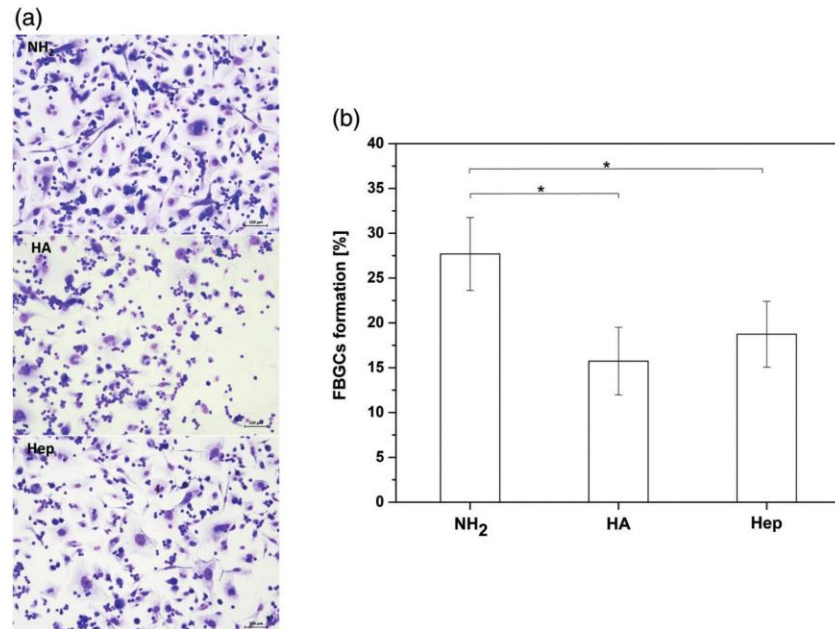


FIGURE 3 (a) Transmitted light microscopic images of multinucleated giant cells (MNGCs) stained with 10% (v/v) Giemsa after 10 days incubation on the amino-terminated surfaces (NH₂) and NH₂ modified with covalent immobilization of either hyaluronic acid (HA) or heparin (Hep). (Scale bar: 100 μm). (b) The area percentage of formed MNGCs on NH₂, HA and Hep surfaces by quantitative evaluation of micrographs. Results are the means ± SD, **p* < .05, *n* = 10



On the other hand, the GAG-modified surfaces significantly lowered the IL-1β release, which was observed under both conditions. In addition, it can be noticed that IL-1β secretion by THP-1 derived macrophages was

upregulated in all samples when stimulated with LPS, which indicates their responsiveness and functional activity of THP-1-derived macrophages during the studies.

3.2.2 | IF staining of NF-κB in macrophages

Figure 5a shows TO-PRO-3 staining (blue) of macrophage nuclei and staining of nonphosphorylated p65 subunit of NF-κB (green) that was found both in cell cytoplasm and nuclei. The quantitative evaluation of the ratio of nuclear to cytoplasmic was used as an indicator for translocation of NF-κB and is shown in Figure 5b. It was highest in macrophages on the control NH₂ surfaces; both in the presence and absence of LPS. A significant reduction of the nuclear to cytoplasmic

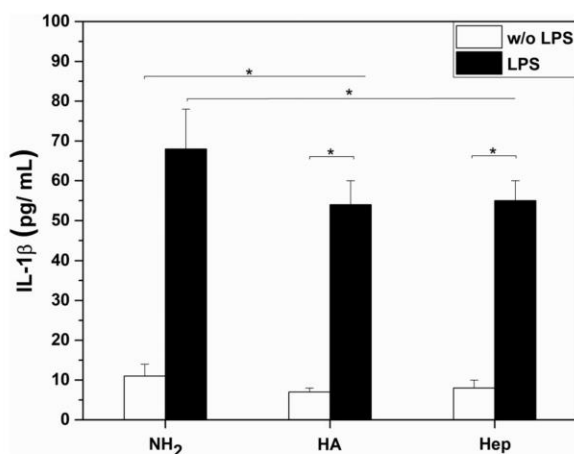


FIGURE 4 IL-1β production by macrophages after 24 hr of cultivation in the absence (white bars) and presence (black bars) of lipopolysaccharide (LPS) on the amino-terminated surface (NH₂) and NH₂ modified by covalent immobilization of either hyaluronic acid (HA) or heparin (Hep). Data represent mean ± SD, n = 6, *p ≤ .05

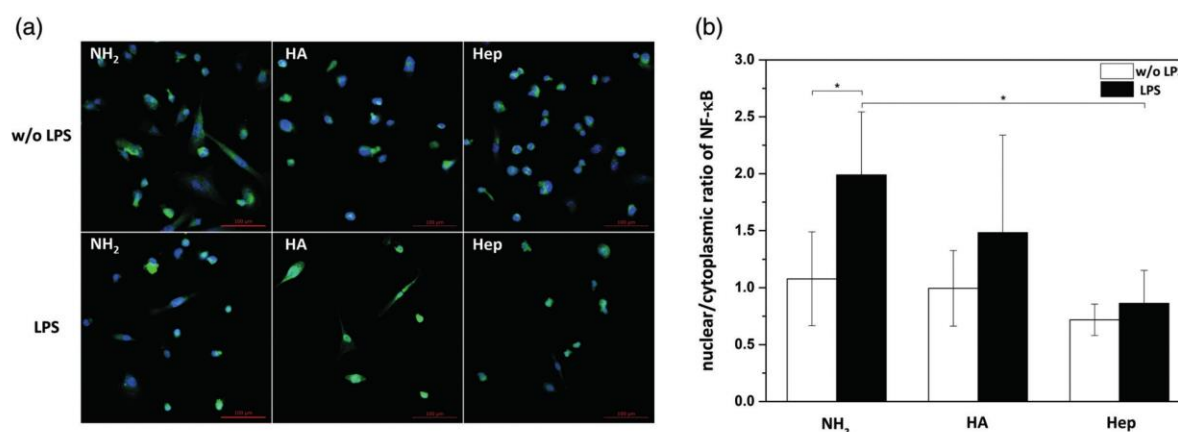


FIGURE 5 (a) TO-PRO-3 (blue color) and p65 followed by CY2 staining (green color) of the nucleus and the cytoplasm are shown for unstimulated (upper row) and of 1 μg ml⁻¹ Lipopolysaccharide (LPS) stimulated macrophages (lower row). The cells were seeded for 48 hr on the amino-terminated surfaces (NH₂) and NH₂ modified with covalent immobilization of either hyaluronic acid (HA) or heparin (Hep). The sequential processing using the ImageJ software is shown to produce binary masks of nuclear and cytoplasmic regions of interest (ROI). (Scale bar: 100 μm). (b) Quantification of nuclear to cytoplasmic ratio in the absence (white bars) and the presence (black bars) of LPS on the NH₂, HA and Hep surfaces, which can be translated as amount of p65 in the nucleus compared to the cytosol. Data represent mean ± SD, n = 10, *p ≤ .05

ratio was found comparing NH₂ surfaces with that of GAG immobilization. Hep shows the highest suppression of translocation of p65 into the nucleus both in absence and presence of LPS

3.2.3 | Western blotting

Figure 6a shows the blots from macrophage cell lysates showing both the bands for phosphorylated p65 of NF-κB (pNF-κB) and actin with the latter used for normalization of densitometry data. The bands of two cell lysates from duplicate samples illustrate higher phosphorylation of NF-κB on NH₂-terminated surfaces in comparison to GAG-modified. It was also observed that the LPS stimulation upregulated the phosphorylation of pNF-κB. Furthermore, Figure 6b shows the quantitative values of pNF-κB in macrophages plated on GAG compared to the NH₂ samples evaluated by densitometry. Similar effects were found for both HA and Hep in terms of a reduced intensity of pNF-κB in the blots

3.2.4 | Association of GAG with macrophages studied by CLSM

Figure 7 shows selected images of DID-stained macrophages cultured on FITC-labeled GAG. The confocal images of macrophages on NH₂ terminated surfaces show the red staining of the cell membrane by DID. On the other hand, macrophages cultured on FITC-GAG-modified samples clearly show an association of FITC-labeled HA and Hep with DID stained cells. The 3D images in Figure 7 show that FITC-labeled HA seems to be mainly co-localized with the cell surface. By contrast, FITC-labeled Hep is seen rather intracellularly, with some apparent presence in the nuclear area. Higher amounts of FITC-labeled HA can

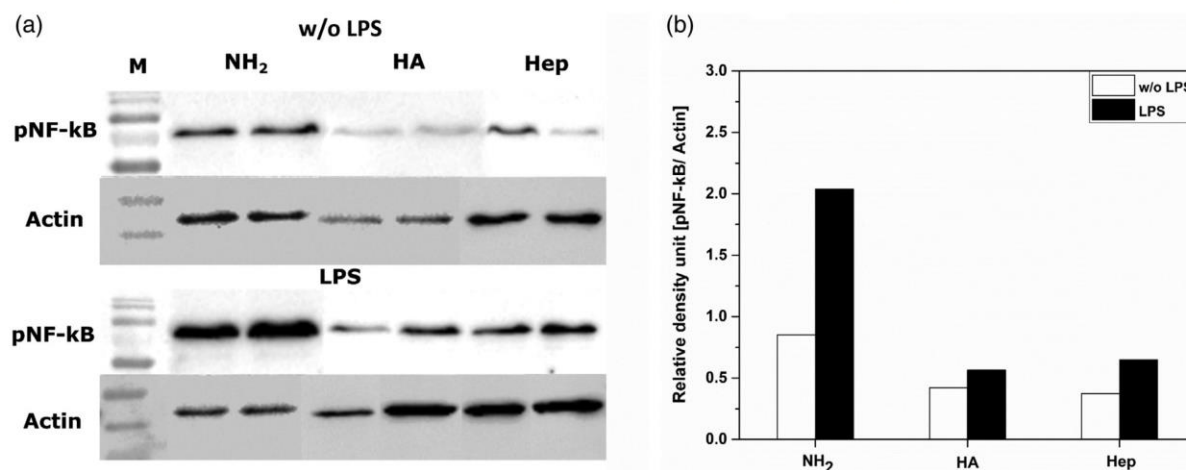


FIGURE 6 (a) Lysates from macrophages cultured on amino-terminated surfaces (NH₂) and NH₂ modified with covalent immobilization of either hyaluronic acid (HA) or heparin (Hep) in the absence and presence of lipopolysaccharide (LPS). The two cell lysates from duplicates of samples were collected after 48 hr and were blotted toward phosphorylated p65 subunit of NF-κB (pNF-κB). The blot was stripped and re-probed with anti-actin antibody (b) The immunoblotting bands were analyzed densitometrically and normalized to the actin content. The relative density of pNF-κB was evaluated in the absence (white bars) and the presence (black bars) of LPS. Data represent mean ± SD, *n* = 2

be seen on the surface of macrophages compared to smaller quantities of Hep inside the cells. Additional cell images are visualized in Figure S3 and S4.

3.2.5 | Association of FITC-labeled GAG with macrophages studied by flow cytometry

Two sets of samples were investigated in the absence (left column) and presence (right column) of 1 μg ml⁻¹ LPS. Figure 8a shows the flow cytometry histograms with side scatter (SSC). The raw data were obtained after setting the negative controls to a baseline by determining a threshold, beyond which, any signal was considered as a positive signal indicating association of FITC-labeled GAG with macrophages.

Here, the number of cells with fluorescence was measured, which represents the quantity of macrophages that are able to take up or associate with FITC-labeled-GAG. Figure 8b demonstrates that a significant difference between HA-coated and Hep-coated samples was found. The FITC-labeled HA showed a higher affinity to be associated with macrophages in comparison to FITC-labeled Hep. These findings are in accordance to the 3D images in Figure 7 obtained by CLSM.

4 | DISCUSSION

In this study, we tried to shed a light on the potential mechanism of anti-inflammatory action of HA or Hep regarding the signaling pathway of NF-κB, when these GAG were used to modify model biomaterials in a covalent manner. We confirmed here findings of previous studies that immobilization of these GAG diminishes activation of macrophages (Köwitsch, Zhou, & Groth, 2018). The observed effects

are related to a lowered translocation of NF-κB subunit p65 to the nuclear area and reduced phosphorylation of NF-κB on GAG-modified surfaces compared to a NH₂-terminated "pro-inflammatory" control surface.

Physical characterization of the surfaces showed that NH₂-terminated control surfaces were less hydrophilic and negatively charged than GAG-modified, which is related to the presence of amino groups (Fauchoux, Schweiss, Lützwow, Werner, & Groth, 2004). HA and Hep-modified surfaces were more hydrophilic and negatively charged indicated by lower WCA and zeta potentials, which is related to presence of carboxylic and sulfate groups. These findings correspond also well to our previous studies immobilizing oxidized GAG on NH₂-terminated surfaces (Yang et al., 2016). The different adhesion of macrophages might be related to differences adsorption of adhesion-mediating proteins like fibronectin from serum. NH₂-terminated surfaces bind significantly more than hydrophilic carboxyl or hydroxyl-terminated surfaces that promote adhesion and spreading of cells by integrin-mediated mechanisms (Fauchoux et al., 2004). Also other authors stated that highly hydrophilic and negatively charged surfaces lead to lower adhesion of cells when compared moderately wetttable materials (Bacakova, Filova, Parizek, Ruml, & Svorcik, 2011). Hence, coating of substrata with GAGs like HA and Hep may reduce adhesion of macrophages, which by itself diminishes propensity of inflammatory reactions. Indeed, this is not the only mechanism by which these GAGs are acting.

Studies on NF-κB signaling pathway were performed in an attempt to investigate the mechanism of anti-inflammatory action of GAG-modified surfaces that goes beyond making surfaces more hydrophilic and negatively charged. Based on IF staining of nonphosphorylated form of p65 subunit of NF-κB (Figure 5) lowest translocation of p65 to the nuclear region occurred in macrophages cultured on Hep-, followed

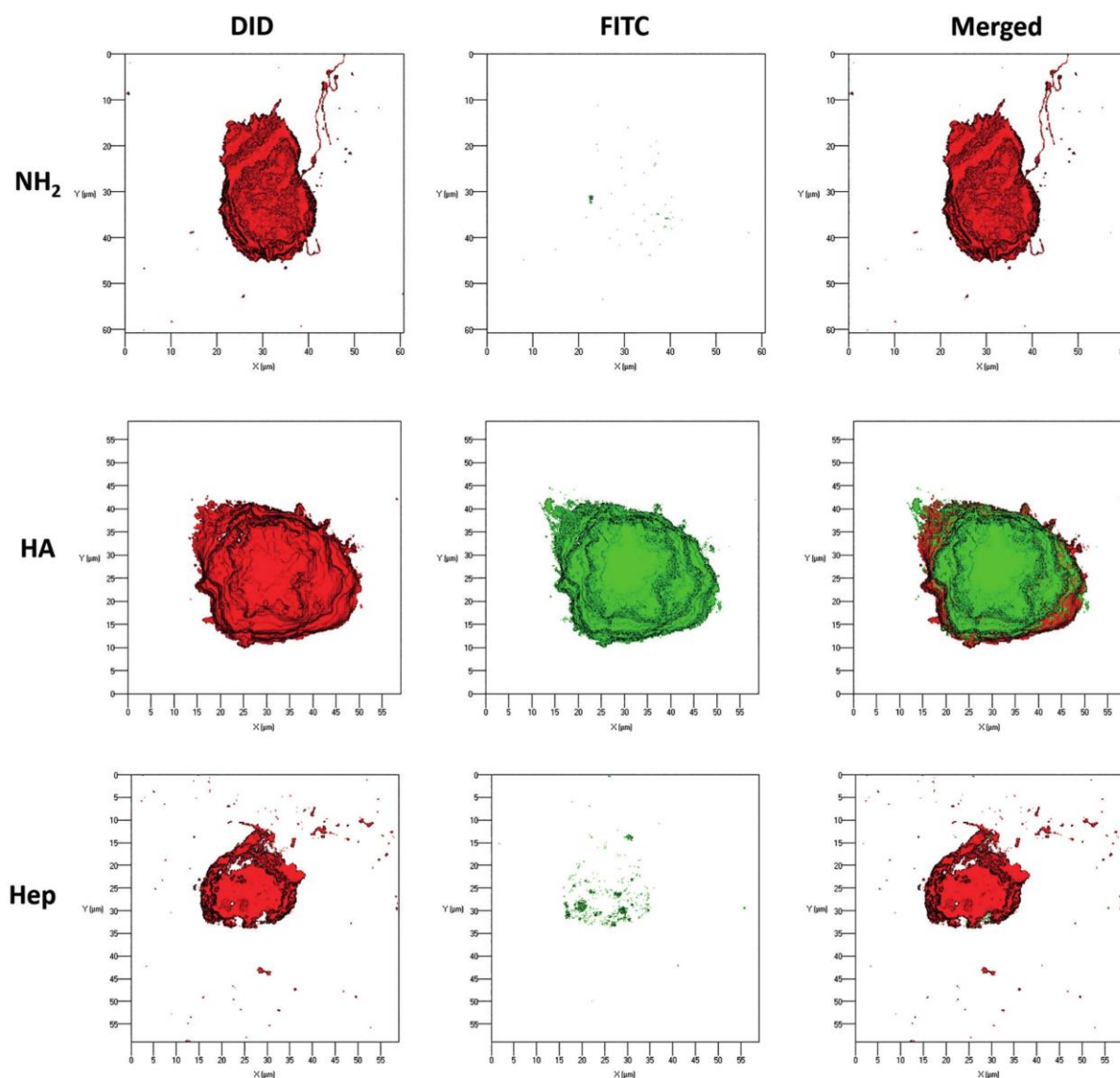


FIGURE 7 Representative 3D view of a z-stack in surface projection with confocal laser scanning microscopy (CLSM). Macrophages were cultured for 24 hr on amino-terminated surfaces (NH₂) and NH₂ modified with covalent immobilization of either hyaluronic acid (HA) or heparin (Hep). The cells were stained for DID (red, membrane staining) and the FITC-labeled GAG (green). (63-fold oil immersion objective, scale: 20 μ m). In this mode, pixel values are computed as solids, which allows no transparency

by HA-modified surfaces, which corresponds to the findings of others with soluble forms of heparin and related compounds (Young, 2008). In parallel, the immunoblotting of phosphorylated NF- κ B illustrated a lower intensity of bands in whole cell lysates from macrophages cultured on GAG-modified surfaces in comparison to NH₂-modified surfaces. This was considered as an additional evidence of the inhibitory effects of immobilized GAG on NF- κ B signaling pathways. These results are supported by reports from other groups indicating that Hep has two different mechanism of action on NF- κ B signaling pathway. One is through partial inhibition of NF- κ B translocation inside the nucleus

through the electrostatic binding of the positively charged transcription factor to the anionic Hep, taken up by endocytosis (Young, 2008; Young et al., 1999). The second is that Hep can activate the NF- κ B pathway through the phosphorylation of p65 allowing its translocation to the nucleus which further inhibits the binding of NF- κ B to DNA sequences (Lee et al., 2007). By contrast, HA possesses anti-inflammatory effects through its interactions to the cell surface receptor CD44, but also by suppression of toll-like receptors (TLR) signaling (Ruppert et al., 2014). The confocal images of DID stained macrophages demonstrated an association of FITC-labeled HA with the surface of

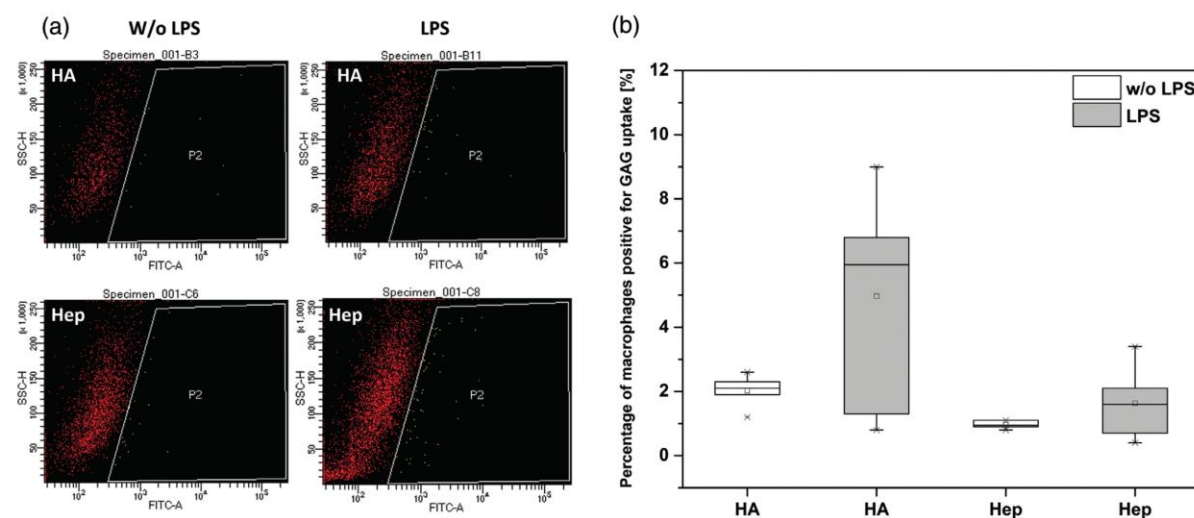


FIGURE 8 (a) Illustrative images of the flow cytometry measurements of macrophages cultured with either FITC-labeled hyaluronic acid (HA) or heparin (Hep) in the absence (left column) and presence (right column) of lipopolysaccharide (LPS). (b) The percentage of macrophages positive for GAG uptake after 48 hr cultivation on amino-terminated (NH_2) and NH_2 modified with covalent immobilization of either FITC-labeled hyaluronic acid (HA) or heparin (Hep), in the absence (white bars) and the presence (black bars) of LPS. Data represent mean \pm SD, $n = 6$, $*p \leq .05$

macrophages while on the other side an internalization of Hep in macrophages was found. The reason beyond the presence of anionic Hep inside macrophages might be due to either endocytosis or anionic transporters (Young, 2008). Indeed, the preparation of samples was based on covalent binding, which should provide a stable bond formation due to the chemical cross-linking process of GAG to amino groups on the substratum (Hermanson, 1996; Köwitsch et al., 2011). This was also observed here as we found no release of FITC-labeled GAG after covalent immobilization on NH_2 -modified surfaces (see Figure S2) Thus, we assume a partial release of GAG molecules from the samples through the activity of secreted reactive oxygen species (ROS), hyaluronidases and heparinases by macrophages that could be responsible for the mobilisation of HA and Hep (Li & Vlodavsky, 2009; Puissant & Boonen, 2016). In conclusion, Hep showed less translocation of the p65 into the cell nucleus as well as less intensity of pNF- κ B in whole cell lysates indicating the suppressive effect of Hep toward the NF- κ B signaling pathway, which was addressed recently by Young (Young, 2008). On the other hand, HA exerts its anti-inflammatory properties most likely through its association with the cell membrane by binding to CD44 as we did not find any evidence for an intracellular presence of HA and its way of action (Altman, Manjoo, Fierlinger, Niazi, & Nicholls, 2015).

5 | CONCLUSION

It can be concluded that HA and Hep possess a high potential to be used for making anti-inflammatory surface coatings based on the suppression of the canonical NF- κ B signaling pathway. This effect supports the idea of making hydrophilic coatings on biomaterial surfaces that reduce opsonisation (protein adsorption) and thus inflammatory response after implantation, but can be also combined directly with pharmaceutical effects by the anti-inflammatory activity of GAG like

hyaluronan and heparin. Hence, we conclude that coating of biomaterials with HA and Hep may have a significant impact in reducing the inflammatory response after implantation, which may increase functionality and lifetime of sensors and other implanted medical devices.

ACKNOWLEDGMENT

This work was financially supported through a PhD grant to Hala by the German Academic Exchange Service (DAAD). The study was also part of the project of bilateral cooperation funded by DAAD and Ministry of Education, Science and Technological Development of the Republic of Serbia (period 2019–2020). The kind support by Dr. rer.nat. Alexander Navarrete Santos from University Hospital of Martin Luther University Halle-Wittenberg doing flow cytometry is greatly appreciated.

CONFLICT OF INTEREST

There are no conflicts to declare.

ORCID

Thomas Groth  <https://orcid.org/0000-0001-6647-9657>

REFERENCES

- Al-Khoury, H., Espinosa-Cano, E., Rosa Aguilar, M., San Román, J., Syrowatka, F., Schmidt, G., & Groth, T. (2019). Anti-inflammatory surface coatings based on polyelectrolyte multilayers of heparin and polycationic nanoparticles of naproxen-bearing polymeric drugs. *Biomacromolecules*, 20(10), 4015–4025.
- Altman, R., Bedi, A., Manjoo, A., Niazi, F., Shaw, P., & Mease, P. (2019). Anti-inflammatory effects of intra-articular hyaluronic acid: A systematic review. *Cartilage*, 10(1), 43–52.
- Altman, R. D., Manjoo, A., Fierlinger, A., Niazi, F., & Nicholls, M. (2015). The mechanism of action for hyaluronic acid treatment in the osteoarthritic knee: A systematic review. *BMC Musculoskeletal Disorders*, 16(1), 321.

- Avenoso, A., D'Ascola, A., Scuruchi, M., Mandraffino, G., Calatroni, A., Saitta, A., ... Campo, G. M. (2018). Hyaluronan in the experimental injury of the cartilage: Biochemical action and protective effects. *Inflammation Research*, 67(1), 5–20.
- Bacakova, L., Filova, E., Parizek, M., Ruml, T., & Svorcik, V. (2011). Modulation of cell adhesion, proliferation and differentiation on materials designed for body implants. *Biotechnology Advances*, 29(6), 739–767.
- Brovold, M., Almeida, J. I., Pla-Palacin, I., Sainz-Arnal, P., Sánchez-Romero, N., Rivas, J. J., & Baptista, P. M. (2018). Naturally-derived biomaterials for tissue engineering applications. In *Novel Biomaterials for Regenerative Medicine* (pp. 421–449). USA: Springer.
- Caughman, G. B., Boackle, R. J., & Vesely, J. (1982). A postulated mechanism for heparin's potentiation of C1 inhibitor function. *Molecular Immunology*, 19(2), 287–295.
- Chanput, W., Mes, J. J., & Wichers, H. J. (2014). THP-1 cell line: an *in vitro* cell model for immune modulation approach. *International Immunopharmacology*, 23(1), 37–45.
- Chen, M., Li, L., Wang, Z., Li, P., Feng, F., & Zheng, X. (2019). High molecular weight hyaluronic acid regulates P. gingivalis-induced inflammation and migration in human gingival fibroblasts via MAPK and NF-κB signaling pathway. *Archives of Oral Biology*, 98, 75–80.
- Fauchoux, N., Schweiss, R., Lützw, K., Werner, C., & Groth, T. (2004). Self-assembled monolayers with different terminating groups as model substrates for cell adhesion studies. *Biomaterials*, 25(14), 2721–2730.
- Franz, S., Rammelt, S., Scharnweber, D., & Simon, J. C. (2011). Immune responses to implants—a review of the implications for the design of immunomodulatory biomaterials. *Biomaterials*, 32(28), 6692–6709.
- Golan, M., Burger, R., & Loos, M. (1982). Conformational changes in C1q after binding to immune complexes: Detection of neoantigens with monoclonal antibodies. *The Journal of Immunology*, 129(2), 445–447.
- Hayden, M. S., & Ghosh, S. (2004). Signaling to NF-κB. *Genes & Development*, 18(18), 2195–2224.
- Hayden, M. S., & Ghosh, S. (2008). Shared principles in NF-κB signaling. *Cell*, 132(3), 344–362.
- Hermanson, G. (1996). *Bioconjugate techniques* (pp. 185–186). USA: Academic Press.
- Kastellorizios, M., Tipnis, N., & Burgess, D. J. (2015). Foreign body reaction to subcutaneous implants. In *Immune Responses to Biosurfaces* (pp. 93–108). USA: Springer.
- Köwitsch, A., Yang, Y., Ma, N., Kuntsche, J., Mäder, K., & Groth, T. (2011). Bioactivity of immobilized hyaluronic acid derivatives regarding protein adsorption and cell adhesion. *Biotechnology and Applied Biochemistry*, 58(5), 376–389.
- Köwitsch, A., Zhou, G., & Groth, T. (2018). Medical application of glycosaminoglycans: A review. *Journal of Tissue Engineering and Regenerative Medicine*, 12(1), e23–e41.
- Köwitsch, A., Abreu, M. J., Chhalotre, A., Hielscher, M., Fischer, S., Mäder, K., & Groth, T. (2014). Synthesis of thiolated glycosaminoglycans and grafting to solid surfaces. *Carbohydrate Polymers*, 114, 344–351.
- Lawrence, T. (2009). The nuclear factor NF-κB pathway in inflammation. *Cold Spring Harbor Perspectives in Biology*, 1(6), a001651.
- Lee, J. H., Lee, J., Seo, G. H., Kim, C. H., & Ahn, Y. S. (2007). Heparin inhibits NF-κB activation and increases cell death in cerebral endothelial cells after oxygen-glucose deprivation. *Journal of Molecular Neuroscience*, 32(2), 145–154.
- Li, J.-p., & Vlodavsky, I. (2009). Heparin, heparan sulfate and heparanase in inflammatory reactions. *Thrombosis and Haemostasis*, 102(11), 823–828.
- Loos, M., Volanakis, J. E., & Stroud, R. M. (1976). Mode of interaction of different polyanions with the first (C1, C1), the second (C2) and the fourth (C4) component of complement-III: Inhibition of C4 and C2 binding site (s) on C1s by polyanions. *Immunochemistry*, 13(9), 789–791.
- Macek, M. (1993). A review of advanced wet cleaning. *Informacije MIDEM*, 23(4), 275–283.
- Moore, L. B., & Kyriakides, T. R. (2015). Molecular characterization of macrophage-biomaterial interactions. In *Immune Responses to Biosurfaces* (pp. 109–122). USA: Springer.
- Noursadeghi, M., Tsang, J., Hausteiner, T., Miller, R. F., Chain, B. M., & Katz, D. R. (2008). Quantitative imaging assay for NF-κB nuclear translocation in primary human macrophages. *Journal of Immunological Methods*, 329(1–2), 194–200.
- Oishi, Y., & Manabe, I. (2018). Macrophages in inflammation, repair and regeneration. *International Immunology*, 30(11), 511–528.
- Paschoa, A. F. (2016). Heparin: 100 years of pleiotropic effects. *Journal of Thrombosis and Thrombolysis*, 41(4), 636–643.
- Poterucha, T. J., Libby, P., & Goldhaber, S. Z. (2017). More than an anticoagulant: Do heparins have direct anti-inflammatory effects? *Thrombosis and Haemostasis*, 117(03), 437–444.
- Puissant, E., & Boonen, M. (2016). Monocytes/macrophages upregulate the hyaluronidase HYAL1 and adapt its subcellular trafficking to promote extracellular residency upon differentiation into osteoclasts. *PLoS One*, 11(10), e0165004.
- Qi, L., Zhang, X., & Wang, X. (2016). Heparin inhibits the inflammation and proliferation of human rheumatoid arthritis fibroblast-like synoviocytes through the NF-κB pathway. *Molecular Medicine Reports*, 14(4), 3743–3748.
- Rent, R., Ertel, N., Eisenstein, R., & Gewurz, H. (1975). Complement activation by interaction of polyanions and polycations: I. Heparin-protamine induced consumption of complement. *The Journal of Immunology*, 114 (1 Part 1), 120–124.
- Ruppert, S. M., Hawn, T. R., Arrigoni, A., Wight, T. N., & Bollyky, P. L. (2014). Tissue integrity signals communicated by high-molecular weight hyaluronan and the resolution of inflammation. *Immunologic Research*, 58(2–3), 186–192.
- Shastri, M. D., Peterson, G. M., & Patel, R. P. (2017). Redefining approaches to asthma: Bridging the gap between heparin and its anti-inflammatory activities. *Current Allergy and Asthma Reports*, 17(10), 70.
- Suarez, P., Rojo, L., González-Gómez, A., & San Román, J. (2013). Self-assembling gradient copolymers of vinylimidazol and (acrylic)ibuprofen with anti-inflammatory and zinc chelating properties. *Macromolecular Bioscience*, 13(9), 1174–1184.
- Thourani, V. H., Brar, S. S., Kennedy, T. P., Thornton, L. R., Watts, J. A., Ronson, R. S., & Vinten-Johansen, J. (2000). Nonanticoagulant heparin inhibits NF-κB activation and attenuates myocardial reperfusion injury. *American Journal of Physiology-Heart and Circulatory Physiology*, 278(6), H2084–H2093.
- Vasconcelos, D. P., Águas, A. P., Barbosa, M. A., Pelegrín, P., & Barbosa, J. N. (2019). The inflammasome in host response to biomaterials: Bridging inflammation and tissue regeneration. *Acta Biomaterialia*, 83, 1–12.
- Velnar, T., Bunc, G., Klobucar, R., & Gradisnik, L. (2016). Biomaterials and host versus graft response: A short review. *Bosnian Journal of Basic Medical Sciences*, 16(2), 82–90.
- Vroman, L., Adams, A. L., Fischer, G. C., & Munoz, P. C. (1980). Interaction of high molecular weight kininogen, factor XII, and fibrinogen in plasma at interfaces. *Blood*, 55(1), 156–159.
- Wan, F., & Lenardo, M. J. (2009). Specification of DNA binding activity of NF-κB proteins. *Cold Spring Harbor Perspectives in Biology*, 1(4), a000067.
- Weiler, J. M., Edens, R. E., Linhardt, R. J., & Kapelanski, D. P. (1992). Heparin and modified heparin inhibit complement activation *in vivo*. *The Journal of Immunology*, 148(10), 3210–3215.
- Wu, F., Li, J., Zhang, K., He, Z., Yang, P., Zou, D., & Huang, N. (2015). Multifunctional coating based on hyaluronic acid and dopamine conjugate for potential application on surface modification of cardiovascular implanted devices. *ACS Applied Materials & Interfaces*, 8(1), 109–121.
- Wynn, T. A., & Vannella, K. M. (2016). Macrophages in tissue repair, regeneration, and fibrosis. *Immunity*, 44(3), 450–462.

Reprinted with permission from Journal of Biomedical Materials Research (JBMR) part A, Hala Alkhoury, Adrian Hautmann, Frank Erdmann, Guoying Zhou, Sanja Stojanović, Stevo Najman and Thomas Groth (2020), Study on the potential mechanism of anti-inflammatory activity of covalently immobilized hyaluronan and heparin, *J Biomed Mater Res*. 108A:1099–1111.

- Yang, Y., Köwitsch, A., Ma, N., Mäder, K., Pashkuleva, I., Reis, R. L., & Groth, T. (2016). Functionality of surface-coupled oxidised glycosaminoglycans towards fibroblast adhesion. *Journal of Bioactive and Compatible Polymers*, 31(2), 191–207.
- Young, E. (2008). The anti-inflammatory effects of heparin and related compounds. *Thrombosis Research*, 122(6), 743–752.
- Young, E., Venner, T., Ribau, J., Shaughnessy, S., Hirsh, J., & Podor, T. J. (1999). The binding of unfractionated heparin and low molecular weight heparin to thrombin-activated human endothelial cells. *Thrombosis Research*, 96(5), 373–381.
- Zhang, X., Zhang, G., Zhang, H., Li, J., Yao, X., & Tang, B. (2018). Surface immobilization of heparin and chitosan on titanium to improve hemocompatibility and antibacterial activities. *Colloids and Surfaces B: Biointerfaces*, 172, 338–345.
- Zhou, G., Al-Khoury, H., & Groth, T. (2016). Covalent immobilization of glycosaminoglycans to reduce the inflammatory effects of biomaterials. *The International Journal of Artificial Organs*, 39, 37–44.
- Zhou, G., Niepel, M. S., Saretia, S., & Groth, T. (2016). Reducing the inflammatory responses of biomaterials by surface modification with glycosaminoglycan multilayers. *Journal of Biomedical Materials Research. Part A*, 104(2), 493–502.
- Zhou, L., Shen, L. H., Hu, L. H., Ge, H., Pu, J., Chai, D. J., ... He, B. (2010). Retinoid X receptor agonists inhibit phorbol-12-myristate-13-acetate (PMA)-induced differentiation of monocytic THP-1 cells into macrophages. *Molecular and Cellular Biochemistry*, 335(1–2), 283–289.

SUPPORTING INFORMATION

Additional supporting information may be found online in the Supporting Information section at the end of this article.

How to cite this article: AlKhoury H, Hautmann A, Erdmann F, et al. Study on the potential mechanism of anti-inflammatory activity of covalently immobilized hyaluronan and heparin. *J Biomed Mater Res*. 2020;108A:1099–1111. <https://doi.org/10.1002/jbm.a.36885>

Chapter 4



Summary – Studies on the mechanisms of anti-inflammatory activity of heparin- and hyaluronan-containing multilayer coatings-targeting NF-κB signalling pathway:

In the study described in this chapter another method named as polyelectrolyte multilayers (PEMs) formation was utilized. The PEMs were fabricated with layer-by-layer (LbL) technique represented by alternating adsorption of polyanions of either HA or Hep in combination with the polycation Chi on top of a priming layer of poly (ethylene imine) (PEI). This study was performed to shed a light on the potential mechanism of anti-inflammatory effects of GAGs toward NF-κB signalling pathway. To evaluate surface properties with physical adsorption of GAGs, various physicochemical characterizations were carried out in terms of wettability, thickness and topography. The characterization results showed significant higher thickness and hydrophilicity with the multilayer formation when compared to the control PEI samples. In addition, surface topography, which was identified by scanning electron microscopy (SEM) and AFM visualized complete coverage of surfaces with the PEMs. The surface characterization results were important for studying the macrophage related inflammatory responses with GAGs immobilization. The same set of experiments as described in chapter 3 was performed by also using THP-1 derived macrophages. Macrophage inflammatory responses in terms of adhesion, fusion and IL-1β were all significantly reduced on GAGs-modified samples. Moreover, partial inhibitory effect of p65 translocation into the nucleus together with lower expression profiles of NF-κB blots in the whole macrophage lysates were illustrated on the PEMs in comparison to the control PEI samples. In addition, macrophages showed the ability to associate or uptake FITC-labelled GAGs. However, the Hep-based system demonstrated the most significant inhibitory effects of both macrophage inflammatory responses as well as of NF-κB pathway. The physical adsorption of GAGs with LbL introduced an advantage of allowing substantial quantities of GAGs adsorption on the surfaces, which may significantly modulate the biomaterial- host induced reactions. In conclusion, the potential anti-inflammatory effect of GAGs was not solely related to the hydrophilic and anionic nature the GAGs but also to their partial inhibition on the NF-κB signalling pathway.



Article

Studies on the Mechanisms of Anti-Inflammatory Activity of Heparin- and Hyaluronan-Containing Multilayer Coatings—Targeting NF-κB Signalling Pathway

Hala Alkhoury^{1,2}, Adrian Hautmann¹, Bodo Fuhrmann², Frank Syrowatka², Frank Erdmann³, Guoying Zhou¹, Sanja Stojanović^{4,5}, Stevo Najman^{4,5}  and Thomas Groth^{1,2,6,*} 

¹ Department Biomedical Materials, Institute of Pharmacy, Martin Luther University Halle Wittenberg, Heinrich Damerow Strasse 4, 06120 Halle (Saale), Germany; hala.al-khoury@student.uni-halle.de (H.A.); adrian.hautmann@pharmazie.uni-halle.de (A.H.); guoying.zhou@pharmazie.uni-halle.de (G.Z.)

² Interdisciplinary Center of Materials Science, Martin Luther University Halle-Wittenberg, 06120 Halle (Saale), Germany; bodo.fuhrmann@cmat.uni-halle.de (B.F.); frank.syrowatka@cmat.uni-halle.de (F.S.)

³ Pharmaceutical Biology and Pharmacology Department, Institute of Pharmacy, Martin Luther University Halle Wittenberg, Wolfgang-Langenbeck-Str. 4, 06120 Halle (Saale), Germany; frank.erdmann@pharmazie.uni-halle.de

⁴ Department of Biology and Human Genetics, Faculty of Medicine, University of Niš, 18000 Niš, Serbia; s.sanja88@gmail.com (S.S.); stevo.najman@gmail.com (S.N.)

⁵ Department for Cell and Tissue Engineering, Scientific Research Center for Biomedicine, Faculty of Medicine, University of Niš, 18000 Niš, Serbia

⁶ Laboratory of Biomedical Nanotechnologies, Institute of Bionic Technologies and Engineering, I.M. Sechenov First Moscow State University, Trubetskaya street 8, 119991 Moscow, Russia

* Correspondence: thomas.groth@pharmazie.uni-halle.de

Received: 22 April 2020; Accepted: 22 May 2020; Published: 25 May 2020



Abstract: The use of implants can be hampered by chronic inflammatory reactions, which may result in failure of the implanted device. To prevent such an outcome, the present study examines the anti-inflammatory properties of surface coatings made of either hyaluronic acid (HA) or heparin (Hep) in combination with chitosan (Chi) prepared as multilayers through the layer-by-layer (LbL) technique. The properties of glycosaminoglycan (GAG)-modified surfaces were characterized in terms of surface topography, thickness and wettability. Results showed a higher thickness and hydrophilicity after multilayer formation compared to poly (ethylene imine) control samples. Moreover, multilayers containing either HA or Hep dampened the inflammatory response visible by reduced adhesion, formation of multinucleated giant cells (MNGCs) and IL-1β release, which was studied using THP-1 derived macrophages. Furthermore, investigations regarding the mechanism of anti-inflammatory activity of GAG were focused on nuclear transcription factor-κB (NF-κB)-related signal transduction. Immunofluorescence staining of the p65 subunit of NF-κB and immunoblotting were performed that showed a significant decrease in NF-κB level in macrophages on GAG-based multilayers. Additionally, the association of FITC-labelled GAG was evaluated by confocal laser scanning microscopy and flow cytometry showing that macrophages were able to associate with and take up HA and Hep. Overall, the Hep-based multilayers demonstrated the most suppressive effect making this system most promising to control macrophage activation after implantation of medical devices. The results provide an insight on the anti-inflammatory effects of GAG not only based on their physicochemical properties, but also related to their mechanism of action toward NF-κB signal transduction.

Keywords: inflammation; glycosaminoglycans; LbL technique; macrophages adhesion; multinucleated giant cell (MNGCs) formation; NF-κB; immunoblotting; endocytosis

1. Introduction

Biomaterial implants can trigger an undesired host response upon surgical insertion in the human body leading to limited functionality, longevity and eventually to failure of the biomedical device [1,2]. Therefore, it is desirable to design biomaterials that will guide the inflammation process to achieve the desired function of the device. The series of events that will determine implant fate is initiated by adsorption of blood proteins and the recruitment of leukocytes. Monocytes represent key players at the implantation site, where they differentiate to macrophages [3,4] that secrete pro-inflammatory cytokines such as IL-1β and tumour necrosis factor-α (TNFα), chemokines and growth factors [5,6]. Furthermore, the surrounding tissue may also be damaged by the biocide activity of reactive oxygen and nitrogen species secreted by macrophages [7]. The persistent stimulation of the immune system may shift acute to chronic inflammation, which is characterized by the formation of multinucleated giant cells (MNGCs) as a result of macrophage fusion in an attempt to phagocytose biomaterials larger in size than a single cell [8,9]. Eventually, fibroblasts are recruited upon the prolonged inflammatory phase, which may finally result in encapsulation of the biomedical device causing its failure [10,11].

A passive mechanism to control inflammation after implantation is based on making biomaterial surfaces hydrophilic or to exploit steric repulsion to reduce the opsonization of the implant by plasma proteins, which is achieved for example by covalent immobilisation of polyethylene glycol [12]. This requires often an activation of the biomaterial surface by chemical or plasma treatment [13]. However, the effect is often limited due to the lack of the ability to inhibit protein adsorption completely and for longer periods of time [14,15]. Another approach is the development of controlled-release systems of nonsteroidal anti-inflammatory drugs (NSAIDs) to reduce the inflammatory response, which can be achieved by blending polymers with NSAID or immobilisation of NSAID nanoparticles on biomaterial surfaces [16,17]. A non-covalent modification of implant materials can be achieved by building up multilayer systems using the layer-by-layer (LbL) method [18]. The LbL method is based on the alternating deposition of oppositely charged polyelectrolytes among them also biopolymers like chitosan (Chi), hyaluronan (HA), heparin (Hep) and others [19,20]. The obvious advantage of LbL is that no chemical or plasma activation of implants is required and that a broad range of molecules is available. Moreover, physical surface properties like wettability can be tuned to achieve hydrophilic surfaces like those based on Chi as polycation and Hep and HA as polyanions that adsorb lower quantities of proteins [21,22]. It is interesting to note that beside their hydrophilic nature the glycosaminoglycans (GAG) HA and Hep possess anti-inflammatory properties through their effect on the nuclear transcription factor-κB (NF-κB) signalling pathway, which makes them interesting candidates for regulation of inflammatory processes [23,24].

The NF-κB transcription factor family consists of a variety of homodimers and heterodimers that regulate and play a crucial role in apoptosis, cell proliferation, differentiation, cell migration, inflammation as well as angiogenesis and metastasis [25,26]. The activation of NF-κB involves two major signalling pathways, the canonical (classic) and non-canonical (alternative) that depends on different stimuli and responding proteins [27]. The NF-κB transcription factor is a key factor in inflammation having a direct influence on the regulation of cytokine release as well as inflammatory-related gene activation and gene expression [26,28]. The anti-inflammatory properties of high molecular weight HA (HMW-HA) is achieved by its binding to cell receptor CD44 leading to down regulation of toll-like-receptor (TLR) signalling, which mediates NF-κB activation [29,30]. In addition, the binding of HA to CD44 promotes the release of anti-inflammatory cytokines like IL-2 and IL-10 [24,31]. On the other hand, Hep has two different mechanisms of inhibition on the NF-κB signalling pathway in which one is focused on inhibiting the translocation of the transcription factor into the nucleus. The second

is explained as the ability of Hep to interfere non-specifically with the binding of NF-κB to DNA in the nucleus [32]. Hence, leukocyte adhesion and activation as well as pro-inflammatory cytokine production is downregulated as a result of the inhibitory effect of Hep toward the NF-κB signalling [33].

In previous studies, we could show that covalent or adsorptive binding of HA and Hep make surface coatings that reduce macrophage adhesion and activation [21,34]. Here, we extend our findings shedding light on the underlying mechanism of action of multilayers made of Chi and HA or Hep focussing on the inhibition of the p65 subunit of NF-κB protein family as a target of canonical NF-κB pathway in THP-1 monocyte-derived macrophages. A survey on the general structure of polyelectrolyte multilayers (PEMs) and their effect on macrophages investigated by different biological studies are shown in Figure 1.

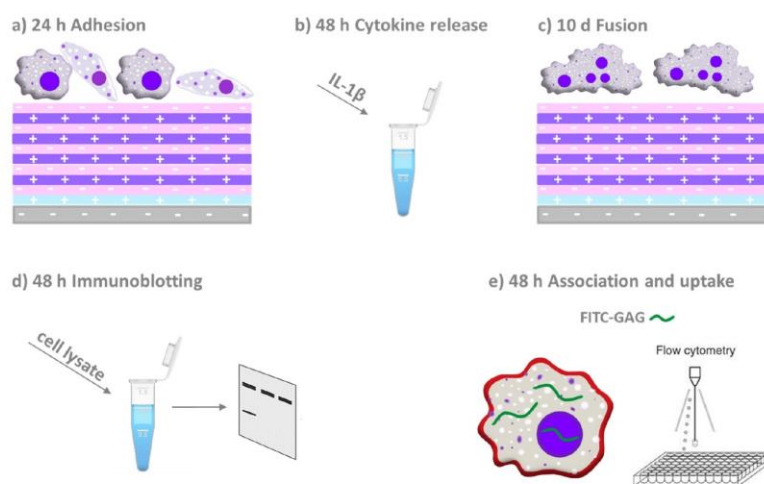


Figure 1. Schematic overview on the material system and design of the biological studies. Polyelectrolyte multilayers were assembled on model substrata glass or silicone (grey base layer with negative charge) on which a priming layer of poly (ethylene imine; blue layer with positive charge) was adsorbed first. Then alternately the polyanions heparin or hyaluronan (pink layer with negative charge) and chitosan as polycation (purple layer with positive charge) were adsorbed until 10 layers in total were assembled. Macrophages derived from the THP-1 monocytic cell line were seeded on these multilayers to study (a) adhesion and spreading of cells after 24 h, (b) evaluation of the pro-inflammatory (IL-1 β) cytokine release, (c) multinucleated giant cells formation, (d) immunoblotting and confocal laser scanning microscopy (CLSM) to study the p65 subunit of NF-κB and (e) association and uptake of fluorescein isothiocyanate (FITC)-labelled GAG through macrophages by CLSM and flow cytometry.

2. Results

2.1. Characterization of Physical Properties of Coatings

The thickness of surface coatings prepared on silicon wafers was studied by ellipsometry in the dry state to verify the deposition of polyelectrolytes. The measurements were performed for the primary poly (ethylene imine) (PEI) layer that was used to provide a positive surface charge for binding the polyanions HA and Hep and formation of PEMs. The PEMs made of hyaluronan and chitosan were then designated as PEI(HA/Chi)₄HA. The PEMs made of heparin and chitosan were abbreviated as PEI(Hep/Chi)₄Hep. Altogether, 10 single layers were absorbed subsequently as described in the Materials and Methods Section. In Figure 2A a significantly higher thickness of PEMs was visible in comparison to PEI-modified silicon wafers. Static water contact angle (WCA) measurements were done to identify the wetting properties of the surface coatings. Figure 2B depicted a significantly lower WCA of PEMs compared to PEI surfaces. In addition, a significant difference between the two glycosaminoglycans was observed, showing the lowest WCA for multilayers composed of PEI(Hep/Chi)₄Hep.

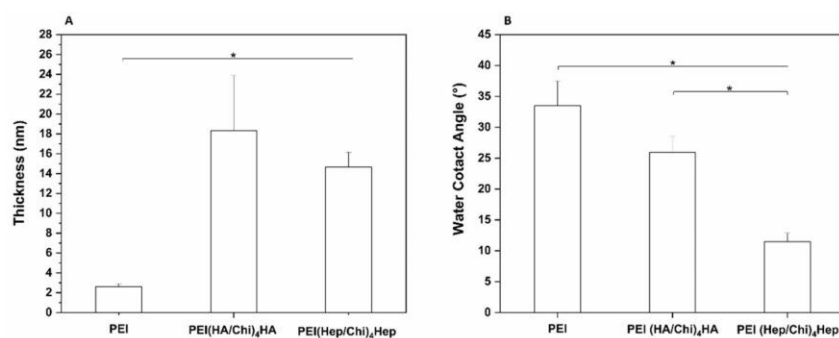


Figure 2. (A) Ellipsometry measurements to obtain the average thickness of poly (ethylene imine) (PEI) coating and multilayers made of either hyaluronic acid (HA) or heparin Hep as polyanions and chitosan (Chi) as a polycation, abbreviated as (PEI, PEI(HA/Chi)₄HA and PEI(Hep/Chi)₄Hep), respectively. Results represent means \pm SD, $n = 6$, * $p < 0.05$. (B) Static water contact angle measurements using the sessile drop method to characterize surface wettability of the same surface coatings. Results represent means \pm SD, $n = 10$, * $p < 0.05$.

A deposition of a 15 nm Cr layer to achieve a sufficient conductivity of samples was performed prior to surface topography visualization with scanning electron microscopy shown in Figure 3A. PEMs containing HA demonstrated island-like structures while PEMs containing Hep expressed a more homogenous, smooth surface coverage. On the other hand, atomic force microscopy studies of surface topography shown in Figure 3B indicated smaller differences between both PEM, since the observed surface features had a similar range of 40–60 nm in the z scale though PEMs with HA as a terminal layer looked more homogenous here than those with Hep as a polyanion.

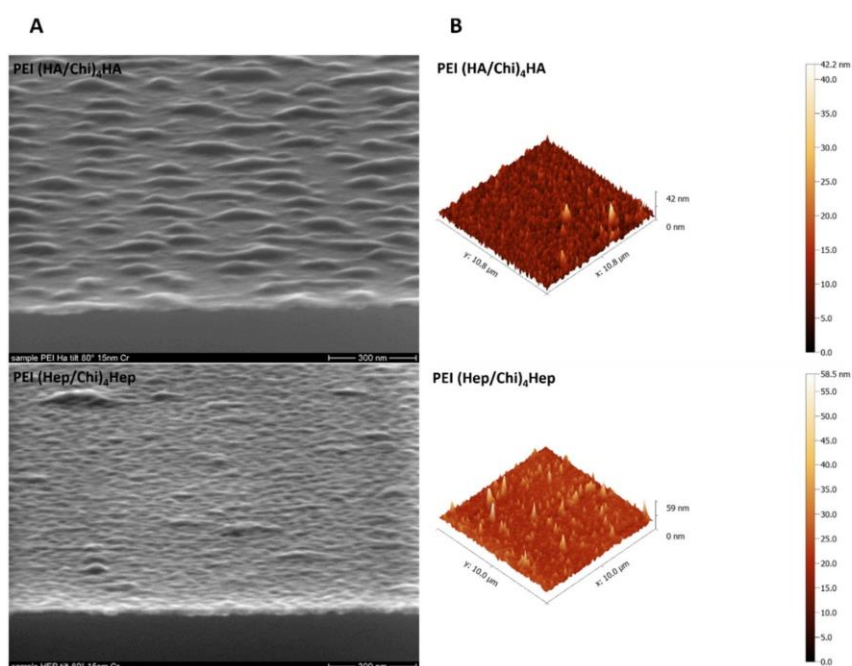


Figure 3. (A) Scanning electron microscopy (SEM), Scale bar: 300 nm and (B) atomic force microscopy (AFM) for studying topography of samples poly (ethylene imine) (PEI) and terminal layers of polyelectrolyte multilayers (PEMs) composed of either hyaluronic acid (HA) or heparin (Hep) as polyanions and chitosan (Chi) as polycation abbreviated as (PEI(HA/Chi)₄HA, PEI(Hep/Chi)₄Hep), respectively.

2.2. Adhesion of Macrophages and Multinucleated Giant Cell Formation

Micrographs visualizing the adhesion and shape of macrophages after 24 h of culture are shown in Figure 4A. Cells showed the highest adherence on PEI with a spread and elongated phenotype. On the other hand, a smaller number of predominantly round, less elongated macrophages were observed on PEMs. Quantitative data based on image analysis shown in Figure 4B displayed that the number of adherent macrophages was highest on the control substratum PEI, while the number of cells was significantly lower on PEMs with the smallest number on PEI(Hep/Chi)₄Hep.

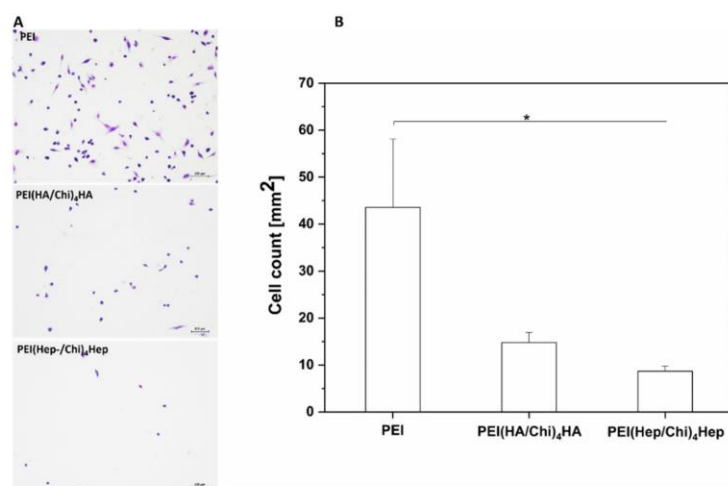


Figure 4. (A) Transmitted light microscopy images of adherent macrophages stained with 10% (v/v) Giemsa after 24 h on poly (ethylene imine) (PEI) and terminal layers of PEMs composed of either hyaluronic acid (HA) or heparin (Hep) as polyanions and chitosan (Chi) as polycation abbreviated as PEI(HA/Chi)₄HA, PEI(Hep/Chi)₄Hep, respectively. Scale: 100 μm . (B) Number of adherent macrophages per surface area after 24 h of cultivation. Data represent means \pm SD, $n = 5$, $* p \leq 0.05$.

Image analysis was also used to quantify the size and shape of adherent macrophages. Figure 5A shows that the aspect ratio of adherent macrophages was higher related to an enhanced polarization of macrophages on PEI samples compared to cells on PEMs, where it was significantly lower. Figure 5B shows that also spreading of macrophages was significantly lower on PEMs in comparison to PEI.

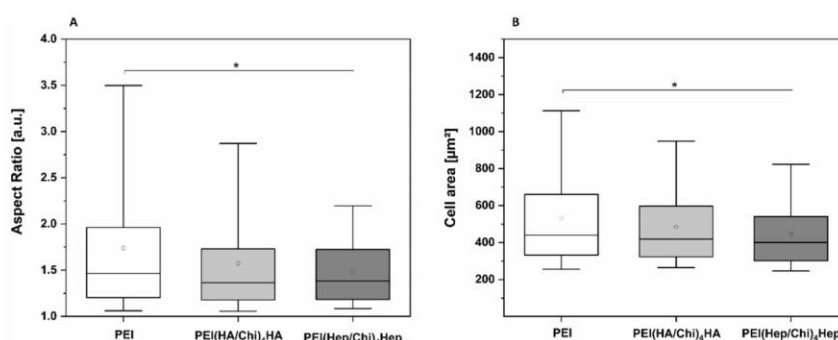


Figure 5. (A) Aspect ratio of adherent macrophages on poly (ethylene imine) (PEI) and terminal layers of PEMs composed of either hyaluronic acid (HA) or heparin (Hep) as polyanions and chitosan (Chi) as polycation abbreviated as PEI(HA/Chi)₄HA, PEI(Hep/Chi)₄Hep, respectively. (B) Cell area of adherent macrophages per surface area after 24 h of cultivation. The box plot indicates the 25th and 75th percentile; the lowest and highest values are represented by the whiskers, whereas the median (dash) and mean value (white circle) are shown as well. $n = 15$, $* p \leq 0.05$.

Furthermore, micrographs presented in Figure 6A visualized significantly higher numbers of multinucleated giant cells (MNGCs) on PEI samples, which can be identified by the number of nuclei (≥ 2) per cell body as well as the larger cell size. By contrast, on PEMs a lower number of MNGCs was seen. The quantitative analysis of area percentage of MNGCs presented in Figure 6B shows that fusion of macrophages was significantly lower on PEMs in comparison to PEI. In addition, the formation of MNGCs was also significantly lower on PEI(Hep/Chi)₄Hep in comparison to PEI(HA/Chi)₄HA.

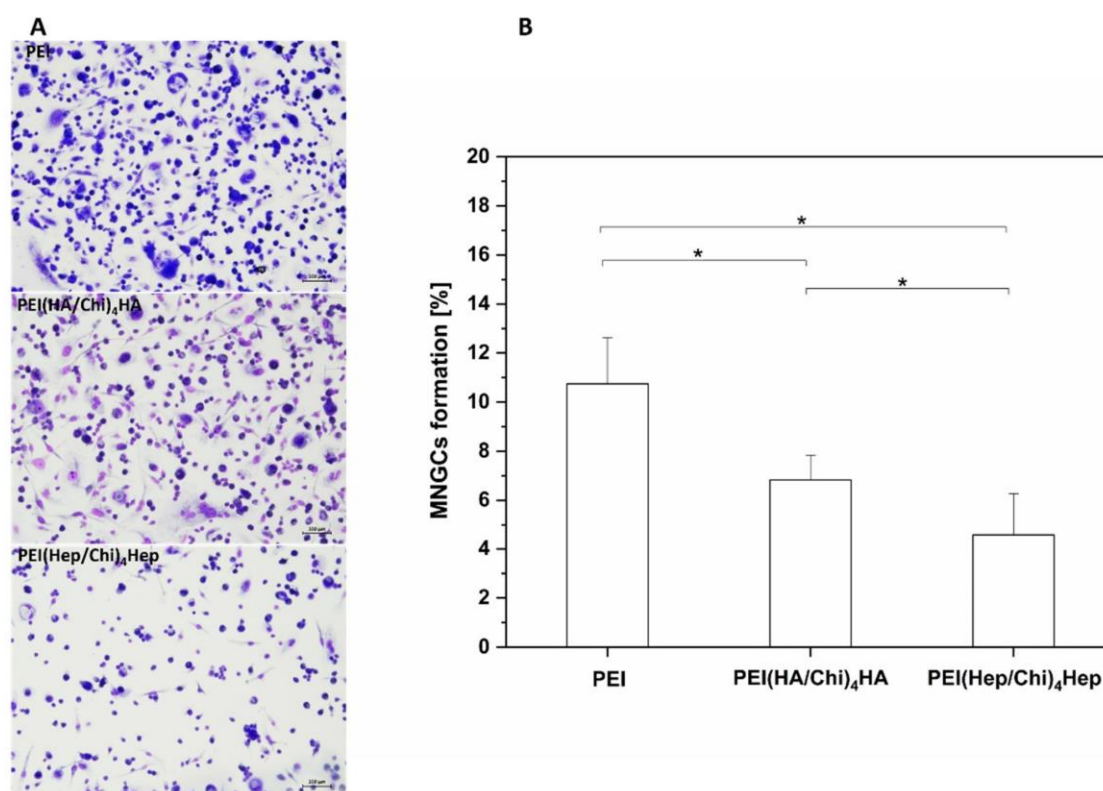


Figure 6. (A) Images of multinucleated giant cells (MNGCs) stained with 10% (v/v) Giemsa after 10 days cultivation on poly (ethylene imine) (PEI) and terminal layers of PEMs composed of either hyaluronic acid (HA) or heparin (Hep) as polyanions and chitosan (Chi) as polycation abbreviated as PEI(HA/Chi)₄HA, PEI(Hep/Chi)₄Hep, respectively. Scale bar: 100 μm. (B) The area percentage of MNGCs on PEI, PEI(HA/Chi)₄HA and PEI(Hep/Chi)₄Hep surfaces based on quantitative image analysis of micrographs. Results represent means ± SD, * $p < 0.05$, $n = 15$.

2.3. IL-1β Pro-Inflammatory Cytokine Release

Results of studies on the release of Interleukin-Iβ are shown in Figure 7. Two sets of samples were studied with the absence (white bars) and presence (black bars) of lipopolysaccharide (LPS). LPS stimulation leads to an up regulation of IL-1β in THP-1 derived macrophages, which is also an indicator of the functionality of these cells. Macrophages adhering on PEI-coated surfaces produced the highest quantity of IL-1β under both conditions (with or without LPS). By contrast macrophages cultured on both PEMs had a significantly reduced release of this cytokine in the presence and absence of LPS. In addition, IL-1β release from macrophages cultured on PEI(Hep/Chi)₄Hep was significantly lower in comparison to PEI(HA/Chi)₄HA.

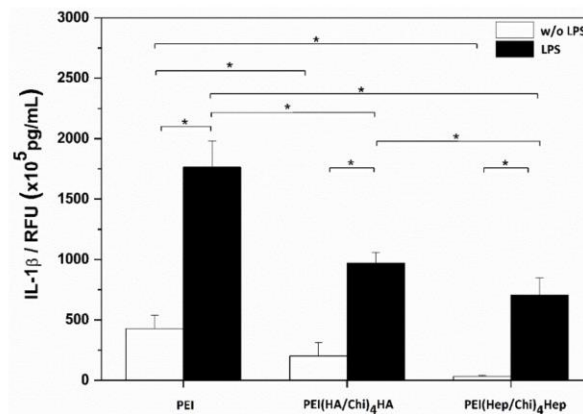


Figure 7. IL-1 β release from macrophages after 24 h incubation in absence (white bars) and presence (black bars) of lipopolysaccharide (LPS) on poly (ethylene imine) (PEI) and terminal layers of PEMs composed of either hyaluronic acid (HA) or heparin (Hep) as polyanions and chitosan (Chi) as polycation abbreviated as (PEI(HA/Chi) $_4$ HA and PEI(Hep/Chi) $_4$ Hep), respectively. Data represent means \pm SD, $n = 6$, * $p \leq 0.05$.

2.4. Immunofluorescence Staining of NF- κ B in Macrophages

In Figure 8A the cell nuclei have been stained with the nuclear stain TO-PRO-3 (blue colour) and the non-phosphorylated p65 subunit of NF- κ B with a monoclonal antibody (green colour). It is visible that the p65 subunit of NF- κ B can be found both in the cell cytoplasm and nuclei. The nuclear to cytoplasmic ratio of NF- κ B was quantitatively evaluated and used as an indicator for the translocation of the transcription factor into the nuclear area. The highest extent of p65 translocation was observed in macrophages on PEI; both in the presence and absence of LPS (Figure 8B). By contrast, a significantly lower nuclear to cytoplasmic ratio was found in macrophages cultured on PEMs. Indeed, the lowest quantity of p65 translocation into the nuclear area both in the absence and presence of LPS was found in cells cultured on PEI(Hep/Chi) $_4$ Hep (Figure 8B).

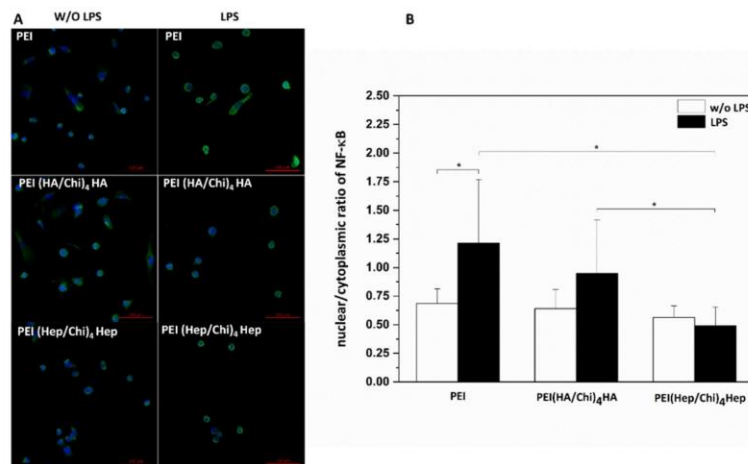


Figure 8. (A) TO-PRO-3 (blue colour) staining of nuclei and monoclonal antibody detection (green colour) of NF- κ B p65 subunit shown for non-stimulated (left row) and stimulated ($1 \mu\text{g}\cdot\text{mL}^{-1}$ LPS) macrophages (right row). The cells were cultured for 48 h on poly (ethylene imine) (PEI) and terminal layers of PEMs composed of either hyaluronic acid (HA) or heparin (Hep) as polyanions and chitosan (Chi) as polycation abbreviated as (PEI(HA/Chi) $_4$ HA, PEI(Hep/Chi) $_4$ Hep), respectively. Scale bar: 100 μm . (B) Quantification of nuclear/cytoplasmic ratio in absence (white bars) and presence (black bars) of LPS in cells cultured on PEI and PEMs. Data represent means \pm SD, $n = 10$, * $p \leq 0.05$.

2.5. Western Blotting

Figure 9A depicts the bands for the non-phosphorylated p65 subunit of NF-κB (named here as NF-κB only) and actin, in which the latter was used for normalization of data in the quantitative evaluation by densitometry. It is visible that a higher expression of NF-κB was observed in cell lysates from macrophages cultured on PEI samples compared to cells on PEMs. Figure 9B shows the quantitative evaluation of band intensities of NF-κB expression in macrophages cultured on PEI and PEMs, quantified by densitometry. The lowest intensity of NF-κB in cell lysates was observed in macrophages cultured on PEI(Hep/Chi)₄Hep. The original blots from different gels can be found in Figures S2 and S3.

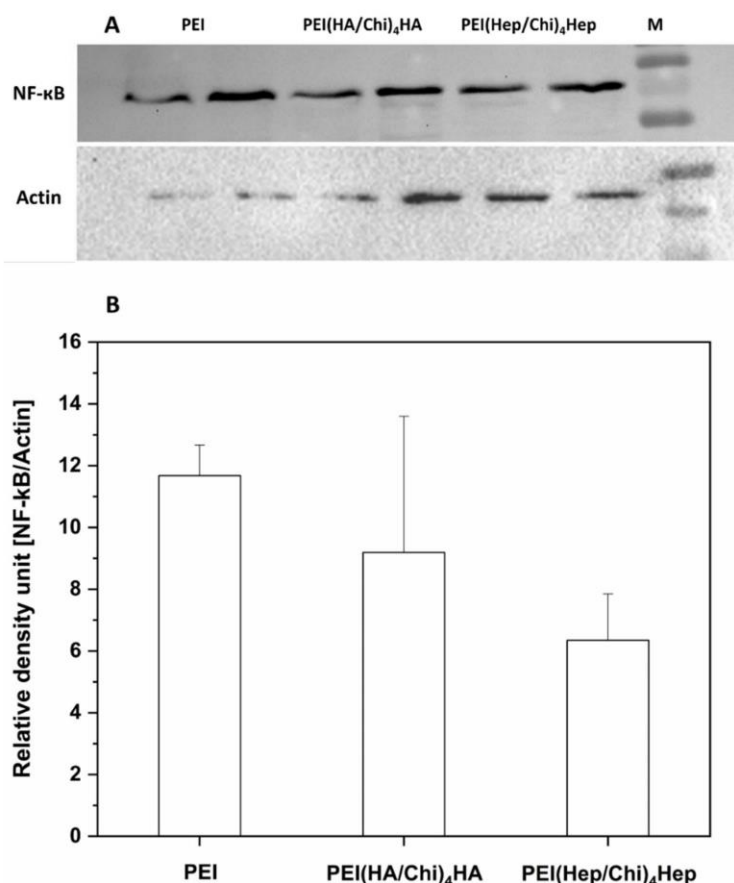


Figure 9. (A) Western blots with bands of p65 of NF-κB and actin from two samples of lysates of macrophages cultured on poly (ethylene imine) (PEI) and terminal layers of PEMs composed of either hyaluronic acid (HA) or heparin (Hep) as polyanions and chitosan (Chi) as a polycation abbreviated as PEI(HA/Chi)₄HA, PEI(Hep/Chi)₄Hep, respectively. The lysates, collected after 48 h, were blotted toward (NF-κB) and actin. (B) The immunoblotting bands were analysed by densitometry. Bands of p65 subunit of NF-κB were normalized to expression of actin. The ratio was named as relative density units. Data represent means, $n = 2$.

2.6. Association of GAG with Macrophages Studied by Confocal Laser Scanning Microscopy (CLSM)

DID-stained macrophages cultured on terminal layers of PEMs containing fluorescent FITC-labelled glycosaminoglycans (GAG, green colour) visualized by CLSM are shown in Figure 10. Here, the macrophages cultured on PEI expressed a red staining of DID of the cell membrane, only because no FITC-labelled GAG were present on this surface (Figure 10A). The macrophages cultured on PEMs with FITC-labelled GAG show an association of FITC-labelled HA or Hep (green in

confocal images) with DID-stained (red) cells. 3D images of FITC-labelled HA and Hep are shown in Figure 10B. Here, it is visible that HA or Hep were either co-localized with the cell surface or found intracellularly. Figure 10A,B shows the ability of macrophages to associate with and the uptake of the immobilized FITC-GAG. Additional cell images are provided in Figures S4 and S5.

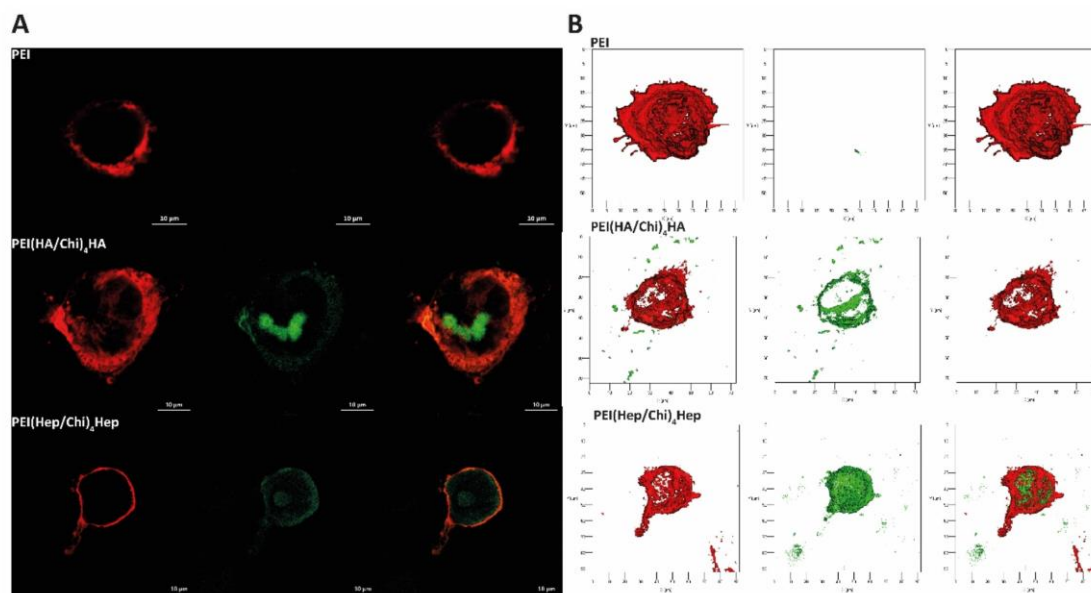


Figure 10. (A) Representative confocal laser microscopy (CLSM) images of adherent macrophages stained with the membrane stain DID (red colour) after 24 h cultivation on poly (ethylene imine) (PEI) and terminal layers of PEMs composed of either hyaluronic acid (HA) or heparin (Hep) as polyanions (stained with FITC, green colour) and chitosan (Chi) as a polycation abbreviated as (PEI(HA/Chi)₄HA, PEI(Hep/Chi)₄Hep), respectively (63-fold oil immersion objective, Scale bar: 10 μm). (B) Representative 3D view of a z-stacks in surface projection with CLSM (63-fold oil immersion objective, scale: 20 μm). In this mode, pixel values are computed as solids, which allows no transparency.

2.7. Association of FITC-Labelled GAG with Macrophages Studied by Flow Cytometry

The results of flow cytometry with dot blots of the side scatter (SSC, y axis) versus the FITC fluorescence (x axis) are shown in Figure 11A. Macrophages located in the P4 region were considered to be negative for GAG-FITC due to cell auto-fluorescence. An uptake of FITC-labelled-GAG by macrophages is denoted by an increase of the cellular fluorescence related to the emission of fluorescein (FITC). Hence, the P5 region shows the number of macrophages positive for FITC-labelled-GAG. Figure 11B shows the quantitative evaluation of macrophages positive for FITC-GAG demonstrating that cells cultured on multilayers containing HA expressed a significantly lower uptake of FITC-labelled GAG in comparison to the cell cultured on PEM with FITC-heparin.

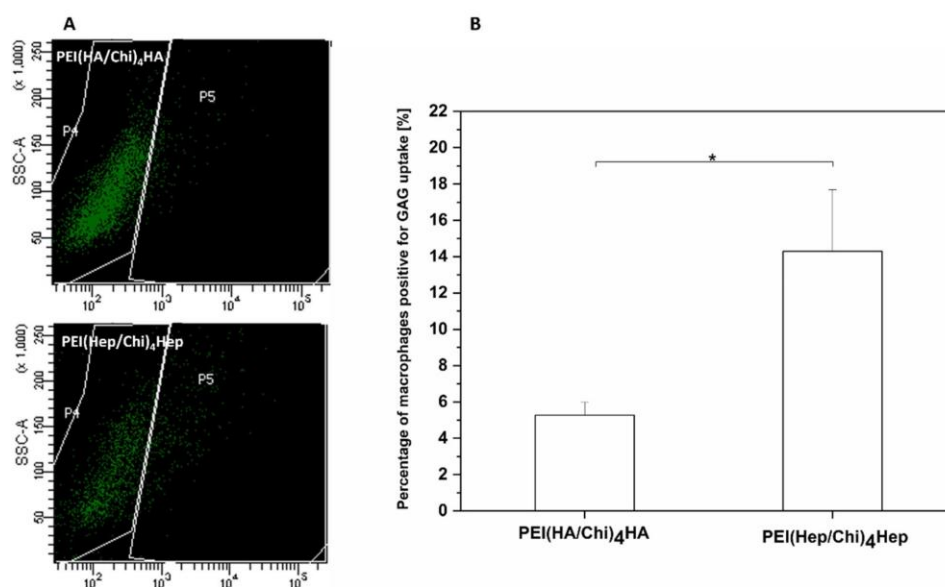


Figure 11. (A) Illustrative images of the flow cytometry measurements of GAG association and uptake by macrophages cultured on either FITC-labelled hyaluronic acid or FITC-heparin multilayers abbreviated as PEI(HA/Chi)₄HA, PEI(Hep/Chi)₄Hep), respectively. (B) The percentage of macrophages positive for GAG uptake after 48 h cultivation on PEI(HA/Chi)₄HA and PEI(Hep/Chi)₄Hep. Data represent means \pm SD, $n = 4$, * $p \leq 0.05$.

3. Discussion

This study aimed to investigate the mechanism of the anti-inflammatory action of PEMs systems based on either HA or Hep as polyanions in combination with Chi as a polycation fabricated by the LbL technique to explore their potential for making implantable biomedical devices more immune compatible to avoid chronic inflammation and subsequent fibrosis. The polyethylene imine (PEI) that serves often as an anchoring layer in the LbL technique [35] was used here for comparison because it is known that amino-terminated surfaces provoke an activation of macrophages [36], which is also known for PEI-modified substrata [34].

Physicochemical studies were performed to characterize surface properties like wettability and topography that have an impact on protein adsorption and cell adhesion [37]. Studies of the topography and thickness showed that the LbL technique was able to achieve a complete coating of substrata (glass or silicone) with PEMs of a dry thickness in the range of 15–20 nm with a rather smooth surface topography in the micrometre scale with differences between HA and Hep multilayer systems. Indeed, multilayers with HA showed a more island-like structure when studied with SEM, which might be related to the much larger molecular weight of hyaluronan compared to heparin used as polyanions in multilayer formation. Wettability studies showed that both glycosaminoglycans HA and Hep formed multilayer coatings of more hydrophilic character despite the presence of chitosan as found also in previous studies [38,39]. By contrast, highest WCA was found for the PEI modified surface, which also corresponds typically to increased protein adsorption, adhesion, and spreading of cells in comparison to more hydrophilic substrata [34].

Accordingly, the result of macrophage adhesion and spreading corresponded to the wetting properties of surfaces showing that it was highest on PEI, while PEMs with GAG reduced their adhesion and spreading with lowest on PEI(Hep/Chi)₄Hep. However, macrophage adhesion was not statistically different between HA and Hep-terminated PEMs. In contrast to that MNGC formation was significantly decreasing from PEI to HA and then Hep. Although, MNGC formation is related to the number of adhering macrophages that are required to aggregate before their fusion, other factors like cytokine release play a more dominant role [40]. Therefore, studies on the release of IL-1 β were

performed that demonstrated a significant reduction of release of this pro-inflammatory cytokine from macrophages cultured on PEMs. It should be noted that IL-1 β release was normalized to the number of viable cells. Hence, the reduced adhesion of macrophages due to higher wettability of PEM alone as a physical effect was not sufficient to explain the suppressive effect of multilayer coatings based on HA and Hep on macrophage activation.

Since, wetting properties of HA and Hep-based PEMs were quite similar, pharmaceutical effects of both GAG might play an important role for the observed inhibition on macrophage fusion and release of pro-inflammatory cytokines. It is known that reduced secretion of pro-inflammatory cytokines like IL-1 β is related to the inhibition of NF- κ B signalling pathway [41,42]. Hence, the focus was set on the study of the NF- κ B signalling pathway, which plays a pivotal role during the activation of macrophages and other cells [26]. As it could be expected from the studies on macrophage adhesion, fusion and cytokine release, translocation of the p65 subunit of NF- κ B to the nuclear area and its concentration were highest in macrophages on the control surface PEI. On the other hand, all parameters were lower in macrophages cultured on PEMs based on either HA or Hep. However, most effective in this regard was the multilayer system PEI(Hep/Chi)₄Hep. A question how both GAG can control the activation of macrophages was related to the fact that both GAGs were physically bound to chitosan in multilayers. Indeed, we have shown previously that such multilayer systems made of biogenic polyelectrolytes represent a living interface, in which polyelectrolytes can interact with and be translocated by cells [43]. Hence, we studied association and potential internalization of FITC-labelled GAG by macrophages using CLSM showing that both association as well as internalization of these GAG can occur. Moreover, studies with flow cytometry confirmed such an association and showed also that a larger quantity of FITC-Hep was found to be associated with macrophages in comparison to FITC-HA.

Indeed, heparin can be internalized by cells either through anionic membrane transporters or by endocytosis [44]. It is known that heparin, taken up by endocytosis, may bind to the positively charged p50–p65 subunits of NF- κ B, leading to a partial inhibition of the phosphorylation process and a reduced translocation of the transcription factor to the nucleus [44,45]. A further mechanism is that intracellular heparin can interfere non-specifically with DNA binding of NF- κ B in the nucleus [32]. On the other hand, the high molecular weight form of hyaluronan (HMW-HA) used here for fabrication of PEMs possesses an anti-inflammatory potential through cross-linking the surface receptor CD44 on cells like macrophages, which suppresses the pro-inflammatory signaling by toll-like receptors (TLR), resulting in down-regulation the phosphorylation cascade of NF- κ B pathway [46]. In addition, CD44 is thought to play an important role in the reduction of pro-inflammatory cytokines release by other pathways [13,47]. The intracellular presence of FITC-HA shown by CLSM may be related to CD44 by receptor endocytosis with the bound ligand [48], but probably not affecting intracellular signal transduction. Since, NF- κ B signalling is one of the important pathways of the regulation of cytokine gene expression, an inhibition by both hyaluronan and heparin, may eventually decrease the potential inflammatory response of macrophages [49,50], which is obviously the case for both multilayer systems that have been presented in this study.

4. Materials and Methods

4.1. Chemicals for Surface Modification

Glass cover slips, \varnothing 12 mm and 15 mm, were provided from Menzel GmbH (Bielefeld, Germany). Silicon wafers of $10 \times 10 \text{ mm}^2$ surface were obtained from LG Siltron Inc. (Gumi, Korea). Poly (ethylene imine) (PEI, $M_w \approx 750 \text{ kDa}$) was purchased from Polysciences Inc. (Warrington, PA, USA). Heparin (Hep, $M_w \approx 15 \text{ kDa}$) and hyaluronic acid (HA, $M_w \approx 1.3 \text{ MDa}$) were provided from Serva (Heidelberg, Germany) and Innovent e.V. (Jena, Germany), respectively. Labelling of GAG was done with fluorescein isothiocyanate (FITC) according to the protocol published recently to obtain 10% labelled carboxylic groups of either HA or Hep with FITC [51]. Chitosan 85/500 with a deacetylation degree of 85% (Chi, $M_w \approx 500 \text{ kDa}$) was delivered from Hepepe Medical Chitosan GmbH (Halle, Germany). Sodium

chloride (NaCl) was obtained from Roth (Karlsruhe, Germany), while acetic acid was provided from Applichem (Darmstadt, Germany). Ammonia (25%) and hydrogen peroxide (30%) were purchased from TH-Geyer GmbH and Co. KG and Roth (Renningen, Karlsruhe, Germany), respectively. AFM tips were provided from AppNano (Applied Nanostructures Inc., Santa Clara, CA, USA).

4.2. Substrates and Polyelectrolyte (PEL) Preparation

The physicochemical and biological properties of multilayers were investigated by using model substrates, such as silicon wafers and glass cover slips. A solution of ammonia, hydrogen peroxide and water (1:1:5, v/v/v) at 75 °C for 10 min was used for cleaning of substrata. Thereafter, the wafers as well as the glass cover slips were washed with ultrapure water (6 × 5 min), and dried with a stream of nitrogen [52]. Hyaluronic acid, heparin and chitosan solutions were prepared at a concentration of (2 mg·mL⁻¹) by dissolution in 150 mM NaCl at pH 4.0. Poly (ethylene imine) was dissolved at a concentration of 5 mg·mL⁻¹ in 150 mM NaCl at pH 7.0 as in previous studies [17]. Poly (ether sulfone) filters of 0.2 μm pore size was used for sterilization of solutions.

4.3. Polyelectrolyte Multilayers (PEMs) Formation

An anchoring base layer of poly (ethylene imine) was applied to obtain a positive surface net charge on silicon and glass substrates for subsequent adsorption of polysaccharides as done in previous studies [17]. In addition, this substrate was used as a control for comparison with multilayers. PEI was adsorbed for 30 min on glass or silicone slides and rinsed with 150 mM NaCl at pH 7.0, three times for 5 min each. Subsequently, multilayers of HA or Hep as polyanions, followed by washing with PBS and subsequent adsorption of Chi for 15 min each until 4 double layers and a final GAG layer were obtained. The control surface was always abbreviated as PEI, while the multilayer systems were always abbreviated as either (PEI, PEI(HA-Chi)₄HA or PEI(Hep-Chi)₄Hep). In studies on association and uptake of FITC-GAG, the last two GAG layers consisted of either FITC-HA or FITC-Hep [17].

4.4. Characterization of Surface Properties and Multilayer Formation

4.4.1. Scanning Electron Microscopy (SEM)

The coated silicon wafers with PEMs were analysed by Philips ESEM XL 30 FEG (Eindhoven, Netherlands) in high vacuum ($p = 10^{-6}$ mbar) to visualize the surface topography. A conductive layer of 15 nm thick chromium (Cr) was deposited by sputtering.

4.4.2. Atomic Force Microscopy (AFM)

AFM (Nano-R, Pacific Nanotechnology, Santa Clara, CA, USA) was also used to study surface topography of PEI- and GAG-modified silicon wafers (Si) in a three-dimensional view. A contact mode under ambient (air) laboratory conditions of temperature and humidity was selected in order to probe the coated Si wafers (10 × 10 mm²). Images were taken by using AFM tips with 125 μm length, 35 μm width, 14–16 μm height and a tip radius of <10 nm. A resolution of (512 × 512 pixel²) as well as a scan area of 10 × 10 μm² per image was applied with a scan rate of 0.2 Hz. Gwiddy software (Nano-R, Pacific Nanotechnology, Santa Clara, CA, USA) (version 2.40) was used for image processing [17].

4.4.3. Water Contact Angle (WCA)

The wettability of the samples was determined with static water contact angle (WCA). An OCA 15+ device from Dataphysics (Filderstadt, Germany) using the sessile drop method was applied here. Ultrapure water of 2 μL with a minimum of five droplets was investigated to each sample (2 for each material) at room temperature. The obtained values were used to calculate the means and standard deviations [38].

4.4.4. Measurement of Multilayer Thickness by Ellipsometry

The average thickness of the PEMs was determined by the spectroscopic ellipsometry (M-2000 V, J.A. Woollam Company, Lincoln, NE, USA). The used reference substrate was a cleaned Si wafer with a SiO₂ layer thickness of 2.5 nm. A Cauchy model was used to extract the optical constants of the multilayers, which was previously described in the literature [51].

4.5. Studies with THP-1 Derived Macrophages

4.5.1. Cell Culture

RPMI-1640 medium (Lonza, Wuppertal, Germany) supplemented with 10% (v/v) foetal bovine serum (FBS, Biochrom AG, Berlin, Germany) and 1% (v/v) antibiotic–antimycotic solution (AAS, Lonza, Wuppertal, Germany) was used for culturing THP-1 human monocytic cells (DSMZ, Braunschweig, Germany) at 37 °C in a humidified 5% CO₂/95% air atmosphere in a NUAIRE® DH Autoflow incubator (NuAire, Plymouth, MN, USA). Cells were passaged every second day to maintain a cell density of 1×10^6 cells mL⁻¹. Macrophages were differentiated from floating THP-1 cells by incubation with 200 nM phorbol-12-myristate-13-acetate (PMA, Sigma Aldrich, Darmstadt, Germany) in T75 cell culture flasks (Greiner Bio-One GmbH and Co.KG, Frickenhausen, Germany) for 48 h. Afterwards, 0.25% trypsin/0.02% EDTA (Biochrom AG, Berlin, Germany) was used to detach the adherent macrophages with further addition of serum-containing RPMI-1640 medium to stop the trypsin effect. Finally, the harvested cells were used for seeding on the different PEMs-modified surfaces [34].

4.5.2. Cell Adhesion Studies

An ultraviolet light chamber (Bio-Link BLX, LTF Labortechnik GmbH and Co. KG, Wasserburg, Germany) set at 254 nm ($50 \text{ J} \cdot \text{cm}^{-2}$) was used for sterilization of PEM modified samples and PEI coated control surfaces (samples were placed in 24-well tissue culture plates, Greiner Bio-One GmbH and Co.KG, Frickenhausen, Germany). Sterilization by UV light was done for 60 min prior to cell studies. Macrophages were seeded at a cell density of 2.5×10^4 cells·mL⁻¹ in serum-containing RPMI-1640 medium. Cells were cultured on the samples for 24 h at 37 °C in a humidified 5% CO₂/95% air atmosphere. Thereafter, gentle washing with phosphate buffer saline (PBS) was done twice to remove non-adherent cells. The attached cells were fixed with cold methanol (Roth, (Karlsruhe, Germany)) for 10 min and stained with 10% (v/v) Giemsa (Merck KGaA, Darmstadt, Germany) in ultrapure water for another 10 min. Micrographs were taken by a light microscope (Nikon ECLIPSE Ti2, Tokyo, Japan) equipped with a CMOS camera (Nikon DS-Fi3, Tokyo, Japan). ImageJ software (version 1.52p, <https://imagej.nih.gov>) was used to quantify the number of adhering cells of the images [21].

4.5.3. Analysis of Multinucleated Giant Cells (MNGCs) Formation

The formation of MNGCs was evaluated through MNGCs area percentage after culturing macrophages, initially seeded at density of 2.5×10^5 cells·mL⁻¹, on the PEMs and PEI surfaces for 10 days. Samples were gently washed twice with PBS followed by fixation of attached cells with cold methanol and staining with 10% (v/v) Giemsa in ultrapure water. Cells were imaged using light microscopy. The area percentage of MNGCs was calculated by ImageJ software [38].

4.5.4. IL-1β Production Measurement

The pro-inflammatory cytokine release was investigated using an enzyme linked immunosorbent assay (ELISA). The measurements were performed according to the manufacturer's instructions (Thermo Scientific, Germany) for the medium supernatants of samples. Two sets of samples were collected after 24 h of incubation in the absence and presence of LPS and stored at -20 °C until needed for investigation. A QBlue® cell viability assay (BioChain, California, USA) was used to estimate the

cell viability in attempt to normalize the cytokine production to the quantity of metabolic active cells on the different PEMs surfaces.

Therefore, the attached cells of the different surfaces were washed carefully with sterile PBS after supernatant collection. Then, a pre-warmed, colourless Dulbecco's modified Eagle's medium (DMEM) with QBlue® assay reagent (10:1) were added and incubated for 2 h at 37 °C in humidified 5% CO₂/95% air atmosphere. Eventually, the relative fluorescence unit (RFU) values were measured after transferring 100 µL of the supernatant from each well to a black 96-well plate. The values were measured at an excitation wavelength of 544 nm and emission wavelength of 590 nm with plate reader [34].

4.5.5. Immunofluorescence (IF) Staining of NF-κB

Immunostaining was performed to study the translocation of the p65 subunit of NF-κB according to the method developed by Noursadeghi et al. [53]. Macrophages were seeded like in the aforementioned section and cultured for 48 h. Samples were analysed in two sets in the absence and presence of 1 µg·mL⁻¹ lipopolysaccharide (LPS, Sigma Aldrich, Darmstadt, Germany). Thereafter, fixation of the cultured cells on PEI and PEMs surfaces was performed with 4% paraformaldehyde (Sigma Aldrich, Darmstadt, Germany) for 15 min, permeabilized with 0.1% (v/v) Triton® X-100 (Sigma-Aldrich, Taufkirchen, Germany) for 10 min at RT, and rinsed twice with PBS. The non-specific binding sites were blocked by using bovine serum albumin (BSA, ≥98%, Carl Roth GmbH, Halle (Saale), Germany; 1%, w/v) in PBS for 30 min. Afterwards, cells were incubated with a monoclonal p65 subunit of the NF-κB antibody (1:100, Santa Cruz Biotechnology, Dallas, TX, USA) at 4 °C overnight. A secondary monoclonal anti-rabbit IgG antibody conjugated with CY2 (1:200, Jackson ImmunoResearch, Ely, UK) was applied for another 30 min at RT after washing with PBS for 5 min on a shaker. TO-PRO-3 (1:500, Invitrogen, CA, USA) for 40 min at RT was used for the nuclei staining. Eventually, confocal microscope LSM 710 (Carl Zeiss, Oberkochen, Germany) applying a 40-fold oil immersion objective was utilized to examine the samples that were mounted on glass slides with polyvinyl alcohol (PVA, Sigma Aldrich, Darmstadt, Germany). ImageJ (v.1.52i) software was used for image processing. The TO-PRO-3 channel was used to mask a region of interest (ROI). Then the nuclear ROI was subtracted from the cellular ROI to obtain a cytosolic ROI. Finally, the fluorescence intensity was evaluated in the nuclear and cytosolic ROI and a ratio calculated [21]. The principle of the method is visualized in Figure S1.

4.5.6. Cell Lysis for Immunoblotting (IB)

THP-1 derived macrophages were differentiated as described above and cultured for 48 h at a cell density of 52 × 10⁵ cells·mL⁻¹ on the prepared PEMs and PEI on objective glass slides with a total area of 19.76 cm² (Menzel GmbH, Bielefeld, Germany) in the four well plates (Greiner Bio-one, Leipzig, Germany). Thereafter, plates were placed on ice and the cells were washed twice with ice-cold PBS. Afterwards, the macrophages were scraped using a cold plastic cell scraper after adding a cell lysate buffer (RIPA buffer) with protease and phosphatase inhibitors (Thermo Fisher scientific, Waltham, MA, USA). Then, a constant agitation at 4 °C for 30 min was maintained beyond the gentle transfer of cell lysates into pre-cooled tubes. Subsequently, the cell lysates were centrifuged at 4 °C and 13,000 rpm for 20 min then the supernatants were stored at -80 °C up to one month before performance of IB [21].

4.5.7. SDS-PAGE and Western Blotting

The same amount of proteins from each samples cell lysate were separated in 15% SDS-polyacrylamide gels and transferred onto nitrocellulose membranes (Schleicher and Schuell GmbH, Munich, Germany). In TBS-T, 3% (w/v) milk powder was used to block membranes, probed with monoclonal antibodies against phospho-NF-κB (CST, #3033), NF-κB (Santa Cruz Biotechnology, sc-8008) and β-actin (MERCK, A1978), followed by incubation with HRP-labelled secondary antibodies and visualized with the enhanced chemiluminescence reaction (Thermo Fisher Scientific, Waltham, MA, USA) in a ChemiDoc Imaging System (Bio-Rad, CA, USA). Obtained grayscale images were

densitometrically analysed by Li-Cor Image Studio software using automatic background determination and subtraction function [21].

4.5.8. Association of FITC-GAG with Macrophages Studied by Confocal Laser Scanning Microscopy

The same density as in the MNGCs formation analysis was used for culturing macrophages for 24 h on PEI and PEMs with terminal layers of FITC-labelled GAG. Cell fixation was performed by adding 4% paraformaldehyde (Sigma Aldrich, Darmstadt, Germany) for 10 min. Thereafter, each sample and incubated for 10 min after adding 0.5 mL of membrane dye carbocyanine (DID, Biotium, Fremont, CA, USA) solution (5 µL of dye in 1 mL PBS). Eventually, CLSM using 63-fold oil immersion objective (LSM 710, Carl Zeiss, Oberkochen, Germany) was used to examine all samples that were washed twice with PBS, mounted on objective slides using polyvinyl alcohol (PVA, Sigma Aldrich, Darmstadt, Germany). ZEN2011 software (Carl Zeiss, Oberkochen, Germany) was utilized for image processing [21].

4.5.9. Uptake of FITC-GAG by Macrophages Studied with Flow Cytometry

Cells were seeded on PEI and PEMs with the terminal two single layers of FITC-labelled GAG and cultured for 48 h as described in the aforementioned section of CLSM. The cells were scraped after trypsinization, centrifuged, washed once with PBS and resuspended in 200 µL PBS. Then, a flow cytometry device (LSR Fortessa II, BD Bioscience, Germany) was used to measure the 100 µL cell suspension, which was transferred to 96-well plate. FACS-Diva software (LSR Fortessa II, BD Bioscience, Germany) (version 6.2) was used for data analysis [21].

4.6. Statistics

An origin 8 Pro software (Origin Lab, Northampton, MA, USA) was used here for the statistical calculations. The one-way analysis of variance (ANOVA) followed by post-hoc Tukey's test was applied. The mean values ± standard deviations (SD) represented all used data. It is indicated in the respective figure captions, the samples' number. Statistical significance was considered for $p \leq 0.05$ and is visualized by asterisks in the figures.

5. Conclusions

In this study, it was shown that the anti-inflammatory effect of PEMs made of either heparin or hyaluronan with chitosan as a polycation were related to reduced adhesion, interleukin I-β release and macrophage fusion, when compared to a pro-inflammatory model surface based on the highly cationic polyethylene imine. It was evident that the observed effects are not solely based on the hydrophilic character of these PEMs when compared to PEI. Indeed, it was shown that the pharmaceutical effects of heparin and hyaluronan known from other studies came into play when macrophages adhering on PEMs associated with and took up these molecules through different membrane receptors that may lead to the suppression of the canonical NF-κB signalling pathway. Hence, such multilayer systems may be of great interest and potential to modulate inflammatory responses of biomaterials improving function and lifetime of implantable biomedical devices.

Supplementary Materials: Supplementary materials can be found at <http://www.mdpi.com/1422-0067/21/10/3724/s1>.

Author Contributions: Conceptualization, T.G. and H.A.; methodology, H.A.; formal analysis, H.A. and A.H.; investigation, H.A., A.H., B.F., F.S., F.E. and G.Z.; data curation, H.A. and A.H.; writing—original draft preparation, H.A.; writing—review and editing, S.S., S.N. and T.G.; supervision, T.G.; project administration, T.G. All authors have read and agreed to the published version of the manuscript.

Funding: This research was funded by German Academic Exchange Service (DAAD) as well as by a bilateral cooperation between DAAD and Ministry of Education, Science and Technological Development of the Republic of Serbia (period 2019–2020).

Acknowledgments: This work was financially supported by the German Academic Exchange service (DAAD) through a PhD grant to Hala Alkhoury. The study was also part of the project of bilateral cooperation funded by DAAD and Ministry of Education, Science and Technological Development of the Republic of Serbia (period 2019–2020). The kind support by Alexander Navarrete Santos from the university hospital, in the core facility of cell analysis and cell sorting at Martin Luther University Halle-Wittenberg, in the flow cytometry is greatly appreciated.

Conflicts of Interest: The authors declare no conflict of interest.

References

1. Tang, L.; Eaton, J.W. Inflammatory responses to biomaterials. *Am. J. Clin. Pathol.* **1995**, *103*, 466–471. [[CrossRef](#)]
2. Anderson, J.M. In vitro and in vivo monocyte, macrophage, foreign body giant cell, and lymphocyte interactions with biomaterials. In *Biological Interactions on Materials Surfaces*; Springer: Berlin, Germany, 2009; pp. 225–244.
3. Mariani, E.; Lisignoli, G.; Borzì, R.M.; Pulsatelli, L. Biomaterials: Foreign bodies or tuners for the immune response? *Int. J. Mol. Sci.* **2019**, *20*, 636. [[CrossRef](#)]
4. Murray, P.J.; Wynn, T.A. Protective and pathogenic functions of macrophage subsets. *Nat. Rev. Immunol.* **2011**, *11*, 723. [[CrossRef](#)]
5. Schutte, R.J.; Parisi-Amon, A.; Reichert, W.M. Cytokine profiling using monocytes/macrophages cultured on common biomaterials with a range of surface chemistries. *J. Biomed. Mater. Res.* **2009**, *88*, 128–139. [[CrossRef](#)]
6. Wynn, T.A.; Barron, L. Macrophages: Master regulators of inflammation and fibrosis. *Semin. Liver Dis.* **2010**, *30*, 245–257. [[CrossRef](#)]
7. Fialkow, L.; Wang, Y.; Downey, G.P. Reactive oxygen and nitrogen species as signaling molecules regulating neutrophil function. *Free Radic. Biol. Med.* **2007**, *42*, 153–164. [[CrossRef](#)]
8. Underhill, D.M.; Goodridge, H.S. Information processing during phagocytosis. *Nat. Rev. Immunol.* **2012**, *12*, 492. [[CrossRef](#)]
9. Xia, Z.; Triffitt, J.T. A review on macrophage responses to biomaterials. *Biomed. Mater.* **2006**, *1*, R1. [[CrossRef](#)]
10. Serini, G.; Bochaton-Piallat, M.-L.; Ropraz, P.; Geinoz, A.; Borsi, L.; Zardi, L.; Gabbiani, G. The fibronectin domain ED-A is crucial for myofibroblastic phenotype induction by transforming growth factor-β1. *J. Cell Biol.* **1998**, *142*, 873–881. [[CrossRef](#)]
11. Barron, L.; Wynn, T.A. Fibrosis is regulated by Th2 and Th17 responses and by dynamic interactions between fibroblasts and macrophages. *Am. J. Physiol. -Gastrointest. Liver Physiol.* **2011**, *300*, G723. [[CrossRef](#)]
12. Ratner, B.D.; Bryant, S.J. Biomaterials: Where we have been and where we are going. *Annu. Rev. Biomed. Eng.* **2004**, *6*, 41–75. [[CrossRef](#)]
13. Altman, R.D.; Manjoo, A.; Fierlinger, A.; Niazi, F.; Nicholls, M. The mechanism of action for hyaluronic acid treatment in the osteoarthritic knee: A systematic review. *Bmc Musculoskelet. Disord.* **2015**, *16*, 321. [[CrossRef](#)]
14. Franz, S.; Rammelt, S.; Scharnweber, D.; Simon, J.C. Immune responses to implants—a review of the implications for the design of immunomodulatory biomaterials. *Biomaterials* **2011**, *32*, 6692–6709. [[CrossRef](#)]
15. Vroman, L.; Adams, A.; Fischer, G.; Munoz, P. Interaction of high molecular weight kininogen, factor XII, and fibrinogen in plasma at interfaces. *Blood* **1980**, *55*, 156–159. [[CrossRef](#)]
16. Suarez, P.; Rojo, L.; Gonzalez-Gomez, A.; Roman, J.S. Self-assembling gradient copolymers of vinylimidazol and (acrylic)ibuprofen with anti-inflammatory and zinc chelating properties. *Macromol. Biosci.* **2013**, *13*, 1174–1184. [[CrossRef](#)]
17. Al-Khoury, H.; Espinosa-Cano, E.; Aguilar, M.a.R.; Romaán, J.S.; Syrowatka, F.; Schmidt, G.; Groth, T. Anti-inflammatory Surface Coatings Based on Polyelectrolyte Multilayers of Heparin and Polycationic Nanoparticles of Naproxen-Bearing Polymeric Drugs. *Biomacromolecules* **2019**, *20*, 10. [[CrossRef](#)]
18. Borges, J.; Mano, J.F. Molecular interactions driving the layer-by-layer assembly of multilayers. *Chem. Rev.* **2014**, *114*, 8883–8942. [[CrossRef](#)]
19. Benkirane-Jessel, N.; Schwinte, P.; Falvey, P.; Darcy, R.; Haikel, Y.; Schaaf, P.; Voegel, J.C.; Ogier, J. Build-up of polypeptide multilayer coatings with anti-inflammatory properties based on the embedding of piroxicam-cyclodextrin complexes. *Adv. Funct. Mater.* **2004**, *14*, 174–182. [[CrossRef](#)]
20. Shao, J.; Wen, C.; Xuan, M.; Zhang, H.; Frueh, J.; Wan, M.; Gao, L.; He, Q. Polyelectrolyte multilayer-cushioned fluid lipid bilayers: A parachute model. *Phys. Chem. Chem. Phys.* **2017**, *19*, 2008–2016. [[CrossRef](#)]

21. AlKhoury, H.; Hautmann, A.; Erdmann, F.; Zhou, G.; Stojanovic, S.; Najman, S.; Groth, T. Study on the potential mechanism of anti-inflammatory activity of covalently immobilized hyaluronan and heparin. *J. Biomed. Mater. Res.* **2020**. [[CrossRef](#)]
22. Aggarwal, N.; Altgärde, N.; Svedhem, S.; Michanetzis, G.; Missirlis, Y.; Groth, T. Tuning Cell Adhesion and Growth on Biomimetic Polyelectrolyte Multilayers by Variation of p H During Layer-by-L ayer Assembly. *Macromol. Biosci.* **2013**, *13*, 1327–1338. [[CrossRef](#)]
23. Mehta, V.B.; Besner, G.E. Inhibition of NF-κB activation and its target genes by heparin-binding epidermal growth factor-like growth factor. *J. Immunol.* **2003**, *171*, 6014–6022. [[CrossRef](#)]
24. Neumann, A.; Schinzel, R.; Palm, D.; Riederer, P.; Münch, G. High molecular weight hyaluronic acid inhibits advanced glycation endproduct-induced NF-κB activation and cytokine expression. *FEBS Lett.* **1999**, *453*, 283–287. [[CrossRef](#)]
25. Karin, M.; Greten, F.R. NF-κB: Linking inflammation and immunity to cancer development and progression. *Nat. Rev. Immunol.* **2005**, *5*, 749. [[CrossRef](#)]
26. Lawrence, T. The nuclear factor NF-kappaB pathway in inflammation. *Cold Spring Harb. Perspect Biol.* **2009**, *1*, a001651. [[CrossRef](#)]
27. Liu, T.; Zhang, L.; Joo, D.; Sun, S.-C. NF-κB signaling in inflammation. *Signal Transduct. Target. Ther.* **2017**, *2*, 17023. [[CrossRef](#)]
28. Ghosh, S.; Hayden, M.S. New regulators of NF-κB in inflammation. *Nat. Rev. Immunol.* **2008**, *8*, 837. [[CrossRef](#)]
29. Avenoso, A.; D’Ascola, A.; Scuruchi, M.; Mandraffino, G.; Calatroni, A.; Saitta, A.; Campo, S.; Campo, G.M. Hyaluronan in the experimental injury of the cartilage: Biochemical action and protective effects. *Inflamm. Res.* **2018**, *67*, 5–20. [[CrossRef](#)]
30. Altman, R.; Bedi, A.; Manjoo, A.; Niazi, F.; Shaw, P.; Mease, P. Anti-inflammatory effects of intra-articular hyaluronic acid: A systematic review. *Cartilage* **2019**, *10*, 43–52. [[CrossRef](#)]
31. Naor, D.; Nedvetzki, S.; Walmsley, M.; Yayon, A.; Turley, E.A.; Golan, I.; Caspi, D.; Sebban, L.E.; Zick, Y.; Garin, T. CD44 involvement in autoimmune inflammations. *Ann. N. Y. Acad. Sci.* **2007**, *1110*, 233–247. [[CrossRef](#)]
32. Lee, J.H.; Lee, J.; Seo, G.H.; Kim, C.H.; Ahn, Y.S. Heparin inhibits NF-κB activation and increases cell death in cerebral endothelial cells after oxygen-glucose deprivation. *J. Mol. Neurosci.* **2007**, *32*, 145–154. [[CrossRef](#)] [[PubMed](#)]
33. Köwitsch, A.; Zhou, G.; Groth, T. Medical application of glycosaminoglycans: A review. *J. Tissue Eng. Regen. Med.* **2018**, *12*, e23–e41. [[CrossRef](#)]
34. Zhou, G.; Niepel, M.S.; Saretia, S.; Groth, T. Reducing the inflammatory responses of biomaterials by surface modification with glycosaminoglycan multilayers. *J. Biomed. Mater. Res.* **2016**, *104*, 493–502. [[CrossRef](#)] [[PubMed](#)]
35. Kolasinska, M.; Krastev, R.; Warszynski, P. Characteristics of polyelectrolyte multilayers: Effect of PEI anchoring layer and posttreatment after deposition. *J. Colloid Interface Sci.* **2007**, *305*, 46–56. [[CrossRef](#)] [[PubMed](#)]
36. Zhou, G.; Loppnow, H.; Groth, T. A macrophage/fibroblast co-culture system using a cell migration chamber to study inflammatory effects of biomaterials. *Acta Biomater* **2015**, *26*, 54–63. [[CrossRef](#)]
37. Bacakova, L.; Filova, E.; Parizek, M.; Ruml, T.; Svorcik, V. Modulation of cell adhesion, proliferation and differentiation on materials designed for body implants. *Biotechnol. Adv.* **2011**, *29*, 739–767. [[CrossRef](#)]
38. Zhou, G.; Al-Khoury, H.; Groth, T. Covalent immobilization of glycosaminoglycans to reduce the inflammatory effects of biomaterials. *Int. J. Artif. Organs* **2016**, *39*, 37–44. [[CrossRef](#)]
39. Hernández-Montelongo, J.; Nascimento, V.F.; Murillo, D.; Taketa, T.B.; Sahoo, P.; de Souza, A.A.; Beppu, M.M.; Cotta, M.A. Nanofilms of hyaluronan/chitosan assembled layer-by-layer: An antibacterial surface for *Xylella fastidiosa*. *Carbohydr. Polym.* **2016**, *136*, 1–11. [[CrossRef](#)]
40. Sheikh, Z.; Brooks, P.; Barzilay, O.; Fine, N.; Glogauer, M. Macrophages, foreign body giant cells and their response to implantable biomaterials. *Materials* **2015**, *8*, 5671–5701. [[CrossRef](#)]
41. Min, Y.-D.; Choi, C.-H.; Bark, H.; Son, H.-Y.; Park, H.-H.; Lee, S.; Park, J.-W.; Park, E.-K.; Shin, H.-I.; Kim, S.-H. Quercetin inhibits expression of inflammatory cytokines through attenuation of NF-κB and p38 MAPK in HMC-1 human mast cell line. *Inflamm. Res.* **2007**, *56*, 210–215. [[CrossRef](#)]

42. Blackwell, T.S.; Blackwell, T.R.; Christman, J.W. Impaired activation of nuclear factor-kappaB in endotoxin-tolerant rats is associated with down-regulation of chemokine gene expression and inhibition of neutrophilic lung inflammation. *J. Immunol.* **1997**, *158*, 5934–5940. [PubMed]
43. Zhao, M.; Altankov, G.; Grabiec, U.; Bennett, M.; Salmeron-Sanchez, M.; Dehghani, F.; Groth, T. Molecular composition of GAG-collagen I multilayers affects remodeling of terminal layers and osteogenic differentiation of adipose-derived stem cells. *Acta Biomater.* **2016**, *41*, 86–99. [CrossRef] [PubMed]
44. Young, E. The anti-inflammatory effects of heparin and related compounds. *Thromb. Res.* **2008**, *122*, 743–752. [CrossRef]
45. Young, E.; Venner, T.; Ribau, J.; Shaughnessy, S.; Hirsh, J.; Podor, T.J. The binding of unfractionated heparin and low molecular weight heparin to thrombin-activated human endothelial cells. *Thromb. Res.* **1999**, *96*, 373–381. [CrossRef]
46. Ruppert, S.M.; Hawn, T.R.; Arrigoni, A.; Wight, T.N.; Bollyky, P.L. Tissue integrity signals communicated by high-molecular weight hyaluronan and the resolution of inflammation. *Immunol. Res.* **2014**, *58*, 186–192. [CrossRef]
47. Neuman, M.G.; Nanau, R.M.; Oruña, L.; Coto, G. In vitro anti-inflammatory effects of hyaluronic acid in ethanol-induced damage in skin cells. *J. Pharm. Pharm. Sci.* **2011**, *14*, 425–437. [CrossRef]
48. Knudson, W.; Chow, G.; Knudson, C.B. CD44-mediated uptake and degradation of hyaluronan. *Matrix Biol.* **2002**, *21*, 15–23. [CrossRef]
49. Yamamoto, Y.; Gaynor, R.B. Therapeutic potential of inhibition of the NF-κB pathway in the treatment of inflammation and cancer. *J. Clin. Investig.* **2001**, *107*, 135–142. [CrossRef]
50. Zang, Y.C.; Halder, J.B.; Hong, J.; Rivera, V.M.; Zhang, J.Z. Regulatory effects of estriol on T cell migration and cytokine profile: Inhibition of transcription factor NF-κB. *J. Neuroimmunol.* **2002**, *124*, 106–114. [CrossRef]
51. Köwitsch, A.; Abreu, M.J.; Chhalotre, A.; Hielscher, M.; Fischer, S.; Mäder, K.; Groth, T. Synthesis of thiolated glycosaminoglycans and grafting to solid surfaces. *Carbohydr. Polym.* **2014**, *114*, 344–351. [CrossRef]
52. Macek, M. A review of advanced wet cleaning. *Inf. Midem* **1993**, *23*, 275–283.
53. Noursadeghi, M.; Tsang, J.; Hausteiner, T.; Miller, R.F.; Chain, B.M.; Katz, D.R. Quantitative imaging assay for NF-κB nuclear translocation in primary human macrophages. *J. Immunol. Methods* **2008**, *329*, 194–200. [CrossRef]



© 2020 by the authors. Licensee MDPI, Basel, Switzerland. This article is an open access article distributed under the terms and conditions of the Creative Commons Attribution (CC BY) license (<http://creativecommons.org/licenses/by/4.0/>).

Chapter 5

Summary – Tissue response to biphasic calcium phosphate covalently modified with either heparin or hyaluronic acid in a mouse subcutaneous implantation model:

The encouraging results of *in vitro* studies with macrophages on the anti-inflammatory effects of GAGs spiked further for *in vivo* investigations in mice. In this chapter, a special focus is set on tissue response in terms of ectopic bone-formation together with limiting inflammatory responses studied in a mouse subcutaneous implantation model. Biphasic calcium phosphate (BCP) was used as reference control for its resorption/degradation properties while either HA or Hep were covalently immobilized on top of the BCP particles by using EDC/NHS cross linking chemistry as described in chapter 2. Surface characterizations investigated the topography by SEM, the ZP measurements and the surface composition with X-ray photoelectron spectroscopy (XPS) in attempt to examine the immobilization process of the GAGs. Results displayed an increase of the negative ZP on BCP-HA and BCP-Hep coated particles in comparison to the control BCP particles, giving an indication of a successful immobilization process. However, the focus of the study was placed on the histological analysis, which indicated that both BCP-HA and BCP-Hep coated particles showed reduced vascularization as well as higher vasculogenic-related genes (Flt1 and Vcam1) expression after 30 days in comparison to plain BCP. In contrast, the osteogenic genes Sp7 and Bglap after 30 days had the highest expression with the control BCP followed BCP-Hep while the lowest expression was in BCP-HA. Moreover, the BCP- HA coated particles limited inflammatory responses with formation of new bone-like tissue while BCP-Hep coated particles delayed the onset of inflammation and permitted the osteogenesis in this subcutaneous bone-forming model. In conclusion, the present study showed for the first time the covalent immobilization of HA and Hep on BCP to be eventually used for tissue response modulation in bone tissue regeneration as well as of ectopic bone formation.



Tissue response to biphasic calcium phosphate covalently modified with either heparin or hyaluronic acid in a mouse subcutaneous implantation model

Journal:	<i>Journal of Biomedical Materials Research: Part A</i>
Manuscript ID	JBMR-A-20-0298
Wiley - Manuscript type:	Original Article
Date Submitted by the Author:	06-May-2020
Complete List of Authors:	Stojanović, Sanja; Faculty of Medicine, University of Niš, Serbia, Department for Cell and Tissue Engineering, Department of Biology and Human Genetics Alkhoury, Hala; Martin Luther University Halle Wittenberg, Biomedical Materials Group; Martin Luther University Halle Wittenberg, Interdisciplinary Center of Materials Science Radenković, Milena; Faculty of Medicine, University of Niš, Serbia, Department for Cell and Tissue Engineering Cvetković, Vladimir; Faculty of Sciences and Mathematics, University of Niš, Department of Biology and Ecology Jablonska, Magdalena; Fraunhofer Institute for Microstructure of Materials and Systems IMWS, Department of Biological and Macromolecular Materials Schmelzer, Christian; Fraunhofer Institute for Microstructure of Materials and Systems, IMWS Syrowatka, Frank; Martin Luther University Halle Wittenberg, Interdisciplinary Center for Materials Science Živković, Jelena; Faculty of Medicine, University of Niš, Serbia, Department for Cell and Tissue Engineering, Department of Biology and Human Genetics Groth, Thomas; Martin Luther University Halle-Wittenberg, Biomedical Materials Group Najman, Stevo; Faculty of Medicine, Cell and Tissue engineering; Faculty of Medicine University of Niš, Biology and Human Genetics
Keywords:	glycosaminoglycans, biphasic calcium phosphate, covalent modification, subcutaneous tissue reaction, ectopic osteogenesis

SCHOLARONE™
Manuscripts

Tissue response to biphasic calcium phosphate covalently modified with either heparin or hyaluronic acid in a mouse subcutaneous implantation model

Sanja Stojanović^{1,2*}, Hala AlKhoury^{3,4*}, Milena Radenković², Vladimir Cvetković⁵,
Magdalena Jablonska⁶, Christian E.H. Schmelzer⁶, Frank Syrowatka⁴, Jelena M.
Živković^{1,2}, Thomas Groth^{3,4,7,#}, Stevo Najman^{1,2,#,§}

¹Department of Biology and Human Genetics, Faculty of Medicine, University of Niš, 18000 Niš, Serbia

²Department for Cell and Tissue Engineering, Scientific Research Center for Biomedicine, Faculty of Medicine, University of Niš, 18000 Niš, Serbia

³Department Biomedical Materials, Institute of Pharmacy, Martin Luther University Halle Wittenberg, Heinrich Damerow Strasse 4, D 06120 Halle (Saale), Germany

⁴Interdisciplinary Center of Materials Science, Martin Luther University Halle-Wittenberg, 06120 Halle (Saale), Germany

⁵Department of Biology and Ecology, Faculty of Sciences and Mathematics, University of Niš, 18000 Niš, Serbia

⁶Fraunhofer Institute for Microstructure of Materials and Systems IMWS, Department of Biological and Macromolecular Materials, 06120 Halle (Saale), Germany

⁷Laboratory of Biomedical Nanotechnologies, Institute of Bionic Technologies and Engineering, I.M. Sechenov First Moscow State University, 119991, Trubetskaya street 8, Moscow, Russian Federation

* These Authors contributed equally to this manuscript

These Authors contributed equally to this manuscript

§ *Corresponding author*. Full Prof. Stevo Najman, PhD, Faculty of Medicine, University of Niš, Blvd. Dr Zorana Đinđića 81, 18000 Niš, Republic of Serbia

E-mail: stevo.najman@gmail.com

Abstract

Biphasic calcium phosphate materials (BCP) are widely employed as bone substitute materials due their resorption/degradation properties. Inflammation after implantation of such materials represents a pre-requisite for bone tissue repair and regeneration but can be also problematic if not only transient followed by fibrosis and scarring. Here, we modified BCP covalently with hyaluronan (HA) and heparin (Hep), glycosaminoglycans that possess anti-inflammatory properties. Beside the characterization of particle surface properties, the focus was on *in vivo* tissue response after subcutaneous implantation in mice. Histological analysis revealed a decrease in signs of inflammatory response to BCP when modified with either HA or Hep. Reduced vascularization after 30 days was noticed when BCP was modified with either HA or Hep with greater cellularity in all examined time points. Compared to plain BCP, expression of vasculogenic-related genes *Flt1* and *Vcam1* was higher in BCP-HA and BCP-Hep group at day 30. Expression of osteogenic genes *Sp7* and *Bglap* after 30 days was the highest in BCP group, followed by BCP-Hep, while the lowest expression was in BCP-HA group which correlates with collagen amount. Hence, coating of BCP particles with HA seems to suppress inflammatory response together with formation of new bone-like tissue, while the presence of Hep delays the onset of inflammatory response but permits osteogenesis in this subcutaneous bone-forming model. Transferring the results of this study to other coated materials intended for biomedical application may also pave the way to reduction of inflammation after their implantation.

Keywords: glycosaminoglycans, biphasic calcium phosphate, covalent modification, subcutaneous tissue reaction, ectopic osteogenesis

1. INTRODUCTION

Inflammation represents one of the major factors that direct the course and outcome of bone repair after injury as well as the fate of any biomaterial used for guided bone regeneration. In cases of biomaterials implantation into the defect site, these processes are largely influenced by the properties of used material such as chemical composition, surface and mechanical properties and stability versus degradability [1]. Although it is necessary, prolonged and excessive inflammation can lead to the scar tissue formation and inappropriate tissue regeneration and repair [2]. There are various types of biomaterials that are used in bone tissue engineering and regeneration. Important characteristics of the most suitable biomaterial for bone tissue regeneration are, besides biocompatibility, to be biomechanically stable, moderately resorbable, not inducing chronic inflammation and foreign body reaction, to integrate into surrounding tissue and to initiate and enable appropriate formation of new bone [3,4].

Calcium phosphate-based synthetic biomaterials are commonly used in guided bone regeneration due to their osteoconductive properties, osteogenic and osteoinductive potential [5,6]. This is based on the ability of these materials to adsorb proteins supportive for bone tissue formation and to be resorbed by releasing calcium ions and phosphate, which can be used by progenitor cells to form new bone [7]. A challenge in the development of these materials is to achieve degradation and resorption in an appropriate time frame that permits the formation of sufficient new bone tissue. To address this issue biphasic calcium phosphate have been developed, which represents a mixture of faster degrading calcium phosphate and hydroxyapatite which degrades slowly [7-9].

Since the inflammatory response to biomaterials is crucial for functional integration of implants on one hand, but also is responsible for adverse events like fibrosis and scarring on the other, modification of biomaterials with anti-inflammatory agents and immunomodulatory molecules is an emerging area of research [10]. Some glycosaminoglycans (GAGs) like heparin and hyaluronan represent very good candidates due to their immunomodulatory and especially anti-inflammatory properties [11-14]. Hyaluronic acid (HA) is a component of tissue extracellular matrix (ECM) which plays a key role in various processes such as cell adhesion, chemotaxis, differentiation, proliferation, cellular migration, wound healing, inflammation,

angiogenesis and tissue regeneration via specific receptors and signaling pathways [15-18]. Heparin is a highly sulfated GAG that is used as anti-coagulant drug but exerts other biological activities such as anti-inflammatory, inhibiting leukocyte adhesion to endothelium and accumulation of cells in inflamed tissues by binding directly to several adhesion molecules expressed during inflammation [12, 19-21]. Due to its high affinity for large variety of cytokines and growth factors it is also used as a carrier and as a component of drug delivery systems and scaffolds in tissue engineering [22].

In recent years potential benefits of blending hyaluronic acid with BCP were analyzed. Some studies revealed that the addition of HA to BCP did not significantly enhance bone regeneration [23], while others reported beneficial effects of HA addition on bone healing [24,25]. It has been also reported that the effects HA on osteoblasts are varying and dependent on the molecular weight and concentration of HA added to bone substitute materials [16, 26]. For example, the addition of high doses of HA to a biphasic bone substitute significantly decreased the occurrence of pro-inflammatory macrophages during the healing of rat calvaria defects [27]. Unlike HA, there are little data in the literature on the use of heparin as additive to bone substitutes. However, there are some *in vitro* studies that examined heparinized substrates on stem cells and it has been shown that these substrates support adhesion and proliferation of MSCs and enhance osteogenic differentiation [14]. Heparin loading onto PCL- α -TCP membrane, which was engineered as a drug carrier to be used as hemocompatible and bioactive substrate for bone tissue engineering, was shown to enhance MSCs attachment and proliferation in heparin concentration-dependent manner [28]. Increased proliferation and osteogenic differentiation of hBMSC was also observed *in vitro* when these cells were cultured within heparin-modified scaffolds [29].

In summary, there is a lack of data on the effect of covalently immobilized HA and Hep, on bone substitute materials regarding inflammatory response and osteogenic processes *in vivo* as well as the connection of their osteogenic and vasculogenic potential. In the present study, tissue response, osteogenic and vasculogenic potential of the biphasic calcium phosphate (BCP) covalently modified with either hyaluronic acid or heparin was analyzed in a mouse subcutaneous bone-forming model. Results are reported herein.

2. MATERIALS AND METHODS

2.1. Chemicals

As biomaterial in this study Maxresorb® (Botiss, Germany) was used. Maxresorb® is 100% synthetic bone graft substitute, biphasic calcium phosphate (BCP), with homogenous, biphasic composition of 60% hydroxyapatite (HA) and 40% beta-tricalcium phosphate (β -TCP). 3-Aminopropyltriethoxysilane (APTES), 98% was delivered from abcr GmbH & CO. KG (Karlsruhe, Germany). Heparin (Hep) and hyaluronic acid (HA) were obtained from Serva (Heidelberg, Germany) and Innovent e.V. Technologie (Jena, Germany), respectively. In addition, 1-(3-dimethylaminopropyl)-3-ethylcarbodiimide hydrochloride, 98+% (EDC) was purchased from ThermoFischer Kandel GmbH (Karlsruhe, Germany), while N-hydroxy-succinimide 98% (NHS) was obtained from Sigma-Aldrich (Taufkirchen, Germany). Acetone \geq 99.5% was provided from Roth (Karlsruhe, Germany) and ethylene diamine from Sigma-Aldrich (Taufkirchen, Germany). 2-(N-morpholino) ethaneulphonic acid monohydrate (MES) was purchased from VWR International Ltd (Hunter Boulevard, England).

2.2. Animals

C57BL/6 mice used in this study were purchased from Military Medical Academy, Belgrade, Serbia and kept in the Vivarium of the Faculty of Medicine, University of Niš, Serbia, where experiments were performed. Mice were 8 to 10 weeks old and held in standard laboratory conditions at a temperature of 23 °C and 12/12 hours day-night regime. They were allowed to eat and drink *ad libitum* during the whole experimental period. All animal procedures in this study were performed in accordance with the Animal Welfare Act (Republic of Serbia), which is in compliance with European Union guidelines for experimental animals. On the request of the Ethical Committee of the Faculty of Medicine University of Niš, the animal procedures were approved by the Veterinary Directorate of the Ministry of Agriculture, Forestry and Water Management of the Republic of Serbia.

2.3. Preparation of BCP particles

2.3.1. Preparation of the amino-terminated BCP particles

Biphasic calcium phosphate (BCP) particles were first wetted with 70% followed by 99% ethanol and subsequently with acetone for three times. All wetting steps were done for 5 min. Thereafter, APTES was used to obtain amino groups on BCP for subsequent covalent immobilization of GAG. Two percent solution (v/v) of APTES in 99.8% acetone was prepared and BCP particles were immersed for 2 h at room temperature (RT). Subsequently, the BCP particles were rinsed for 5 min with acetone and then washed with autoclaved and filtered MilliQ water (8×5 min).

2.3.2. Immobilization of GAGs onto amino-terminated BCP particles

Both GAGs were immobilized on BCP particles following a protocol developed by Zhou et al. [13]. MES buffer (50 mM, pH 4.70) was prepared by dissolving MES in pre-autoclaved and filtered MilliQ water. Hyaluronic acid (HA, $M_w \approx 1.3$ MDa) and heparin (Hep, $M_w \approx 15$ kDa) were dissolved in MES buffer at a concentration of 2 mg mL⁻¹. Subsequently, EDC and NHS (concentration 5 mg mL⁻¹ and 3 mg mL⁻¹, respectively) were added for 1 hour at RT to GAG solutions. The EDC/NHS-activated GAG solutions were added to APTES-modified BCP particles for 24 h under light protection. Afterwards, an inactivation of the remaining reactive carboxyl species was achieved by immersing the materials in 1 M ethylene diamine solution for 10 min. The BCP particles were rinsed with 99% ethanol for 5 min and washed with pre-autoclaved and filtered double-distilled water (6×5 min). The wet particles were placed in a vacuum chamber for 24 h to insure complete and sterile drying. The dry particles were stored in the desiccator using sealed sterile tubes until use.

2.4. Characterization of surface properties of BCP particles

2.4.1. Scanning electron microscopy (SEM)

Philips ESEM XL 30 FEG (Endoven, Netherlands) with high vacuum ($p = 10^{-6}$ mbar) was used to study the topography of the plain or GAG-modified BCP particles.

2.4.2. Zeta potential measurements

The zeta potential of BCP particles was determined by a SurPASS device (Anton Paar, Graz, Austria). Two identical filters discs were added on both sides of the fiber measuring cell (Anton Paar) that was filled with particles. One mM potassium chloride was used as electrolyte for streaming potential measurements. A flow rate between 100-150 mL min⁻¹, not exceeding 300 mbar as the maximum pressure was adjusted during the experiment. Hydrochloric acid (HCl) at concentration of 1 M was used to adjust the pH value of KCl to pH 3.0. Then, 100 mM sodium hydroxide (NaOH) was used for pH titration. Measurements were carried out by an automated titration program using titration steps of 0.02 µL from pH 3 to pH 11.0.

2.4.3. X- ray photoelectron spectroscopy (XPS)

X- ray photoelectron spectroscopy was performed to study the atomic composition of plain and GAG-modified BCP particles using a Kratos Ultra^{DLD} spectrometer with a monochromated Al K α source (emission: 10 mA, anode: 15 kV). For survey spectra (binding energy 0-1200 eV; measured area 300 x 700 µm²), a pass energy of 160 eV and charge neutralization were applied. The pressure in the analysis chamber was at 1x10⁻⁸ Torr. All spectra were normalized to the C1s peak (285 eV). The obtained spectra were analyzed using the software CasaXPS 2.3.15.

2.5. Subcutaneous implantation in mice

Experimental groups were formed based on the biomaterials' coatings that were examined and were as follows: 1) BCP pure particles (BCP); 2) BCP with covalently immobilized hyaluronic acid (BCP/HA) and 3) BCP with covalently immobilized heparin (BCP/Hep). All biomaterials were shortly soaked with sterile saline solution prior to implantation to form compact constructs. Prior to implantation of materials, animals were anesthetized by intraperitoneal administration of the ketamine/xylazine mixture according to the guidelines for mouse anaesthesia. Interscapular skin was shaved, washed with povidone iodine and small incision was made. Two implants made of the same biomaterial were implanted per animal, subcutaneously, into the interscapular region using biopsy needle as previously published [30-34]. Each experimental group consisted of ten animals carrying the same material. Implants were extracted and

analyzed after 15 and 30 days (five animals from each group were sacrificed per each experimental period). Extracted implants were further used for different analyses. For gene expression analysis explants were immediately stored in RNA stabilization reagent (RNAlater, Qiagen, Venlo, the Netherlands) at -80 °C until subsequent RNA isolation. For histological analysis explants were fixed in 10% neutral buffered formalin (NBF) until further tissue processing.

2.6. Histological procedures

After fixation in 10% NBF, extracted implants were decalcified in 10% ethylenediaminetetraacetic acid (EDTA) solution (pH 7.4). Tissue dehydration was performed by applying ascending concentrations of ethanol. Implants were then cleared in xylene, embedded in paraffin and sliced on a microtome CUT 5062 (SLEE medical GmbH, Mainz, Germany). The haematoxylin and eosin (H&E) and Azan trichrome (AT) staining were performed on tissue sections from at least four different animals per group for each experimental period.

2.7. Histomorphometrical analysis

Histomorphometrical measurements were performed in NIS-Elements software version 3.2 (Nikon, Tokyo, Japan) on imaged tissue slides. The images were obtained on a microscope Leica DMLS equipped with the camera CMEX-10 Pro (Euromex Microscopen BV, Netherlands) at × 100 magnification. Total implant area, total vessel area, area of material granules and number of blood vessels on H&E stained tissue sections were measured using “Annotations and Measurements” software tool. Results are presented as percentage of infiltrated tissue per total implant area, percentage of vascularization per total implant area, percentage of vascularization in infiltrated tissue, vessel density per total implant area and vessel density in infiltrated tissue.

2.8. Quantitative real time polymerase chain reaction (Real-Time qPCR)

Isolation of total RNA from extracted implants was performed by using RNeasy Mini Kit (Qiagen, Venlo, The Netherlands) according to the manufacturer's instructions. During RNA purification, DNase I RNase free set (Qiagen) was used for on-column digestion of residual genomic DNA, according to manufacturer's instructions. Concentration of RNA in samples was determined immediately after RNA isolation on BioSpec-nano Micro-volume UV-Vis Spectrophotometer (Shimadzu, Japan). Isolated RNA was stored at -80 °C until it was reversely transcribed prior to quantitative real time polymerase chain reaction (Real-Time qPCR). Total RNA was reversely transcribed into single-stranded cDNA by using High-capacity cDNA Reverse Transcription Kit (Applied Biosystems®, Thermo Fisher Scientific, Waltham, MA, USA) according to the manufacturer's protocol. Reactions were performed in PCR thermal cycler SureCycler8800 (Agilent Technologies, Santa Clara, CA, USA) according to the following protocol: 10 minutes at 25 °C; 120 minutes at 37 °C, 5 minutes at 85 °C and cooling at 4 °C. Obtained cDNA was stored at -80 °C until the further use for gene expression analysis. Quantitative Real-Time PCR reactions were performed, monitored and analyzed by real time thermal cycler Stratagen Mx3005P (Agilent Technologies, Santa Clara, CA, USA). The qPCR reactions were prepared by using SYBR Fast Universal 2x qPCR Master Mix (Kapa Biosystems, Wilmington, MA, USA), according to the manufacturer's instructions. ROX dye was used as a reference dye. Pre-designed primer sets (QuantiTect primer assay kits) were purchased from Qiagen. Primer kits, consisted of both forward and reverse primers, were used for the following endothelial- and osteogenic-related genes: *Flt1* (QT00096292), *Vcam1* (QT00128793), *Sp7* (QT00293181), *Bglap* (QT01057049) and *Actb* (QT01136772). The protocol conditions were: (1) enzyme activation: 3 min at 95 °C (1 cycle); (2) denaturation: 3 s at 95 °C and annealing/extension (with data acquisition): 30 s at 60 °C (40 cycles). The specific binding of primers was confirmed by melting curve analysis and specific length product visualization on electrophoresis gel. The expression level of each target gene was normalized to the expression of β -actin gene (*Actb*) in the same sample. The relative gene expression data analysis was performed by the relative quantification method $2^{-\Delta\Delta C_t}$. Mouse XpressRef Universal Total RNA (338114, Qiagen) was used as calibrator for all qPCR reactions.

2.9. Statistics

All quantitative data were statistically processed. One-way analysis of variance (ANOVA) was used for statistical calculations followed by post-hoc Tukey's test as well as Mann–Whitney U-test using Origin 8 Pro software (Origin Lab, Northampton, Massachusetts, USA). All data are represented as mean values \pm standard deviations (SD). The statistical significance is shown by asterisks in the figures for $p \leq 0.05$.

3. RESULTS

3.1. Characterization of BCP particle surface properties

Figure 1 (A) shows surface topography of modified materials by using SEM. The immobilization of hyaluronic acid (HA) and heparin (Hep) resulted in slight changes of the surface topography of BCP particles. It can be seen, that there is a deposition of material after the immobilization of GAGs, which is considered as a result of coating of BCP with either HA or Hep. **Figure 1 (B)** shows the zeta potentials of samples in dependence on the pH of electrolyte solution (1 mM KCl). Here it is apparent that pure BCP particles possess higher potentials throughout the range of pH during the titration compared to GAG-modified BCP particles that have lower, more negative zeta potentials. However, a strong difference of zeta potentials between BCP-HA and BCP-Hep particles was not observed.

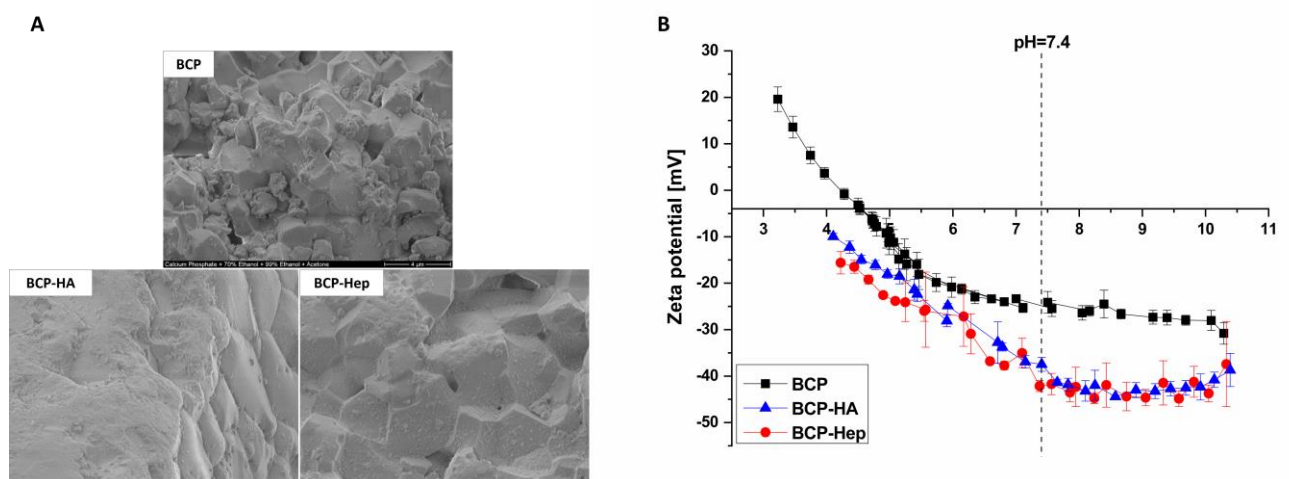


Figure 1. (A) Scanning electron microscopy images visualize surface topography of pure BCP particles (BCP) and BCP-modified by covalent immobilization of either hyaluronic acid (BCP-HA) or heparin (BCP-Hep). **(B)** Zeta potentials of plain BCP and after covalent immobilization of either HA or Hep, abbreviated as [BCP (■), BCP-HA (▲) and BCP-Hep (●)]. Results are presented as means \pm SD in the pH range from 3.0 to 11.0.

3.2. X- ray photoelectron spectroscopy (XPS)

The elemental composition of the particle surfaces was determined by XPS measurements comparing pure BCP, after the silanization with APTES and covalent immobilization of hyaluronic acid and heparin (**Figure 2**). **Figure 2** shows that BCP particles predominantly contain calcium, phosphorus and oxygen as expected by their composition. However, it was also found that considerable quantities of carbon were found (around 20%) and also some sulfur (2.3%). The activation of BCP with APTES reduced those quantities of Ca, P, and O slightly, while the carbon content increased. A new peak of silicon was found (3.5%) that is related to the chemical composition of APTES as silane. Sulfur was not detectable anymore, which indicates that a coating of BCP with APTES was achieved. Furthermore, the elemental composition illustrates a decrease of Si percentage after hyaluronic acid as well as heparin immobilization together with an emerging presence of nitrogen and an increase of carbon compared to the plain BCP particles.

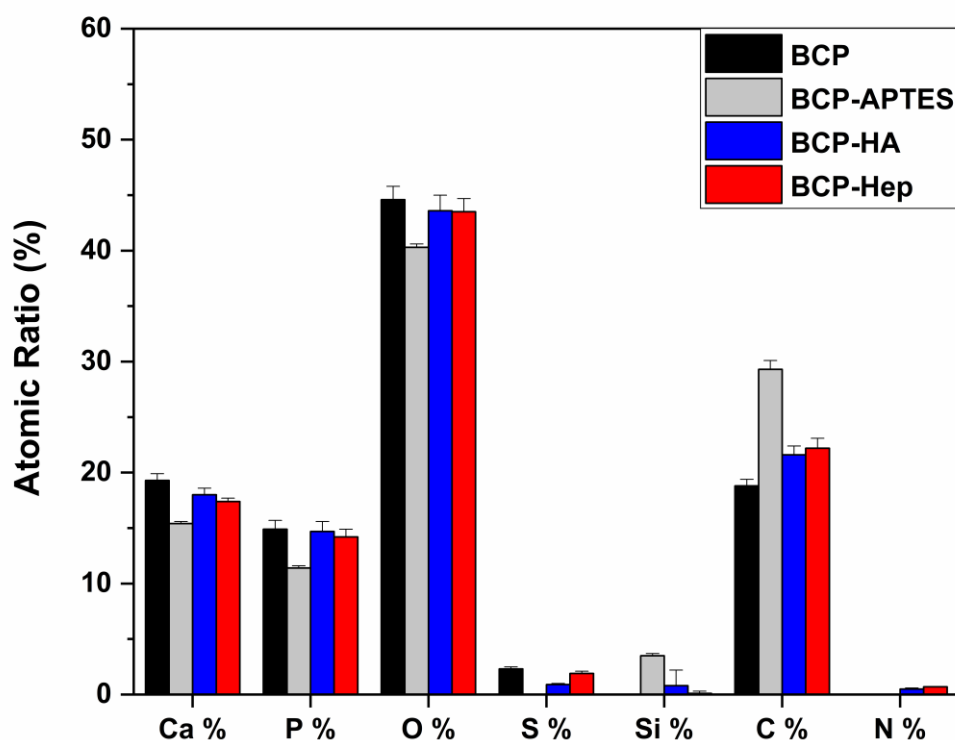


Figure 2. X-ray photoelectron spectroscopy (XPS) of atomic ratio percentage of BCP, BCP with a silanization step of APTES (BCP-APTES) and BCP-modified with either hyaluronic acid (BCP-HA) or heparin (BCP-Hep).

3.3. Histological analysis

More cellularity and presence of various cell populations can be observed on H&E stained histological slides of explants BCP-HA and BCP-Hep compared to BCP material at both examined time points, 15 days (Figure 3) and 30 days (Figure 4). Large cell infiltrates in close proximity to the materials' granules can be seen, consisting of fibroblast, immune cells and mesenchymal stem cells. Higher number of multinucleated giant cells (MNGCs) can be observed in BCP group compared to GAGs immobilized materials at day 15. At this time point signs of material resorption can also be seen in BCP group while this process is continued at day 30 at which premature bone-forming like structures can be seen indicating the primary steps of ectopic bone

tissue formation. At day 30, greater number of MNGCs can be seen in group BCP-Hep compared to other examined groups at this time point. Also, osteoclast-like cells can be seen in BCP-Hep group at day 30 (Figures 4f, 6f)) and signs of material resorption.

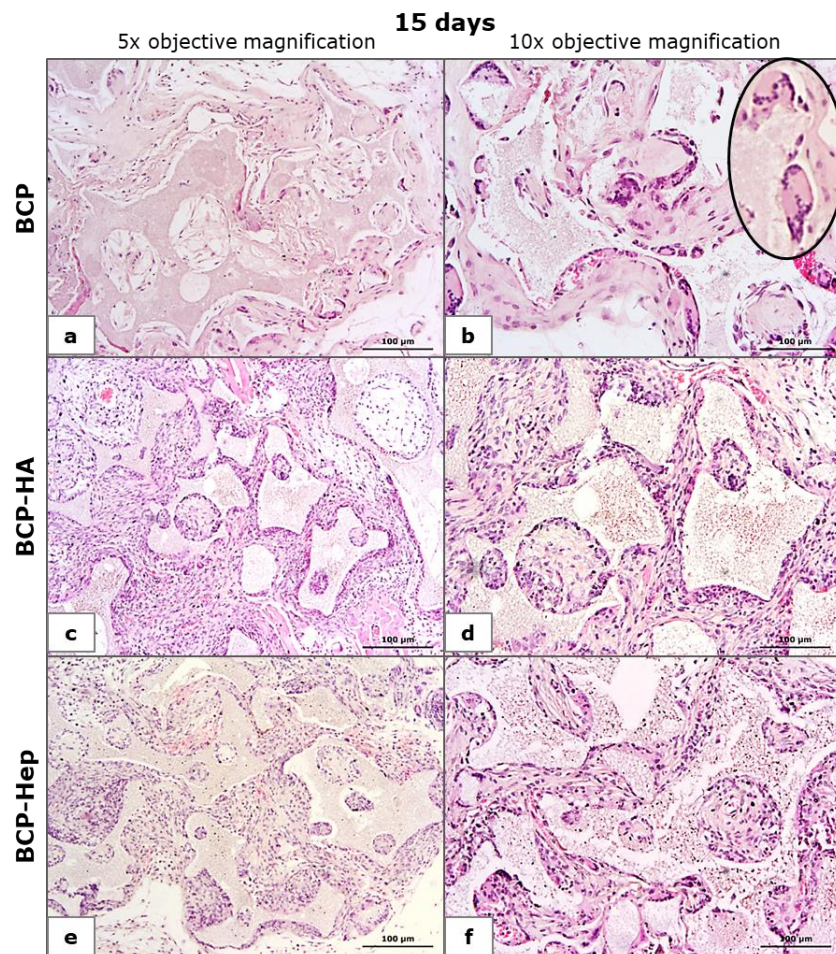


Figure 3. Tissue sections of implants explanted after 15 days, H&E staining, brightfield, objective magnification 5x (a, c, e) and 10x (b, d, f), scale bars show 100 µm; ellipse denotes MNGCs.

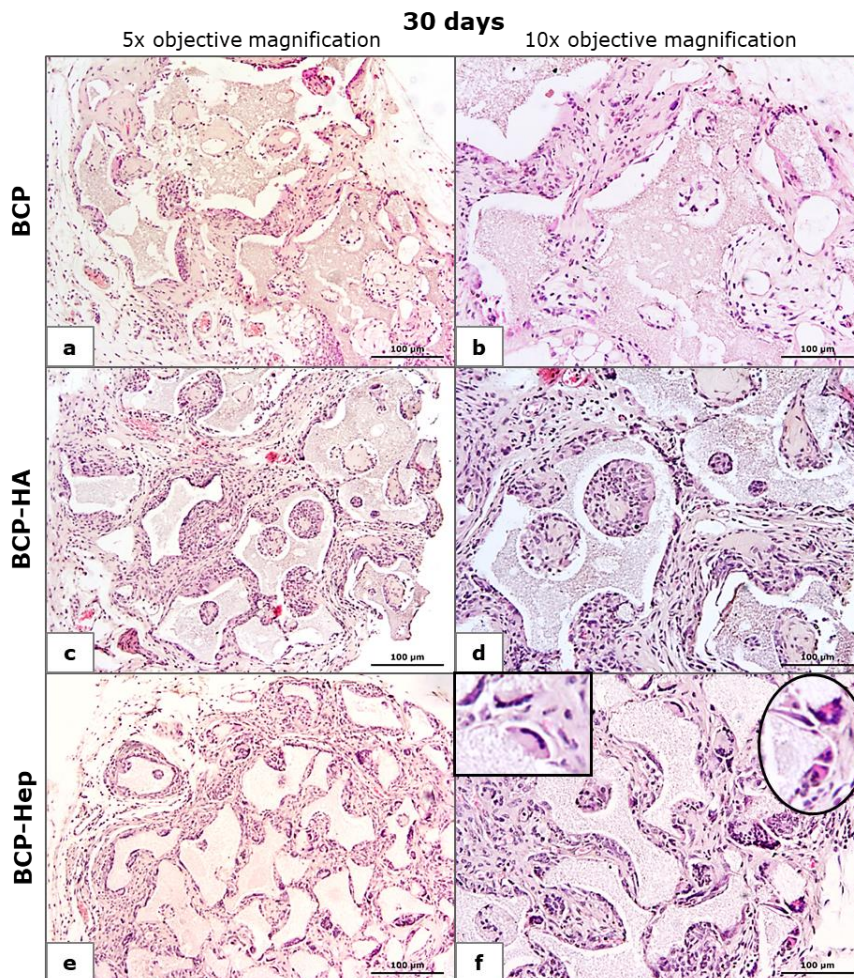


Figure 4. Tissue sections of implants explanted after 30 days, H&E staining, brightfield, objective magnification 5x (a, c, e) and 10x (b, d, f), scale bars show 100 µm; ellipse denotes MNGCs, rectangle denotes osteoclast-like cells.

Greater amount of collagen, visualized by Azan Trichrome staining and indicated as blue colored fibers on images, can be observed at day 30 (Figure 6) compared to day 15 (Figure 5) in all examined groups. However, noticeable difference in collagen amount can be seen among groups. More collagen fibers are observed in BCP and BCP-Hep compared to BCP-HA group at both time points).

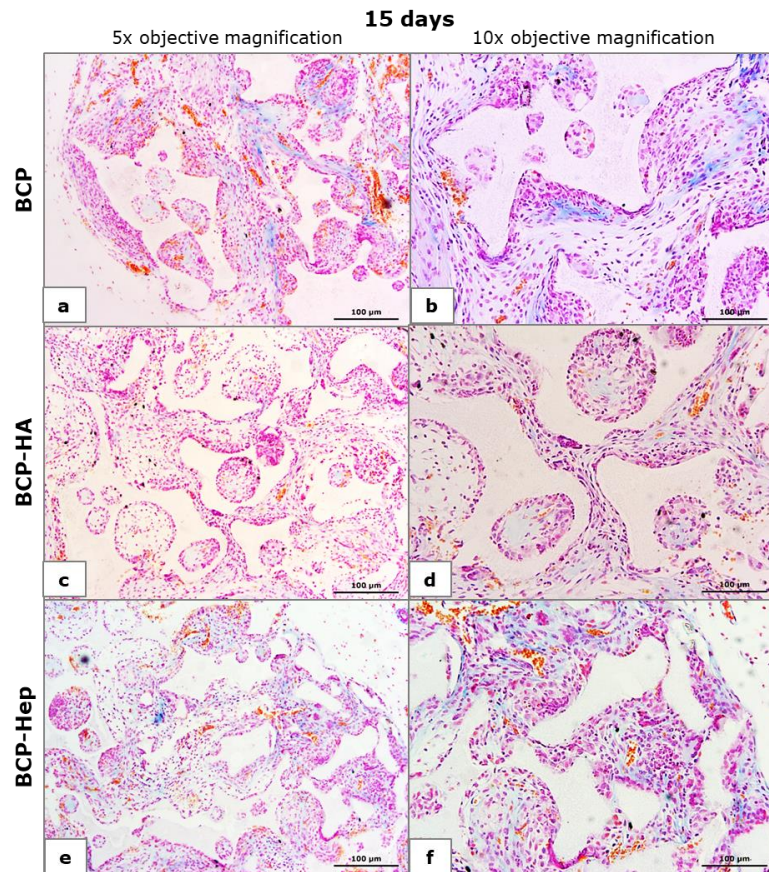


Figure 5. Tissue sections of implants explanted after 15 days, Azan Trichrome staining for collagen, brightfield, objective magnification 5x (a, c, e) and 10x (b, d, f), blue color on the images indicates collagen staining.

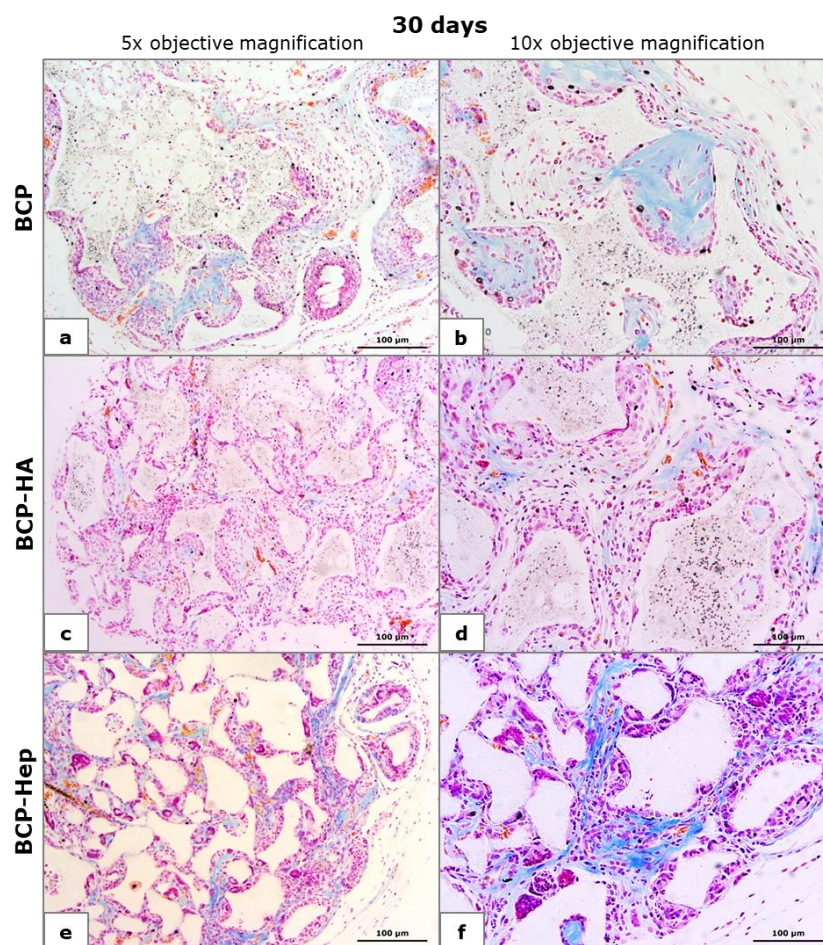


Figure 6. Tissue sections of implants explanted after 30 days, Azan Trichrome staining for collagen, brightfield, objective magnification 5x (a, c, e) and 10x (b, d, f); blue color on the images indicates collagen staining.

3.4. Histomorphometrical analysis

No statistically significant difference was observed in the percentage of infiltrated tissue among examined groups and analyzed time points (Figure 7a). Higher percentage of vascularization per total implant area was observed in BCP group at day 30 compared to other examined groups and the same group at day 15 (Figure 7b), while lower percentage of vascularization per total implant area was observed in both BCP-HA and BCP-Hep groups at day 30 compared to day 15. These changes from 15 to 30 days were not statistically significant while there is a significant difference between all examined groups at day 30. Statistically significant decrease in

vascularization was observed at day 30 in BCP-Hep group compared to BCP group. Percentage of vascularization in infiltrated tissue showed the same trend (Figure 7c).

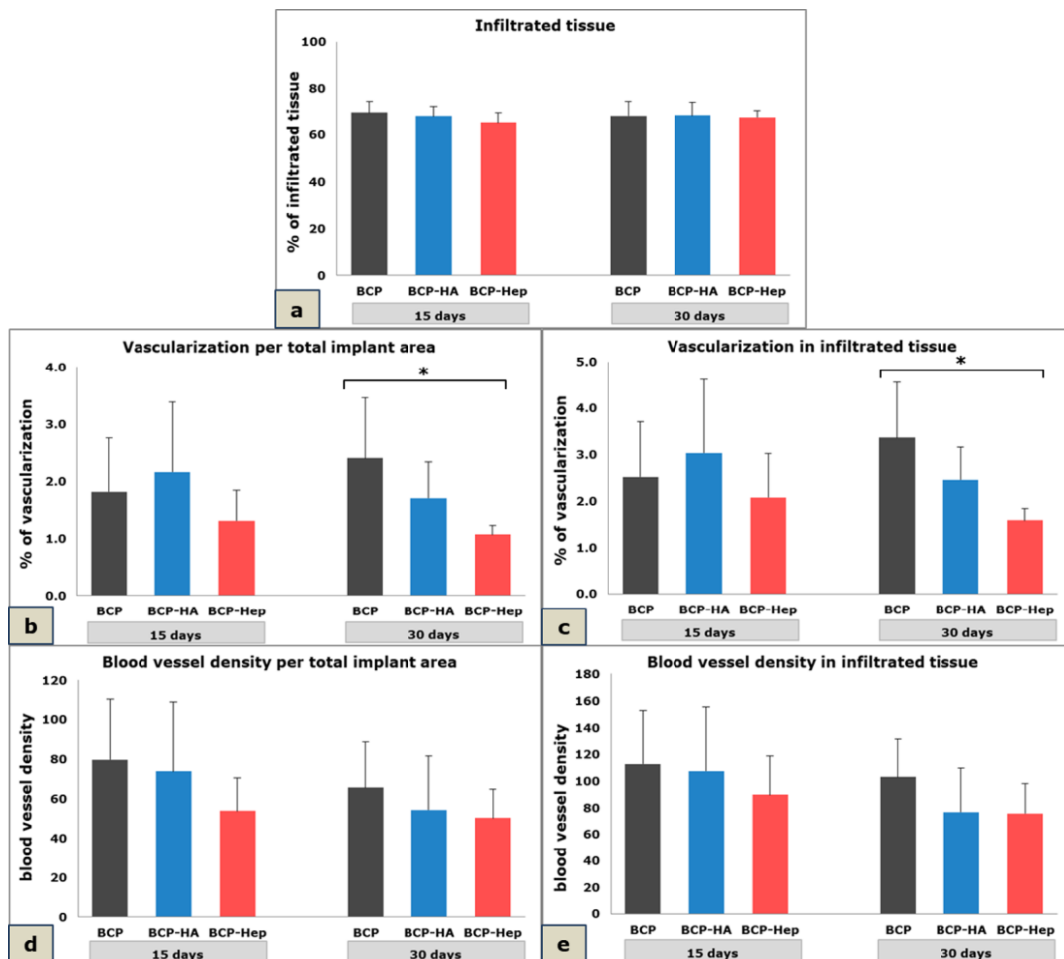


Figure 7. Histomorphometrical parameters measured on stained tissue sections of implants explanted after 15 and 30 days, results are presented as mean \pm SD, (*) $p \leq 0.05$.

Vessel density calculated per total implant area was higher in all groups at day 15 compared to the day 30 while in both time points it was the highest in BCP group compared to both BCP-HA and BCP-Hep coated material. Differences among groups and time points were noticeable but not statistically significant. Noticeable decrease in vessel density per infiltrated tissue was observed in BCP-HA and BCP-Hep groups compared to BCP group especially at day 30, however, no statistically significant probably due to the large SD.

3.5. Gene expression analysis

To analyze the effects of covalent immobilization of hyaluronic acid and heparin on the ectopic osteogenic and vasculogenic potential of synthetic resorbable BCP, endothelial- and osteogenesis-related genes' expression was analyzed. Results of the expression of endothelial-related genes *Flt1* and *Vcam1* are presented in Figure 8.

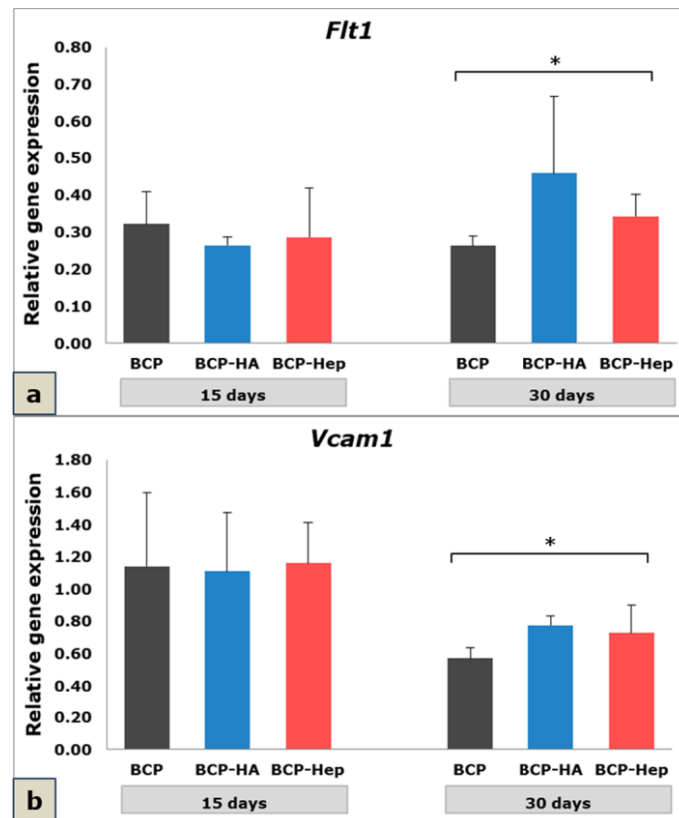


Figure 8. Relative expression of *Flt1* (a) and *Vcam1* (b) genes in implants explanted after 15 and 30 days, results are presented as mean \pm SD, (*) $p \leq 0.05$.

Slightly lower expression of *Flt1* was observed in BCP-HA and BCP-Hep compared to BCP at 15 days, but not statistically significant (Figure 8a). At day 30, statistically significant difference in *Flt1* expression was observed among examined groups with the highest expression in BCP-HA group (Figure 8a). Statistically significant increase in *Flt1* expression in BCP-HA group was observed at day 30 compared to day 15. Expression of *Vcam1* was significantly lower in all examined groups at day 30 compared to day 15 (Figure 8b). Expression of *Vcam1* was significantly different

among examined groups at day 30 with the same expression pattern as for *Flt1* at this time point.

Higher expression of both examined osteogenesis-related genes *Sp7* (gene for early osteoblast marker Osterix) and *Bglap* (gene for late osteoblast marker osteocalcin) was observed in group BCP compared to groups BCP-HA and BCP-Hep at both examined time points, with pronounced increase at day 30 (Figure 9). Statistically significant difference among groups was observed only for *Bglap* at day 30. Significant increase in *Bglap* expression from day 15 to day 30 was observed in groups BCP and BCP-Hep but not in the group BCP-HA.

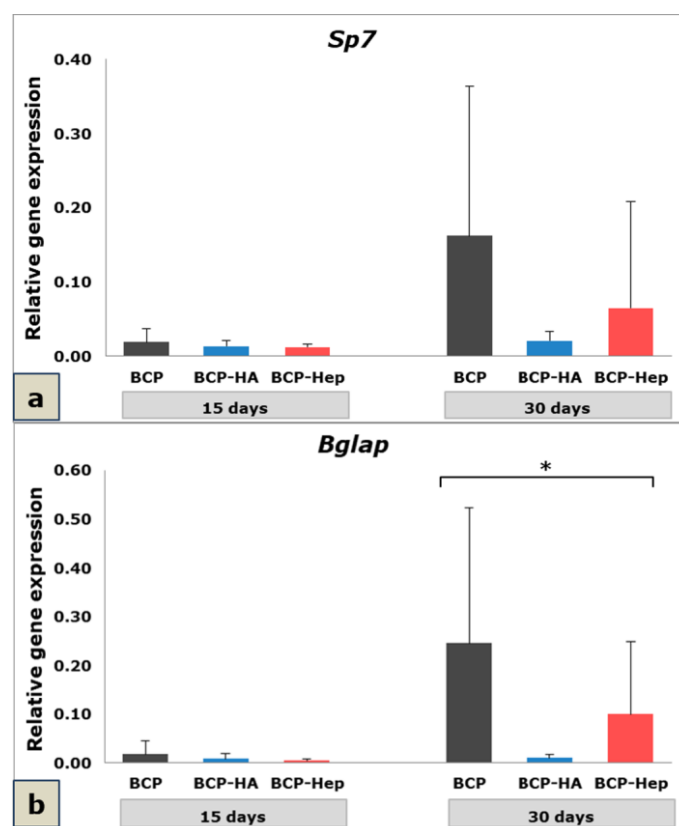


Figure 9. Relative expression of *Sp7* (a) and *Bglap* (b) genes in implants explanted after 15 and 30 days, results are presented as mean \pm SD, (*) $p \leq 0.05$.

4. DISCUSSION

In the present study, we covalently modified the synthetic resorbable bone substitute material, Maxresorb[®], which represents a biphasic material composed of calcium phosphate and hydroxyapatite in a well-balanced ratio, with two GAGs, heparin and

hyaluronic acid, separately. In our previous studies, we have shown that covalent monolayer and adsorptive multilayer immobilization of GAGs on model surfaces led to the reduction of inflammatory response of macrophages [13,35]. In the present study, we wanted to examine how the covalent immobilization of these two GAGs onto BCP will influence the tissue response *in vivo* regarding the course of osteogenesis and vasculogenesis/angiogenesis in subcutaneous bone-forming model in mice. The ectopic bone-forming model in mice was used because it is a suitable model for analyzing the osteogenic potential of the biomaterial itself without any influence of the surrounding bone-related factors that are present in orthotopic bone-forming models [36].

Based on protocols that were developed recently, we immobilized both GAGs covalently after modification of BCP by APTES [13,37]. Studies on SEM revealed the deposition of GAGs by the change in surface topography. Stronger evidence for the success of surface immobilization of both GAG was obtained by zeta potential measurements, which showed more negative zeta potentials of BCP after immobilization of GAGs related to the presence of carboxylic groups in HA and carboxylic and sulfate groups in Hep [20]. XPS studies were somewhat difficult to interpret because of the presence of sulfur in the plain BCP particles and also a larger quantity of carbon that was not expected. Indeed, it is known that synthetic calcium-phosphate based biomaterials may have certain impurities. The presence of carbon is probably due to adsorption of carbohydrates from the environmental air [38] or originated from the starting material in synthesis since it is known that calcium carbonate or associated compounds are used for synthesis of calcium phosphate [39]. Indeed, also the slight changes in the occurrence of nitrogen that is present in the amino sugar subunits of HA and Hep after covalent binding of GAG provided additional evidence for the presence of both GAGs after the chemical immobilization protocol on BCP particles.

Beside the physicochemical data, evidence for the effect of immobilized GAG on the coated BCP granules is based on the different tissue response in terms of mobilization and adhesion of larger number of different cell types onto the material compared to pure BCP, which can be noticed in the histological images. GAGs are major component of ECM and cell surfaces that are involved in the binding of cytokines and mediate

cell–cell and cell–ECM interactions [40]. The finding of greater cellularity in BCP-HA and BCP-Hep implants is in accordance with physiological functions of GAGs [20]. It seemed also that the coating of BCP with GAGs made them less resorbable or postponed the process of resorption for some time. Multinucleated giant cells (MNGCs) appear as a reaction to implanted biomaterials [41-43]. The number of these cells and their persistence greatly influence the further inflammation course of the tissue and healing outcome and are greatly dependent on the physico-chemical properties of implanted biomaterials [41,42,44]. These cells are also very important in regeneration and healing process since they are involved in the biodegradation of the biomaterial and are related to expression of both pro- and anti-inflammatory molecules, which represent signals for other cells and events that lead to tissue regeneration [41, 42]. In our study lesser number of MNGCs was noticed after 15 days in both BCP-HA and BCP-Hep group, suggesting anti-inflammatory properties of the coated material are in line with our previous *in vitro* studies showing that HA and Hep-modified glass surfaces significantly reduced the formation of MNGCs [13,45]. Interestingly, in the present study, we noticed larger number of MNGCs in BCP-Hep group after 30 days compared to other groups and earlier time point which indicates a delayed reaction to the BCP material. Moreover, among MNGCs some of them look like osteoclasts and indicate intensive resorption of the material. Recently, similar findings to ours were reported by Diez-Escudero et al. [37] who showed that functionalization of biomimetic calcium-deficient hydroxyapatite with covalently immobilized heparin fostered the formation and activity of osteoclasts *in vitro*. In BCP-HA group, these cells are very rare which indicates strong suppressive effect of covalently bound HA that is line with the anticipated anti-inflammatory effect of high molecular weight HA also observed in other studies [27]. Since greater vascularization can be considered as a sign of inflammation, decreased vascularization obtained by histomorphometrical analyses in BCP-HA and BCP-Hep group compared to BCP group at both time points, 15 and 30 days, might indicate that both HA and Hep immobilization onto BCP granules led to the lowering inflammatory tissue response caused by pure BCP as it was expected from our previous *in vitro* studies [13,45]. These differences were statistically significant at day 30.

Although vascularization can be an indicator of the course of inflammation, it also plays a crucial role in bone regeneration. Vasculogenesis/angiogenesis and osteogenesis are tightly coupled and have to be well regulated for successful bone regeneration and function [46]. Here, we analyzed the expression level of the two endothelial-related genes: *Flt1*, gene for vascular endothelial growth factor receptor-1 (VEGFR-1) and *Vcam1*, gene for vascular cell adhesion molecule 1 (VCAM-1) and the two osteogenesis-related genes: *Sp7*, gene for Osterix (transcription factor that regulates osteoblast differentiation and bone development) and *Bglap*, gene for osteocalcin, mature osteoblasts' marker that plays a significant role in the mineralization process during osteogenic differentiation.

VEGF protein family and VEGF receptors, the most important regulators of vascular development and angiogenesis, play also an important role in bone repair and regeneration and skeletal development [47]. It has been shown that VEGFR-1 plays an important role in the recruitment of endothelial precursor cells during vasculogenesis and that its activation by VEGF induces cell migration [48]. Higher expression of VEGFR-1 compared to VEGFR-2 was found in osteoblasts and fibroblast-like cells in mandibular distraction osteogenesis suggesting that VEGFR-1 plays crucial role in osteogenesis [48]. Some non-endothelial cells express VEGF and VEGF receptors as well, including osteoprogenitors, pericytes, MSCs, osteoblasts and osteoclasts, and all of them respond to VEGF signalling by increased recruitment, differentiation and activity [46,49]. Although expression of VEGF receptors in osteoblasts is reported to be variable, there are indications that VEGF directly affect osteoblast differentiation and has indirect effects on postnatal bone homeostasis maintenance and development through autocrine and paracrine mechanisms by affecting various cell types involved in the process [46,49]. It has been shown that expression of VEGFR1 is dependent on the differentiation state of osteoblasts and low levels of VEGFR1 were only detected in differentiating osteoblasts during the mineralization phase [50]. Slightly lower *Flt1* expression in BCP group but significantly higher in BCP-HA and BCP-Hep groups at day 30 compared to day 15 was observed in our study. This increase in *Flt1* expression in GAGs immobilized groups might be due to the presence of greater number of osteoprogenitors, pericytes and MSCs in these groups. VCAM-1 (CD106) is predominantly expressed in endothelial cells and

its expression is induced by various factors such as proinflammatory cytokines and reactive oxygen species (ROS) [51,52]. VCAM-1 is minimally expressed in resting vascular endothelial cells and is inducible in many tissue vascular beds following injury or stress [51,52]. It is constitutively expressed in bone marrow (BM) stromal/endothelial cells and certain classes of hematopoietic cells [53] but also in MSCs [54]. CD106 was reported to be strongly expressed in MSCs, but its expression was decreased after osteogenic differentiation [54]. Other authors also reported that expression of CD106 decrease during osteogenic differentiation *in vitro* indicating the usefulness of CD106 as a differentiation-predicting marker of BMSC [55]. Lower expression of *Vcam1* at day 30 compared to day 15 in all examined groups in our study could indicate that starting inflammatory response, which was induced by implantation of the biomaterial, was lowered at day 30. Slightly, but significantly higher expression of *Vcam1* in BCP-HA and BCP-Hep groups compared to BCP group might indicate as well the late response of cells to BCP or is a consequence of the presence of greater number of hematopoietic cells and MSCs in the groups with immobilized GAGs compared to the pure BCP, which can be seen on histological images and which is in accordance with the *Flt1* expression pattern.

Both *Sp7* and *Bglap* genes were expressed in greater extent in BCP group compared to the other examined groups at both examined time points, with pronounced increase in expression after 30 days. The lowest expression of these osteogenesis-related genes was noticed in BCP-HA group and these differences among groups are statistically significant at day 30. This means that ectopic osteogenic process had occurred in BCP group and had progressed from day 15 to day 30. In groups of GAGs immobilized BCP, osteogenic process obviously started at day 30 in BCP-Hep group since both *Sp7* and *Bglap* gene expression increased compared to day 15 while no increase in expression of these genes was noticed in BCP-HA group. On the other hand, expression of *Flt1* gene was the highest in BCP-HA group at day 30 which may indicate different pattern and dynamic of ectopic bone formation. This osteogenesis-related gene expression pattern corresponds to the collagen content in examined groups, analyzed by AT staining, and increase in collagen content can be observed in BCP and BCP-Hep groups from day 15 to day 30. Positive correlation between

collagen amount and expression of *Sp7* and *Bglap* was also observed in our previous study in the same model but different implant composition [30].

Our results are among the first showing the comparative osteogenic and vasculogenic potential of BCP covalently modified with hyaluronic acid and heparin in subcutaneous bone-forming model *in vivo*, and comparison of the BCP tissue response modulation by these two GAGs with anti-inflammatory properties.

5. CONCLUSION

Based on obtained results we can conclude that the covalent immobilization of either hyaluronic acid or heparin, representing GAGs with anti-inflammatory properties, on biphasic calcium phosphate material significantly influences the tissue response to this biomaterial. Osteoinductive potential of BCP was changed by immobilization of GAGs while osteogenic process and vasculogenesis/angiogenesis were at different stages in examined groups and time points. The results of this study are promising in the field of bone tissue regeneration since they show, for the first time, that hyaluronic acid and heparin can be used for covalent modification of the biphasic calcium phosphate for modulation of the tissue response to this biomaterial and ectopic bone formation. However, further studies including prolonged observation periods and orthotopic bone formation analysis may also be required prior to the application of this approach in bone tissue engineering.

Acknowledgements. The German Academic Exchange service (DAAD) supported this work financially through a PhD grant to Hala AlKhoury. The study was also part of the project of bilateral cooperation funded by DAAD and Ministry of Education, Science and Technological Development of the Republic of Serbia (period 2019 – 2020). This study was also supported by the Ministry of Education, Science and Technological development of the Republic of Serbia (Grant No. III 41017).

Conflicts of interest

“There are no conflicts to declare”.

REFERENCES

1. Anderson JM. Biological responses to materials. *Annu Rev Mater Res* 2001;31:81-110.
2. Landén NX, Li D, Ståhle M. Transition from inflammation to proliferation: a critical step during wound healing. *Cell Mol Life Sci* 2016;73(20):3861-85.
3. Janicki P, Schmidmaier G. What should be the characteristics of the ideal bone graft substitute? Combining scaffolds with growth factors and/or stem cells. *Injury* 2011;42(Suppl 2):S77-81.
4. Kapusetti G, More N, Choppadandi M. Introduction to Ideal Characteristics and Advanced Biomedical Applications of Biomaterials. In: Paul S, editor. *Biomedical Engineering and its Applications in Healthcare*. Singapore: Springer; 2019. p 171-204.
5. LeGeros RZ. Calcium phosphate-based osteoinductive materials. *Chem Rev* 2008;108(11):4742-53.
6. Jeong J, Kim JH, Shim JH, Hwang NS, Heo CY. Bioactive calcium phosphate materials and applications in bone regeneration. *Biomater Res* 2019;23:4.
7. Lobo SE, Livingston Arinzeh T. Biphase Calcium Phosphate Ceramics for Bone Regeneration and Tissue Engineering Applications. *Materials (Basel)* 2010;3(2):815–826.
8. LeGeros RZ, Lin S, Rohanizadeh R, Mijares D, LeGeros JP. Biphase calcium phosphate bioceramics: preparation, properties and applications. *J Mater Sci Mater Med* 2003;14(3):201-209.
9. Ebrahimi M, Botelho MG, Dorozhkin SV. Biphase calcium phosphates bioceramics (HA/TCP): Concept, physicochemical properties and the impact of standardization of study protocols in biomaterials research. *Mater Sci Eng C Mater Biol Appl* 2017;71:1293-1312.
10. Bridges AW, García AJ. Anti-inflammatory polymeric coatings for implantable biomaterials and devices. *J Diabetes Sci Technol* 2008;2(6):984-994.
11. Severin IC, Soares A, Hantson J, Teixeira M, Sachs D, Valognes D, Scheer A, Schwarz MK, Wells TN, Proudfoot AE, Shaw J. Glycosaminoglycan ana-logs as a novel anti-inflammatory strategy. *Front Immunol* 2012;3:293.

12. Zhou G, Groth T. Host Responses to Biomaterials and Anti-Inflammatory Design-a Brief Review. *Macromol Biosci* 2018;18(8):e1800112.
13. Zhou G, Al-Khoury H, Groth T. Covalent immobilization of glycosaminoglycans to reduce the inflammatory effects of biomaterials. *Int J Artif Organs* 2016;39(1):37-44.
14. Diez-Escudero A, Espanol M, Bonany M, Lu X, Persson C, Ginebra MP. Heparinization of Beta Tricalcium Phosphate: Osteo-immunomodulatory Effects. *Adv Healthc Mater* 2018;7(5):1700867.
15. Allison DD, Grande-Allen KJ. Review. Hyaluronan: a powerful tissue engineering tool. *Tissue Eng* 2006;12(8):2131-2140.
16. Huang L, Cheng YY, Koo PL, Lee KM, Qin L, Cheng JC, Kumta SM. The effect of hyaluronan on osteoblast proliferation and differentiation in rat calvarial-derived cell cultures. *J Biomed Mater Res A* 2003;66(4):880–884.
17. Kuo JW, Prestwich GD. Hyaluronic acid. In: Ducheyne P, Healy K, Hutmacher D, Kirkpatrick J, editors. *Materials of biological origin – materials analysis and implant uses, comprehensive biomaterials*. Amsterdam: Elsevier; 2011. p 239–59.
18. Köwitsch A, Yang Y, Ma N, Kuntsche J, Mäder K, Groth T. Bioactivity of immobilized hyaluronic acid derivatives regarding protein adsorption and cell adhesion. *Biotechnol Appl Biochem* 2011;58(5):376-89.
19. Lever R, Page CP. Non-anticoagulant Effects of Heparin: An Overview. In: Lever R, Mulloy B, Page C, editors. *Heparin - A Century of Progress. Handbook of Experimental Pharmacology*, vol 207. Berlin, Heidelberg: Springer; 2012. p 281-305.
20. Köwitsch A, Zhou G, Groth T. Medical application of glycosaminoglycans: a review. *J Tissue Eng Regen Med* 2018;12(1):e23-e41.
21. Young E. The anti-inflammatory effects of heparin and related compounds. *Thromb Res* 2008;122(6):743-752.
22. Hettiaratchi MH, Krishnan L, Rouse T, Chou C, McDevitt TC, Guldberg RE. Heparin-mediated delivery of bone morphogenetic protein-2 improves spatial localization of bone regeneration. *Sci Adv* 2020;6(1):eaay1240.
23. Ahmed AG, Awartani FA, Niazy AA, Jansen JA, Alghamdi HS. A Combination of Biphasic Calcium Phosphate (Maxresorb®) and Hyaluronic Acid Gel (Hyadent®) for Repairing Osseous Defects in a Rat Model. *Applied Sciences* 2020;10(5):1651.

24. Aslan M, Simsek G, Dayi E. The effect of hyaluronic acid-supplemented bone graft in bone healing: experimental study in rabbits. *J Biomater Appl* 2006;20(3):209-220.
25. Koca C, Komerik N, Ozmen O. Comparison of efficiency of hyaluronic acid and/or bone grafts in healing of bone defects. *Niger J Clin Pract* 2019;22(6):754-762.
26. Rayahin JE, Buhrman JS, Zhang Y1, Koh TJ, Gemeinhart RA. High and low molecular weight hyaluronic acid differentially influence macrophage activation. *ACS Biomater Sci Eng* 2015;1(7):481-493.
27. Sieger D, Korzinskas T, Jung O, Stojanovic S, Wenisch S, Smeets R, Gosau M, Schnettler R, Najman S, Barbeck M. The Addition of High Doses of Hyaluronic Acid to a Biphasic Bone Substitute Decreases the Proinflammatory Tissue Response. *Int J Mol Sci* 2019;20(8):1969.
28. Alehosseini M, Golafshan N, Kharaziha M, Fathi M, Edris H. Hemocompatible and Bioactive Heparin-Loaded PCL- α -TCP Fibrous Membranes for Bone Tissue Engineering. *Macromol Biosci* 2018;18(6):e1800020.
29. Quade M, Knaack S, Weber D, König U, Paul B, Simon P, Rösen-Wolff A, Schwartz-Albiez R, Gelinsky M, Lode A. Heparin modification of a biomimetic bone matrix modulates osteogenic and angiogenic cell response in vitro. *Eur Cell Mater* 2017;33:105-120.
30. Najman SJ, Cvetković VJ, Najdanović JG, Stojanović S, Vukelić-Nikolić MĐ, Vučković I, Petrović D. Ectopic osteogenic capacity of freshly isolated adipose-derived stromal vascular fraction cells supported with platelet-rich plasma: a simulation of intraoperative procedure. *J Craniomaxillofac Surg* 2016;44(10):1750-1760.
31. Najdanović JG, Cvetković VJ, Stojanović S, Vukelić-Nikolić MĐ, Čakić-Milošević MM, Živković JM, Najman SJ. Effects of bone tissue engineering triad components on vascularization process: comparative gene expression and histological evaluation in an ectopic bone forming model. *Biotechnol Biotec Eq* 2016;30(6):1122-1131.
32. Cvetković VJ, Najdanović JG, Vukelić-Nikolić MĐ, Stojanović S, Najman SJ. Osteogenic potential of in vitro osteo-induced adipose-derived mesenchymal stem cells combined with platelet-rich plasma in an ectopic model. *Int Orthop* 2015;39(11):2173-2180.

33. Najdanović JG, Cvetković VJ, Stojanović S, Vukelić-Nikolić MĐ, Stanisavljević MN, Živković JM, Najman SJ. The Influence of adipose-derived stem cells induced into endothelial cells on ectopic vasculogenesis and osteogenesis. *Cel Mol Bioeng* 2015;8(4):577-590.
34. Barbeck M, Najman S, Stojanović S, Mitić Ž, Živković JM, Choukroun J, Kovačević P, Sader R, Kirkpatrick CJ, Ghanaati S. Addition of blood to a phylogenetic bone substitute leads to an increased *in vivo* vascularization. *Biomed Mater* 2015;10(5):055007.
35. Zhou G, Niepel MS, Saretia S, Groth T. Reducing the inflammatory responses of biomaterials by surface modification with glycosaminoglycan multilayers. *J Biomed Mater Res A* 2016; 104(2):493-502.
36. Scott MA, Levi B, Askarinam A, Nguyen A, Rackohn T, Ting K, Soo C, James AW. Brief review of models of ectopic bone formation. *Stem Cells Dev* 2012;21(5):655-667.
37. Diez-Escudero A, Torreggiani E, Di Pompo G, Espanol M, Persson C, Ciapetti G, Baldini N, Ginebra MP. Effect of calcium phosphate heparinization on the *in vitro* inflammatory response and osteoclastogenesis of human blood precursor cells. *J Tissue Eng Regen Med* 2019;13(7):1217-1229.
38. Ratner BD. Surface properties and surface characterization of materials. In: Ratner BD, Hoffmann AS, Schoen FJ, Lemons JE, editors. *Biomaterials Science. An Introduction to Materials in Medicine*. San Diego: Academic Press, Elsevier; 2004. p 40-59.
39. Osseni SA, Bonou SAS, Sagbo EV, Ahouansou R, Agbahoungbata MY, Neumeyer D, Verelst M, Mauricot R. Synthesis of Calcium Phosphate Bioceramics Based on Snail Shells: Towards a Valorization of Snail Shells from Republic of Benin. *Am J Chem* 2018;8(4):90-95.
40. Bishop JR, Schuksz M, Esko JD. Heparan sulphate proteoglycans fine-tune mammalian physiology. *Nature* 2007;446(7139):1030-1037.
41. Miron RJ, Bosshardt DD. Multinucleated Giant Cells: Good Guys or Bad Guys? *Tissue Eng Part B Rev* 2018;24(1):53-65.
42. Al-Maawi S, Orłowska A, Sader R, James Kirkpatrick C, Ghanaati S. *In vivo* cellular reactions to different biomaterials-Physiological and pathological aspects and their consequences. *Semin Immunol* 2017;29:49-61.

43. Anderson JM, Rodriguez A, Chang DT. Foreign body reaction to biomaterials. *Semin Immunol* 2008;20(2):86-100.
44. Al-Maawi S, Rutkowski J, Sader R, Kirkpatrick CJ, Ghanaati S. The biomaterial-induced cellular reaction allows a novel classification system regardless of the biomaterials origin. *J Oral Implantol* 2020. doi: 10.1563/aid-joi-D-19-00201. [Epub ahead of print]
45. AlKhoury H, Hautmann A, Erdmann F, Zhou G, Stojanović S, Najman S, Groth T. Study on the potential mechanism of anti-inflammatory activity of covalently immobilized hyaluronan and heparin. *J Biomed Mater Res A* 2020;108(5):1099-1111.
46. Grosso A, Burger MG, Lunger A, Schaefer DJ, Banfi A, Di Maggio N. It Takes Two to Tango: Coupling of Angiogenesis and Osteogenesis for Bone Regeneration. *Front Bioeng Biotechnol* 2017;5:68.
47. Hu K, Olsen BR. The roles of vascular endothelial growth factor in bone repair and regeneration. *Bone* 2016;91:30-38.
48. Byun JH, Park BW, Kim JR, Lee JH. Expression of vascular endothelial growth factor and its receptors after mandibular distraction osteogenesis. *Int J Oral Maxillofac Surg* 2007;36(4):338-344.
49. Dirckx N, Van Hul M, Maes C. Osteoblast recruitment to sites of bone formation in skeletal development, homeostasis, and regeneration. *Birth Defects Res C Embryo Today* 2013;99(3):170–191.
50. Deckers MM, Karperien M, van der Bent C, Yamashita T, Papapoulos SE, Löwik CW. Expression of vascular endothelial growth factors and their receptors during osteoblast differentiation. *Endocrinology* 2000;141(5):1667-1674.
51. Cook-Mills JM, Marchese ME, Abdala-Valencia H. Vascular cell adhesion molecule-1 expression and signaling during disease: regulation by reactive oxygen species and antioxidants. *Antioxid Redox Signal* 2011;15(6):1607-38.
52. Kong DH, Kim YK, Kim MR, Jang JH, Lee S. Emerging Roles of Vascular Cell Adhesion Molecule-1 (VCAM-1) in Immunological Disorders and Cancer. *Int J Mol Sci* 2018;19(4):1057.
53. Ulyanova T, Scott LM, Priestley GV, Jiang Y, Nakamoto B, Koni PA, Papayannopoulou T. VCAM-1 expression in adult hematopoietic and

nonhematopoietic cells is controlled by tissue-inductive signals and reflects their developmental origin. *Blood* 2005;106(1):86-94.

54. Liu F, Akiyama Y, Tai S, Maruyama K, Kawaguchi Y, Muramatsu K, Yamaguchi K. Changes in the expression of CD106, osteogenic genes, and transcription factors involved in the osteogenic differentiation of human bone marrow mesenchymal stem cells. *J Bone Miner Metab* 2008;26(4):312-320.
55. Fukiage K, Aoyama T, Shibata KR, Otsuka S, Furu M, Kohno Y, Ito K, Jin Y, Fujita S, Fujibayashi S, Neo M, Nakayama T, Nakamura T, Toguchida J. Expression of vascular cell adhesion molecule-1 indicates the differentiation potential of human bone marrow stromal cells. *Biochem Biophys Res Commun* 2008;365(3):406-412.

Chapter 6

Summary – Anti-inflammatory surface coatings based on polyelectrolyte multilayers of heparin and polycationic nanoparticles of Naproxen-bearing polymeric drugs:

In this chapter, studies were expanded for the integration of multiple anti-inflammatory strategies in an *in vitro* release system. The novelty of the work based on combining the short-term anti-inflammatory effects of Hep as polyanion with the long-term and potential release of Naproxen from polymeric nanoparticle (NP) as a polycation. The LbL technique was used to build up PEMs. The PEMs were characterized with quartz crystal microbalance (QCM) to testify the exponential growth, SEM and AFM to visualize the surface topography as well as ZP measurements. In this study, PEI was used as a positive control. In addition, polystyrene sulfonate (PSS) and Chi were used here as alternative polyanion and polycation respectively in multilayer formation. The physicochemical characterization showed complete surface coverage of multilayers containing NPs with certain roughness while multilayers containing only Hep, PSS as well as Chi had smoother surface coatings. In addition, NP-containing multilayers expressed a viscoelastic behaviour and had negative ZP. By contrast, reference PEM composed of Hep/Chi and PSS/Chi had lower ZP. THP-1-derived macrophages were used to study the short and long term anti-inflammatory activity of Hep and NPs, respectively. Short-term studies showed reduced cell adhesion and IL1- β secretion with Hep when compared to PSS. The long-term study was related to a reduced FBGCs formation after 15 days of NP-containing multilayers in comparison to PEM that contained Chi. Macrophages also showed the ability to take up NPs by endocytosis, indicating release of Naproxen by digestion of NP in the lysosomal compartment. This work represents a proof-of-concept study in reducing inflammatory responses as the mechanism of action was not examined. In conclusion, novel biomaterial coating was established here by having the potential to attenuate foreign body reaction after implantation and thus improve the longevity of implants such as sensors and other soft or hard tissue implants.

Anti-inflammatory Surface Coatings Based on Polyelectrolyte Multilayers of Heparin and Polycationic Nanoparticles of Naproxen-Bearing Polymeric Drugs

Hala Al-Khoury,^{†,||,∇} Eva Espinosa-Cano,^{‡,§,∇} María Rosa Aguilar,^{*,‡,§} Julio San Román,^{‡,§} Frank Syrowatka,^{||} Georg Schmidt,^{||} and Thomas Groth,^{†,||,⊥}

[†]Department Biomedical Materials, Institute of Pharmacy, Martin Luther University Halle Wittenberg, Heinrich Damerow Strasse 4, 06120 Halle (Saale), Germany

[‡]Biomaterials Group, Department of Polymeric Nanomaterials and Biomaterials, Institute of Polymer Science and Technology, ICTP-CSIC, Juan de la Cierva 3, 28006 Madrid, Spain

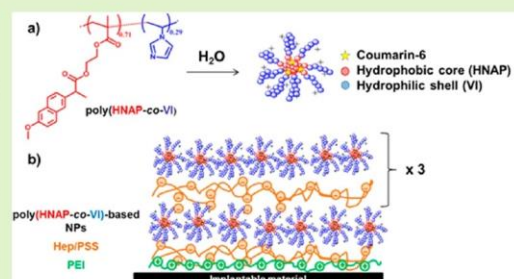
[§]Networking Biomedical Research Centre in Bioengineering, Biomaterials and Nanomedicine, CIBER-BBN, 28029 Madrid, Spain

^{||}Interdisciplinary Centre of Materials Science, Martin Luther University Halle-Wittenberg, 06120 Halle (Saale), Germany

[⊥]Interdisciplinary Centre of Applied Science, Martin Luther University Halle-Wittenberg, 06099 Halle (Saale), Germany

Supporting Information

ABSTRACT: Immune response to biomaterials can produce chronic inflammation and fibrosis leading to implant failure, which is related to the surface properties of the biomaterials. This work describes the preparation and characterization of polyelectrolyte multilayer (PEM) coatings that combine the anti-inflammatory activity of heparin as polyanion with the potential release of Naproxen, a nonsteroidal anti-inflammatory drug from polymeric nanoparticles (NP) with cationic surface charge. The polyelectrolyte multilayers were characterized by physical methods to estimate multilayer growth, thickness, zeta potential, and topography. It was found that multilayers with NP had negative zeta potentials and expressed a viscoelastic behavior, while studies of topography showed that nanoparticles formed continuous surface coatings. THP-1-derived macrophages were used to study short-term anti-inflammatory activity (time scale 48 h), showing that PEM that contained heparin reduced cell adhesion and IL-1 β secretion, when compared to those with polystyrenesulfonate, used as alternative polyanion in multilayer formation. On the other hand, the presence of NP in PEM was related to a reduced foreign body giant cell formation after 15 days, when compared to PEM that contained chitosan as alternative polycation, which suggests a long-term anti-inflammatory effect of Naproxen-containing nanoparticles. It was also shown that macrophages were able to take up NP from multilayers, which indicates a release of Naproxen by digestion of NP in the lysosomal compartment. These findings indicate that surface coatings composed of heparin and Naproxen-based NP on implants such as biosensors have the potential to attenuate foreign body reaction after implantation, which may improve the long-term functionality of implants.



INTRODUCTION

Long-term use of biomaterials is often hampered by the inflammatory response elicited after implantation. Early adsorption of proteins on the biomaterial surface triggers the activation of the innate and acquired immunity.¹ Macrophages are considered as key effectors in this inflammatory response known as foreign body reaction (FBR).² Their direct contact with the implant surface can induce the secretion of chemokines, growth factors, and pro-inflammatory cytokines such as interleukin 1 β (IL-1 β), among others.³ Prolonged unresolved inflammation leads to the fusion of macrophages into foreign body giant cells (FBGCs) in an attempt to phagocytose the implant⁴ and ultimately to the attraction of

fibroblasts with subsequent fibrous encapsulation,⁵ isolation, and premature failure of the implant.¹ Chemical and physical modifications of biomaterials and immunomodulatory approaches have been developed to reduce macrophage adhesion at early stages and to block pro-inflammatory cytokine release and long-term FBGC formation.⁶ This can be based on reducing or blocking protein adsorption, which is achieved by immobilization of poly(ethylene glycol) or zwitterionic compounds such as phosphatidylcholine with reduction of opsonization. Since these approaches have limited long-term

Received: August 9, 2019

Published: August 26, 2019

stability, more efficient methods to suppress inflammation are based on immobilization of drugs with anti-inflammatory effects such as nonsteroidal anti-inflammatory drugs (NSAID) or biomolecules such as heparin.¹ The layer-by-layer (LbL) technique, which is based on the alternative deposition of oppositely charged polyelectrolytes, has been introduced recently for the preparation of anti-inflammatory coatings⁷ because of its simplicity, applicability to a variety of materials (metals, glasses, ceramics, and polymers), and control of surface properties at the nanometer scale.⁸

Previous studies have demonstrated the immediate anti-inflammatory capacity of coatings based on glycosaminoglycans (GAGs).^{9–12} In particular, heparin (Hep) can bind a variety of chemokines, cytokines, and growth factors, which can modulate inflammatory processes. As an example, when taken up by endocytosis, Hep inhibits the nuclear transcription factor- κ B (NF- κ B), which in turn suppresses leukocyte activation turning down pro-inflammatory cytokines production.^{13–15} Moreover, Hep-based coatings have demonstrated superior properties when compared to other GAGs-based systems due to high wettability, negative surface charge, and intrinsic anti-inflammatory activity.¹⁶ Although these surface coatings eventually reduce FBR,¹⁷ there is still lack of definitive solutions.^{18,19}

The LbL technique can be used to fabricate polyelectrolyte multilayers from polyanions such as heparin.¹⁶ The inherent thickness of PEM that depends on the number of single layers, molecular weight of polyelectrolytes and complexation conditions makes them useful as carriers for localized controlled drug release.²⁰ The simplest approach represents the incorporation of bioactive molecules, such as nucleic acids, growth factors, or other cytokines embedded in the multilayer system,²¹ covalently linked to PEM components or adsorbed on the top layer after PEM preparation.²² However, this strategy has some limitations as many anti-inflammatory drugs such as glucocorticoids or nonsteroidal anti-inflammatory drugs are highly hydrophobic, which causes difficulties to achieve uptake in hydrophilic multilayer systems²³

For example, Naproxen (NAP) is a widely known NSAID with anti-inflammatory, analgesic, and antipyretic properties of superior pharmacokinetics and lower risk of cardiovascular adverse effects compared to other NSAIDs.²⁴ To overcome the problem of solubility, embedding cyclodextrin/hydrophobic drug complexes, liposomes, and polymeric NP with hydrophobic core in PEM films emerged as a promising solution.^{25,26} Another option is the linkage of NSAID such as NAP through an ester bond to a polymer and subsequent formation of NP. Such NP can be taken up by endocytosis and release the cargo by activity of esterases and the acidic pH in lysosomes.²⁷ Hence, immobilization of NP in PEM systems shall permit a localized control on drug release at the implantation site.²³

This work describes for the first time the combination of Hep (polyanion) with NAP-bearing cationic NP to prepare surface coatings by the LbL technique with potential short-term and long-term anti-inflammatory activity (Figure 1). Reference multilayer systems were prepared using polystyrenesulfonate (PSS) as alternative polyanion to replace Hep, showing biocompatibility, but no anti-inflammatory activity, while chitosan (Chi), a biocompatible natural polymer, was employed as further polycation to replace NP to have a system without NAP. Physicochemical characterization of PEM formation and surface properties was performed to study the effect of PEM properties on cellular responses. THP-1-derived

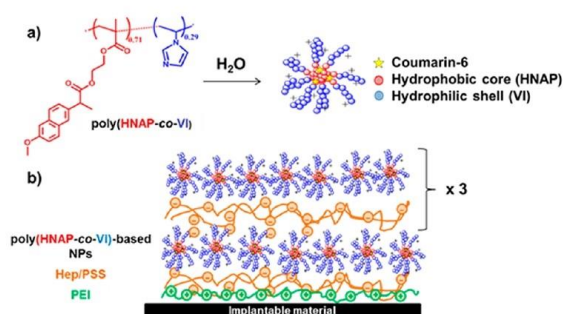


Figure 1. Schematic representation of (a) the HNAP71 copolymer and nanoparticles obtained after self-assembly in aqueous media entrapping coumarin-6 as a model hydrophobic drug and fluorescent tracer molecule; and (b) polyelectrolyte multilayer composed of polyethylene imine as bonding layer with alternating deposition of heparin (Hep) or polystyrenesulfonate (PSS) as polyanions and nanoparticles (NP) as cationic element prepared by a layer-by-layer method.

macrophages were used to study the short- and long-term anti-inflammatory activity of PEM by evaluating cell adhesion and IL1- β secretion after 48 h and FBGCs formation after 15 days, respectively. Results are reported herein.

MATERIALS AND METHODS

Materials. Dichloromethane (DCM), 4-dimethylaminopyridine (DMAP), hydroxyethyl methacrylate (HEMA), magnesium sulfate (MgSO₄), and dicyclohexylcarbodiimide (DCC) were purchased from Merck (Madrid, Spain). (+)-(-)-S-2-(6-Methoxynaphthalen-2-yl) propanoic acid (naproxen) from TCI (Montgomeryville, PA, USA) and sodium bicarbonate (NaHCO₃) and sodium chloride (NaCl) were obtained from Panreac (Madrid, Spain). All reagents were used without further purification for the synthesis and purification of the naproxen-based methacrylic monomer. Dimethyl sulfoxide (DMSO) from Scharlau (Madrid, Spain) was used without further purification. 1-Vinylimidazole (VI) and 2,2'-azobis(isobutyronitrile) (AIBN) from Merck (Madrid, Spain) were distilled and recrystallized from ethanol, respectively, for the preparation of amphiphilic copolymers. Ethanol (EtOH) and acetone (AcetOH) were purchased from Scharlau (Madrid, Spain) and coumarin-6 (c6) from Merck (Madrid, Spain). They were used without further purification for the preparation of NP.

Glass slides were purchased from Menzel GmbH (Bielefeld, Germany) of (\varnothing 12 mm and 15 mm) surfaces. Silicon wafers were obtained from LG Siltron Inc. (Gumi, Korea) of (10 \times 10) mm² surface. In addition, gold sensors for quartz crystal microbalance (QCM) were delivered from 3T analytic GmbH (Tuttlingen, Germany). Poly(ethylene imine) (PEI, $M_w \approx 750$ kDa) was purchased from Polysciences Inc. (Warrington, USA). Heparin (Hep, $M_w \approx 15$ kDa) and polystyrenesulfonate (PSS, 30 wt % in H₂O, $M_w \approx 70$ kDa) were obtained from Serva and Sigma-Aldrich (Heidelberg, Darmstadt, Germany), respectively. Chitosan 85/500 (Chi, $M_w \approx 500$ kDa) was obtained from Heppel Medical Chitosan GmbH (Halle (Saale), Germany) with a deacetylation degree of 85%. Sodium Chloride (NaCl) was purchased from Roth (Karlsruhe, Germany), while acetic acid was provided from Applichem (Darmstadt, Germany).

Methods. Nanoparticles (NP) Preparation and Characterization. Monomer and Copolymer Synthesis. The synthesis of the methacrylic derivatives of naproxen (HNAP) was carried out through a carbodiimide mediated Steglich esterification reaction. The copolymer poly(HNAP-co-VI) was synthesized by free radical polymerization in solution combining HNAP and vinylimidazole (VI) as previously described by our group for a methacrylic derivative of ibuprofen.²⁸ In the current study, a feed molar ratio of 50:50

(HNAP:VI) and a monomer concentration of 0.25 M were used. The copolymer was named HNAP71 according to its molar content in HNAP.

Preparation and Characterization of Unloaded and Coumarin-6-Loaded Nanoparticles. Unloaded and coumarin-6 (c6)-loaded NP were prepared by a nanoprecipitation method. C6 was encapsulated at a low concentration (i.e., 1% w/w in respect to the polymer) in order to avoid fluorescence quenching. Briefly, HNAP71 copolymer (10 mg mL⁻¹) or HNAP71 (10 mg mL⁻¹) and coumarin-6 were dissolved in a mixture of acetone and ethanol (8:2; vol/vol), added dropwise to an aqueous buffer solution (100 mM acetic acid and 100 mM NaCl) at pH 4.0 under magnetic stirring. The final polymer concentration was 1.0 mg mL⁻¹. Thereafter, the solution was dialyzed against the same buffer solution at pH 4.0 for 72 h in order to eliminate the organic solvent and soluble nonencapsulated c6, in the case of loaded NP. Then, the resultant NP were filtered through 1 μm Nylon filters to remove the remaining insoluble c6.

The hydrodynamic properties of NP (i.e., particle size distribution and zeta potential (ξ)) were determined at room temperature by dynamic light scattering (DLS) and laser Doppler electrophoresis (LDE), respectively, using a Malvern Nanosizer NanoZS Instrument (Madrid, Spain) equipped with a 4 mW He–Ne laser (λ = 633 nm) at a scattering angle of 173°. The autocorrelation function was converted in an intensity particle size distribution with ZetaSizer Software 7.10 version, to obtain mean hydrodynamic diameter (D_h) and particle dispersion index (PDI) based on 0 (monodisperse particles) and 1 (polydisperse particles) between the Stokes–Einstein equation, assuming the particle to be spherical. For each sample, the statistical average and standard deviation of D_h and PDI data were calculated from 3 measurements of 11 runs each, while the ξ statistical average and standard deviation were calculated from 3 measurements of 20 runs each.

Coumarin-6 Encapsulation Efficiency and Loading. C6-loaded NP were prepared as described above, but in a NaCl-free buffer solution and freeze-dried in order to eliminate the aqueous phase. The white amorphous powder was dissolved in a mixture of acetone and ethanol (8:2, vol/vol) overnight to dissolve the self-assembled structure releasing all encapsulated c6. After that, ethanol was added and the sample was kept in agitation over 24 h to dissolve c6 in supernatant and precipitate the polymer. Samples were centrifuged at 10,000 rpm for 5 min at room temperature, and the UV absorbance of the supernatant was measured at λ = 459 nm by a NanoDrop One spectrophotometer (Thermo Scientific, Madrid, Spain). A standard curve was prepared from c6 and used for calculation of the c6 concentration in the samples. The encapsulation efficiency (EE) was defined as the ratio of the c6 detected experimentally and the original concentration of c6 encapsulated in the inner core of the NP (eq 1) and the loading capacity (LC) as the ratio of the mass of c6 detected and the mass of NPs (eq 2).

$$\text{Encapsulation Efficiency (\%)} = \frac{[\text{coumarin-6}]_{\text{measured}}}{[\text{coumarin-6}]_{\text{initial}}} \times 100 \quad (1)$$

$$\text{Loading capacity (\%)} = \frac{\text{mass of c6 measured}}{\text{mass of NPs}} \times 100 \quad (2)$$

Cryogenic Transmission Electron Microscopy (Cryo-TEM). The images of Cryo-TEM of the NP were taken with a Jeol 1230 electron microscope (Bergen, Norway) operated at 100 kV and equipped with a Gatan liquid nitrogen specimen holder (Warrendale, PA, United States) and a CMOS Tvipis TemCam-F416 camera (Gauting, Germany), at 40,000 nominal magnification under low dose conditions. Samples were applied to holey carbon grids (Quantifoil, Großlobichau, Germany) after glow-discharge and immediately blotted and vitrified using a FEI Vitrobot cryo-plunger (Thermo Scientific, Madrid, Spain).

NP Density Determination. Nanoparticles density was assessed using a previously described isopycnic centrifugation method with slight modifications.²⁹ Briefly, aqueous glucose solutions at concentrations of 10, 20, 30, 35, 40, 45, 50, 55, and 60% (w/v) were

prepared. Five mL of successive layers of glucose solutions at decreasing concentrations are let to diffusion for 12 h to create different density gradients. Then, a NP sample (1 mg/mL, 2 mL) was placed on top of each glucose gradient and centrifuged for 6 h at room temperature and 10,000 rpm. Immediately after centrifugation, 5 mL fractions were collected and their density was determined by a pycnometer method. UV absorption is measured at λ = 239 nm by a NanoDrop One spectrophotometer to determine the content in NP of each collected volume. The density of the fraction showing the highest UV absorbance (λ = 239 nm) was retained as the value of the nanoparticle density. Results of density measurements are shown in Table S1 in the Supporting Information.

Substrates and Polyelectrolyte (PEL) Preparation. Silicon wafers and glass slides were used for deposition and physicochemical and biological characterization of multilayers. Glass was used as a model surface because the LbL technique is a method that permits adsorption of polyelectrolytes to virtually all kind of surfaces.^{8,10,20–23} In addition, glass and silicon permit the use of different analytical techniques such as atomic force microscopy, zeta potential measurements, and optical microscopy. The substrates were cleaned with a solution of ammonia (TH-Geyer GmbH & Co. KG 25%, Renningen, Germany), hydrogen peroxide (Roth 30%, Karlsruhe, Germany), and water (1:1:5, v/v/v) at 75 °C for 10 min, subsequently washed with ultrapure water (6 × 5 min), and dried with a stream of nitrogen.³⁰

C6-loaded NP and unloaded NP were prepared as described above (1 mg mL⁻¹). Polyelectrolyte (PEL) solutions (2 mg mL⁻¹), heparin (Hep, M_w ≈ 15 kDa), and polystyrenesulfonate (PSS, 30 wt % in H₂O, M_w ≈ 70 kDa) were also prepared by dissolution in 100 mM NaCl + 100 mM acetic acid at pH 4.0 and 7.0, respectively. Poly(ethylene imine) (PEI, M_w ≈ 750 kDa) was dissolved in the same buffer solution as well at pH 7.0 with a concentration of 5 mg mL⁻¹. Moreover, the same concentrations of the polyelectrolyte PEI, Hep, and PSS were prepared in 150 mM NaCl solution. Chitosan (Chi, M_w ≈ 500 kDa) was also dissolved in 150 mM NaCl, pH 4.0 adjusted by hydrochloric acid. All solutions were sterile filtered with poly(ether sulfone) filters of 0.2 μm pore size.

Polyelectrolyte Multilayer Formation. Four different systems were prepared made of 8 single layers on top of the primary PEI layer. They were composed of either NP-containing PEM with Hep or PSS as polyanions or Chi-containing PEM with Hep or PSS as polyanions denominated as [PEI(Hep-NP)₄, PEI(PSS-NP)₄, PEI(Hep-Chi)₄, and PEI(PSS-Chi)₄]. PEI was used as anchoring base layer to obtain a positive surface net charge on silicon and glass substrates. PEI was adsorbed for 30 min and rinsed with either 100 mM NaCl + 100 mM acetic acid or 150 mM NaCl at pH 7, three times for 2.5 min. Subsequently, multilayers of Hep or PSS as polyanions together with Chi or NP as polycations were formed on top of PEI in which they were adsorbed for 15 min while NP were adsorbed for 60 min. Furthermore, the NP-containing Hep or PSS multilayers were rinsed with 100 mM NaCl + 100 mM acetic acid and the Chi-containing Hep or PSS rinsed with 150 mM NaCl, three times for 2.5 min. An ultraviolet light chamber (Bio-Link BLX, LTF Labortechnik GmbH & Co. KG, Wasserburg, Germany) was used, set at 254 nm (50 J cm⁻²) to sterilize the PEM modified samples for 60 min, placing them in 24-well tissue culture plates (Greiner Bio-One GmbH & Co.KG, Frickenhausen, Germany) for further cell studies.

Characterization of Surface Properties and Multilayer Formation. Multilayer Growth. The growth of PEM was studied in real-time by means of a quartz crystal microbalance with dissipation monitoring (QCM-D, qCell T, 3T Analytik, Tuttlingen, Germany). Temperature was set to 25 °C according to the manufacturer's protocol. Quartz gold sensors were used as the model substrates to immobilize the PEL and NP. The formation of PEM was monitored by real-time variations in oscillatory frequency and damping. A continuous flow rate of 100 μL min⁻¹ was used for all PEL for 15 min, while NPs were incubated for 1 h. Rinsing steps were done for 15 min after each layer deposition. All measurements were repeated twice, and average values were calculated. qGraph viewer software (3T Analytik) was used to calculate adsorbed mass and film thickness by applying the Voigt viscoelastic model.³¹ Calculations were made using

viscosity and density of water (0.001 Pa and 1,000 kg/m³) and film density based on the density of nanoparticles as shown in the Supporting Information.

Scanning Electron Microscopy (SEM). The structure of PEM on silicon wafers was studied with Philips ESEM XL 30 FEG (Eindhoven, Netherlands) used in high vacuum ($p = 10^{-6}$ mbar). PEM were coated with 20 nm chromium.

Atomic Force Microscopy (AFM). Three-dimensional images of the topographic of PEM were obtained with an AFM Nano-R (Pacific Nanotechnology Inc., Santa Clara, USA) in close contact mode. AFM tips from AppNano (Applied Nanostructures Inc., Santa Clara, USA) with 125 μm length, 35 μm width, 14–16 μm height and tip radius of <10 nm were used for imaging. Images with scan areas of $10 \times 10 \mu\text{m}^2$ were taken with a scan rate of 0.2 Hz and a resolution of 512×512 pixel². All scans were performed in an environmental atmosphere with air as ambience. Image processing was done using Gwiddyon software (version 2.40).

Zeta Potential Measurements. The zeta potential of PEM was determined with a SurPASS streaming potential device (Anton Paar, Graz, Austria). Two identical glass substrates covered with the different PEM were mounted oppositely into the adjustable gap cell. The gap size was adjusted to achieve a flow rate between 100 and 150 mL min⁻¹, not exceeding 300 mbar as the maximum pressure, which was checked to ensure a consistency in both directions. 1 mM potassium chloride (KCl) was used as electrolyte. 0.1 N hydrochloric acid (HCl) was used to adjust the pH value of KCl to pH 3.0 as starting pH titration. 0.1 N sodium hydroxide solution (NaOH) was used for an automated titration ranging from pH 3.0 to 10 using volume increments of 20 μL for adjustment of pH values in 0.25 pH steps.

Cell Experiments. Cell Culture. THP-1 human monocytic cells (DSMZ, Braunschweig, Germany) were cultured in RPMI-1640 medium (Lonza, Wuppertal, Germany) supplemented with 10% (v/v) fetal bovine serum (FBS, Biochrom AG, Berlin, Germany) and 1% (v/v) antibiotic–antimycotic solution (AAS, Lonza, Wuppertal, Germany) at 37 °C in a humidified 5% CO₂/95% air atmosphere using a NUAIRE DH Autoflow incubator (NuAire, Plymouth, Minnesota, USA). The nonadherent cells were passaged every second day to maintain a cell density of about 1×10^6 cells mL⁻¹. THP-1 cells were differentiated to macrophages by incubation with 200 nM phorbol-12-myristate-13-acetate (PMA, Sigma-Aldrich, Darmstadt, Germany) in T75 cell culture flasks (Greiner Bio-One GmbH & Co.KG, Frickenhausen, Germany) for 48 h. Thereafter, 0.25% trypsin/0.02% EDTA (Biochrom AG, Berlin, Germany) was used to detach the adherent macrophages with further addition of serum-containing RPMI-1640 medium to stop the trypsin effect. Eventually, the harvested cells were used for seeding on the different PEM.

Cell Adhesion Studies. THP-1- derived macrophages were seeded on PEM at a cell density of 2.5×10^4 cells mL⁻¹ in serum-containing RPMI-1640 medium. Cultures were incubated for 24 h at 37 °C in a humidified 5% CO₂/95% air atmosphere. Afterward, the surfaces were gently washed twice with phosphate buffer saline (150 mM NaCl, 5.8 mM NaH₂PO₄, Na₂HPO₄, pH 7.4; PBS) to remove nonadherent cells. Attached cells were fixed with cold methanol (Roth, Karlsruhe, Germany) for 10 min and stained with 10% (v/v) Giemsa (Merck KGaA, Darmstadt, Germany) in ultrapure water for another 10 min, which is a standard method to stain macrophages. A transmitted light microscope (Axiovert 100, Carl Zeiss MicroImaging GmbH, Oberkochen, Germany) equipped with a CCD camera (MC-3254, AVTHorn, Oberkochen, Germany) was used to photograph the cells. The images were used to quantify the number of adhering cells using ImageJ software (version 1.46r).

Pro-inflammatory Cytokine Production and Metabolic Activity of Macrophages. The IL-1 β release was evaluated after 48 h of culture of macrophages in serum-containing RPMI-1640 medium in the presence and absence of 1 μg mL⁻¹ lipopolysaccharide (LPS, Sigma-Aldrich, Darmstadt, Germany) on the different PEM. The medium supernatants of the LPS-treated and untreated samples were collected after 48 h of incubation and stored at -80 °C until needed for investigating the pro-inflammatory IL-1 β cytokine release. An

enzyme linked immunosorbent assay (ELISA) was used here according to the manufacturer's instructions (Invitrogen, Thermo Scientific, San Diego, USA).

The cell viability was determined by a Q-Blue assay (BioChain, Heidelberg, Germany), which was later used to normalize the cytokine production on the different PEM surfaces to the quantity of viable cells. Briefly, after collecting the supernatant for IL-1 β studies, cells were washed carefully with sterile PBS twice. Then, 500 μL of prewarmed, colorless Dulbecco's modified Eagle's medium (DMEM, Biochrom, Berlin, Germany) supplemented with the QBlue reagent (10:1) was added to each well. After incubation at 37 °C for 2 h, 100 μL of supernatants from each well was transferred to a black 96-well plate and fluorescence was measured at 544 nm excitation and 590 nm emission wavelength with a plate reader (BMG Labtech, Fluostar optima, Offenburg, Germany). Finally, the cytokine release was normalized to the fluorescence values, which correspond to the quantity of viable cells.

NP Internalization by Macrophages Studied with Flow Cytometry. Macrophages were seeded in RPMI 1640 medium with 10% FBS at a concentration of 2.5×10^5 cells mL⁻¹ on the primary PEI surfaces in the presence of c6-loaded NP in suspension, which was considered as positive control. Further seeding of cells was performed on the terminal fourth bilayer of c6-loaded NP embedded on multilayers composed of either Hep or PSS as polyanions with incubation for 48 h. Thereafter, all PEM systems and control were transferred to new well plates and gently washed with PBS. Then, 300 μL of 0.25% Trypsin was added for 3 min to detach adhering macrophages, followed by addition of serum-containing RPMI 1640 medium to stop the trypsin effect. The cells were scraped, centrifuged, washed once with PBS, and resuspended in 200 μL PBS. Finally, 100 μL of cell suspension was transferred to a 96-well plate and measured with a flow cytometry device (LSR Fortessa II, BD Bioscience, Germany) to detect nanoparticles associated with macrophages. For the quantification of macrophages positive to c6-NP in the gating strategy, dead cells and debris were excluded. From the remaining cells the percentage of c6 NP-positive macrophages is represented. The data were analyzed with FACS-Diva software (version 6.2).

Foreign Body Giant Cell (FBGCs) Formation. The quantity of FBGCs on the different PEM was evaluated in serum-containing RPMI-1640 medium in the presence and absence of 1 μg mL⁻¹ LPS. Macrophages were seeded as described above and cultured for 15 days. PEM covered glass slides were gently washed twice with PBS, and attached cells were fixed with cold methanol and stained with 10% (v/v) Giemsa in ultrapure water as described above. Micrographs were taken by transmitted light microscope equipped with a CCD camera. The area percentage of FBGC covering the surface of different PEM was calculated by ImageJ software.

Statistics. Statistical calculations were performed with one-way analysis of variance (ANOVA) followed by posthoc Tukey's test using Origin 8 Pro software (Origin Lab, Northampton, Massachusetts, USA). All data are represented as mean values \pm standard deviations (SD). The number of samples has been indicated in the respective figure captions. Statistical significance was considered for $p \leq 0.05$ and is indicated by asterisks in the figures.

RESULTS AND DISCUSSION

HNAP71 Copolymer Synthesis. The copolymer was synthesized following a protocol described previously²⁸ with yields higher than 75%. According to ¹H NMR, a 0.5 molar fraction of HNAP in the feed (F_{HNAP}) lead to a molar fraction of HNAP in the copolymer (f_{HNAP}) of 0.71. The copolymer showed a molecular weight of 75 kDa with a polydispersity of the molecular weight distribution of 2.0 both obtained by size exclusion chromatography (SEC). It should be noted that Naproxen is covalently linked to the copolymer structure through an ester bond that is hydrolyzable at acidic pH and esterases encountered in the lumen of lysosomes and at the site of inflammation.²⁷

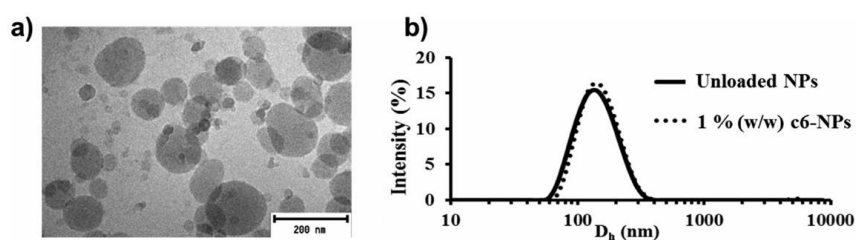


Figure 2. (a) Cryogenic transmission electron microscopy (cryoTEM) micrograph of the nanoparticulated system [Scale: 200 nm]. (b) Comparative graph of the unloaded NP and coumarin-6-loaded NP size distribution (by intensity) obtained by DLS.

Table 1. C6 Encapsulation Efficiency Loading Capacity and Hydrodynamic Properties of Unloaded NP and c6-Loaded NP

Sample	EE ^a (%)	LC ^b (%)	D _h ^c (nm)	PDI ^d	ξ ^e (mV)
Unloaded	-	-	131.5 ± 3.3	0.115 ± 0.016	+ 29.5 ± 1.0
C6-loaded	92 ± 2	0.92	140.0 ± 1.1	0.132 ± 0.026	+ 28.9 ± 0.6

^aEE (%) – percentage of encapsulation efficiency. ^bLC (%) – percentage of loading capacity. ^cD_h – mean hydrodynamic diameter. ^dPDI – polydispersity index studied by DLS. ^eξ – mean zeta potential measured by LDE (*n* = 3).

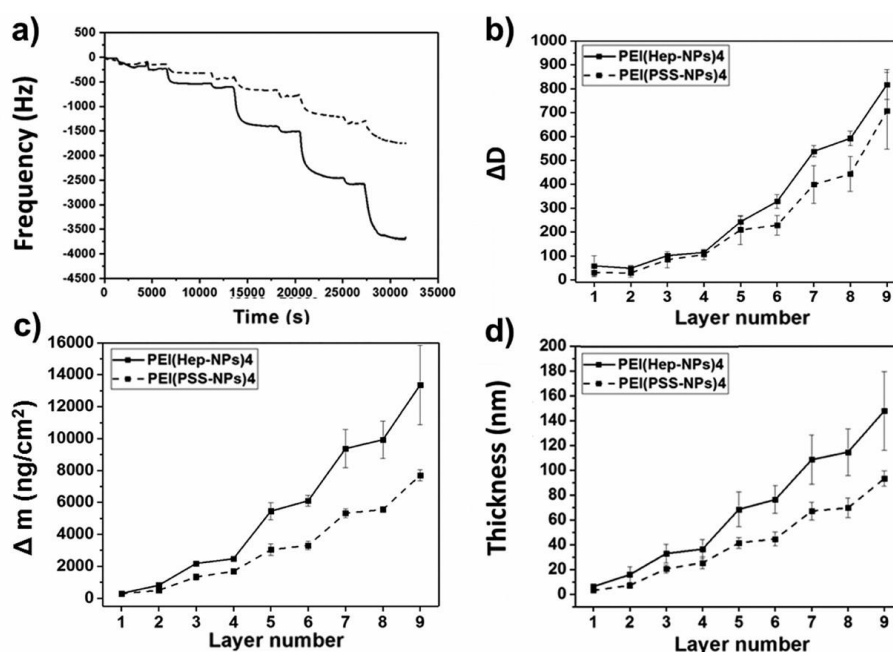


Figure 3. Representative quartz microbalance with dissipation monitoring (QCM-D) graphs depicting (a) real-time variations of frequency during construction, (b) dissipation change (ΔD) after each layer, (c) the corresponding QCM-D mass change ($-\Delta m$) per unit area, and (d) thickness change obtained by applying the Voigt model for viscoelastic films of the PEI(Hep-NP)₄ (solid lines) and PEI(PSS-NP)₄ (dashed lines). Layer 1: PEI. Even layers: Hep or PSS. Odd Layers: NP. Results are means \pm SD of two independent experiments.

Characterization of Unloaded and Coumarin6-Loaded NP. The CryoTEM image (see Figure 2a) shows the spherical morphology of NP obtained by the nanoprecipitation method in aqueous media. Figure 2b presents the size distribution (by intensity) of NP. In addition, results of hydrodynamic diameter (D_h) (by intensity) and polydispersity (PDI) were obtained by DLS and zeta potential (ξ) values by LDE (Table 1).

C6 was used simultaneously as a fluorescent probe for NP internalization studies with macrophages but also as a model for the ability of NP to encapsulate another hydrophobic drug molecule. HNAP71-based nanoparticles encapsulated c6 with

high efficiency (encapsulation efficiency = $92 \pm 2\%$, *n* = 3) (eq 1). Only a slight increase of 10 nm in NP diameter was observed with no significant changes in surface charge (Table 1). This result demonstrates that HNAP71-NP represent an appropriate hydrophobic reservoir for nonpolar small molecules such as most anti-inflammatory drugs. Moreover, their highly positive surface charge close to +30 mV demonstrates the presence of protonable amine groups of VI monomer on the surface of NP, which makes them useful as a polycationic component for immobilization by the LbL technique in combination with polyanions.

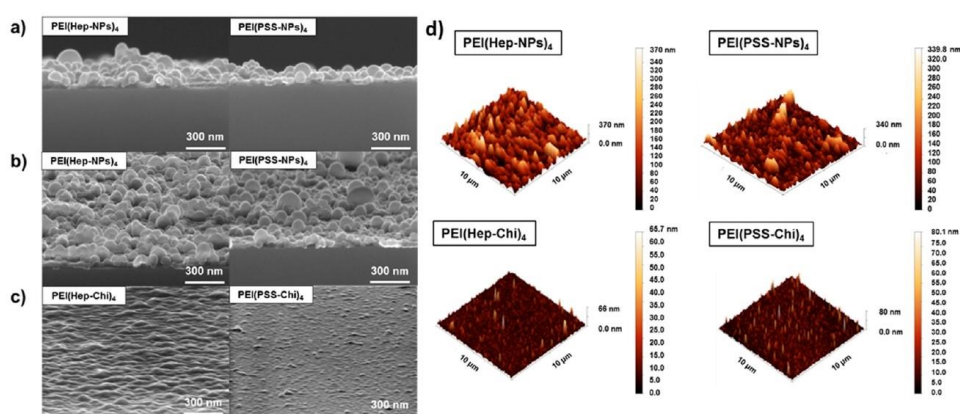


Figure 4. Scanning electron microscopy (SEM) images: (a) cross-sectional view of terminal layer with NP, (b) top view of the terminal layer with NP, and (c) top view of terminal layer Chi in combination with either heparin (Hep) or polystyrenesulfonate (PSS) as polyanions [Scale: 300 nm]. (d) Atomic force microscopy (AFM) images of surface topography in dry state of terminal layers of nanoparticles (NP) or chitosan (Chi) in combination with either heparin (Hep) or polystyrenesulfonate (PSS) as polyanions. [Scale: 10 μm]. LbL systems are abbreviated as [PEI(Hep-NP)₄], [PEI(PSS-NP)₄], [PEI(Hep-Chi)₄], and [PEI(PSS-Chi)₄], respectively.

Multilayer Growth. The PEM growth was studied in real-time by QCM-D. The reported values are averaged from two independent measurements. The decrease in quartz crystal oscillation frequency after each adsorption step (see Figure 3a) demonstrates film growth when NP were combined with either Hep or PSS. The energy dissipation ΔD provides information about the mechanical properties of the film. In this case, film formation leads to a significant increase in dissipation as shown in Figure 3b and Supporting Information Figure 1b, when using either PSS or Hep as polyanion representing a typical viscoelastic behavior.^{31,32} Therefore, there is no direct relationship between adsorbed mass and frequency variations, which requires the application of the Kelvin–Voigt model for viscoelastic films instead of the Sauerbrey equation³³ to determine the adsorbed mass per unit area and the film thickness (see Figure 3c and Figure 3d).

ΔD values followed a staircase increasing trend (Figure 3b), which indicates a swelling or stiffening of the system upon adsorption of NP or polyanions, respectively. These results point toward NP as the main contributors to the viscoelastic behavior of the film, owing to their highly hydrophilic corona. Figure 3c shows a staircase growth for both PEM. The mass adsorption was always higher for NP than for the polyanion as they present higher molecular weight and can absorb large amounts of water. However, it is noticeable that the assembly of PEI(Hep-NP)₄ PEM followed an exponential growth. By contrast, PEI(PSS-NP)₄ PEM growth shows a more linear trend (Figure 3c and Figure 3d) resulting in higher thickness for the Hep-based PEM. This exponential growth has been related to the presence of diffusible components.³⁴ Hep diffusion through the PEM layer has already been described and identified as a reason for such growth behavior.¹⁶ From these data one can conclude more adsorption of Hep compared to PSS with NP as polycationic component that may be attributed to the higher charge density of heparin. The fact that Hep-based systems present a larger thickness than PSS-containing PEMs (Figure 3d) might be related to higher water content. This assumption is supported by findings from others that films made of polysaccharides such as Hep are more hydrated than films made of synthetic polyelectrolytes.¹⁶

Regarding the multilayer systems PEI(PSS-Chi)₄ that was introduced here for comparison of the effect of polycationic components (either PP or Chi), an exponential growth was found (see Supporting Information Figure 1a), which leads to relatively soft films (Supporting Information Figure 1b), as found by others, too.³⁵ Previous studies have also described the growth kinetics of the comparative PEM PEI(Hep-Chi)₄ with similar formation conditions that also match the findings of our study (Supporting Information Figure 1a and b).^{16,36}

Surface Characterization of Multilayer. The surface topography of PEM was characterized by SEM (Figure 4a–c) and AFM (Figure 4d) under dry conditions to visualize the immobilization of NP. The SEM micrographs of NP-containing Hep and PSS PEM (Figure 4b) show the distribution of NP across the surface with a certain roughness confirming their presence in accordance with QCM-D studies. In fact, the spherical NP are clearly visible on top of PEM, while a smoother surface is observed with Chit-based PEM (Figure 4c). Moreover, Figure 4b indicates the presence of higher quantities of NP when Hep is used as polyanion compared to PSS, which is also supported by the higher thickness visible in the cross sections (Figure 4a). These findings support the observations and conclusions made in QCM-D experiments. The findings of SEM were supported by AFM studies. Figure 4d shows a comparison of surface topography, which was highly different between multilayers containing NP (upper row) and those that only contained chitosan as polycation (lower row). AFM images demonstrate that the topography was highly dependent on the presence of NP with a topography in z scale in the range of 300 nm, while the PEM made of Hep and PSS with chitosan as polycation were much smoother in the range of 30 nm.

Results of QCM-D studies and SEM/AFM microscopy show that there was no perfect hexagonal packing of nanoparticles but rather a more chaotic deposition. This might be due to polydispersity of NP size distribution together with the fact that even after long adsorption time of 60 min for NP, thermodynamic equilibrium of adsorption has not been reached. In addition, subsequent washing steps may also lead to some detachment of more loosely adsorbed NP. Hence, a theoretical four layer deposition of NP was not found, because

the thickness derived from QCM-D studies of about 150 nm maximum corresponds to around two deposited NP layers.

Interaction of materials surfaces with proteins and cells is driven by interfacial energy, including Coloumb interaction and other physical forces.³⁷ The surface (zeta) potential of biomaterials is related to Coloumb interaction with charged proteins and cells playing a key role in cell–surface interactions.³⁸ Despite the fact that charges are screened by small counterions, it has been demonstrated that negatively charged surfaces inhibit whereas positively charged surfaces favor cell adhesion.^{39,40} Streaming potential measurements were performed by a pH titration at low ionic strength. Results are shown in Figure 5. The zeta potential of PEM showed a

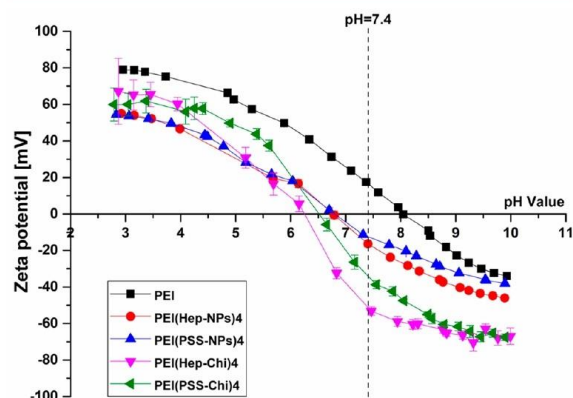


Figure 5. Zeta potential of primary poly(ethylene imine) (PEI) layer and the terminal (fourth) layer of nanoparticles (NP) or chitosan (Chi) in combination with either heparin (Hep) or polystyrenesulfonate (PSS) as polyanions on glass slides, abbreviated as [PEI (black squares), PEI(Hep-NP)₄ (red circles), PEI(PSS-NP)₄ (blue triangles), PEI (Hep-Chi)₄ (pink triangles), and PEI (PSS-Chi)₄ (green triangles)], respectively. Results are means \pm SD of two independent experiments in the pH range 3–10.

sigmoid behavior during titration with positive potentials at acidic and negative at basic pH values as observed in previous studies.^{16,41} This is related to the existence of a swollen surface layer that represents an amphoteric behavior through the

presence of both cationic and anionic groups from both polyelectrolytes as described in more detail by Zimmermann and Werner.⁴² NP-containing multilayers did show different surface potentials across the pH titration, which indicates that the outermost layer was dominated by the charge contribution of the protonable amine groups of VI at the surface of NP.⁴³ By contrast, reference PEM composed of Hep/Chi and PSS/Chi had lower zeta potentials in the basic region, which indicates a dominance of polyanions in this pH range and less than that of the polycation Chi. As was expected, the polycation PEI coated surfaces possessed the highest positive zeta potential and a point of zero charge (PZC) at pH 8.5, which is related to a net positive charge of this surface at physiological conditions.⁴⁴

Studies on Macrophage Adhesion and IL-1 β Release.

To evaluate the immediate anti-inflammatory capacity of the systems, studies on adhesion of macrophages that represent a prerequisite for the onset of inflammatory processes on biomaterials were carried out after 48 h. Figure 6a shows the micrographs of Giemsa-stained macrophages and Figure 6b the quantitative analysis of cell adhesion. The highest adhesion was observed on the positively charged PEI surfaces. Macrophages on PEI showed a spread and elongated morphology together with significantly higher number of adhering cells ($p \leq 0.05$) in comparison to PEM, which possessed a lower elastic modulus and a negative surface charge as demonstrated by QCM-D and zeta-potential measurements, respectively. These results are in accordance with previous studies claiming that surfaces presenting high wettability, low elastic modulus, or negative charge can reduce macrophage adhesion.³⁴ Giemsa staining suggested also that Hep as polyanion in combination with either NP or Chi reduced macrophage adhesion (Figure 6a), which goes along with the anionic, hydrophilic nature of heparin and cell repulsive properties of multilayer films prepared at low pH with this glycosaminoglycan as found in other studies.^{16,41}

Macrophages can respond to biomaterial implantation by release of pro-inflammatory cytokines leading to systemic (acute phase response) and local effects such as recruitment and activation of other leukocytes resulting in acute and chronic inflammation.⁴⁵ However, a reduced secretion of pro-inflammatory cytokines such as IL-1 β , TNF- α , or IL-6 indicates limited inflammatory responses indicating a better

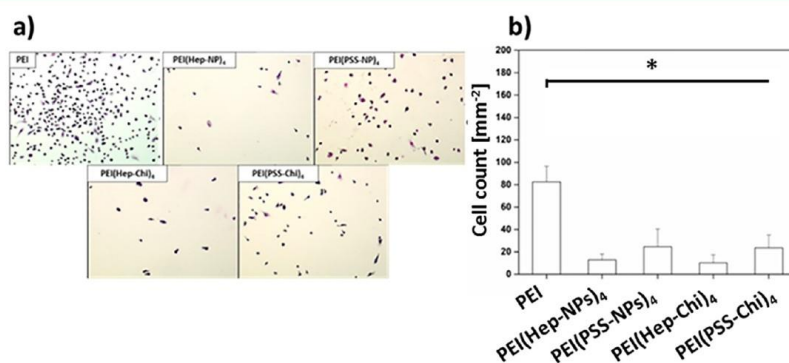


Figure 6. (a) Micrographs of Giemsa-stained macrophages on the primary layer of poly(ethylene imine) (PEI) and the terminal layer of nanoparticles (NP) or chitosan (Chi) in combination with either heparin (Hep) or polystyrenesulfonate (PSS), abbreviated as [PEI, PEI(Hep-NP)₄, PEI(PSS-NP)₄, PEI(Hep-Chi)₄, and PEI(PSS-Chi)₄], respectively. [Scale: 200 μ m]. (b) Number of adherent macrophages per mm² after 24 h of incubation obtained by image analysis. Data represent means \pm SD, $n = 10$, * $p \leq 0.05$.

biocompatibility of biomaterials.⁴⁶ Figure 7 depicts the normalized secretion of IL-1 β by macrophages seeded on

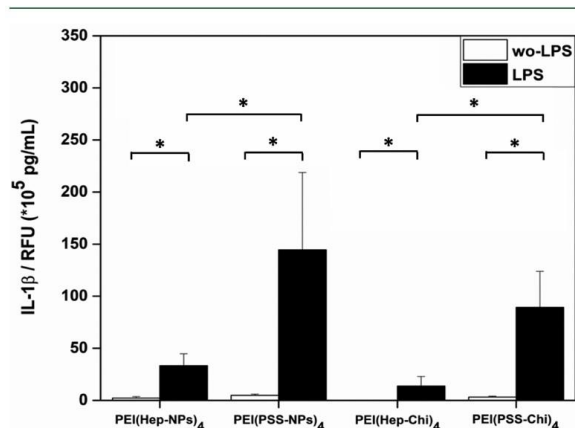


Figure 7. IL-1 β release from macrophages incubated for 48 h in absence (white bars) or presence (black bars) of lipopolysaccharide (LPS). Macrophages were seeded in RPMI medium with 10% FBS on the terminal layers of either NP or Chi as polycations with Hep or PSS as polyanions, abbreviated as [PEI(Hep-NP)₄, PEI(PSS-NP)₄, PEI(Hep-Chi)₄, and PEI(PSS-Chi)₄], respectively. Results were normalized to the quantity of viable cells measured by QBlue assay given as relative fluorescence units (RFU) and represent mean \pm SD of two experiments, $n = 4$, $*p \leq 0.05$.

PEM in the presence or absence of LPS after 48 h. LPS was used as a strong inducer of macrophage activation because of the binding of the CD14/TLR4/MD2 receptor complex in macrophages.^{47,48} ANOVA test was performed to compare IL-1 β secretion in the presence and absence of LPS (e.g., Hep/NP with LPS was compared to Hep/NP without LPS) and to compare PEM that had the same polyelectrolytes (e.g., Hep/NP was compared to Hep/Chi and PSS/NP). Results in Figure 7 show that the release of IL-1 β was up-regulated in all samples after LPS stimulation. The lowest release of IL-1 β was found on PEI(Hep-Chi)₄ PEM with no significant differences

($*p \leq 0.05$) to PEI(Hep-NP)₄. Moreover, PEM based on PSS that lacks any specific anti-inflammatory activity lead to significantly higher release of the IL-1 β compared to the Hep-containing PEM. Hence, it is evident that PEM with Hep as polyanion possesses an anti-inflammatory activity as found in previous studies.¹⁶ Polyelectrolyte multilayers represent a substrate that interacts in a dynamic manner with adhering cells permitting reorganization of terminal layers but also uptake of polyelectrolytes and other multilayer components by cells.⁴⁹ Hep immediate anti-inflammatory capacity could be attributed to its capacity to diffuse through PEM systems followed by release and potential uptake by macrophages, leading to a reduction of NF- κ B nuclear translocation and cytokine expression.

In contrast, NP seem to have no contribution regarding the short-term anti-inflammatory capacity of PEM since IL-1 β values were much higher when LPS was used for stimulation of macrophages leading to significantly more secretion of this pro-inflammatory cytokine. This might be attributed to the fact that NAP release from NP occurs through hydrolysis of ester bonds, which is a very slow process at physiological conditions. However, hydrolysis is much faster in the presence of esterases and acidic pH encountered in lysosomes after NP internalization in macrophages.²⁸

NP Internalization by THP-1 Derived Macrophages.

Therefore, it was studied whether macrophages are able to take up NP from PEM as previous studies of our group have shown that cells are able to remodel PEM in an active manner.⁴⁹ Studies with macrophages incubated for 48 h either with fluorescent c6-labeled NP in supernatant on PEI or on PEM with c6-labeled NP were done with flow cytometry to quantify the percentage of macrophages positive for c6-loaded NP. Figure 8a shows flow cytometry histograms with side scatter (SSC) here, the raw data were obtained after setting the negative controls to a baseline by determining a threshold, beyond which any signal would be considered as positive for association of macrophages with c6-NP represented by the blue dots. Figure 8b shows the quantitative evaluation of experiments, which confirms that addition of c6-loaded NP to macrophages adhering on PEI-coated surfaces resulted in NP

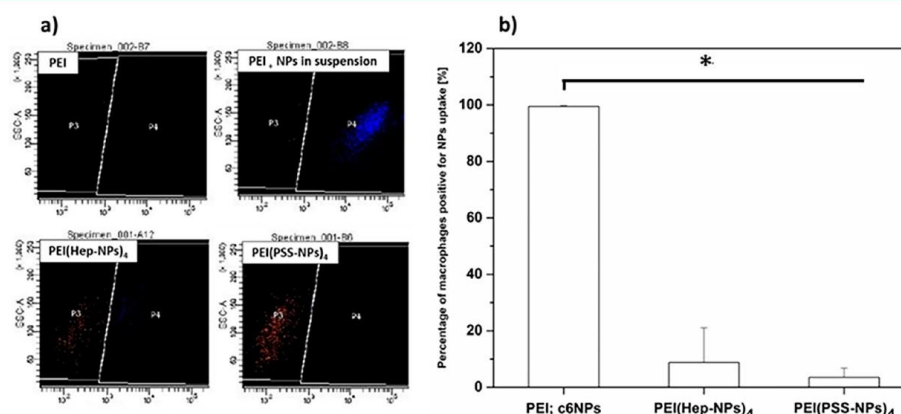


Figure 8. (a) Flow cytometry histograms of macrophages cultured on PEI (PEI) with addition of coumarin-6-labeled NP in supernatant (PEI; c6NP in suspension) or on multilayers with coumarin-6-labeled nanoparticles (PEI(Hep-NP)₄ and PEI(PSS-NP)₄) for a period of 48 h. Histograms show a plot of side scatter vs fluorescence intensity of coumarin-6 measured at the Alexa Fluor 466-A wavelength. The threshold was set in such a way to separate fluorescent from nonfluorescent cells. (b) The percentage of macrophages positive for c6-NP endocytosis of macrophages as calculated from flow cytometry histograms. Data represent means \pm SD, $n = 6$, $*p \leq 0.05$.

uptake by all cells demonstrating their fast uptake. By contrast, only 10% and 5% of macrophages seeded on PEI(Hep-NP)₄ and PEI(PSS-NP)₄ multilayers, respectively, were positive for c6-loaded NP uptake, which confirms that the immobilization of NP delays uptake by macrophages. On the other hand, it provides also evidence that macrophages may mobilize multilayer-bound NP with Naproxen, which may have an effect on the long-term response through release of the drug after digestion of NP in the lysosomal compartment.²⁸

Studies on Fusion of THP-1 Derived Macrophages. FBGCs formation is considered as a hallmark of chronic inflammation, which occurs at later stages of FBR, approximately after 15 days.⁵⁰ FBGCs are characterized by more than one nucleus in one cell body as well as a large area of cell cytoplasm as a result of macrophage fusion. The appearance of giant cells indicates the nonbiocompatibility of a material. Fusion of macrophages seeded on PEM was studied in the presence (upper row) and absence (lower row) of LPS after 15 days of incubation. Figure 9a shows the micrographs of

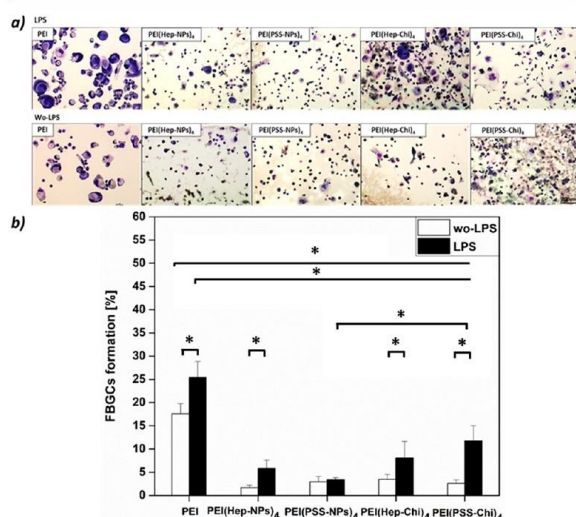


Figure 9. (a) Transmitted light microscopy images of macrophages and foreign body giant cells (FBGCs) stained with 10% (v/v) Giemsa after 15 days incubation in the presence (upper part) and absence (lower part) of LPS on the primary PEI surface and terminal fourth layer of either NP or Chi in combination with either Hep or PSS, abbreviated as [PEI, PEI(Hep-NP)₄, PEI(PSS-NP)₄, PEI(Hep-Chi)₄, and PEI(PSS-Chi)₄], respectively. [Scale: 200 μ m] (b) Area percentage of FBGCs covering the surface by quantitative image analysis of micrographs. Data represent means \pm SD, $n = 5$, $*p < 0.05$.

macrophages, while Figure 9b represents the quantitative evaluation of images. Here again, the ANOVA test was performed to compare LPS and no LPS conditions and PEM composed of the same polyelectrolytes (e.g., Hep-containing formulations or PSS-containing formulations). The addition of LPS increased significantly macrophage fusion on PEM, except PEI(PSS-NP)₄, which is visible when one compares macrophages cultured in the presence or absence of LPS (Figure 9a). Moreover, on the PSS/NPs system there is a significant reduction in the FBGCs formation when comparing to the system using Chi as polycation. We hypothesize that the long-term NPs release is slightly faster in the PSS-based system when compared to the Hep-based system due to the previously

discussed weaker interactions between NPs and PSS when compared to Hep owing to its lower charge density. This might explain the slightly better long-term anti-inflammatory activity (i.e., FBGCs formation) of the PSS/NPs system when compared to Hep/NPs, regardless of its lower short-term anti-inflammatory activity (i.e., higher macrophage adhesion and levels of IL-1 β released). The reduced FBGC formation on PEM with terminal NP layers supports the idea that they can exert an anti-inflammatory effect with either Hep or PSS as polyanions in the long term that is most probably a result of their uptake by macrophages. However, this needs to be studied in more detail probably in an animal model in future investigations.

CONCLUSIONS

In this study it was shown for the first time that a combination of cationic nanoparticles that bear a NSAID Naproxen can be combined with different polyanions such as heparin or polystyrenesulfonate to form PEM. As a further novelty of this work we consider the possibility to combine the immediate anti-inflammatory effects of heparin as polyanion, which has been visible here by reduction of IL-1 β secretion as a master regulator of inflammation, with a long-term anti-inflammatory effect of Naproxen that becomes most probably effective after endocytosis of NP through macrophages and subsequent hydrolysis of the ester bond between the polymer backbone and the Naproxen. This has been concluded from studies on FBGC formation. Although the exact mechanism of anti-inflammatory activity has not been explored here to its full detail, this work represents a proof-of-concept study to establish novel surface coatings that can suppress inflammatory reactions of macrophages to biomaterials, which may pave the way to modulate or reduce foreign body reaction after implantation of medical devices, such as sensors and other soft or hard tissue implants.

ASSOCIATED CONTENT

Supporting Information

The Supporting Information is available free of charge on the ACS Publications website at DOI: 10.1021/acs.biomac.9b01098.

Additional results, density of nanoparticles obtained by pycnometer method, and UV absorbance at $\lambda = 239$ nm obtained by NanoDrop One spectrophotometer for the fractions obtained after isopycnic centrifugation of glucose; and representative quartz crystal microbalance with dissipation monitoring (QCM-D) acquisition graphs depicting cumulative frequency shift (Δf) during PEM formation and dissipation change (ΔD) (PDF)

AUTHOR INFORMATION

Corresponding Author

*E-mail: mraguilar@ictp.csic.es.

ORCID

Georg Schmidt: 0000-0002-4151-6543

Thomas Groth: 0000-0001-6647-9657

Author Contributions

^vH.A.-K. and E.E.-C. contributed equally.

Notes

The authors declare no competing financial interest.

■ ACKNOWLEDGMENTS

This work was partly supported by the German Academic Exchange service (DAAD) through a PhD grant to Hala Alkhoury. Further financial support was provided by High Performance Center Chemical and Biosystems Technology Halle/Leipzig supported by the European Regional Development Fund (ERDF) and the Federal State Saxony-Anhalt. The authors would also like to thank CIBER-BBN, the Spanish Ministry of Science, Innovation and Universities (MAT2017-84277-R), and the training program for Academic Staff (FPU15/06109) of the Spanish Ministry of Education Culture and Sport for the funding to this project. The kind support by Mrs. Marlis Porobin from Department Biomedical Materials, Muhamad Tariq from Institute of Physics at Martin Luther University Halle-Wittenberg, and Rafael Nuñez from the Center for Biological Research (CIB-CSIC), in zeta potential, AFM and cryoTEM experiments, is greatly appreciated.

■ REFERENCES

- (1) Zhou, G.; Groth, T. Host Responses to Biomaterials and Anti-inflammatory Design—a Brief Review. *Macromol. Biosci.* **2018**, *18* (8), 1800112 (1–15).
- (2) Yu, T.; Tutwiler, V. J.; Spiller, K., The Role of Macrophages in the Foreign Body Response to Implanted Biomaterials. In *Biomaterials in Regenerative Medicine and the Immune System*; Santambrogio, L., Ed.; Springer International Publishing: Cham, 2015; pp 17–34.
- (3) Wynn, T. A.; Barron, L. Macrophages: master regulators of inflammation and fibrosis. *Semin. Liver Dis.* **2010**, *30* (3), 245–57.
- (4) Helming, L.; Gordon, S. Macrophage fusion induced by IL-4 alternative activation is a multistage process involving multiple target molecules. *Eur. J. Immunol.* **2007**, *37* (1), 33–42.
- (5) Barron, L.; Wynn, T. A. Fibrosis is regulated by Th2 and Th17 responses and by dynamic interactions between fibroblasts and macrophages. *Am. J. Physiol.: Gastrointest. Liver Physiol.* **2011**, *300* (5), 723–728.
- (6) Kzhyshkowska, J.; Gudima, A.; Riabov, V.; Dollinger, C.; Lavalle, P.; Vrana, N. E. Macrophage responses to implants: prospects for personalized medicine. *J. Leukocyte Biol.* **2015**, *98* (6), 953–62.
- (7) Benkirane-Jessel, N.; Schwinte, P.; Falvey, P.; Darcy, R.; Haikel, Y.; Schaaf, P.; Voegel, J. C.; Ogier, J. Build-up of polypeptide multilayer coatings with anti-inflammatory properties based on the embedding of piroxicam–cyclodextrin complexes. *Adv. Funct. Mater.* **2004**, *14* (2), 174–182.
- (8) Park, K.; Choi, D.; Hong, J. Nanostructured Polymer Thin Films Fabricated with Brush-based Layer-by-Layer Self-assembly by Site-selective Construction and Drug release. *Sci. Rep.* **2018**, *8* (1), 3365 (1–9).
- (9) Korn, P.; Schulz, M. C.; Hintze, V.; Range, U.; Mai, R.; Eckelt, U.; Schnabelrauch, M.; Müller, S.; Becher, J.; Scharmweber, D.; Stadlinger, B. Chondroitin sulfate and sulfated hyaluronan-containing collagen coatings of titanium implants influence peri-implant bone formation in a minipig model. *J. Biomed. Mater. Res., Part A* **2014**, *102* (7), 2334–2344.
- (10) Hsieh, C. Y. C.; Hu, F.-W.; Chen, W.-S.; Tsai, W.-B. Reducing the Foreign Body Reaction by Surface Modification with Collagen/Hyaluronic Acid Multilayered Films. *ISRN Biomater.* **2014**, *2014*, 718432 (1–8).
- (11) Altgärde, N.; Nilebäck, E.; de Battice, L.; Pashkuleva, I.; Reis, R. L.; Becher, J.; Möller, S.; Schnabelrauch, M.; Svedhem, S. Probing the biofunctionality of biotinylated hyaluronan and chondroitin sulfate by hyaluronidase degradation and aggrecan interaction. *Acta Biomater.* **2013**, *9* (9), 8158–8166.
- (12) Thierry, B.; Winnik, F. M.; Merhi, Y.; Silver, J.; Tabrizian, M. Bioactive Coatings of Endovascular Stents Based on Polyelectrolyte Multilayers. *Biomacromolecules* **2003**, *4* (6), 1564–1571.
- (13) Taylor, K. R.; Gallo, R. L. Glycosaminoglycans and their proteoglycans: host-associated molecular patterns for initiation and modulation of inflammation. *FASEB J.* **2006**, *20* (1), 9–22.
- (14) Gandhi, N. S.; Mancera, R. L. The structure of glycosaminoglycans and their interactions with proteins. *Chem. Biol. Drug Des.* **2008**, *72* (6), 455–482.
- (15) Köwitsch, A.; Zhou, G.; Groth, T. Medical application of glycosaminoglycans: a review. *J. Tissue Eng. Regen. Med.* **2018**, *12* (1), 23–41.
- (16) Zhou, G.; Niepel, M. S.; Saretia, S.; Groth, T. Reducing the inflammatory responses of biomaterials by surface modification with glycosaminoglycan multilayers. *J. Biomed. Mater. Res., Part A* **2016**, *104* (2), 493–502.
- (17) Swartzlander, M. D.; Barnes, C. A.; Blakney, A. K.; Kaar, J. L.; Kyriakides, T. R.; Bryant, S. J. Linking the foreign body response and protein adsorption to PEG-based hydrogels using proteomics. *Biomaterials* **2015**, *41*, 26–36.
- (18) Hyung Park, J.; Bae, Y. H. Hydrogels based on poly (ethylene oxide) and poly (tetramethylene oxide) or poly (dimethyl siloxane). III. In vivo biocompatibility and biostability. *J. Biomed. Mater. Res.* **2003**, *64* (2), 309–319.
- (19) Zhou, G.; Al-Khoury, H.; Groth, T. Covalent immobilization of glycosaminoglycans to reduce the inflammatory effects of biomaterials. *Int. J. Artif. Organs* **2016**, *39* (1), 37–44.
- (20) Park, S.; Han, U.; Choi, D.; Hong, J. Layer-by-layer assembled polymeric thin films as prospective drug delivery carriers: design and applications. *Biomater. Res.* **2018**, *22*, 29 (1–13).
- (21) Anandhakumar, S.; Raichur, A. M. Polyelectrolyte/silver nanocomposite multilayer films as multifunctional thin film platforms for remote activated protein and drug delivery. *Acta Biomater.* **2013**, *9* (11), 8864–8874.
- (22) Yang, M.; Choi, D.; Choi, M.; Hong, J. Nanoporous multilayer films for controlled antigen protein release. *J. Ind. Eng. Chem.* **2016**, *33*, 221–225.
- (23) Vrana, N.; Erdemli, O.; Francius, G.; Fahs, A.; Rabineau, M.; Deby, C.; Tezcaner, A.; Keskin, D.; Lavalle, P. Double entrapment of growth factors by nanoparticles loaded into polyelectrolyte multilayer films. *J. Mater. Chem. B* **2014**, *2* (8), 999–1008.
- (24) Patrono, C. Cardiovascular Effects of Nonsteroidal Anti-inflammatory Drugs. *Curr. Cardiol. Rep.* **2016**, *18* (3), 25 (1–8).
- (25) Martín-Saldaña, S.; Palao-Suay, R.; Aguilar, M. R.; Ramírez-Camacho, R.; San Román, J. Polymeric nanoparticles loaded with dexamethasone or α -tocopheryl succinate to prevent cisplatin-induced ototoxicity. *Acta Biomater.* **2017**, *53*, 199–210.
- (26) d'Arcy, R.; Tirelli, N. Fishing for fire: strategies for biological targeting and criteria for material design in anti-inflammatory therapies. *Polym. Adv. Technol.* **2014**, *25* (5), 478–498.
- (27) DiCiccio, J. E.; Steinberg, B. E. Lysosomal pH and analysis of the counter ion pathways that support acidification. *J. Gen. Physiol.* **2011**, *137* (4), 385–390.
- (28) Suarez, P.; Rojo, L.; Gonzalez-Gomez, A.; Roman, J. S. Self-assembling gradient copolymers of vinylimidazol and (acrylic)-ibuprofen with anti-inflammatory and zinc chelating properties. *Macromol. Biosci.* **2013**, *13* (9), 1174–1184.
- (29) Vauthier, C.; Schmidt, C.; Couvreur, P. Measurement of the Density of Polymeric Nanoparticulate Drug Carriers by Isopycnic Centrifugation. *J. Nanopart. Res.* **1999**, *1* (3), 411–418.
- (30) Macek, M. A review of advanced wet cleaning. *Informacije MIDEM* **1993**, *23* (4), 275–283.
- (31) Cho, N. J.; Kanazawa, K. K.; Glenn, J. S.; Frank, C. W. Employing two different quartz crystal microbalance models to study changes in viscoelastic behavior upon transformation of lipid vesicles to a bilayer on a gold surface. *Anal. Chem.* **2007**, *79* (18), 7027–7035.
- (32) Notley, S. M.; Eriksson, M.; Wågberg, L. Visco-elastic and adhesive properties of adsorbed polyelectrolyte multilayers determined in situ with QCM-D and AFM measurements. *J. Colloid Interface Sci.* **2005**, *292* (1), 29–37.
- (33) Voinova, M. V.; Rodahl, M.; Jonson, M.; Kasemo, B. Viscoelastic Acoustic Response of Layered Polymer Films at Fluid-

Solid Interfaces: Continuum Mechanics Approach. *Phys. Scr.* **1999**, *59* (5), 391–413.

(34) Picart, C. Polyelectrolyte multilayer films: from physico-chemical properties to the control of cellular processes. *Curr. Med. Chem.* **2008**, *15* (7), 685–697.

(35) Chen, L. H.; Ang, X. M.; Chan, C. C.; Shaillender, M.; Neu, B.; Wong, W. C.; Zu, P.; Leong, K. C. Layer-by-layer (chitosan/polystyrene sulfonate) membrane-based Fabry–Perot interferometric fiber optic biosensor. *IEEE J. Sel. Top. Quantum Electron.* **2012**, *18* (4), 1457–1464.

(36) Aggarwal, N.; Groth, T. Multilayer films by blending heparin with semisynthetic cellulose sulfates: Physico-chemical characterization and cell responses. *J. Biomed. Mater. Res., Part A* **2014**, *102* (12), 4224–4233.

(37) Bongrand, P.; Capo, C.; Depieds, R. Physics of cell adhesion. *Prog. Surf. Sci.* **1982**, *12* (3), 217–285.

(38) Altankov, G.; Richau, K.; Groth, T. The role of surface zeta potential and substratum chemistry for regulation of dermal fibroblasts interaction. *Materialwiss. Werkstofftech.* **2003**, *34* (12), 1120–1128.

(39) Xu, L.-P.; Meng, J.; Zhang, S.; Ma, X.; Wang, S. Amplified effect of surface charge on cell adhesion by nanostructures. *Nanoscale* **2016**, *8* (25), 12540–12543.

(40) Li, H.-L.; Zhang, H.; Huang, H.; Liu, Z.-Q.; Li, Y.-B.; Yu, H.; An, Y.-H. The effect of amino density on the attachment, migration, and differentiation of rat neural stem cells in vitro. *Mol. Cells* **2013**, *35* (5), 436–443.

(41) Aggarwal, N.; Altgärde, N.; Svedhem, S.; Zhang, K.; Fischer, S.; Groth, T. Effect of molecular composition of heparin and cellulose sulfate on multilayer formation and cell response. *Langmuir* **2013**, *29* (45), 13853–13864.

(42) Dukhin, S. S.; Zimmermann, R.; Duval, J. F.; Werner, C. On the applicability of the Brinkman equation in soft surface electrokinetics. *J. Colloid Interface Sci.* **2010**, *350* (1), 1–4.

(43) Annenkov, V. V.; Danilovtseva, E. N.; Tenhu, H.; Aseyev, V.; Hirvonen, S. P.; Mikhaleva, A. I. Copolymers of 1-vinylimidazole and (meth)acrylic acid: Synthesis and polyelectrolyte properties. *Eur. Polym. J.* **2004**, *40* (6), 1027–1032.

(44) Lungu, C. N.; Diudea, M. V.; Putz, M. V.; Grudzinski, I. P. Linear and Branched PEIs (Polyethylenimines) and Their Property Space. *Int. J. Mol. Sci.* **2016**, *17* (4), 555 (1–12).

(45) Anderson, J. M.; Rodriguez, A.; Chang, D. T. Foreign body reaction to biomaterials. *Semin. Immunol.* **2008**, *20* (2), 86–100.

(46) Anderson, J. M.; Miller, K. M. Biomaterial biocompatibility and the macrophage. *Biomaterials* **1984**, *5* (1), 5–10.

(47) Park, E. K.; Jung, H. S.; Yang, H. I.; Yoo, M. C.; Kim, C.; Kim, K. S. Optimized THP-1 differentiation is required for the detection of responses to weak stimuli. *Inflammation Res.* **2007**, *56* (1), 45–50.

(48) Loppnow, H.; Brade, H.; Rietschel, E. T.; Flad, H.-D., Induction of cytokines in mononuclear and vascular cells by endotoxin and other bacterial products. In *Methods in Enzymology*; Academic Press: 1994; Vol. 236, pp 3–10.

(49) Zhao, M.; Altankov, G.; Grabiec, U.; Bennett, M.; Salmeron-Sanchez, M.; Dehghani, F.; Groth, T. Molecular composition of GAG-collagen I multilayers affects remodeling of terminal layers and osteogenic differentiation of adipose-derived stem cells. *Acta Biomater.* **2016**, *41*, 86–99.

(50) Anderson, J. M. Biological responses to materials. *Annu. Rev. Mater. Res.* **2001**, *31* (1), 81–110.

Chapter 7

Summary and future perspectives

In conclusion, this PhD thesis provided a demonstration of the anti-inflammatory properties of GAGs as well as Naproxen-conjugated NPs that are meant to control the inflammation process as well as to reduce or avoid the fibrotic encapsulation of implants. The studies provide an insight on the anti-inflammatory effects of GAGs like HA and Hep based on their physicochemical properties as well as on the mechanism of action toward the canonical NF- κ B signalling pathway. In addition, the integration of multiple anti-inflammatory strategies such as Naproxen-conjugated NPs provided a potential long-term anti-inflammatory effect. Thereafter, a specific novelty was established by animal studies in an attempt to expand the screening toward studying tissue reaction in vivo. Surface characterization of the two used methods of covalent immobilization as well as PEMs formation involved investigation of wettability, ZP and topography. THP-1 derived macrophages were used in all studies since they are considered as key dominant cells in the inflammatory cascade. Results showed that the anti-inflammatory properties of GAGs were based on one hand by making GAGs-modified samples more hydrophilic and anionic, which in turn had an effect in significantly reducing macrophages adhesion, fusion and IL-1 β pro-inflammatory cytokine release in comparison to control surfaces. On the other hand, HA and Hep inhibited significantly the NF- κ B signalling pathway in terms of p65 subunit translocation into the nucleus, which was related to findings of immunoblotting and flow cytometry showing the ability of macrophages to associate with or uptake the labelled GAGs. Indeed, the Hep-coated samples showed the most significant inhibitory effect toward the canonical NF- κ B pathway with both immobilization methods. Moreover, NPs resulted in potential long-term anti-inflammatory effect, which was shown by reduced macrophage fusion after 15 days. In addition, tissue responses illustrated that both BCP-HA and BCP-Hep coated particles reduced multinucleated giant cell formation as well as the vascularization after 30 days, which was taken as a sign of reducing inflammatory in vivo response.

Based on these findings, additional experiments should focus on the amount of immobilized GAGs as well as the release ratio at different time points. Employing toluidine blue dye binding assay, for example, could be used to estimate the amount of immobilized GAGs by calculating the difference in the absorbance of the GAG

solution before and after the immobilization process. In addition, future perspectives shall focus on the medical application of the coatings developed in this work to treat various inflammatory related diseases. For instance, multilayer coatings with hyaluronic acid on glucose biosensors on one hand would eventually delay the fibrous capsule formation and thus enable a long-term measurement of glucose levels. On the other hand, the pharmacokinetics and pharmacodynamics of heparin is improved by attaching to solid supports, which will eventually lead to a reduced metabolic turnover. Hence, it can be covalently immobilized on poly(lactic acid-co-glycolic acid) (PLGA) by using EDC/ NHS cross linker chemistry to enhance the poor blood biocompatibility of the PLGA polymer. Eventually, it is essential to apply different modification methods to reach biocompatible biomaterials to be used in the market.

Acknowledgment

Five years of intensive work, five years to unlimited challenges came to the end now. Before completely closing the chapter of this period of my life;

I would like to express my immense gratitude for my first reviewer Prof. Dr. rer. nat. habil. Thomas Groth for his kindness, generative hints and support throughout the whole period I spent in his lab. I would like to thank him for giving me the opportunity to obtain my PhD degree under his supervision. Moreover, I want to extend my thanks for his concern and guidance, which helped me to overcome all the obstacles I faced.

I want to thank all reviewers for investing the time reading my thesis.

Special thanks to Dr. Bodo Fuhrmann and Dr. Alexander Navarrete Santos for the unlimited kindness and support. I enjoyed all the scientific discussion we had.

Sincere thanks to the colleagues who were helpful; Dr.-Ing. Marcus S. Niepel, thanks a lot for the resourceful ideas, support and numerous inspiring discussions; Dr. rer. nat. Alexander Köwitsch, I would like to thank you for being helpful with many different tasks at the lab; M.Sc.-Pharm. Adrian Hautmann thanks for the nice team work we achieved together as well as for your kindness. Last but not least, special thanks for my colleague and close friend Dipl. Pharm. Reema Anouz for being encouraging, concerned, understanding and supportive, I owe you a lot of admire.

Moreover, I would like to thank Mrs. Marlis Porobin for her help with the zeta potential measurements, buffer preparation and all other official paper work.

On the other pages of the chapter there were other people who helped in making this work successful;

To Syria, where I opened my eyes for the first time, where I was born, I grew up, I learned and I collected experience. To the place where I left my heart, my memories, my people who made me successful in each step of my life, to my home country Syria. To the strong unbreakable sad and happy country at the same time. To the country of

civilization with the great history, to the wrinkles I saw in your roads and walls due to the many different populations who passed over your ground, to Syria...

I would deeply tell you how proud I feel being a daughter of you. Moreover, I highly want to express my huge desire to come back, to construct, to develop and to build up all what gone in the war as a kind of modest thanks to what you offered me throughout the 26 years.

Furthermore, I would like to thank Germany, my second home country. I am deeply grateful for the hand of support you gave to me, to the door you opened, to the chances, to the diverse rich experience, to the tears and laughter. Germany is the mother who cuddled me as a mature child and opened my vision as well as my perspectives to learn hundreds of new things during the time of my stay. For this, I would say thanks a lot and I would be always a grateful and faithful scientist.

To DAAD, I would like to thank this great organization for playing a key role in making this work achievable. In addition, I would like to thank Mrs. Brigit Klaes for her continuous support.

To my former bosses, Musab Zedan and Mohamed Okasha who always believed I can perform complex tasks, I would like to express my appreciation to keep motivating me along the whole way.

To the person who I consider my real hero. I would like to let you know that you have a special spot in my heart for standing beside me in my distress and showing me love when I was unloved. Many thanks for being genuine and for believing in me.

In addition, sincere thanks to my best friend Wasim Khouri for supporting me on daily basis. I want to highly express my profound grateful for being so faithful over the years.

Finally, I would like to dedicate this thesis to the people who I owe them the most, my family...

I would like to present them the hard work, the years I spent without them, the success, and all the efforts I did. Thank you a lot for being caring, reassuring and super funny. I owe you all immense appreciation for each single detail you did to me to reach this step.

With closing the chapter and before the last full stop I would say;

Jesus, thank you for being always around when I felt lonely. You gave me all the courage, energy, capability to wake up each day with a different motivation. It was always renewable and exchangeable. You were my secret source of ability and positivity. You gave me hope even I was unable to see in the dark tunnel, Thank you...

With this I can press the last full stop to open again a different chapter with a different story.

Treasuring the whole period; with gratitude.

Publication list with declaration of self-contribution to research articles

1. G. Zhou, H. Al-Khoury, T. Groth; Covalent immobilization of glycosaminoglycans to reduce the inflammatory effects of biomaterials, *Int J Artif Organs* 2016.

My contribution was about 50%. I performed all experimental work. The manuscript was prepared and written by G. Zhou and with my support.

2. H. Alkhoury, A. Hautmann, F. Erdmann, G. Zhou, S. Stojanović, S. Najman, T. Groth, Study on the potential mechanism of anti-inflammatory activity of covalently immobilized hyaluronan and heparin, *Journal of Biomedical Materials Research (JBMR) part A*, 2020.

My contribution was about 70%. I performed most of the experiments except the immunofluorescence (IF) staining of NF- κ B and association of FITC-GAGs with macrophages studied by confocal laser scanning microscopy, who were performed by A. Hautmann. I assembled and wrote all parts except for the part 2.3.8. method section “SDS-PAGE and Western blotting”, which was mainly written by Dr. F. Erdmann.

3. H. Alkhoury, A. Hautmann, B. Fuhrmann, F. Syrowatka, F. Erdmann, G. Zhou, S. Stojanović, S. Najman, T. Groth, Studies on the mechanisms of anti-inflammatory activity of heparin- and hyaluronan-containing multilayer coatings-targeting NF- κ B signalling pathway, *International Journal of Molecular Sciences (IJMS)*, 2020.

My contribution was about 70%. I performed most of the experiments except the immunofluorescence (IF) staining of NF- κ B and Association of FITC-GAGs with macrophages studied by confocal laser scanning microscopy done by A. Hautmann. I assembled and wrote all parts except part 4. method section “SDS-PAGE and Western blotting”, which was mainly written by Dr. F. Erdmann.

-
4. S. Stojanović, H. Alkhoury, M. Radenković, V. Cvetković, M. Jablonska, C. E.H. Schmelzer, F. Syrowatka, J. M. Živković, T. Groth, S. Najman, Tissue response to biphasic calcium phosphate covalently modified with either heparin or hyaluronic acid in a mouse subcutaneous implantation model, *Journal of Biomedical Materials Research (JBMR) part A*, 2020.

My contribution was about 40%. I developed the protocol of immobilizing GAGs molecules on BCP particles. I performed the preparation of the samples as well as the characterizations with physical methods. I wrote the synthesis, the characterization methods as well as the results section and made further contributions during the writing of manuscript with the cooperation partners.

5. H. Alkhoury, E. Espinosa-Cano, M.R. Aguilar, J. San Román, F. Syrowatka, G. Schmidt, T. Groth, Anti-inflammatory surface coatings based on polyelectrolyte multilayers of heparin and polycationic nanoparticles of Naproxen- bearing polymeric drugs, *ACS publications-Biomacromolecules* 2019.

My contribution was about 80%. I performed most of the experiments and wrote the related paragraph.

Oral presentations

1. H. AlKhoury, A. Hautmann, F. Erdmann, S. Stojanović, S. Najman, T. Groth, Study on the potential mechanism of anti-inflammatory activity of covalent versus layer by layer immobilized glycosaminoglycans, 18th Young Researchers' Conference; Materials Science and Engineering, 4th – 6th December **2019**, Belgrade/Serbia.
 2. H. AlKhoury, E.Espinosa, F. Syrowatka, M. R. Aguilar, J. S. Román, G. Schmidt, T. Groth, Immobilization strategies with GAGs- polymeric drug conjugate on biomaterials for anti-inflammatory purposes, young researches initiatives yESAO, 11th – 12th September **2018**, Madrid/ Spain.
 3. H. AlKhoury, F.Heyroth, F. Syrowatka, M. R. Aguilar, E. Espinosa, J. S. Roman, G. Schmidt, T. Groth, Immobilization strategies with glycosaminoglycans- polymeric drug conjugate on biomaterials for anti-inflammatory purposes, 44th Annual Congress of the European Society for Artificial Organs (ESAO), 4th – 10th September **2017**, Vienna/ Austria.
 4. H. AlKhoury, F.Heyroth, F. Syrowatka, M. R. Aguilar, E. Espinosa, J. S. Roman, G. Schmidt, T. Groth, Reducing inflammatory responses to biomaterials with glycosaminoglycan- polymeric drug conjugate immobilization in a multilayer system, 8th BiNanoMed International Congress of Nanotechnology in Medicine and Biology, 20th – 22nd March **2017**, Krems/ Austria.
 5. G. Zhou, H. AlKhoury, S. Saretia, T. Groth, Immobilization strategies for glycosaminoglycans on biomaterials for anti-inflammatory purposes, XLIII Annual Congress of the European Society for Artificial Organs (ESAO), 14th– 18th September **2016**, Warsaw/ Poland.
 6. G. Zhou, H. AlKhoury, T. Groth, Anti-inflammatory surface coatings with glycosaminoglycans on biomaterials, young researches initiative yESAO, 12th – 14th September **2016**, Warsaw/ Poland.
-

-
7. G. Zhou, H. AlKhoury, T. Groth, Anti-inflammatory surface coatings with glycosaminoglycans on biomaterials, *20. Chirurgische Forschungstage*, 9th–10th September **2016**, Magdeburg/ Germany.

 8. G. Zhou, H. AlKhoury, T. Groth, Glycosaminoglycans as efficient tool to reduce inflammatory response to biomaterials for anti-inflammation targeting, *the 7th BioNanoMed International Congress of Nanotechnology in Medicine and Biology*, 6th – 8th April **2016**, Krems/Austria.
-

Posters

1. H. AlKhoury, A. Hautmann, F. Erdmann, G. Zhou, S. Stojanović, S. Najman, T. Groth, Covalent immobilization and multilayer formation of glycosaminoglycans and their anti-inflammatory mechanism of action, *the European Society for Artificial Organs (ESAO) winter school*, 26th –29th February **2020**, Lutherstadt Wittenberg/Germany.
 2. H. AlKhoury, A. Hautmann, F. Erdmann, G. Zhou, T. Groth, Covalent immobilization and multilayer formation of glycosaminoglycans and their anti-inflammatory mechanism of action, *the 30th Conference of the European Society for Biomaterials (ESB) together with the 26th Conference of the German Society for Biomaterials (DGBM)*, 9th –13th September **2019**, Dresden/Germany.
 3. H. AlKhoury, A. Hautmann, F. Erdmann, T. Groth, The anti-inflammatory action of physically adsorbed versus covalently bounded glycosaminoglycans, *Controlled Release Society (CRS) local chapter meeting*, 7th –8th March **2019**, Leipzig/Germany.
 4. H. AlKhoury, B. Fuhrmann, F. Syrowatka, G. Schmidt, T. Groth, Development of anti-inflammatory surfaces using microtopographies, *XLV Annual Congress of the European Society for Artificial Organs (ESAO)*, 12th – 15th September **2018**, Madrid / Spain.
 5. H. AlKhoury, A. Hautmann, G. Zhou, T. Groth, Development of anti-inflammatory strategies for implant material, *7th International Conference of Osteoimmunology*, 3rd – 7th June **2018**, Crete/ Greece.
 6. G. Zhou, H. AlKhoury, S. Saretia, T. Groth, Reduced inflammatory responses to biomaterials after glycosaminoglycans immobilization, *TERM summer school on Biomaterials and regenerative medicine*, 4th – 9th July **2016**, Riva del Garda/ Italy.
-

Curriculum vitae

Personal data

Name: Hala Alkhoury

Date of birth: 10. September 1988 in Damascus, Syria

Academic degree: Dipl. Pharm. (Diplom-Pharmacist)

Work Experience

- | | |
|-------------|---|
| 2013 – 2014 | Pharmaceutical representative at the vaccine department and a product specialist at the oncology department at GlaxoSmithKline. |
| 2011 – 2013 | Pharmaceutical representative in the cardiology, Chronic Venous Insufficiency (CVI) and osteoporosis field at Servier Laboratories. |

Education

- | | |
|-------------------|---|
| 10/2015 – 06/2020 | PhD student in the group of Prof. Dr. rer. nat. habil. Thomas Groth, Institute of Pharmacy, Martin-Luther-University Halle-Wittenberg

Title of PhD thesis: “Different strategies to prepare anti-inflammatory biomaterial coatings with in vitro and in vivo studies on efficacy and mechanisms” |
| 06/2014 – 07/2015 | Diploma student in the group of Prof. Dr. rer. nat. habil. Thomas Groth, Institute of Pharmacy, Martin-Luther-University Halle-Wittenberg

Title of diploma thesis: “Anti-inflammatory studies of Glycosaminoglycans” |
| 01/2006 – 08/2011 | Pharmacy student at Arab International University |
-

Awards / Grants

- | | |
|---------|---|
| 02/2020 | Golden Poster Award from the European Society for Artificial Organs (ESAO) Winterschool, Lutherstadt Wittenberg, Germany. |
| 06/2018 | Travel Award from the 7 th International Conference of Osteoimmunology in Chania, Crete, Greece. |
| 01/2018 | Exchange Award for Young Scientists from the Young European Society for Artificial Organs (yESAO) |
| 11/2016 | The Diploma Thesis Award from Serumwerk Bernburg |

Halle (Saale), 30. Juni 2020

Hala Alkhoury

Selbstständigkeitserklärung

Hiermit erkläre ich gemäß § 5 der Promotionsordnung der Naturwissenschaftlichen Fakultät I der Martin-Luther-Universität Halle-Wittenberg, dass ich die Ergebnisse der vorliegenden kumulativen Dissertationsarbeit

Different strategies to prepare anti-inflammatory biomaterial coatings with in vitro and in vivo studies on efficacy and mechanisms

am Institut für Pharmazie in der Arbeitsgruppe Biomedizinische Materialien unter Anleitung von Prof. Dr. rer. nat. habil. Thomas Groth selbständig erarbeitet und die Dissertation ohne fremde Hilfe verfasst habe.

Weiterhin erkläre ich, dass ich keine anderen als die von mir angegebenen Quellen und Hilfsmittel zur Erstellung meiner Dissertation verwendet habe. Den benutzen Werken wörtlich oder inhaltlich entnommene Stellen sind als solche gekennzeichnet.

Ferner erkläre ich, dass ich mich mit der vorliegenden Dissertationsarbeit erstmals um die Erlangung eines Doktorgrades bewerbe.

Halle (Saale), den 30. Juni 2020

Dipl. Pharm. Hala Alkhoury
